Parisa Aris

Exploring the Multifaceted Pharmacological Potential of Griseofulvin: From Genomic Insights to Therapeutic Applications

Thesis submitted to the University of Ottawa

in partial fulfilment of the requirements for the degree

Doctorate in Philosophy in Biology

Department of Biology

Faculty of Science

University of Ottawa

Thèse soumise à l'Université d'Ottawa

envers la réalisation partielle des exigences du

Doctorat en Philosophie en Biologie

Département de Biologie

Faculté des Sciences

Université d'Ottawa

Abstract

Griseofulvin (C17H17ClO6) is a natural compound first isolated from *Penicillium griseofulvum* in 1939. Besides Penicillium, it can also be found in other types of fungi such as *Xylaria flabelliformis*, *Abieticola koreana*, and *Stachybotrys levispora*. Its applications span agriculture and medicine: in agriculture, griseofulvin acts as a protective agent against fungal infections in crops, while in medicine, it serves as a low-toxicity antifungal treatment for ringworm and dermatophyte infections in both humans and animals. In cancer research, griseofulvin has shown potential by inhibiting cancer cell division, possibly inducing cell death through its interaction with microtubules in the mitotic spindle. Furthermore, griseofulvin exhibits promising activity against hepatitis C virus by disrupting microtubule formation in human cells, thereby inhibiting viral replication. These diverse applications underscore the broad utility of griseofulvin across different fields, suggesting further avenues for exploration in therapeutic and biotechnological contexts.

This research encompasses four distinct chapters, each probing different aspects of griseofulvin and its derivatives. The first chapter introduces griseofulvin, presenting an extensive review of both past and current knowledge on the subject. It provides a foundation for understanding the compound's properties and uses, setting the stage for the subsequent chapters.

The second chapter explores the genomic evidence pertaining to the preservation and distribution of genes involved in griseofulvin biosynthesis across various fungal species. Through comprehensive sequencing and comparative genomic analyses, the study sheds light on the evolutionary dynamics and ecological significance of the gsf gene cluster, which orchestrates the synthesis of griseofulvin, a bioactive compound with antifungal properties. By examining multiple fungal genomes, the research elucidates patterns of gene conservation and divergence,

providing insights into the evolutionary forces shaping the distribution of griseofulvin-producing fungi. Furthermore, the identification of conserved gsf genes and their shared sequence orders among fungal species offers valuable insights into the functional roles and evolutionary constraints governing griseofulvin biosynthesis. We hypothesize that nonessential gsf genes would provide minimal evolutionary benefit, leading to these genes accumulating significant sequence variability or being completely lost in the gsf BGC of many fungal genomes. Overall, this study contributes to our understanding of the genetic basis of griseofulvin production in fungi and lays the groundwork for future research aimed at harnessing the therapeutic potential of this bioactive compound.

Subsequently, the third chapter investigates the therapeutic potential of griseofulvin and its derivatives against COVID-19 through computational molecular dynamics simulations. With the urgent need for effective treatments against the novel coronavirus, this study explores the binding interactions between griseofulvin compounds and key viral proteins implicated in the replication and transcription processes of SARS-CoV-2. Through in silico analyses, the research identifies promising candidates among griseofulvin derivatives that exhibit significant binding affinity to essential viral proteins, such as the main protease (6LU7), ACE2 receptor, receptor-binding domain (RBD), and RNA-dependent RNA polymerase (RdRp). We hypothesize that griseofulvin and its derivatives can effectively inhibit SARS-CoV-2 by binding to the virus's main protease, RdRp, and RDB proteins, as well as the human ACE2 receptor. Molecular docking and molecular dynamics simulations will reveal strong interactions between these compounds and the target proteins. These findings highlight the potential of griseofulvin derivatives as inhibitors of COVID-19 viral replication and offer valuable insights for further

experimental validation and drug development efforts aimed at combating the ongoing global pandemic.

The fourth chapter undertakes a thorough investigation into the antibacterial properties of newly formulated derivatives of griseofulvin using computational techniques. Utilizing molecular docking and molecular dynamics simulations, the study assesses how these derivatives interact and remain stable when bound to bacterial targets such as penicillin-binding protein 2 (PBP2), tyrosine phosphatase, and filamenting temperature-sensitive mutant Z (FtsZ) protein. The research identifies critical structural characteristics necessary for antibacterial effectiveness, including the presence of a β-lactam moiety, sulfonyl group, and chlorine substitution. Notably, certain derivatives exhibit robust binding affinities and stability within the active sites of bacterial proteins, suggesting their potential as potent antibacterial agents. The hypothesis posits that deliberate structural adjustments to griseofulvin can enhance its antibacterial properties, positioning it as a promising candidate for new antibiotic development. These findings offer significant insights for the strategic design and advancement of griseofulvin derivatives with enhanced antibacterial activity, presenting promising avenues for combatting bacterial infections and addressing the challenge of antibiotic resistance.

Acknowledgements

I express my profound gratitude to my supervisor, Dr. Xuhua Xia, for his unwavering support amentorship throughout my academic journey. His guidance, encouragement, and boundless supply of research ideas tailored to my interests have been invaluable. I am indebted to him for fostering my scientific growth through constructive feedback and providing opportunities for teaching and research mentorship. My heartfelt appreciation extends to the professors who have supported and contributed to my PhD studies, including Dr. Ashkan Golshani, and Dr. Francois-Xavier Campbell-Valois. I am grateful for their guidance, encouragement, and invaluable contributions to my research. I also extend my thanks to all past and present members of the Xia lab for their support and friendship. Special thanks to Yulong Wei, Alibek Kruglikov, Mahbubeh Askarirad, and Heba Farookhi. My deepest appreciation goes to my family and friends for their unwavering love and support. I am especially grateful to my parents for their sacrifices and encouragement. Lastly, I acknowledge the funding provided by NSERC Discovery Grant to Dr. Xuhua Xia, and Ontario Graduate Scholarship, which have made this research possible.

Table of Contents

List of Tables

List of Figures

List of Abbreviations

SARS-CoV-2 - Severe acute respiratory syndrome coronavirus 2

BGCs -biosynthetic gene clusters

gsf BGC - griseofulvin biosynthetic gene cluster

HGT - horizontal gene transfer

AF - aflatoxins

ST - sterigmatocystin

MGEs - mobile genetic elements

NR-PKS – nonreducing polyketide synthase

SAT - transacylase

KS - ketosynthase

PT - product template

ACP - acyl carrier protein

6-DMG - 6-desmethylgriseofulvin

4-DMG - 4- desmethylgriseofulvin

MT - microtubule

VCAM-1 - vascular cell adhesion molecule 1

HDMEC - IL-1 stimulated human dermal microvascular endothelial cells

MBs - Mallory bodies

K8/18 - keratins 8 and 18

PDB - Protein Data Bank

RdRp - RNA-dependent RNA polymerase

RBD - spike protein receptor-binding domain

ACE2 - angiotensin-converting enzyme 2

RAAS - renin-angiotensin-aldosterone system

ANG I - angiotensin I

ANG II - angiotensin II

SMRT - Single Molecule Real-Time

NCBI - National Center for Biotechnology Information

INSDC - International Sequence Database Collaboration

AntiSMASH - Antibiotic Secondary Metabolite Analysis Shell

MIBiG - Minimum Information about a Biosynthetic Gene cluster

BiG-SCAPE - Biosynthetic Gene Similarity Clustering And Prospecting Engine

JI - Jaccard Index

AI - Adjacency Index

DSS - Domain Sequence Similarity

3CLpro - 3C-like main protease

PLpro - papain-like protease

Mpro - main protease

MD - Molecular dynamics

CASTp - Computed Atlas of Surface Topography of proteins

ACPYPE - AnteChamber PYthon Parser interface

RMSD - root mean square deviation

RMSF - root mean square fluctuations

Rg - radius of gyration

SASA - solvent accessible surface area

HCV - hepatitis C virus

6-APA - 6-aminopenicillanic acid

7-ACA - 7-aminocephalosporanic acid

ftsZ - Filamenting temperature-sensitive mutant Z

PBP2 - Penicillin binding protein 2

GyrB - DNA gyrase subunit B

SAR - structure-activity relationships

PASS - Prediction of Activity Spectra for Substances

PTPs - tyrosine phosphatase

TbpA - Tyrosine phosphatase A

c-di-GMP - cyclic diguanylic acid

List of Publications

Publications related to my Thesis Chapters

1. Aris P, Mohamadzadeh M, Zarei M, Xia X. Computational Design of Novel Griseofulvin Derivatives Demonstrating Potential Antibacterial Activity: Insights from Molecular Docking and Molecular Dynamics Simulation. International Journal of Molecular Sciences. 2024;25(2):1039. 2.
2. Aris P, Mohamadzadeh M, Wei Y, Xia X. In Silico Molecular Dynamics of Griseofulvin and Its Derivatives Revealed Potential Therapeutic Applications for COVID-19. International journal of molecular sciences. 2022;23(13):6889.
3. 3. Aris P, Wei Y, Mohamadzadeh M, Xia X. Griseofulvin: An Updated Overview of Old and Current Knowledge. Molecules. 2022;27(20):7034.
4. 4. Aris P, Yan L, Wei Y, Chang Y, Shi B, Xia X. Conservation of griseofulvin genes in the gsf gene cluster among fungal genomes. G3. 2022;12(2):jkab399.

Other publications at the Xia lab

1. Aris P, Mohamadzadeh M, Kruglikov A, Askari Rad M, Xia X. In Silico Exploration of Microtubule Agent Griseofulvin and Its Derivatives Interactions with Different Human β-Tubulin Isotypes. Molecules. 2023;28(5):2384.
2. Wei Y, Aris P, Farookhi H, Xia X. Which mammalian species are at risk of being infected by SARS-CoV-2: an ACE2 perspective. 2020.
3. Wei Y, Aris P, Farookhi H, Xia X. Predicting mammalian species at risk of being infected by SARS-CoV-2 from an ACE2 perspective. Scientific reports. 2021;11(1):1-10.
4. Wei Y, Silke JR, Aris P, Xia X. Coronavirus genomes carry the signatures of their habitats. BioRxiv. 2020.

CHAPTER ONE

This chapter is published as a review article in Molecules Journal in 2022.

Aris P, Wei Y, Mohamadzadeh M, Xia X. Griseofulvin: An Updated Overview of Old and Current Knowledge. Molecules. 2022;27(20):7034.

1.1.Author Contributions

Parisa Aris[1], Yulong Wei[2], Masoud Mohamadzadeh[3], Xuhua Xia[1,4]*

1. Department of Biology, University of Ottawa, 30 Marie Curie, P.O. Box 450, Station A, Ottawa, Ontario, K1N 6N5, Canada. Tel: (613) 562-5800 ext. 6886, Fax: (613) 562-5486.

2. Department of Microbial Pathogenesis, Yale University School of Medicine, New Haven, CT 06519, USA

3. Department of Chemistry, Faculty of Sciences, University of Hormozgan, Bandar Abbas 71961, Iran

4. Ottawa Institute of Systems Biology, Ottawa, Ontario, K1H 8M5, Canada.

P.A. designed the study, collected the data, and wrote the original draft of the manuscript. M.M. conducted molecular docking. Y.W. and X.X. reviewed and edited the manuscript. X.X. designed, supervised, and coordinated the study. All authors have read and agreed to the published version of the manuscript.

Introduction

1.1.General introduction on griseofulvin

Griseofulvin ($C_{17}H_{17}ClO_6$) is a natural product that was first discovered and isolated from *Penicillium griseofulvum* in the 1939. In addition to *Penicillium*, griseofulvin may be isolated from other genera of ascomycetes including *Xylaria flabelliformis*, *Abieticola koreana*, and *Stachybotrys levispora* (1-4). Griseofulvin has a wide range of applications, from agriculture to medicine. In agriculture, griseofulvin is used as a crop protectant to prevent fungal colonization and infection (5). In medicine, griseofulvin has been widely used as an antifungal drug and in treating ringworm and dermatophyte infections in humans and animals (6, 7) due to its low toxicity. In cancer research, griseofulvin has shown inhibitory effects on cancer cell division and may induce cell death through interaction with the mitotic spindle microtubule (8). Furthermore, griseofulvin may inhibit hepatitis C virus replication by interfering with microtubule polymerization in human cells (9).

Griseofulvin has long been known to cause vasodilation and improve capillary blood flow (10, 11). A new look at this old drug in our study revealed that griseofulvin has a good binding potential with the SARS-CoV-2 main protease and with the human ACE2 receptor (12). ACE2 facilitates the breakdown of ANG II which reduce blood pressure and inflammation (13). Our molecular docking results suggest a promising direction in drug repurposing to enhance ACE2 breakdown to relieve COVID symptoms (12).

In this chapter, we summarized the history of griseofulvin research since its discovery to the recent findings that suggest a promising future for the clinical application of this fungal secondary metabolite. We also studied the griseofulvin interaction with cytoplasmic intermediate filament proteins using molecular docking to find the binding affinity toward keratin 8 and 18 in

human, rat, and mouse. Our findings revealed that griseofulvin has good binding potential with K18 in rat, followed by mouse, which helps explain the significance of mild liver problems in human and the more serious problems in mice.

1.2. Discovery of Griseofulvin and its biosynthetic gene cluster in fungi

In 1939, griseofulvin was first isolated and is still widely used as an antifungal mainly caused by dermatophytes (6, 7). Over the next decade of research, Brian and Hemming (1947) discovered a metabolite of *Penicillium janczawski* that could cause hyphal waving of plant pathogen *Botrytis allii* and named it the 'curling factor' (14). This substance was later shown to be biologically and chemically identical to the product of *P. griseofulvum* which was identified and isolated by Oxford *et al.* (1939) under the name of griseofulvin (15).

Griseofulvin is produced from many species of the genus *Penicillium,* which is one of the most important fungal taxa frequently found around the world (2-4, 16-27). Following *P. griseofulvum, P. lanosocoeruleum,* a plant pathogen, is one of the most significant fungi that has recently been shown to produce griseofulvin (28). Further, *Abieticola koreana*, *Stachybotrys levispor*, and *Xylaria flabelliformis (previously known as X. cubensis)* were also shown to produce griseofulvin (2-4). Of note, fungal endophytes such as *Xylaria* are abundant in plant tissue that produce griseofulvin as an antifungal against plant pathogenic fungi (1, 29, 30).

Griseofulvin is a polyketide derived from acetyl and malonyl CoA precursor molecules to form dehydrogriseofulvin. The A-B-C ring structures of griseofulvin were first discovered by oxidative degradation (31). Findings of Brich *et al*. (1958) showed that 6-methylsalicylic acid (6-MSA), the carbon skeleton of griseofulvin, is assembled from one acetyl CoA and three molecules of malonyl CoA (32, 33). The biosynthetic structure of griseofulvin was elucidated by

^{13}C-NMR study using singly and doubly labeled acetate (34), and the crystal structure of griseofulvin was revealed by X-ray crystallography and UV spectroscopy (35-37).

In 2010, the griseofulvin biosynthetic gene cluster (*gsf* BGC) responsible for griseofulvin production in *P. aethiopicum* was fully discovered through shotgun sequencing and bioinformatics mining (Figure 1) (16). Recently, we performed a comparative genome study of more than 266 fungal species and showed that *Memnoniella echinate, with only* seven out of the thirteen putative *gsf* cluster genes (Figure 1), can still synthesize Griseofulvin (38). A phylogenetic analysis reconstructed with 18S rRNA sequences shows the global relationships among whole *gsf* BGCs of 13 surveyed fungal species including *P. aethiopicum*, *X. flabelliformis*, *M. echinata*, *P. griseofulvum*, *P. vulpinum*, *P. coprophilum*, and *A. alliaceus* (Figure 1). The 18S rRNA sequences do not have strain information, so there is no one to one correspondence between the leaves and the gene clusters when multiple strains are involved.

1.3. Biosynthesis of Griseofulvin

1.3.1. Gene Cluster Evolution Hypothesis

Genes producing secondary metabolites in fungi are frequently linked and located in biosynthetic gene clusters (BGCs) (39). It has been hypothesized that horizontal gene transfer (HGT) plays a vital role in this phenomenon. This is so because genes involved in fungal metabolic pathways are frequently physically clustered, increasing the possibility of pathway transfers occurring in a single event. There is evidence that sterigmatocystin (ST), a highly toxic secondary metabolite that serves as a precursor to aflatoxins (AF), was horizontally transferred from Aspergillus (40). However, it is believed that the metabolic gene clusters may have evolved from bacteria as almost half of the bacterial genes are located in an operon, a group of genes under the control of a promoter, and it may be essential to control the expression of downstream

genes (41). Further investigations have revealed that the gene clusters are usually located at the end of the chromosomes and flanked by mobile genetic elements (MGEs) that facilitate gene transfer within genomes and between species (41-43).

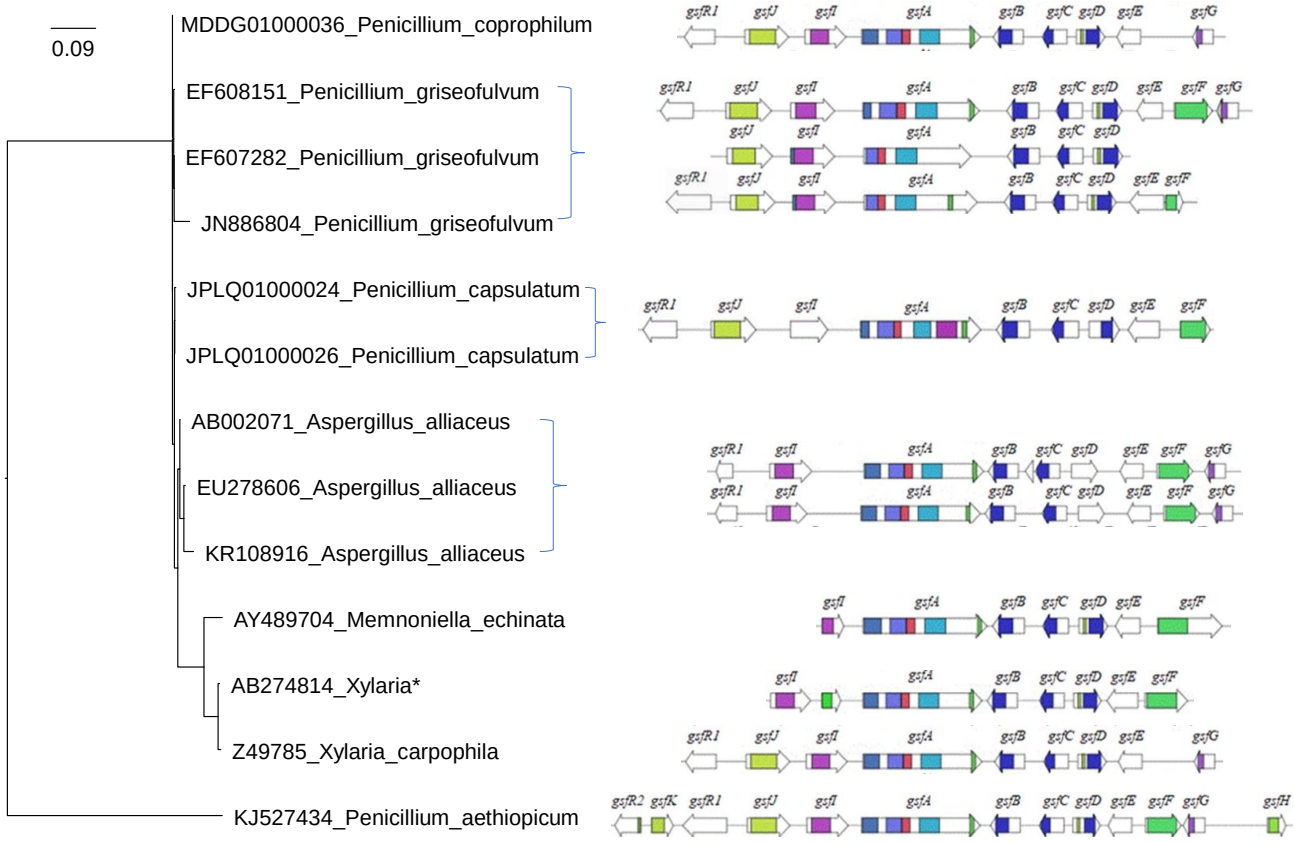

Figure 1.1. Griseofulvin biosynthetic gene cluster in *P. aethiopicum* and other fungal species. The arrows show the *gsf* gene candidates and their orientations in griseofulvin biosynthesis gene cluster. The phylogenetic tree is reconstructed with 18S rRNA sequences (in the format of accession_species) with the PhyML software after alignment with MAFFT. The *gsf* genes for *Xlaria** is *X. flabelliformis* which does not have an 18S rRNA sequence. *X. angulosa* was used instead. *P. aethiopicum* has only 33 nt of the 18S rRNA in contrast to other sequences that are ~1700 nt long.

1.3.2. Griseofulvin Biosynthetic Gene Cluster

In 2010, the putative griseofulvin gene cluster containing the PKS genes *gsfA*—*gsfK*, *gsfR1*, and *gsfR2* was first identified through shotgun sequencing and bioinformatic mining in *P. aethiopicum* (16). Later, single-gene deletion and biochemical test procedures were used to investigate the role of these *gsf* genes in griseofulvin biosynthesis (44), with the key findings summarized in Figure 2. GsfA initiates the biosynthesis of griseofulvin by combining one acetyl CoA and six malonyl CoA molecules to generate heptaketide backbone benzophenone 5a. GsfA is a nonreducing polyketide synthase (NR-PKS) that consists of several functional domains, including starter unit ACP transacylase (SAT), ketosynthase (KS), malonyl-CoA-ACP transacylase (AT), product template (PT), and an acyl carrier protein (ACP). The GsfA PT domain may mediate the cyclization of aromatic rings to form the intermediate benzophenone. The intermediate griseophenone C is produced from the methylation of phenols on benzophenone 5a by the O-methyltransferases (*gsfB* and *gsfC*). Following, griseophenone C is chlorinated to convert into griseophenone B by the halogenase *gsfI*, and the grisan core is produced from griseophenone B by the phenol oxidative activity of *gsf F*. The grisan core is finally transformed into griseofulvin by two further processes, methylation at 5-OH mediated by *gsf D* and enoyl redcution catalyzed by *gsf* E (Figure 2) (44).

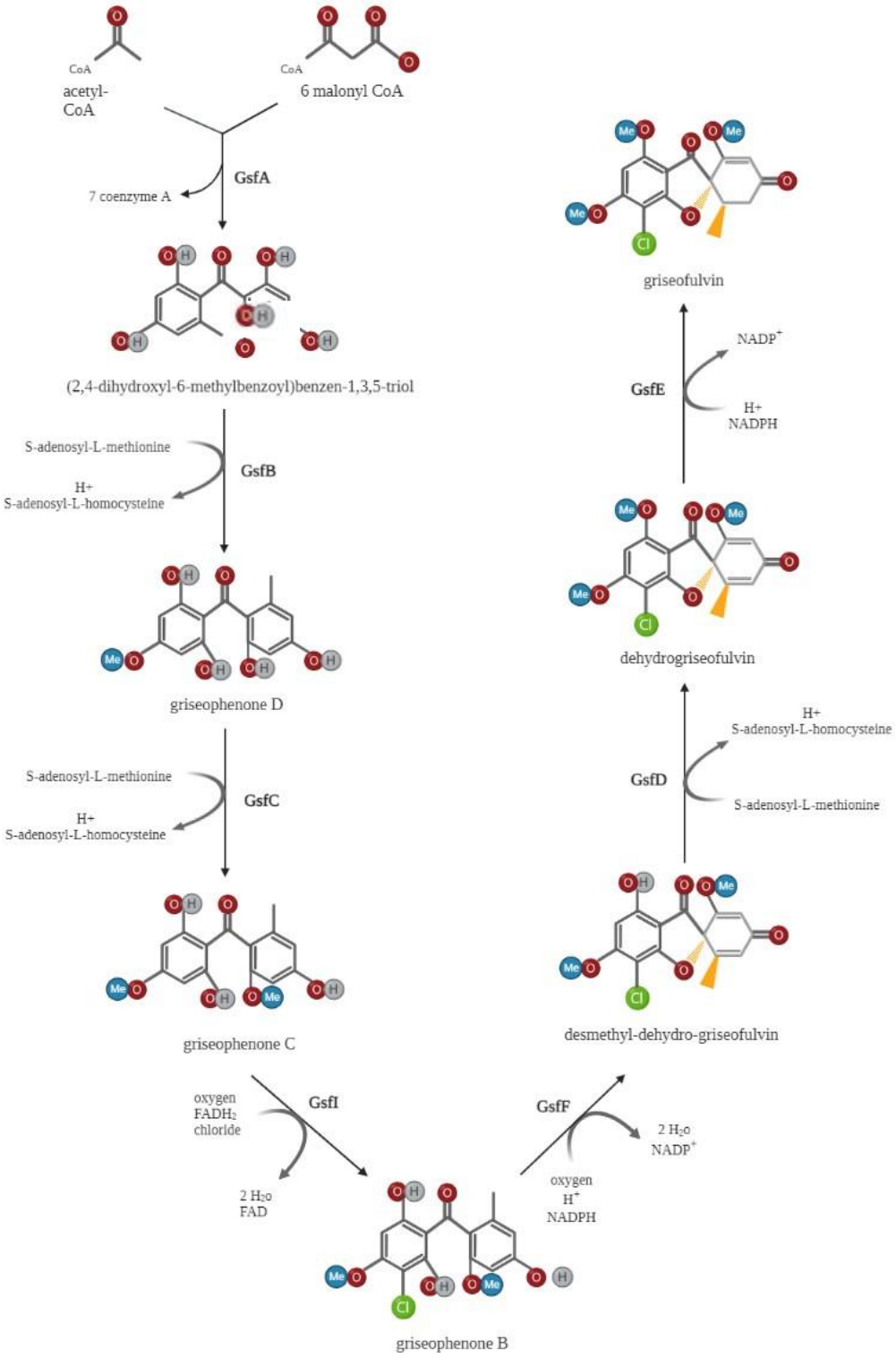
CoA
acetyl-CoA
CoA
6 malonyl CoA
GsfA
7 coenzyme A
(2,4-dihydroxyl-6-methylbenzoyl)benzen-1,3,5-triol
S-adenosyl-L-methionine
H+
S-adenosyl-L-homocysteine
GsfB
griseophenone D
S-adenosyl-L-methionine
H+
S-adenosyl-L-homocysteine
GsfC
griseophenone C
oxygen
FADH2
chloride
GsfI
2 H2o
FAD
GsfF
2 H2o
NADP+
oxygen
H+
NADPH
griseophenone B
desmethyl-dehydro-griseofulvin
H+
S-adenosyl-L-homocysteine
GsfD
S-adenosyl-L-methionine
dehydrogriseofulvin
NADP+
GsfE
H+
NADPH
griseofulvin

Figure 1. 2. Griseofulvin biosynthetic pathway. The nonreducing polyketide synthase *gsfA* initiates the synthesis of griseofulvin by combining one acetyl-CoA and six malonyl-CoA units to form the heptaketide backbone of benzophenone 5a. The O-methyltransferases (*gsfB* and *gsfC*) then methylate phenols on benzophenone 5a to generate the intermediate griseophenone C. Following this process, griseophenone C is chlorinated by the halogenase gsfI to produce griseophenone B, and griseophenone B is then converted to the grisan core by phenol oxidative activity of *gsfF*. The grisan core is ultimately converted into griseofulvin by two further processes: enoyl reduction catalyzed by *gsfE* and methylation at 5-OH mediated by *gsfD*. Created by Biorender.com.

Not all *gsf* genes are essential for griseofulvin biosynthesis and function. For instance, the deletion of *gsfA* or *gsfI* disrupts the production of griseofulvin since both proteins are essential for the *gsf* biosynthetic pathway (16, 44, 45). Additionally, the deletion of *gsfK* had no impact on biosynthesis in *P. aethiopicum* (44). Further, when compared to *P. aethiopicum*, *P. griseofulvum* lacks *gsfK*, *gsfH*, and *gsfR2* in the *gsf* BGC (45).

We recently conducted a comparative genome study in which the *gsf* BGC of 12 fungal genomes was identified, annotated, and compared. In this study, in addition to the *Penecillium* species, *gsf* BGC was found for the first time in *Aspergillus alliaceus*, *Aspergillus burnettii*, and *Memnoniella echinata*. Overall, our findings suggest that a total of seven genes (*gsfA*-*gsfF*, *gsfI*) out of the thirteen in *P. aethiopicum* were conserved by the majority of the genomes investigated and no gene rearrangements were reported at the *gsf* BGC (38).

1.3.3. Genetic Regulation of Griseofulvin Biosynthesis

The *gsfR1* and *gsfR2* encode for putative transcription factors in the griseofulvin gene cluster. However, their functions in the *gsf* gene cluster remain debatable. The *gsfR1* gene may not only impact griseofulvin biosynthesis but also serves as a critical regulator of other secondary metabolisms (46), such as patulin produced by *P. griseofulvum* (47). Indeed, the *gsfR1* gene deletion increased griseofulvin biosynthesis by increasing *gsfA* gene expression when tested on apples and PDA medium in vitro, suggesting *gsfR1* as a negative regulator of the cluster. However, in different culture conditions, such as high concentrations of nitrogen and complex sugars, and on media supplemented with peptone, the *gsfR1* positively regulates griseofulvin biosynthesis (48). These results indicate that *gsfR1* can respond differently depending on external stimulation, particularly nitrogen and carbon availability. Surprisingly, the gene *gsfR1* was missing in the recently released genome of griseofulvin producer *Xylaria flabelliformis* (2), indicating that griseofulvin biosynthesis could be regulated independently of *gsfR1* action.

It is noteworthy that the *gsfR2* gene in *P. griseofulvum* was found in a separate genomic region of the biosynthetic gene cluster, in contrast to *P. aethiopicum* (47) and *gsfR2* deletion did not affect griseofulvin biosynthesis, suggesting that this gene is probably involved in a different pathway or another secondary metabolite biosynthesis (48).

1.3.4. Environmental Factors in Producing Griseofulvin

The gene cluster expression is mostly synchronized in response to environmental conditions. Several factors appear to influence producing griseofulvin, of which organic compounds are one of the most critical environmental components (49). The yield of griseofulvin increases in rich media with glucose, acetate, and succinate. Of note is that a nitrogen concentration of less than 0.04 g% or more than 0.4 g% may inhibit the griseofulvin

biosynthesis (50). Furthermore, the ATP/ADP ratio is a significant parameter of cellular energy status that regulates griseofulvin synthesis; the more the energy level, the more griseofulvin production (51, 52). Another important factor is pH. The highest level of griseofulvin yields in a pH ranging from 5.5 to 6 (53).

Secondary metabolites are mainly synthesized during the stationary phase growth by microorganisms to improve their ability to thrive in diverse environments (54, 55). It may be assumed that the advantages of griseofulvin production are to defend against other fungal species and reduce competition. Even though only species that encounter such competition would preserve the griseofulvin gene cluster in their genomes, given the cost of time and energy. Thus, when the beneficial effects of producing griseofulvin outweigh the energy cost of biosynthesis, the organism would have increased fitness, according to the natural selection theory (56, 57). One example is the fungal endophyte, *Xylaria flabelliformis*, which is commonly found within plant tissue and the synthesis of griseofulvin as an antifungal against plant pathogenic fungi (2).

1.4. Physiochemical Properties of Griseofulvin

Griseofulvin is a fungal secondary polyketide metabolite that is soluble in ethanol and methanol but has poor solubility in water (6). One notable feature of griseofulvin is its ability to tolerate heat stress and maintain its function at a high temperature of 121°C without losing functional properties (49). These properties are important to understand their medical applications because they affect absorption, transportation, excretion and degradation.

1.5. Medical Applications

1.5.1. Antifungal Application

The first use of griseofulvin in medicine can be traced back to treating ringworm infections caused by *Microsporum canis* in guinea pigs (58). Further investigations revealed its effect on not only the genus *Microsporum* but *Trichophyton* and *Epidermophyton* (59). Griseofulvin was approved by Food and Drug Administration (FDA) in 1959, and it is still in use today and is considered one of the most widely used treatments for dermatophytes fungal infections in humans and animals.

1.5.2. Non-fungal Inflammatory Diseases

Further studies reported the effectiveness of griseofulvin in the treatment of non-fungal skin inflammation diseases, including lichen planus (60) and chronic purpuric dermatosis (61), suggesting that it may also have anti-inflammatory and immunomodulatory potential. This is while, earlier studies have shown that griseofulvin is effective in treating of the shoulder-hand syndrome (62), and a few other inflammatory, rheumatic conditions, such as posttraumatic reflex dystrophies and scapulohumeral periarthritis (63).

1.5.3. Cardiovascular Applications

It has been shown that intravenous administration of griseofulvin improves coronary blood flow and decreases blood pressure, indicating its peripheral vasodilation effects. In addition, griseofulvin increases myocardial heart rate by directly acting on the myocardium and vascular smooth muscle rather than through central nervous systems or humoral mechanisms (10, 11).

1.5.4. Antitumor Applications

Griseofulvin has gained attention for its potential application in cancer chemotherapy because of its low toxicity. In tumor cell lines, antifungal drug griseofulvin inhibits tumor growth and several forms of cancer cell proliferation by inhibiting dynamic instability of microtubules, mitotic arrest, and cell death in multipolar spindles, but not in fibroblasts and keratinocytes containing normal centrosome composition. Indeed, griseofulvin binds to the αβ intradimer tubulin interface and induces mitotic arrest by a variety of mitotic abnormalities, such as misaligned chromosomes and multipolar spindles, resulting in cells containing fragmented nuclei. These cells exhibited increased p53 accumulation in the nucleus, indicating that the cells undergo apoptosis (8, 64).

1.5.5. Antiviral Applications

Griseofulvin was used for zoster associated pain relief and prevented the development of further lesions within two days of starting treatment (65). Further studies have shown that griseofulvin suppresses the hepatitis C virus (HCV) replication by arresting the human cell cycle at the G2/M phase and acting on microtubule polymerization but does not affect HCV internal ribosome entry site (IRES) dependent translation. A synergistic inhibitory effect of griseofulvin and interferon alpha (IFNα) was also noted in Huh7/Rep-Feo (hepatoma cell line containing HCV 1b replicons that expresses a chimeric protein consisting of neomycin phosphotransferase and firefly luciferase) cells (9).

1.6. Pharmacokinetics of Griseofulvin

Griseofulvin is commonly used orally, although poor intestinal absorption may lead to failure in treatment. A spectrophotofluorometric study showed that griseofulvin absorption and effectiveness are dramatically increased with the highfat diet (66). Indeed, the oral bioavailability

of griseofulvin-loaded liposomes may be enhanced significantly by high drug encapsulation efficiency and small liposome size (67).

Griseofulvin absorption is greatest from the duodenum and least from the stomach, but colon absorption is hardly noticeable (68). In addition, a higher level of griseofulvin was found in the lung after intravenous administration, while the liver had a significantly higher level after oral administration (69). Furthermore, griseofulvin can be secreted through sweat glands and appears in the keratinized layer within four hours after a single-dose administration to inhibit fungal growth (70). The treatment response time depends on the keratin thickness at the injection site. Accordingly, healing fungal toenail infections may take longer than hair or skin infections (71).

The biological half-life of griseofulvin is 9 to 21 hours in the blood (72), and it is excreted as 6-desmethylgriseofulvin (6-DMG) and 4- desmethylgriseofulvin (4-DMG) metabolites in urine and feces after being metabolized by the liver microsomal enzyme system (68).

1.7. Characterized Interactions between Griseofulvin and Cellular Components

Griseofulvin enters the dermatophyte through energy dependent transport processes, binds to the fungal microtubules, interfering the microtubule function, thus inhibiting mitosis (73). The primary mechanism by which griseofulvin inhibits mitosis at metaphase is to suppress spindle microtubule (MT) dynamics by acting directly at the plus end to increase the stability and suppress the shortening rate at the MT plus ends (74). Griseofulvin has two possible binding sites in tubulin based on docking studies; one of which overlaps with the Taxol, a chemotherapy medication to treat cancer, the binding site at the beta-tubulin H6-H7 hoop, and the other is

located at the interface of αβ tubulin (64). It has been shown that griseofulvin at a concentration of 30 to 60 µM induced both mitotic G2/M arrest and apoptosis in a human malignant cell line (HL-60) using activation of NF-κB pathway with cell division cycle protein (cdc)2 activation and phosphorylation of B-cell lymphoma (Bcl)2 proteins that regulate cell death (75). Notably, the β-tubulin gene expression has been reported to decrease after griseofulvin treatment in *T. rubrum* (76).

Further studies have shown that it can be considered a potential therapeutic option for colon and breast cancer by an inhibitory effect on centrosomal clustering activity by altering the interphase microtubule stability. The findings strongly argued that mitotic irregularities and nuclear localization of p53 in human breast cancer MCF-7 cells are induced by kinetic inhibition of microtubule dynamics (8, 64). Likewise, griseofulvin inhibits hepatitis C virus replication by disrupting microtubule polymerization and interrupting the G2/M phase in human cells (9).

Additionally, griseofulvin has been shown effective for inflammatory skin diseases through inducing inhibitory effects on vascular cell adhesion molecule 1 (VCAM-1) in both TNF-alpha and IL-1 stimulated human dermal microvascular endothelial cells (HDMEC) (77).

1.8. Changes in keratins 8 and 18 in griseofulvin-induced liver injury

Because of the high concentration of griseofulvin in the liver as the major detoxification site, it has also been reported to cause occasional hepatitis (78, 79). While griseofulvin caused hepatitis is extremely rare in human, Mallory bodies (MBs) in hepatocytes associated with griseofulvin treatment were frequently reported in rodents (80, 81). The intermediate filament proteins (IFs), such as cytoplasmic keratins 8 and 18 (K8/18), are one of the most important components of a Mallory body (82). These intermediate filament proteins are believed to play an

important role in hepatocyte protection against toxic or mechanical stress, and regulation of cell response to injuries, cell growth, and death (83, 84). K8 and 18 are present in a 1:1 ratio under normal circumstances (85), but liver diseases such as alcoholic hepatitis, hepatic porphyria , and copper metabolism increase the K8/K18 ratio to more than 1, consequently forming the K8/18-containing aggregates known as Mallory bodies, which impairs centrosome and microtubule network function and results in cell death (86-89). Likewise, treatment of mice with griseofulvin-containing diet induces the Mallory body formation likely caused by overexpression of Krt8 (Keratin 8) gene (90), and griseofulvin binding to K8 and K18 in hepatocytes, which result in changing the keratin solubility, keratin phosphorylation on specific sites, and causing protein misfolding (83). Misfolded proteins are refolded with help of cellular chaperone proteins or tagged by ubiquitin for degradation (91). These findings suggest the binding potential of griseofulvin with cytoskeletons, especially keratin intermediate filaments proteins K8, and K18.

Here, we studied the griseofulvin interaction with K8 and K18 in human, rat, and mouse using molecular docking (Table 1), conducted in AutoDock 4 (92). The 3D protein structures of the K8 and K18 were downloaded from the RCSB Protein Data Bank (PDB) (https://www.rcsb.org/) or AlphaFold database (https://alphafold.ebi.ac.uk/). The interactions between the receptors and the griseofulvin were visualized using Discovery Studio Visualizer v.20 (https://discover.3ds.com/discovery-studio-visualizer-download). Keratin 8 (Krt8) and keratin 18 (Krt18) genes reside on chromosome 12 (GenBank accession NC_000012) in human, chromosome 15 (NC_000081) in mouse (Mus musculus), and chromosome 7 (NC_051342) in rat (Rattus norvegicus). The Krt8 sequences, after alignment with MAFFT, have 493 aligned sites of which human and mouse K8 differ by 44 aa (89% identity, 86% similarity), human and rat K8 differ by 44 aa (89% identity, 86% similarity) and mouse and rat K8 differ by 27 aa (94%

identity, 90% similarity). The alignment of the three Krt18 amino acid sequences have 432 sites, of which human and mouse K18 differ by 48 aa (86% identity, 90% similarity), human and rat K18 differ by 57 aa (84% identity, 89% similarity) and mouse and rat K18 differ by 16 aa (96% identity, 96% similarity). The molecular docking results revealed the K8 residues of Ile 63, Gln 85, and Lys 92 form H bonds with the oxyl groups of griseofulvin, while the K18 residues of Arg 117, Gln 243, Gln 350, Thr 353, and Arg 404 are involved in H-bond interactions (Figure 3). The griseofulvin illustrated low binding energy toward the K8, ranging from -3.17 to -4.6 kcal mol^{-1}. However, a higher binding energy toward K18 was observed in rat and mouse with -5.23 and -5.54 kcal mol^{-1} respectively (Table 1). In conclusion, the best griseofulvin interaction was found with Keratin 18 in rat, followed by mouse, based on the lowest binding energy and highest number of hydrogen bonds. This differential binding to K8 and K18 may disrupt the 1:1 ratio between the two and contribute to liver problems. The stronger binding of griseofulvin to K18 in rodents than in human may also explain the observed difference in the severity of hepatitis between rodents and humans.

Table 1. 1. Molecular docking details of griseofulvin interaction with keratin 8 (K8), and keratin 18 (K18) in human, rat, and mouse.

Keratin	Species	PDB or Alpha Fold IDs	$\Delta G_{binding}$ (Kcal/mol)	Hydrophobic Interaction	Hydrogen Bond
K8	Human	3K3C	−3.17	GLY 61, GLY 62, THR 64	ILE 63
		7K3X	−3.2	GLY 61	ILE 63
		7K3Y	−3.61	SER 58	-
		P05787F1	−4.6	ARG 88, LYS 92	GLN 85, LYS 92
	Mouse	P11679F1	−4.1	LYS 420, THR 421	-
	Rat	Q10758F1	−4.55	SER 15, GLY 16, PRO 17	-
K18	Human	A0A024RAY2F1	−4.72	LEU 87, ARG 90, SER 93, TYR94	-
		P05783F1	−4.99	SER 242, GLN 243, ASP 244, LYS 247, ILE 248, ASP 251	GLN 243
	Mouse	P05784F1	−5.54	LYS 111, ARG 117	ARG 117
	Rat	Q5BJY9F1	−5.23	ARG 346, GLY 349	GLN 350, THR 353, ARG 404

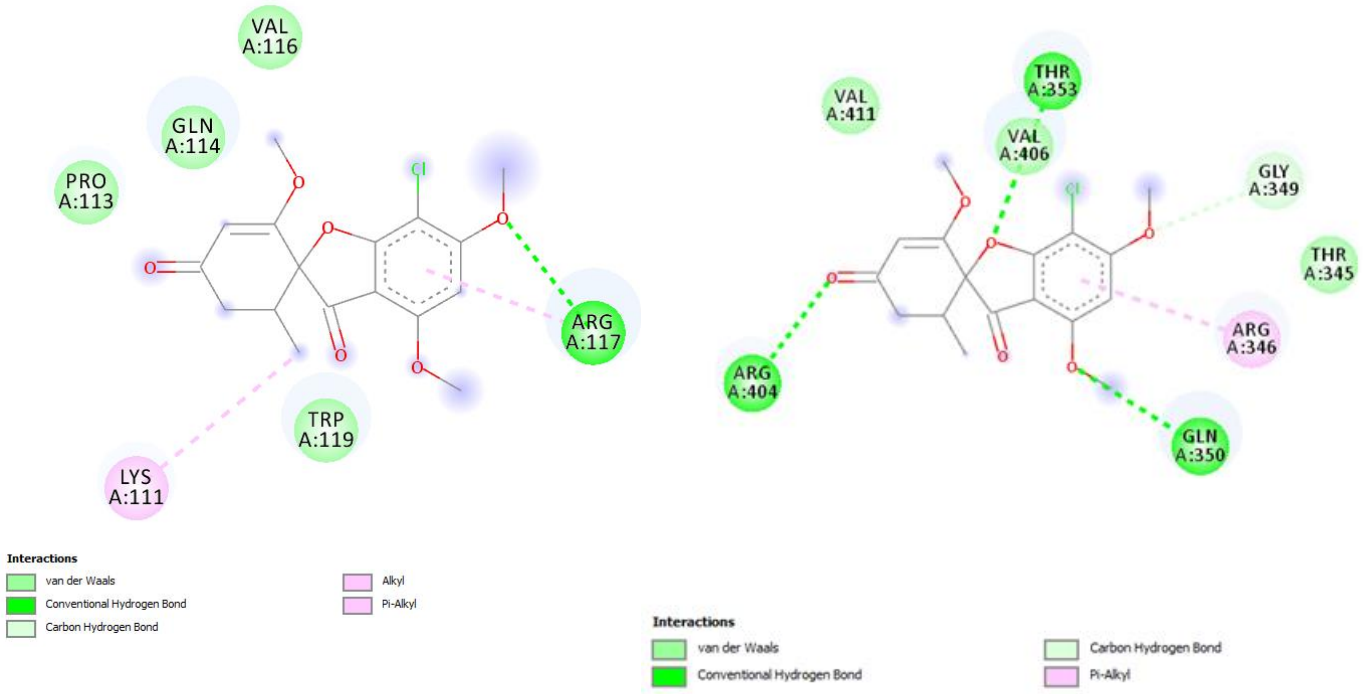

Figure 1. 3. 2D binding model of griseofulvin docked into the active site of keratin 18 (K18) in mouse (left) and rat (right). The dotted lines show the key interacting residues of the K18 toward griseofulvin as a ligand. The green, light green, and pink dotted lines show conventional hydrogen bonds, van der Waals, alkyl or Pi-alkyl interactions, respectively.

Amiodarone (Am), an antiarrhythmic medication used to treat and prevent a number of types of cardiac dysrhythmias (93), was used as positive control in this study, because it could be associated with liver injury and Mallory body formation in hepatocytes (94, 95). The molecular docking analysis showed that Arg90 is the only residue that can form hydrogen bonds in the binding cavity of K18, while the docking pose of amiodarone with K8 revealed three hydrogen bonds interactions with amino acids Gly 61 and Ile 63 in human (Table 2). Amiodarone showed the lowest free energy values (-4.68 and -4.85 kcal mol^{-1}), corresponding to the high affinity

binding site, for human K18. However, the amiodarone exhibited higher binding affinities, with binding energies of −4.14 and -3.64 kcal mol^{-1}, to K8 than K18 of mouse and rat respectively.

Table 1. 2. Molecular docking details of Amiodarone interaction with Keratin 8 (K8), and Keratin 18 (K18) in Human, Rat, and Mouse.

Keratin	Species	PDB or Alpha Fold IDs	$\Delta G_{binding}$ (Kcal/mol)	Hydrogen interaction	Hydrophobic bond
K8	Human	3K3C	−3.38	GLY 61, ILE 63	MET 60, GLY 61, ILE 63
		7K3X	>0	-	-
		7K3Y	>0	-	-
		P05787F1	−4.1	-	MET 406, SER 410, HIS 412
	Mouse	P11679F1	-4.14	-	MET 412, MET 415, ILE 417
	Rat	Q10758F1	−3.64	ARG 49	SER 51, LEU 52, PHE 55
K18	Human	A0A024RAY2F1	−4.69	ARG 90	LEU 87, ARG 90, LEU 91, TYR 94
		P05783F1	−4.85	-	LEU 87, ARG 90, LEU 91, TYR 94
	Mouse	P05784F1	−2.51	-	GLU 414
	Rat	Q5BJY9F1	−0.21	-	ARG 374, GLU 378

We also studied the molecular interactions of griseofulvin metabolites, including 6-desmethylgriseofulvin (6-DMG) and 4- desmethylgriseofulvin (4-DMG) (68), with K8 and K18 in human, mouse, and rat. Our *in silico* analysis exhibited slightly higher affinities for 6-DMG and 4-DMG metabolites than griseofulvin to mouse and rat K18. In addition, the number of hydrophobic and hydrogen bonds between griseofulvin metabolites and cytokeratin proteins (K8 and K18) were greater than griseofulvin in human, mouse, and rat. These findings suggest that griseofulvin metabolites have favorable interactions with keratins 8 and 18 (K8 and K18), and therefore they could be responsible for liver injury and Mallory body formation in hepatocytes of human and rodents treated with griseofulvin. The molecular docking details of 4-DMG and 6-DMG with K8 and K18 are shown in Tables 3 and 4 respectively.

Table 1. 3. Molecular docking details of 4-desmethylgriseofulvin (4-DMG) interaction with Keratin 8 (K8), and Keratin 18 (K18) in Human, Rat, and Mouse.

Keratin	Species	PDB or Alpha Fold IDs	$\Delta G_{binding}$ (Kcal/mol)	Hydrogen interaction	Hydrophobic bond
K8	Human	3K3C	−3.34	GLY 62, THR 64	GLY 61, GLY 62
		7K3X	−3.34	GLY 61, ILE 63	GLY 61, ILE 63
		7K3Y	−3.8	SER 58	SER 58, ALA 57
		P05787F1	−5.43	THR 64, ALA 65	THR 64, ALA 65,VAL 66, THR 67
	Mouse	P11679F1	−4.14	THR 419, LYS 420, THR 421	THR 421, THR 422
	Rat	Q10758F1	−3.93	SER 21, ARG 23	ALA 19, PHE 20, SER 21
K18	Human	A0A024RAY2F1	−4.48	ARG 90	ARG 90
		P05783F1	−4.96	SER 242, ASP 244	GLN 243, LYS 247, ASP 251
	Mouse	P05784F1	−5.28	GLN 114, ARG 117	LYS 111, PRO 113, GLN 114, ARG 117
	Rat	Q5BJY9F1	−5.22	THR 353, ARG 404	ARG 346, GLN 350, VAL 411

Table 1. 4. Molecular docking details of 6-desmethylgriseofulvin (6-DMG) interaction with Keratin 8 (K8), and Keratin 18 (K18) in Human, Rat, and Mouse.

Keratin	Species	PDB or Alpha Fold IDs	$\Delta G_{binding}$ (Kcal/mol)	Hydrogen interaction	Hydrophobic bond
K8	Human	3K3C	−4.04	GLY 62, THR 64	GLY 61, GLY 62
		7K3X	−3.71	ILE 63	ILE 63
		7K3Y	−3.95	GLY 56, SER 58	GLY 56, SER 58
		P05787F1	−4.85	LEU 72	LEU 72, PRO 75, VAL 77
	Mouse	P11679F1	−4.29	GLN 134, SER 138	LEU 131, GLN 134, GLN 135, SER 138
	Rat	Q10758F1	−4.50	SER 21	ARG 18, ALA 19
K18	Human	A0A024RAY2F1	−4.88	TYR94	LEU 91, TYR 94
		P05783F1	−4.81	GLU 236	SER230, SER 231, LEU 233, VAL 235, GLU 236
	Mouse	P05784F1	−5.61	LEU 108, TPR 119	LYS 111, PRO 113, VAL 116
	Rat	Q5BJY9F1	−5.33	ARG 346, GLN 350, ARG 404	ARG 346, GLN 350, VAL 411

1.9. Repurposing of Griseofulvin

Computational drug repurposing accelerates drug development and reduces the time, effort, and expenses associated with the drug discovery process (96, 97). In our recent study, griseofulvin and its derivatives were repurposed as potent inhibitors of SARS-CoV-2 entry and

viral replication. The inhibitory effects of griseofulvin and its derivatives on essential SARS-CoV-2 main protease, RNA-dependent RNA polymerase (RdRp), spike protein receptor-binding domain (RBD), and angiotensin-converting enzyme 2 (ACE2) from humans were investigated using molecular docking and molecular dynamics simulation. Our findings showed the activity of these compounds against SARS-CoV-2 target proteins. The highest docking score with the most hydrogen bond interactions to COVID-19 main protease was observed for griseofulvin. However, griseofulvin was also shown to interact favorably with ACE2, RBD, and RdRb proteins (12).

In addition to these inhibitory effects, griseofulvin may enhance ACE2 function to regulate the renin-angiotensin-aldosterone system (RAAS). ACE converts angiotensin I (ANG I) to angiotensin II (ANG II), which increases blood pressure and causes inflammation. ACE2 facilitates the breakdown of ANG II which lowers blood pressure and inflammation while maintaining homeostasis and preventing tissue damage (13). Inhibition of ACE2 function caused by SARS-CoV-2 binding to the ACE2 receptor leads to an increase in ANG II protein and its deleterious effects. It is well-known that griseofulvin has vasodilation and increased capillary blood flow effects (10, 11), although the molecular mechanism by which griseofulvin affects blood pressure remains unclear. Results from our molecular docking study put forward the hypothesis that griseofulvin binds to ACE2 and competes against SARS-CoV-2 binding to the extracellular domain of ACE2, therefore improving ACE2 vasodilation and tissue protection functions (12). These findings suggest that griseofulvin and its derivatives might be considered when developing future SARS-CoV-2 treatment options.

1.10. Acknowledgments

The authors would like to thank the joint editor and referees for their helpful comments that significantly improved the presentation of the study.

1.11. References

1. Whalley A. The xylariaceous way of life. Mycological Research. 1996;100(8):897-922.
2. Mead ME, Raja HA, Steenwyk JL, Knowles SL, Oberlies NH, Rokas A. Draft Genome Sequence of the Griseofulvin-Producing Fungus Xylaria flabelliformis Strain G536. Microbiology resource announcements. 2019;8(38):e00890-19.
3. Lee HB, Mun HY, Nguyen TTT, Kim J-C, Stone JK. Abieticola koreana gen. et sp. nov., a griseofulvin-producing endophytic xylariaceous ascomycete from Korea. Mycotaxon. 2016;131(4):749-64.
4. Ribeiro AI, Costa ES, Thomasi SS, Brandão DFR, Vieira PC, Fernandes JoB, et al. Biological and chemical control of Sclerotinia sclerotiorum using Stachybotrys levispora and its secondary metabolite griseofulvin. Journal of agricultural and food chemistry. 2018;66(29):7627-32.
5. Dayan FE, Cantrell CL, Duke SO. Natural products in crop protection. Bioorganic & medicinal chemistry. 2009;17(12):4022-34.
6. Oxford AE, Raistrick H, Simonart P. Studies in the biochemistry of micro-organisms: griseofulvin, C17H17O6Cl, a metabolic product of Penicillium griseo-fulvum Dierckx. Biochemical Journal. 1939;33(2):240.
7. Lambert DR, Siegle RJ, Camisa C. Griseofulvin and ketoconazole in the treatment of dermatophyte infections. International journal of dermatology. 1989;28(5):300-4.
8. Rebacz B, Larsen TO, Clausen MH, Rønnest MH, Löffler H, Ho AD, et al. Identification of griseofulvin as an inhibitor of centrosomal clustering in a phenotype-based screen. Cancer research. 2007;67(13):6342-50.
9. Jin H, Yamashita A, Maekawa S, Yang P, He L, Takayanagi S, et al. Griseofulvin, an oral antifungal agent, suppresses hepatitis C virus replication in vitro. Hepatology Research. 2008;38(9):909-18.
10. Rubin AA. Coronary vascular effects of griseofulvin. JAMA. 1963;185(12):971-2.

11. Aldinger EE. Cardiovascular effects of griseofulvin. Circulation Research. 1968;22(5):589-93.
12. Aris P, Mohamadzadeh M, Wei Y, Xia X. In Silico Molecular Dynamics of Griseofulvin and Its Derivatives Revealed Potential Therapeutic Applications for COVID-19. International journal of molecular sciences. 2022;23(13):6889.
13. Atlas SA. The renin-angiotensin aldosterone system: pathophysiological role and pharmacologic inhibition. Journal of managed care pharmacy. 2007;13(8 Supp B):9-20.
14. Brian P, Hemming H. Production of antifungal and antibacterial substances by fungi; preliminary examination of 166 strains of Fungi Imperfecti. Microbiology. 1947;1(2):158-67.
15. Grove JF, MacMillan J, Mulholland T, Rogers MT. 759. Griseofulvin. Part I. Journal of the Chemical Society (Resumed). 1952:3949-58.
16. Chooi Y-H, Cacho R, Tang Y. Identification of the viridicatumtoxin and griseofulvin gene clusters from Penicillium aethiopicum. Chemistry & biology. 2010;17(5):483-94.
17. Tang H-Y, Zhang Q, Li H, Gao J-M. Antimicrobial and allelopathic metabolites produced by Penicillium brasilianum. Natural product research. 2015;29(4):345-8.
18. Roullier C, Bertrand S, Blanchet E, Peigné M, Robiou du Pont T, Guitton Y, et al. Time dependency of chemodiversity and biosynthetic pathways: an LC-MS metabolomic study of marine-sourced penicillium. Marine drugs. 2016;14(5):103.
19. Jadulco R, Edrada RA, Ebel R, Berg A, Schaumann K, Wray V, et al. New Communesin Derivatives from the Fungus Penicillium sp. Derived from the Mediterranean Sponge Axinella v errucosa. Journal of natural products. 2004;67(1):78-81.
20. Petit K, Mondeguer F, Roquebert M, Biard J, Pouchus Y. Detection of griseofulvin in a marine strain of Penicillium waksmanii by ion trap mass spectrometry. Journal of microbiological methods. 2004;58(1):59-65.
21. Xue C, Li T, Deng Z, Fu H, Lin W. Janthinolide AB, two new 2, 5-piperazinedione derivatives from the endophytic Penicillium janthinellum isolated from the soft coral Dendronephthya sp. Die Pharmazie. 2006;61(12):1041-4.
22. Clarke S, McKenzie M. Penicillium sclerotigenum: a new source of Griseofulvin. Nature. 1967;213(5075):504-5.

23. Wang L, Zhou H-B, Frisvad JC, Samson RA. Penicillium persicinum, a new griseofulvin, chrysogine and roquefortine C producing species from Qinghai province, China. Antonie van leeuwenhoek. 2004;86(2):173-9.

24. Nielsen JC, Grijseels S, Prigent S, Ji B, Dainat J, Nielsen KF, et al. Global analysis of biosynthetic gene clusters reveals vast potential of secondary metabolite production in Penicillium species. Nature microbiology. 2017;2(6):1-9.

25. Frisvad JC, Samson RA. Polyphasic taxonomy of Penicillium subgenus Penicillium. A guide to identification of food and air-borne terverticillate Penicillia and their mycotoxins. Studies in mycology. 2004;49(1):1-174.

26. Larsen TO, Smedsgaard J, Nielsen KF, Hansen ME, Frisvad JC. Phenotypic taxonomy and metabolite profiling in microbial drug discovery. Natural product reports. 2005;22(6):672-95.

27. Samson RA, Pitt JI. Modern concepts in Penicillium and Aspergillus classification: Springer Science & Business Media; 2013.

28. Allawi MYA, Al-Taee WSQ. Investigation of A New Local Isolate of Penicillium Lanosocoeruleum That Produces The Antifungal Griseofulvin. Pakistan Journal of Medical & Health Sciences. 2022;16(04):380-.

29. PARK J-H, CHOI G-J, LEE S-W, LEE H-B, KIM K-M, JUNG H-S, et al. Griseofulvin from Xylaria sp. strain F0010, an endophytic fungus of Abies holophylla and its antifungal activity against plant pathogenic fungi. Journal of Microbiology and Biotechnology. 2005;15(1):112-7.

30. Petrini O. Fungal endophytes of tree leaves. Microbial ecology of leaves: Springer; 1991. p. 179-97.

31. Grove JF, MacMillan J, Mulholland T, Rogers MT. 762. Griseofulvin. Part IV. Structure. Journal of the Chemical Society (Resumed). 1952:3977-87.

32. Birch A, Massy-Westropp R, Rickards R, Smith H. 66. Studies in relation to biosynthesis. Part XIII. Griseofulvin. Journal of the Chemical Society (Resumed). 1958:360-5.

33. Birch A, Donovan F. Studies in relation to biosynthesis. I. Some possible routes to derivatives of orcinol and phloroglucinol. Australian Journal of Chemistry. 1953;6(4):360-8.

34. Simpson TJ, Holker JS. 13C-NMR studies on griseofulvin biosynthesis and acetate metabolism in Penicillium patulum. Phytochemistry. 1977;16(2):229-33.

35. Nirmala K, Sakegowda D, Duax WL. Crystal structure of griseofulvin. Journal of Crystallographic and Spectroscopic Research. 1982;12(5):415-23.

36. Brown W, Sim G. 193. Fungal metabolites. Part I. The stereochemistry of griseofulvin: X-ray analysis of 5-bromogriseofulvin. Journal of the Chemical Society (Resumed). 1963:1050-9.
37. Levine SG, Hicks RE. The conformation of griseofulvin. Application of an NMR shift reagent. Tetrahedron Letters. 1971;12(4):311-4.
38. Aris P, Yan L, Wei Y, Chang Y, Shi B, Xia X. Conservation of griseofulvin genes in the gsf gene cluster among fungal genomes. G3 Genes| Genomes| Genetics. 2021.
39. Cimermancic P, Medema MH, Claesen J, Kurita K, Brown LCW, Mavrommatis K, et al. Insights into secondary metabolism from a global analysis of prokaryotic biosynthetic gene clusters. Cell. 2014;158(2):412-21.
40. Slot JC, Rokas A. Horizontal transfer of a large and highly toxic secondary metabolic gene cluster between fungi. Current biology. 2011;21(2):134-9.
41. Dobrindt U, Hochhut B, Hentschel U, Hacker J. Genomic islands in pathogenic and environmental microorganisms. Nature Reviews Microbiology. 2004;2(5):414-24.
42. Keller NP, Turner G, Bennett JW. Fungal secondary metabolism—from biochemistry to genomics. Nature Reviews Microbiology. 2005;3(12):937-47.
43. Wisecaver JH, Slot JC, Rokas A. The evolution of fungal metabolic pathways. PLoS Genetics. 2014;10(12).
44. Cacho RA, Chooi Y-H, Zhou H, Tang Y. Complexity generation in fungal polyketide biosynthesis: a spirocycle-forming P450 in the concise pathway to the antifungal drug griseofulvin. ACS chemical biology. 2013;8(10):2322-30.
45. Banani H, Marcet-Houben M, Ballester A-R, Abbruscato P, González-Candelas L, Gabaldón T, et al. Genome sequencing and secondary metabolism of the postharvest pathogen Penicillium griseofulvum. BMC genomics. 2016;17(1):19.
46. Valente S, Cometto A, Piombo E, Meloni GR, Ballester A-R, González-Candelas L, et al. Elaborated regulation of griseofulvin biosynthesis in Penicillium griseofulvum and its role on conidiation and virulence. International Journal of Food Microbiology. 2020:108687.
47. Banani H, Marcet-Houben M, Ballester A-R, Abbruscato P, González-Candelas L, Gabaldón T, et al. Genome sequencing and secondary metabolism of the postharvest pathogen Penicillium griseofulvum. BMC genomics. 2016;17(1):1-14.

48. Valente S, Cometto A, Piombo E, Meloni GR, Ballester A-R, González-Candelas L, et al. Elaborated regulation of griseofulvin biosynthesis in Penicillium griseofulvum and its role on conidiation and virulence. International journal of food microbiology. 2020;328:108687.
49. Wright JM. The production of antibiotics in soil: ii. Production of griseofulvin by penicillium nigricans. Annals of Applied Biology. 1955;43(2):288-96.
50. Soloveva N, Malkov M. Kil® n, GI; Golubeva, LA: Role of nitrogen nutrition in the cultivation of Penicillium nigricans producing griseofulvin on a synthetic medium. Antibiot. 1972;9:104-6.
51. Rogal I, Malkov M. Effect of the cultivation temperature on the dynamics of the ATP and ADP levels and on the growth of P. nigricans Thom. Strains in the presence of various carbon sources. Antibiotiki. 1978;23(11):971.
52. Dasu VV, Panda T. Studies on production of griseofulvin. Bioprocess engineering. 1999;21(6):489-95.
53. Alan R, Rodger C, Primrose FT. Production of griseofulvin in low nitrogen level medium. Google Patents; 1958.
54. Niu G, Tan H. Biosynthesis and regulation of secondary metabolites in microorganisms. Springer; 2013.
55. Vining LC. Functions of secondary metabolites. Annual review of microbiology. 1990;44(1):395-427.
56. Hurst LD. Genetics and the understanding of selection. Nature Reviews Genetics. 2009;10(2):83-93.
57. Kimura M. The neutral theory of molecular evolution and the world view of the neutralists. Genome. 1989;31(1):24-31.
58. Gentles J. Experimental ringworm in guinea pigs: oral treatment with griseofulvin. Nature. 1958;182(4633):476-7.
59. Gupta AK, Adam P, Dlova N, Lynde CW, Hofstader S, Morar N, et al. Therapeutic options for the treatment of tinea capitis caused by Trichophyton species: griseofulvin versus the new oral antifungal agents, terbinafine, itraconazole, and fluconazole. Pediatric dermatology. 2001;18(5):433-8.
60. Sehgal V, Bikhchandani R, Koranne R, Nayar M, Saxena H. Histopathological evaluation of griseofulvin therapy in lichen planus. Dermatology. 1980;161(1):22-7.

61. Tamaki K, Yasaka N, Osada A, Shibagaki N, Furue M. Successful treatment of pigmented purpuric dermatosis with griseoiulvin. British Journal of Dermatology. 1995;132(1):159-60.
62. Cohen A, Goldman J, Daniels R, Kanenson W. Treatment of shoulder-hand syndrome with griseofulvin. Journal of the American Medical Association. 1960;173(5):542-3.
63. Serre H, Simon L. ACTION THERAPEUTIQUE INATTENDUE EN RHUMATOLOGIE DUN ANTIBIOTIQUE ANTIFONGIQUE-LA GRISEOFULVINE. PRESSE MEDICALE. 1962;70(48):2263-&.
64. Rathinasamy K, Jindal B, Asthana J, Singh P, Balaji PV, Panda D. Griseofulvin stabilizes microtubule dynamics, activates p53 and inhibits the proliferation of MCF-7 cells synergistically with vinblastine. BMC cancer. 2010;10(1):1-13.
65. Livingston WA. GRISEOFULVIN IN TREATMENT OF ZOSTER. Archives of Dermatology. 1965;92(6):761-.
66. CROUNSE RG. Effective use of griseofulvin. Archives of dermatology. 1963;87(2):176-8.
67. Ong SGM, Ming LC, Lee KS, Yuen KH. Influence of the encapsulation efficiency and size of liposome on the oral bioavailability of griseofulvin-loaded liposomes. Pharmaceutics. 2016;8(3):25.
68. Lin C, Symchowicz S. Absorption, distribution, metabolism, and excretion of griseofulvin in man and animals. Drug Metabolism Reviews. 1975;4(1):75-95.
69. BEDFORD C, BUSFIELD D, Child K, Mac Gregor I, SUTHERLAND P, Tomich E. Studies on the biological disposition of griseofulvin, an oral antifungal agent. AMA Archives of Dermatology. 1960;81(5):735-45.
70. Araujo OE, Flowers FP, King MM. Griseofulvin: a new look at an old drug. DICP. 1990;24(9):851-4.
71. Roth Jr FJ. Griseofulvin. Annals of the New York Academy of Sciences. 1960;89(1):247-53.
72. Develoux M, editor Griseofulvin. Annales de dermatologie et de venereologie; 2001.
73. Gull K, Trinci A. Griseofulvin inhibits fungal mitosis. Nature. 1973;244(5414):292-4.
74. Panda D, Rathinasamy K, Santra MK, Wilson L. Kinetic suppression of microtubule dynamic instability by griseofulvin: implications for its possible use in the treatment of cancer. Proceedings of the National Academy of Sciences. 2005;102(28):9878-83.

75. Uen YH, Liu DZ, Weng MS, Ho YS, Lin SY. NF-κB pathway is involved in griseofulvin-induced G2/M arrest and apoptosis in HL-60 cells. Journal of cellular biochemistry. 2007;101(5):1165-75.

76. Zomorodian K, Uthman U, Tarazooie B, Rezaie S. The effect of griseofulvin on the gene regulation of β-tubulin in the dermatophyte pathogen Trichophyton rubrum. Journal of Infection and Chemotherapy. 2007;13(6):373-9.

77. Asahina A, Tada Y, Nakamura K, Tamaki K. Colchicine and griseofulvin inhibit VCAM-1 expression on human vascular endothelial cells—evidence for the association of VCAM-1 expression with microtubules. Journal of dermatological science. 2001;25(1):1-9.

78. Chiprut RO, Viteri A, Jamroz C, Dyck WP. Intrahepatic cholestasis after griseofulvin administration. Gastroenterology. 1976;70(6):1141-3.

79. Watanabe M, Akagi S, Kohge N, Uchida Y, Nguyen T, Hirakawa K, et al. Laparoscopy of Griseofulvin-induced Liver Injury Presenting a Wide Depression. Endoscopy. 1994;26(05):514-5.

80. Zimmerman HJ. Hepatotoxicity: the adverse effects of drugs and other chemicals on the liver. 2nd ed ed: Philadelphia: Lippincott; 1999. 609-11 p.

81. Moseley RH. Hepatotoxicity of antimicrobials and antifungal agents. Drug-induced liver disease. 3rd ed: Amsterdam: Elsevier, ; 2013. p. 470-3.

82. Zatloukal K, French SW, Stumptner C, Strnad P, Harada M, Toivola DM, et al. From Mallory to Mallory–Denk bodies: what, how and why? Experimental cell research. 2007;313(10):2033-49.

83. Fortier A-M, Riopel K, Désaulniers M, Cadrin M. Novel insights into changes in biochemical properties of keratins 8 and 18 in griseofulvin-induced toxic liver injury. Experimental and molecular pathology. 2010;89(2):117-25.

84. Fortier A-M, Asselin E, Cadrin M. Keratin 8 and 18 loss in epithelial cancer cells increases collective cell migration and cisplatin sensitivity through claudin1 up-regulation. Journal of Biological Chemistry. 2013;288(16):11555-71.

85. Golob-Schwarzl N, Bettermann K, Mehta AK, Kessler SM, Unterluggauer J, Krassnig S, et al. High keratin 8/18 ratio predicts aggressive hepatocellular cancer phenotype. Translational oncology. 2019;12(2):256-68.

86. French SW, Bardag-Gorce F, Li J, French BA, Oliva J. Mallory-Denk body pathogenesis revisited. World journal of hepatology. 2010;2(8):295.

87. Redeker AG, Sterling RE, Bronow RS. Effect of griseofulvin in acute intermittent porphyria. JAMA. 1964;188(5):466-8.

88. Berman A, Franklin RL. Precipitation of acute intermittent porphyria by griseofulvin therapy. Jama. 1965;192(11):1005-7.

89. Maitra D, Cunha JB, Elenbaas JS, Bonkovsky HL, Shavit JA, Omary MB. Porphyrin-induced protein oxidation and aggregation as a mechanism of porphyria-associated cell injury. Cellular and Molecular Gastroenterology and Hepatology. 2019;8(4):535-48.

90. Knasmüller S, Parzefall W, Helma C, Kassie F, Ecker S, Schulte-Hermann R. Toxic effects of griseofulvin: disease models, mechanisms, and risk assessment. Critical reviews in toxicology. 1997;27(5):495-537.

91. Zhang X, Qian S-B. Chaperone-mediated hierarchical control in targeting misfolded proteins to aggresomes. Molecular Biology of the Cell. 2011;22(18):3277-88.

92. Morris GM, Huey R, Lindstrom W, Sanner MF, Belew RK, Goodsell DS, et al. AutoDock4 and AutoDockTools4: Automated docking with selective receptor flexibility. Journal of computational chemistry. 2009;30(16):2785-91.

93. Rosenbaum MB, Chiale PA, Halpern MS, Nau GJ, Przybylski J, Levi RJ, et al. Clinical efficacy of amiodarone as an antiarrhythmic agent. The American Journal of Cardiology. 1976;38(7):934-44.

94. Poucell S, Ireton J, Valencia-Mayoral P, Downar E, Larratt L, Patterson J, et al. Amiodarone-associated phospholipidosis and fibrosis of the liver. Light, immunohistochemical, and electron microscopic studies. Gastroenterology. 1984;86(5 Pt 1):926-36.

95. Mason JW. Amiodarone. New England Journal of Medicine. 1987;316(8):455-66.

96. March-Vila E, Pinzi L, Sturm N, Tinivella A, Engkvist O, Chen H, et al. On the integration of in silico drug design methods for drug repurposing. Frontiers in pharmacology. 2017:298.

97. Ashburn TT, Thor KB. Drug repositioning: identifying and developing new uses for existing drugs. Nature reviews Drug discovery. 2004;3(8):673-83.

CHAPTER TWO

Conservation of griseofulvin genes in the *gsf* gene cluster among fungal genomes

This chapter is published.

Aris P, Yan L, Wei Y, Chang Y, Shi B, Xia X. Conservation of griseofulvin genes in the gsf gene cluster among fungal genomes. G3. 2022;12(2):jkab399.

2.1. Author Contributions

Parisa Aris[1,+], Lihong Yan[2,3,+],Yulong Wei[1], Ying Chang[2,3], Bihong Shi[2,3,*], Xuhua Xia[1,4,*]

1. Department of Biology, University of Ottawa, 30 Marie Curie, P.O. Box 450, Station A, Ottawa, Ontario, Canada, K1N 6N5. Tel: (613) 562-5800 ext. 6886, Fax: (613) 562-5486.

2. National Joint Engineering Research Center of Industrial Microbiology and Fermentation Technology, College of Life Sciences, Fujian Normal University, Fuzhou, 350117, China.

3. Department of Bioengineering, College of Life Sciences, Fujian Normal University, Fuzhou, China

4. Ottawa Institute of Systems Biology, Ottawa, Ontario, Canada K1H 8M5.

P. A., Y.W., B.S. and X.X. designed the study and wrote the manuscript. B.S. conceived the genome project of *P. griseofulvum* D-756. L.Y., Y.C. performed the experiments. P.A. collected the data and prepared all figures. P.A., L.Y. analyzed the data. X.X. and B.S. supervised and coordinated the study. All authors reviewed the manuscript.

2.2. Abstract

The polyketide griseofulvin is a natural antifungal compound and research in griseofulvin has been key in establishing our current understanding of polyketide biosynthesis. Nevertheless, the griseofulvin *gsf* biosynthetic gene cluster (BGC) remains poorly understood in most fungal species, including *Penicillium griseofulvum* where griseofulvin was first isolated. To elucidate essential genes involved in griseofulvin biosynthesis, we performed third-generation sequencing to obtain the genome of *Penicillium griseofulvum* strain D-756. Furthermore, we gathered publicly available genome of 11 other fungal species in which *gsf* gene cluster was identified. In a comparative genome analysis, we annotated and compared the *gsf* BGC of all 12 fungal genomes. Our findings show no gene rearrangements at the *gsf* BGC. Furthermore, seven *gsf* genes are conserved by most genomes surveyed whereas the remaining six were poorly

conserved. This study provides new insights into differences between *gsf* BGC and suggests that seven *gsf* genes are essential in griseofulvin production.

2.3. Introduction

` Griseofulvin ($C_{17}H_{17}Cl_1O_6$) is a natural spirocyclic polyketide compound that is produced by ascomycetes. This fungistatic was first isolated from *Penicillium griseofulvum* Dierckx (syn. *Penicillium patulum* Bain.; *Penicillium urticae* Bain.) and had since been detected in many other species of the *Penicillium* genus such as *Penicillium aethiopicum* (1). Griseofulvin synthesis increases with cellular ATP/ADP ratio (2, 3), and one may hypothesize that the benefit of griseofulvin production is to eliminate other fungal species to reduce competition. Nevertheless, given the cost of time and energy, one expects that only species that experience such competition would maintain the griseofulvin gene cluster in their genomes. Indeed, fungal endophytes such as *Xylaria flabelliformis* are commonly found within plant tissue and produces griseofulvin as an antifungal against plant pathogenic fungi (Whalley, 1996, Park et al., 2005). Furthermore, species in Genus *Penicillium* produce many other secondary metabolites in response to environmental changes, and some exometabolites are only expressed under unique circumstances (4).

Mechanistically, griseofulvin interacts with the mitotic spindle microtubule to inhibits cell division and induces cell death in cancer cell lines (5). Due to its low toxicity (6), Griseofulvin has been widely used in many applications. In agriculture, griseofulvin acts as a crop protectant to prevent against fungus infections (7). Notable medical applications of griseofulvin include treatment of ringworm infection in guinea pigs (8) and treatment of dermatophyte infections in both humans and animals (9, 10). Today, griseofulvin is largely

replaced by new antifungal drugs, but the compound retained a niche in treating ringworm infection and athlete's foot (1). Additionally, in recent years, the compound has garnered renewed interest because of its potential therapeutic effects to treat cancer (5) and suppressive activities against the replication of hepatitis C virus (11).

Griseofulvin is synthesized by non-reducing polyketide synthases (NR-PKSs). To optimize the bioengineering of this natural compound for use in veterinary and medical applications, there have been continuous efforts to determine the *gsf* synthase genes and the griseofulvin synthetic pathway. While early degradation (12) and isotope labelling (13, 14) experiments have determined that the biosynthetic process of griseofulvin involves several synthases to convert Acetyl-CoA and Malonyl-CoA (12, 13, 15) into a grisan scaffold (16), it was not until 2010 that the *gsf* biosynthetic gene cluster (BGC) that is responsible for griseofulvin biosynthesis was fully discovered.

Through shotgun sequencing and Bioinformatics mining for PKS genes, *gsfA – gsfK*, *gsfR1* and *gsfR2* were identified in the *gsf* BGC in *P. aethiopicum* (1). The involvement of these *gsf* genes in griseofulvin biosynthesis was later determined through single-gene deletion and biochemical assay experiments (17). To summarize the findings of (17), *gsfA* initiates the biosynthesis of griseofulvin; it is a nonreducing polyketide synthase that combines one Acetyl-CoA and six Malonyl-CoA units to generate the heptaketide backbone benzophenone 5a. Next, the O-methyltransferases (*gsfB* and *gsfC*) methylate phenols on Benzophenone 5a to generate the intermediate griseophenone C. Following this process, griseophenone C is chlorinated and converted into griseophenone B by the halogenase *gsfI*, and griseophenone B is then converted into the grisan core by the phenol oxidative activity of *gsf F*. Finally, the grisan core is converted

into the final griseofulvin through two additional steps: methylation at 5-OH catalyzed by *gsf D* and enoylredcution by dehydrogenase *gsfE*.

While some *gsf* genes are important in griseofulvin biosynthesis, others may not be essential. For instance, both *gsfA* and *gsfI* play crucial roles in the *gsf* biosynthetic pathway, and their deletions disrupt griseofulvin synthesis (1, 17, 18). In contrast, deletion of *gsfK* did not affect biosynthesis in *P. aethiopicum* (17). A simple comparison between two griseofulvin-producing species, *P. aethiopicum* (GenBank accession ID GU574478.1) and *P. griseofulvum* PG3 (GenBank accession ID LHQR00000000.1), shows that *P. griseofulvum* lacks *gsfK*, *gsfH*, and *gsfR2* in the *gsf* biosynthetic gene cluster (Banani et al., 2016). Nonetheless, while experimental studies have detected griseofulvin production in many *Penicillium* species (1, 19-32) and in species such as *Xylaria flabelliformis*, *Abieticola koreana*, and *Stachybotrys levispora* (19, 26, 27), the biosynthetic details of the *gsf* BGC are scarce for most species.

We sequenced the genome of a biochemically unique *P. griseofulvum* strain D-756. It is a mutant strain with a high yield of griseofulvin originally isolated from a wild strain *P. patulum* 4541 (*patulum* is synonym of *griseofuvum*) and subject to multiple generations of mutagenesis (Wu et al. 1980). Strain D-756 features high tolerance of Cl^- which is an ingredient in griseofulvin synthesis. In particular, it can use starch as a carbon source instead of lactose in the original strain. We compared the *gsf* BGC between *P. griseofulvum* strain D-756 and 11 other fungal species that are mostly known to produce griseofulvin. We found that 7 out of 13 identified *gsf* genes are well conserved among 12 fungal species. Optimizing griseofulvin synthesis requires the identification of a set of essential *gsf* genes that are highly conserved in griseofulvin-producing fungi. However, there would be less evolutionary advantage to maintain

non-essential *gsf* genes, and we expect these *gsf* genes to accumulate high sequence variability or are lost entirely at the *gsf* BGC of many fungal genomes.

2.4. Materials and Methods

2.4.1. Strain

Penicillium griseofulvum Dierckx (syn.: *P. patulum* Bainier.; *P. urticae* Bainier) D-756 was a mutant strain with high yield of griseofulvin, which was obtained from the wild strain *P. patulum* 4541 after 13 rounds of artificial mutagenesis (WU et al., 1980). The *P. griseofulvum* D-756 and its parental strain *P. griseofulvum* 4541 (syn.: *P. patulum* Bainier) were identified based on morphology and DNA sequencing of ITS and 18S rRNA (Lu J.J et al., 2019).

2.4.2. Third generation sequencing on *Penicillium griseofulvum* strain D-756

The genome of *P. griseofulvum* strain D-756 was sequenced using the 3rd generation sequencing approach. First, genomic DNA from *Penicillium griseofulvum* D-756 was prepared as described previously by Möller EM et al (33). Briefly, spore suspensions of *P. griseofulvum* D-756 (1.0×10^{7}con/mL) were inoculated on a 25mL solid Czapek-Dox Medium (CDM) plate and incubated at 28℃ for 4 days. Fungal hyphae were collected and quickly grinding in a mortar with liquid nitrogen. DNA was extracted from 0.5g frozen mycelia. DNA concentration and purity were analyzed by ultrafine spectrophotometer (DeNovix DS-11), and the DNA integrity was checked by agarose gel electrophoresis. The genome of strain D-756 was sequenced by Single Molecule Real-Time (SMRT) technology. Sequencing was performed at the Beijing Novogene Bioinformatics Technology Co., Ltd. Low-quality reads were filtered by the SMRT Link v5.0.1, and the filtered reads were assembled to generate contigs without gaps.

2.4.3. Retrieving fungal genomes and their griseofulvin genes

We retrieved known Gsf protein sequences in the reference species *P. aethiopicum* (GenBank accession ID GU574478) as queries in BLASTP. The BLASTP searches were performed using the National Center for Biotechnology Information (NCBI) Nucleotide BLAST program (www.ncbi.nlm.nih.gov/nucleotide) with default options to identify fungal species that may harbor genes involved in griseofulvin synthesis. The top hundred hits for each Gsf proteins (GsfA-GsfR2) were represented in Supplementary file 1. The search results revealed 22 species that each contains at least three homologs with more than 50% BLASTP similarities to reference Gsf proteins in *Penicillium aethiopicum* (supplementary file 1, Table S1). Moreover, some species were previously reported to produce griseofulvin with experimental evidence (supplemental file 2 Data S1, for reports of fungi with griseofulvin production). The genome of these species were retrieved from the NCBI genome database (https://www.ncbi.nlm.nih.gov/genome). We also included more than 200 species from different genus selected from phylum Ascomycetes. In total, the genomes of 266 fungal species were retrieved from the NCBI database for further analysis (Supplementary file 1, Table S2).

Among retrieved genomes were that of two *Penicillium griseofulvum*, strain PG3 and strain MRI314, under the Genome assembly accession GCA_001561935.1 and GCA_001735785.1, respectively. They were sequenced with Illumina MiSeq with an assembly level of sequence contig. While the International Sequence Database Collaboration (INSDC) submitter provided annotation for strain PG3, there is no annotation information for strain MRI314. To better annotate the *gsf* BGC in *P. griseofulvum*, we performed third-generation sequencing on *P. griseofulvum* strain D-756 (see above section) to identify and annotate its *gsf* BGC.

2.4.4. Annotating and comparing the *gsf* BGC between fungal species

The fungal genomes were analyzed using Antibiotic Secondary Metabolite Analysis Shell (antiSMASH), a genome mining tool that integrates NCBI BLAST+, HMMer 3, Muscle 3, and FastTree to predict, identify, and perform secondary analysis of BGCs (34). The 266 genomes (Supplementary file 1, Table S2), including the annotated genome of *P. griseofulvum* strain D-756 using funannotate (v1.5.1) (Love et al., 2018), were processed via antiSMASH v6.0 using the ClusterFinder algorithm with default settings to predict gene cluster borders and to annotate predicted griseofulvin gene cluster. The Minimum Information about a Biosynthetic Gene cluster (MIBiG) repository provides reference gene clusters as a framework for the classification of BGCs (35), and MIBiG accession BGC0000070 (the griseofulvin biosynthetic gene cluster from *P. aethiopicum*) was used as a reference cluster in this study to find the griseofulvin gene cluster in fungal genomes. Nucleotide sequences of interest identified by antiSMASH were used to perform BLASTN against *P. aethiopicum* IBT 5753 (GenBank accession ID GU574478) as query to test consistency of predicted *gsf* genes.

The antiSMASH outputs were analyzed using Biosynthetic Gene Similarity Clustering And Prospecting Engine (BiG-SCAPE), a software package that explores the diversity of biosynthetic gene clusters across genomes (36). Briefly, BiG-SCAPE determines the functional protein domains of the biosynthetic griseofulvin gene cluster for all species from the Pfam database (https://pfam.xfam.org/). Then, every predicted protein domain was aligned using hmmalign, which is a part of the HMMer package that used profile hidden Markov models (HMMs) for biological sequence analysis. In addition, the pairwise distance between gene clusters was calculated using a combination of three indices, including Jaccard Index (JI), the Adjacency Index (AI), and the Domain Sequence Similarity (DSS). The sequence similarity

networks of Biosynthetic Gene Clusters (BGCs), directly from antiSMASH results and MIBiG reference gene clusters, were constructed based on a comparison of their protein domain content, order, copy number and sequence identity (Navarro-muñoz et al., 2018). Following BiG-SCAPE, CORASON provided the phylogenetic relationships of these griseofulvin BGCs using FastTree (default options) with the Jukes-Cantor + CAT model for a nucleotide alignment.

Pfam protein families (http://pfam.xfam.org) and the NCBI conserved domain database (CDD) (https://www.ncbi.nlm.nih.gov/cdd/) were used for interactive domain family analysis of *gsf* BGC in fungal species.

2.4.5. Phylogenetic reconstruction

Gsf protein sequences from antiSMASH results were first aligned using MAFFT with the slow but accurate G-INS-i option (37) and aligned genes were concatenated in order. The phylogenetic tree was then constructed using PhyML (38) with the GTR model which is the best-fitting model for the dataset based on likelihood ratio tests and information-theoretic indices such as AIC and BIC (39). Moreover, FastME with the LG (Le and Gascuel 2008) substitution model was used for phylogenetic inference based on distance methods in order to confirm the analysis. *M. echinata* was selected as the outgroup, and bootstrapping tests were performed with 500 repetitions.

The ITSx program (https://microbiology.se/software/itsx/), a Perl-based software tool that implements hidden Markov models, was used to predict ITS region in *P. griseofulvum* D-756 based on predicted positions of the ribosomal genes (40). The ITS sequences of other species were retrieved from NCBI Fungal ITS RefSeq Targeted Loci Project (accession PRJNA177353). These sequences were then aligned using MAFFT with G-INS-i option, and phylogenetic trees

were constructed in DAMBE (41) using PHYML, with GTR as the best model based on AIC, bootstrap = 500, and outgroup species = *X. flabelliformis*.

2.5. Results and Discussion

The biosynthesis pathway of griseofulvin has been previously elucidated in *P. aethiopicum* strain IBT 5753 (1). A total of 13 genes were identified in the *gsf* BGC, including nonreducing polyketide synthase (NR-PKS), tailoring enzymes, dehydrogenase/reductase, cytochrome P450, halogenase, ketoreductase, and transcription factors (1). In the present study, griseofulvin BGCs were predicted in 11 other fungal species: *Penicillium capsulatum*, *Penicillium coprophilum*, *Penicillium vulpinum*, three *Penicillium griseofulvum*, two *Aspergillus alliaceus*, *Aspergillus burnettii*, *Xylaria flabelliformis*, and *Memnoniella echinata*, which showed homology to MIBiG accession BGC0000070, the reference griseofulvin biosynthetic gene cluster from *P. aethiopicum* (supplementary file 2, Data S2). Of note are *M. echinata* and *X. flabelliformis*, two species that were previous reported to synthesize griseofulvin, yet the genes involved in the biosynthetic pathway were unknown (19, 42).

The antiSMASH result of *P. griseofulvum* D-756 showed the *gsf* gene cluster is located at the genomic positions 1364595 to 1389034 contig 4 (supplementary file 3, Table S10). The BGC of *P. griseofulvum* D-756 contains the same *gsf* genes with more than 99% homology and organized in the same order as those in the BGC of *P. griseofulvum* strain PG3 (supplementary file 2, Data S3). Expectedly, the *gsf* genes are conserved between these two strains except *gsfG*. Additionally, the griseofulvin BGC was annotated in the other 9 species (supplementary file 3, Table S1-S11) belong to the Aspergillaceaea family of the order Eurotiales, also known as the green and blue molds, and 2 species, *M. echinata* and *X. flabelliformis*, belonging to the

Hypocreales order and Xylariales order, respectively (supplementary file 1, Table S2). Species belonging to the Aspergillaceaea family exhibit diverse ecology. For example, genus *Penicillium* have been frequently isolated from different environmental sources such as air, freshwaters, terrestrial, food product, and soil (43), potentially due to their low nutritional requirements and large enzymatic apparatus for primary metabolism (44). Among these species, *Aspergillus alliaceus* has effective biological control of the root parasitic weed (45). *X. flabelliformis* is another griseofulvin producing species which is commonly found within plant tissue (46). These species are usually produce griseofulvin to control other fungi and it allows them to decompose of cellulose in the senescent plant (47). This indicates griseofulvin can be produced by a variety of fungi and not limited to *Penicillium* species. However, our results indicate that the *gsf* BGC is only conserved among some species in the Eurotiomycetes class and the Sordariomycetes class (Supplementary file 1, Table S2). In addition to the presence of *gsf* BGC in the genome, several external factors are also involved in producing griseofulvin including organic materials, such as source of carbon, levels of ATP and nitrogen (48, 49). For example, using glucose or acetate as the source of carbon may generate the high level of ATP which leads to produce more griseofulvin (3, 50). Another important factor is pH; griseofulvin yield increases at pH ranging from 5.5 to 6 (50).

A maximum-likelihood phylogenetic analysis showed the global relationships among whole *gsf* BGCs of 12 surveyed fungal species. Figure 1 shows the three *P. griseofulvum* species clustered together in a clade very distant from *X. flabelliformis* and distinct from other members of the *A. alliaceus* group. Seven out of 12 species including *P. aethiopicum, X. flabelliformis, M. echinata, P. griseofulvum* strain PG3 and D-756, *P. vulpinum*, *P. coprophilum* are known to produce griseofulvin with experimental validations (Chooi et al., 2010, Jarvis et al., 1996,

Samson and Pitt, 1990, Mead et al., 2019, Banani et al., 2016, Nielsen et al., 2017), whereas the remaining 5 were poorly studied. Another phylogenetic tree was generated by the FastME method in order to confirm the analysis (supplementary file 2, Fig. S2). In addition, a reference phylogenetic tree was constructed using the ITS region for 48 species whose ITS sequences were available in NCBI or detected using the ITSx tool (supplementary file 2, Fig. S3).

A nucleotide sequence comparison using BLAST (supplementary file 3) at identified *gsf* genes, with reference being *P. aethiopicum*, revealed that many *gsf* genes are highly conserved (similarity >70%). These include nonreducing polyketide synthase (*gsfA*), tailoring enzymes (*gsfB-D*), dehydrogenase (*gsfE*), cytochrome P450 (*gsfF*), and halogenase (*gsfI*). However, the ankyrin repeats mediate protein-protein interactions (*gsfG*), drug resistance transporter (*gsfJ*), and transcription factor (*gsfR1*) are not well-conserved.

Moreover, we observed that amidohydrolases (*gsfH*), short chain dehydrogenase (*gsfK*), and Zn2Cys6 binuclear cluster domain (*gsfR2*) in *P. aethiopicum* were not located within *gsf* gene cluster in all other fungal genomes. However, the three *gsf* genes including *gsfH*, *gsfK* and *gsfR2* can be found by BLASTN in another region in the genome of *P. griseofulvum* strain D-756 (supplementary file 4, Table S1). This finding is similar to that previously reported in the genome of *P. griseofulvum* strain PG3, in which a homolog of *gsfR2* was identified outside of the *gsf* gene cluster (18). Hence, although these genes are not located within the *gsf* cluster, they may still be involved in griseofulvin production.

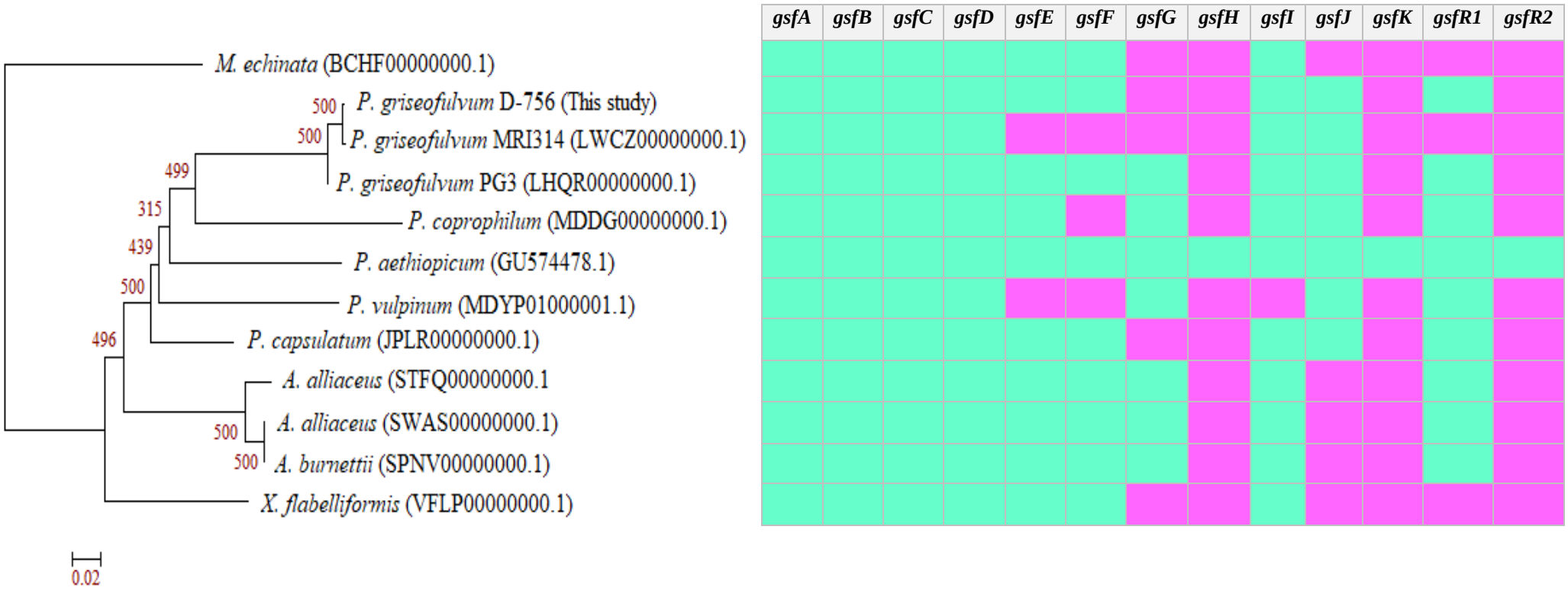

Figure 2.1. Phylogenetic reconstruction at the Gsf protein sequences in BGC of 12 species. The tree was built with the maximum likelihood-based PhyML approach, using aligned and concatenated Gsf protein sequences in BGC, with *M. echinata* as outgroup. Supporting bootstrap values are based on 500 replicates. The heat map on the right indicates the presence (blue) or absence (pink) of *gsf* genes identified in fungal genomes, against the *gsf* BGC of *P. aethiopicum* as reference, with rows representing species and columns representing *gsf* genes.

In brief, the above results revealed that seven strains harbor genes that encode the highly homologous proteins to Gsf BGC in the reference species *P. aethiopicum*. They are *P. griseofulvum* strain PG3 having ten *gsf* genes, followed by *P. griseofulvum* strain D-756, *P. capsulatum*, *P. coprophilum*, *A. burnettii*, and *A. alliaceus* (strain CBS 536.65 and strain IBT 14317) each having nine *gsf* genes. However, the BLASTN analysis against *P. aethiopicum* as query revealed greater number of griseofulvin genes in five fungal genomes, including *P. griseofulvum* strain D-756, *P. griseofulvum* strain MRI314, *P. vulpinum*, *P.coprophilum*, and *P. capsulatum*, compared to antiSMASH (supplementary file 4, Table S1-S5). For example, although BLASTN hits show a homolog of *gsfG* located in the contig 4 of *P. griseofulvum* D-756 genome, that was not identified by antiSMASH prediction. However, this may be a false positive as the annotation shows this hit belongs to an uncharacterized protein. The Known Cluster Blast comparisons made by antiSMASH only show hits for genes with a percentage identity greater than 45% and minimum coverage of 40% (51). Anything below the cut-off points is not considered significant for the comparison. For some of the BLASTN results, some genes appear to be missing entirely in the annotated file, e.g. *gsfG* in *P. capsulatum* genome. In the current study, only the *gsf* genes identified by both antiSMASH and BLASTN were considered for further analysis.

Only seven *gsf* genes (*gsfA*-*gsfF*, *gsfI*) out of the 13 in *P. aethiopicum* of which were presented in more than 70% of species were conserved by other fungi, including close relative *Penicillium* species. This suggests that these seven *gsf* genes could be essential for griseofulvin production. That not all *gsf* genes may be essential is corroborated by a recent study (52) showing that the *gsfR2* does not play a role in griseofulvin biosynthetic cluster and deletion of

gsfR1, a negative regulator, led to an increase in griseofulvin production under specific conditions.

Locally, there are differences at *gsf* genes among fungal species, and our analysis at the *gsf* BGC revealed variable degrees of gene conservation that have not been reported previously (Fig. 2). In the Pfam profiles (supplementary file 2, Data S4 and S5) and nucleotide sequences of *gsf* genes, we found differences in *gsf* genes that may lead to either loss of function (LOF) or gain of function (GOF). For example, BiG-SCAPE reveals that the GsfD (ADI24956.1) functional domains PF08100 (dimerization) and PF00891 (O-methyltransferase) do not exist in the *gsf* BGCs of either *A. alliaceus* stain IBT 14317 or strain CBS 536.65 (Figure 2). Additionally, at GsfA (ADI24953.1), we found that all species shared three typical domains (PKS, PT, and ACP). However, while Pfam profile analysis revealed that *P. griseofulvum* strain D-756 and strain PG3 contain the GsfA domain PF00550 (phosphopantetheine attachment site (PP-binding)), *P. griseofulvum* strain MRI314 does not harbor this domain (supplementary file 2, Data S4 and S5). Additionally, GsfA (ADI24953.1) in *P. capsulatum* has an extra PS-DH domain (PF14765, a polyketide synthase dehydratase) which catalyze dehydrations in the biosynthesis of some polyketides such as the antibiotic rifamycin and erythromycin (53, 54). Furthermore, at GsfI (ADI24948.1) and GsfD (ADI24956.1), although *P. capsulatum* harbors both *gsf* genes, the functional domains of GsfI (PF04820, a halogenase) and GsfD (PF08100, a dimerisation domain) have been lost from the genes (supplementary file 2, Data S4). Further Gsf domain analysis was performed using NCBI CDD (supplementary file 5, Table S1-12). CDD analysis revealed a 5beta-POR_like_SDR_domain (cd08948) in GsfE (ADI24957.1) among all surveyed species that encode homolog of GsfE. In addition, fungal_TF_MHR domain _which plays a regulatory role (55)_ identified in GsfR1 (ADI24950.1) among four *Penicillium* species

including *P. griseofulvin* PG3, *P. capsulatum, P. coprophilum, P. aethiopicum*. However, it seems that this domain has been lost entirely from the genome of other species including *A. alliaceus, A. burnettii, X. flabelliformis,* and *M. echinata*. All of these are potential LOF or GOF events that potentially alter gene activity (56). Future Bioinformatics analyses and experimental research are required to examine and validate these potential LOF and GOF events.

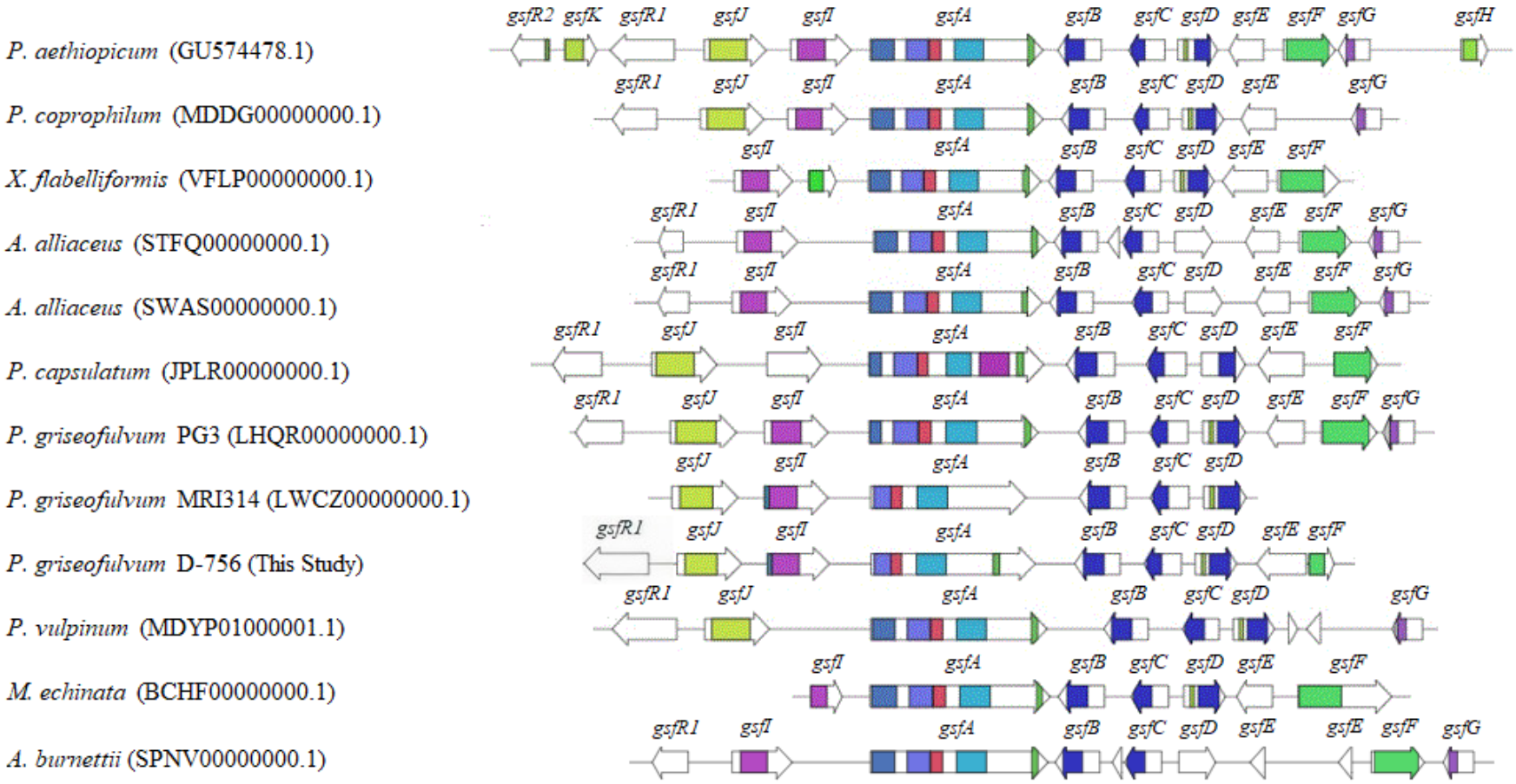

Figure 2. 2. Organization of putative gene clusters involved in griseofulvin biosynthesis in surveyed fungal species. Arrows show the strand directionality of genes. The color codes within the genes denote the functional domains (for more information on Pfam domains, see the supplementary file 2, Data S4 and S5).

Finally, as a comparison of results between CORASON and BiG-SCAPE, figure 3 shows that colored regions red and blue (representing the domain containing genes *gsfA* and *gsfB*), region yellow and brown (representing the domain containing genes *gsfC* and *gsfD*) are well conserved by all fungi species. This CORASON result is consistent with BiG-SCAPE results shown in figure 2. For instance, genes *gsfE* and *gsfI* located at colored region green and purple are conserved in at least 10 out of 12 species, and figure 3 shows that the core domain consisting of these *gsf* genes are indeed shared by more than 80% of species surveyed. In addition, the phylogenetic analysis of griseofulvin gene clusters in figure 1, using sequences aligned by MAFFT and constructed based on the PhyML approach, is consistent with figure 3, which was constructed using FastTree in CORASON. This finding shows an agreement between these two methods.

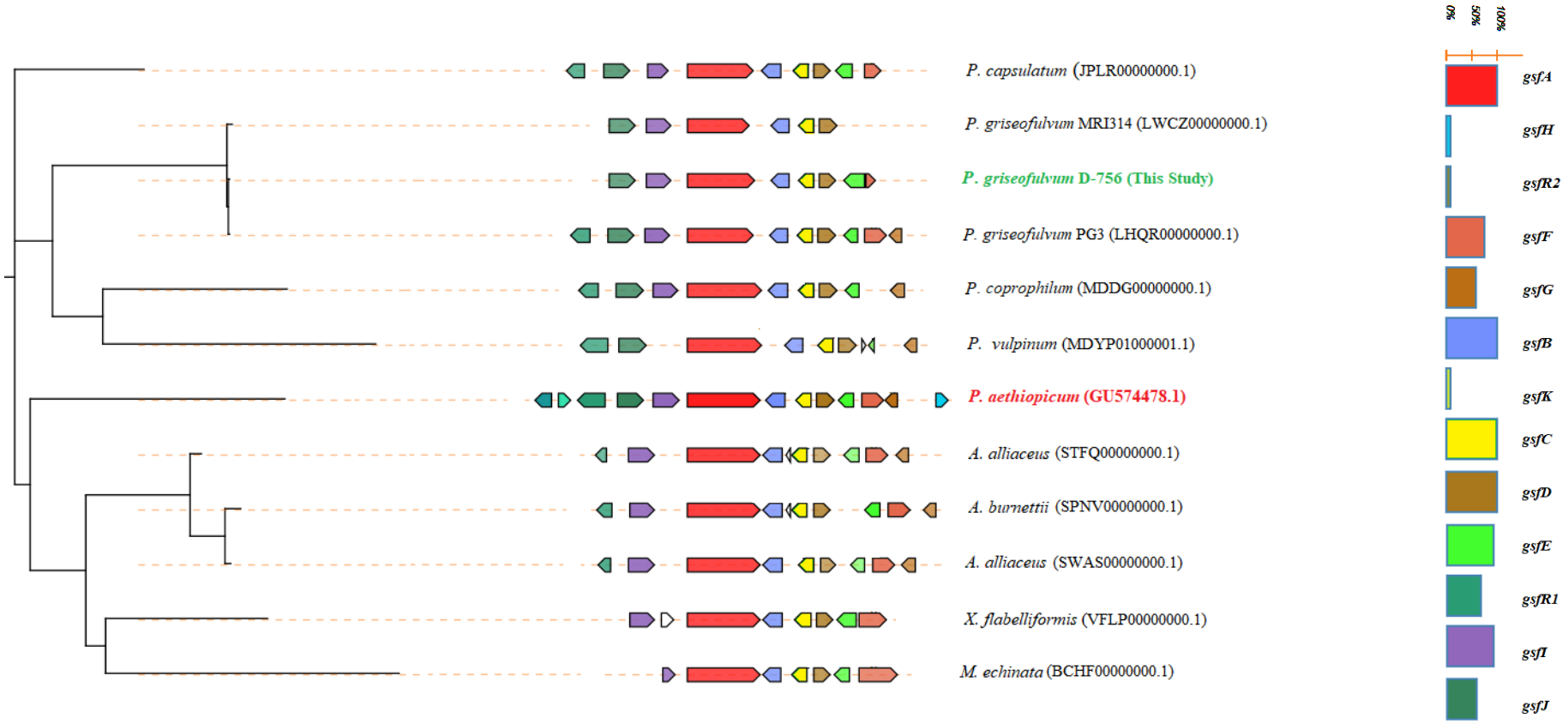

Figure 2. 3. Phylogenetic tree of griseofulvin BGCs generated by CORASON with sequence similarities relative to the griseofulvin BGC in MIBiG (BGC000070), which is highlighted in red (*P. aethiopicum*). Highlighted in bold green (*P. griseofulvum* strain D-756) is sequenced in this study. The histogram on the right shows the name and color code for *gsf* genes and the level the gene is conserved (in percentage) by the 12 species.

2.6. Data Availability

This Whole Genome Shotgun project has been deposited at DDBJ/ENA/GenBank under the accession JAHTKM000000000, BioSample SAMN20034676. The version described in this paper is version JAHTKM010000000. In addition, the whole genome sequence data (the genome assembly and annotation of *P. griseofulvum* D-756) have been deposited in Genome Warehouse in National Genomics Data Center, Beijing Institute of Genomics, Chinese Academy of Sciences /China National Center for Bioinformation, under accession number GWHBEUO00000000, belonging to the BioProject of PRJCA006461 that is publicly accessible at https://ngdc.cncb.ac.cn/gwh.

2.7. Acknowledgments

The authors would like to thank the joint Editor and referees for their helpful comments that greatly improved the presentation of the paper.

2.8. References

1. Chooi Y-H, Cacho R, Tang Y. Identification of the viridicatumtoxin and griseofulvin gene clusters from Penicillium aethiopicum. Chemistry & biology. 2010;17(5):483-94.

2. Rogal I, Malkov M. Effect of the cultivation temperature on the dynamics of the ATP and ADP levels and on the growth of P. nigricans Thom. Strains in the presence of various carbon sources. Antibiotiki. 1978;23(11):971.

3. Dasu VV, Panda T. Studies on production of griseofulvin. Bioprocess engineering. 1999;21(6):489-95.

4. Frisvad JC. Taxonomy, chemodiversity, and chemoconsistency of Aspergillus, Penicillium, and Talaromyces species. Frontiers in Microbiology. 2015;5:773.

5. Rebacz B, Larsen TO, Clausen MH, Rønnest MH, Löffler H, Ho AD, et al. Identification of griseofulvin as an inhibitor of centrosomal clustering in a phenotype-based screen. Cancer research. 2007;67(13):6342-50.

6. Hamdy AK, Sheha MM, Abdel-Hafez AA, Shouman SA. Design, synthesis, and cytotoxicity evaluation of novel griseofulvin analogues with improved water solubility. International journal of medicinal chemistry. 2017;2017.

7. Dayan FE, Cantrell CL, Duke SO. Natural products in crop protection. Bioorganic & medicinal chemistry. 2009;17(12):4022-34.

8. Gentles J. Experimental ringworm in guinea pigs: oral treatment with griseofulvin. Nature. 1958;182(4633):476-7.

9. Oxford AE, Raistrick H, Simonart P. Studies in the biochemistry of micro-organisms: griseofulvin, C17H17O6Cl, a metabolic product of Penicillium griseo-fulvum Dierckx. Biochemical Journal. 1939;33(2):240-8.

10. Lambert DR, Siegle RJ, Camisa C. Griseofulvin and ketoconazole in the treatment of dermatophyte infections. International journal of dermatology. 1989;28(5):300-4.

11. Jin H, Yamashita A, Maekawa S, Yang P, He L, Takayanagi S, et al. Griseofulvin, an oral antifungal agent, suppresses hepatitis C virus replication in vitro. Hepatology Research. 2008;38(9):909-18.

12. Birch A, Massy-Westropp R, Rickards R, Smith H. 66. Studies in relation to biosynthesis. Part XIII. Griseofulvin. Journal of the Chemical Society (Resumed). 1958:360-5.

13. Simpson TJ, Holker JS. 13C-NMR studies on griseofulvin biosynthesis and acetate metabolism in Penicillium patulum. Phytochemistry. 1977;16(2):229-33.

14. Harris CM, Roberson JS, Harris TM. Biosynthesis of griseofulvin. Journal of the American Chemical Society. 1976;98(17):5380-6.

15. Birch A, Donovan F. Studies in relation to biosynthesis. I. Some possible routes to derivatives of orcinol and phloroglucinol. Australian Journal of Chemistry. 1953;6(4):360-8.

16. Kaufman TS, Sindelar RD. A short and efficient synthesis of grisan. Journal of heterocyclic chemistry. 1989;26(3):879-81.

17. Cacho RA, Chooi Y-H, Zhou H, Tang Y. Complexity generation in fungal polyketide biosynthesis: a spirocycle-forming P450 in the concise pathway to the antifungal drug griseofulvin. ACS chemical biology. 2013;8(10):2322-30.

18. Banani H, Marcet-Houben M, Ballester A-R, Abbruscato P, González-Candelas L, Gabaldón T, et al. Genome sequencing and secondary metabolism of the postharvest pathogen Penicillium griseofulvum. BMC genomics. 2016;17(1):19.

19. Mead ME, Raja HA, Steenwyk JL, Knowles SL, Oberlies NH, Rokas A. Draft Genome Sequence of the Griseofulvin-Producing Fungus Xylaria flabelliformis Strain G536. Microbiology resource announcements. 2019;8(38):e00890-19.

20. Tang H-Y, Zhang Q, Li H, Gao J-M. Antimicrobial and allelopathic metabolites produced by Penicillium brasilianum. Natural product research. 2015;29(4):345-8.

21. Roullier C, Bertrand S, Blanchet E, Peigné M, Robiou du Pont T, Guitton Y, et al. Time dependency of chemodiversity and biosynthetic pathways: an LC-MS metabolomic study of marine-sourced penicillium. Marine drugs. 2016;14(5):103.

22. Jadulco R, Edrada RA, Ebel R, Berg A, Schaumann K, Wray V, et al. New Communesin Derivatives from the Fungus Penicillium sp. Derived from the Mediterranean Sponge Axinella v errucosa. Journal of natural products. 2004;67(1):78-81.

23. Petit K, Mondeguer F, Roquebert M, Biard J, Pouchus Y. Detection of griseofulvin in a marine strain of Penicillium waksmanii by ion trap mass spectrometry. Journal of microbiological methods. 2004;58(1):59-65.

24. Xue C, Li T, Deng Z, Fu H, Lin W. Janthinolide AB, two new 2, 5-piperazinedione derivatives from the endophytic Penicillium janthinellum isolated from the soft coral Dendronephthya sp. Die Pharmazie. 2006;61(12):1041-4.

25. Clarke S, McKenzie M. Penicillium sclerotigenum: a new source of Griseofulvin. Nature. 1967;213(5075):504-5.

26. Lee HB, Mun HY, Nguyen TTT, Kim J-C, Stone JK. Abieticola koreana gen. et sp. nov., a griseofulvin-producing endophytic xylariaceous ascomycete from Korea. Mycotaxon. 2016;131(4):749-64.

27. Ribeiro AI, Costa ES, Thomasi SS, Brandão DFR, Vieira PC, Fernandes JoB, et al. Biological and chemical control of Sclerotinia sclerotiorum using Stachybotrys levispora and its secondary metabolite griseofulvin. Journal of agricultural and food chemistry. 2018;66(29):7627-32.

28. Wang L, Zhou H-B, Frisvad JC, Samson RA. Penicillium persicinum, a new griseofulvin, chrysogine and roquefortine C producing species from Qinghai province, China. Antonie van leeuwenhoek. 2004;86(2):173-9.

29. Nielsen JC, Grijseels S, Prigent S, Ji B, Dainat J, Nielsen KF, et al. Global analysis of biosynthetic gene clusters reveals vast potential of secondary metabolite production in Penicillium species. Nature microbiology. 2017;2(6):1-9.

30. Frisvad JC, Samson RA. Polyphasic taxonomy of Penicillium subgenus Penicillium. A guide to identification of food and air-borne terverticillate Penicillia and their mycotoxins. Studies in mycology. 2004;49(1):1-174.

31. Larsen TO, Smedsgaard J, Nielsen KF, Hansen ME, Frisvad JC. Phenotypic taxonomy and metabolite profiling in microbial drug discovery. Natural product reports. 2005;22(6):672-95.

32. Samson RA, Pitt JI. Modern concepts in Penicillium and Aspergillus classification: Springer Science & Business Media; 2013.

33. Möller E, Bahnweg G, Sandermann H, Geiger H. A simple and efficient protocol for isolation of high molecular weight DNA from filamentous fungi, fruit bodies, and infected plant tissues. Nucleic acids research. 1992;20(22):6115.

34. Blin K, Shaw S, Steinke K, Villebro R, Ziemert N, Lee SY, et al. antiSMASH 5.0: updates to the secondary metabolite genome mining pipeline. Nucleic acids research. 2019;47(W1):W81-W7.

35. Kautsar SA, Blin K, Shaw S, Navarro-Muñoz JC, Terlouw BR, van der Hooft JJ, et al. MIBiG 2.0: a repository for biosynthetic gene clusters of known function. Nucleic acids research. 2020;48(D1):D454-D8.

36. Navarro-Muñoz JC, Selem-Mojica N, Mullowney MW, Kautsar S, Tryon JH, Parkinson EI, et al. A computational framework for systematic exploration of biosynthetic diversity from large-scale genomic data. Biorxiv. 2018:445270.

37. Katoh K, Asimenos G, Toh H. Multiple alignment of DNA sequences with MAFFT. Bioinformatics for DNA sequence analysis: Springer; 2009. p. 39-64.

38. Guindon S, Gascuel O. A simple, fast, and accurate algorithm to estimate large phylogenies by maximum likelihood. Systematic biology. 2003;52(5):696-704.

39. Akaike H. Information theory and an extension of the maximum likelihood principle. Selected papers of hirotugu akaike: Springer; 1998. p. 199-213.

40. Bengtsson-Palme J, Ryberg M, Hartmann M, Branco S, Wang Z, Godhe A, et al. Improved software detection and extraction of ITS1 and ITS 2 from ribosomal ITS sequences of fungi and other eukaryotes for analysis of environmental sequencing data. Methods in ecology and evolution. 2013;4(10):914-9.

41. Xia X. DAMBE7: new and improved tools for data analysis in molecular biology and evolution. Molecular biology and evolution. 2018;35(6):1550-2.

42. Jarvis BB, Zhou Y, Jiang J, Wang S, Sorenson W, Hintikka E-L, et al. Toxigenic molds in water-damaged buildings: dechlorogriseofulvins from Memnoniella echinata. Journal of natural products. 1996;59(6):553-4.

43. Zhang N, Wang Z. 3 Pezizomycotina: Sordariomycetes and Leotiomycetes. Systematics and Evolution: Springer; 2015. p. 57-88.

44. Cruz R, Santos C, Lima JSd, Moreira K, Motta CS. Diversity of Penicillium in soil of Caatinga and Atlantic Forest areas of Pernambuco, Brazil: an ecological approach. 2013.

45. Aybeke M, Şen B, Ökten S. Aspergillus alliaceus, a new potential biological control of the root parasitic weed Orobanche. Journal of basic microbiology. 2014;54(S1):S93-S101.

46. Franco ME, Wisecaver JH, Arnold AE, Ju Y-M, Slot JC, Ahrendt S, et al. Secondary metabolism drives ecological breadth in the Xylariaceae. bioRxiv. 2021.

47. Whalley A. The xylariaceous way of life. Mycological research. 1996;100(8):897-922.

48. Wright JM. The production of antibiotics in soil: ii. Production of griseofulvin by penicillium nigricans. Annals of Applied Biology. 1955;43(2):288-96.

49. Soloveva N, Malkov M. Kil® n, GI; Golubeva, LA: Role of nitrogen nutrition in the cultivation of Penicillium nigricans producing griseofulvin on a synthetic medium. Antibiot. 1972;9:104-6.

50. Alan R, Rodger C, Primrose FT. Production of griseofulvin in low nitrogen level medium. Google Patents; 1958.

51. Blin K, Medema MH, Kazempour D, Fischbach MA, Breitling R, Takano E, et al. antiSMASH 2.0—a versatile platform for genome mining of secondary metabolite producers. Nucleic acids research. 2013;41(W1):W204-W12.

52. Valente S, Cometto A, Piombo E, Meloni GR, Ballester A-R, González-Candelas L, et al. Elaborated regulation of griseofulvin biosynthesis in Penicillium griseofulvum and its role on conidiation and virulence. International Journal of Food Microbiology. 2020:108687.

53. Gay D, You Y-O, Keatinge-Clay A, Cane DE. Structure and stereospecificity of the dehydratase domain from the terminal module of the rifamycin polyketide synthase. Biochemistry. 2013;52(49):8916-28.

54. Keatinge-Clay A. Crystal structure of the erythromycin polyketide synthase dehydratase. Journal of molecular biology. 2008;384(4):941-53.

55. Todd RB, Andrianopoulos A. Evolution of a fungal regulatory gene family: the Zn (II) 2Cys6 binuclear cluster DNA binding motif. Fungal Genetics and Biology. 1997;21(3):388-405.

56. Housden BE, Muhar M, Gemberling M, Gersbach CA, Stainier DY, Seydoux G, et al. Loss-of-function genetic tools for animal models: cross-species and cross-platform differences. Nature Reviews Genetics. 2017;18(1):24-40.

CHAPTER THREE

In Silico Molecular Dynamics of Griseofulvin and its Derivatives Revealed Potential Therapeutic Applications for COVID-19

This chapter is published.

Aris P, Mohamadzadeh M, Wei Y, Xia X. In Silico Molecular Dynamics of Griseofulvin and Its Derivatives Revealed Potential Therapeutic Applications for COVID-19. International journal of molecular sciences. 2022;23(13):6889.

3.1. Author Contributions

Parisa Aris[1], Masoud Mohamadzadeh, Yulong Wei[1], Xuhua Xia[1,3]*

1. Department of Biology, University of Ottawa, 30 Marie Curie, P.O. Box 450, Station A, Ottawa, Ontario, Canada, K1N 6N5. Tel: (613) 562-5800 ext. 6886, Fax: (613) 562-5486.

2. Department of Chemistry, Faculty of Sciences, University of Hormozgan, Bandar Abbas 71961, Iran

3. Ottawa Institute of Systems Biology, Ottawa, Ontario, Canada K1H 8M5.

3.2. Abstract

Treatment options for Coronavirus Disease 2019 (COVID-19) remain limited and repurposing approved drugs with promising medicinal properties have gained increasing interest in therapeutic approaches to COVID-19. Using computational approaches, we examined griseofulvin and its derivatives against four key anti-SARS-CoV-2 targets: Main Proteinase, RdRp, Spike protein RBD, and human host ACE2. Molecular docking analysis revealed that griseofulvin (CID 441140) has the best binding affinity (–6.8 kcal/mol) with Main Proteinase (6LU7) of SARS-CoV-2. Moreover, griseofulvin derivative M9 (CID 144564153) demonstrated the most potent inhibitor with -9.49 kcal/mol followed by A3 (CID 46844082) with -8.44 kcal/mol against Mprotease and ACE2 respectively. Additionally, H-bond analysis revealed that compound A3 formed the highest number of hydrogen bonds, indicating the strongest inhibitory efficacy against ACE2. Further, Molecular Dynamics (MD) simulation analysis suggests that griseofulvin and these derivatives are structurally stable. These findings suggest that griseofulvin and its derivatives may be considered in designing future therapeutic inhibitors for SARS-CoV-2 Main Protease and ACE2 receptor.

3.3. Introduction

The COVID-19 pandemic has had an overwhelming long-term impact on healthcare systems globally. Despite vaccine developments and clinical research progress, the fast spread rate of SARS-CoV-2 and its variants has become a serious concern worldwide (1, 2). The World Health Organization reported over 500 million confirmed cases and over six million deaths as of 24 April 2022. During the last week of April 2022, the number of new weekly cases in Americas and the African region increased by 9% and 32%. Remarkably, the number of new weekly deaths in the South-East Asia increased by 41%.

Although extensive efforts have been made to manage this crisis, treatment of COVID-19 remained an urgent need and therapeutic options remained limited (3). So far, different enzymes necessary for viral replication, including 3C-like main protease (3CLpro), papain-like protease (PLpro), and RNA-dependent RNA polymerase (RdRP) have been reported as potential treatment targets for SARS-CoV-2 infection (4, 5). Moreover, SARS-CoV-2 spike protein RBD and its receptor angiotensin converting enzyme 2 (ACE2) are proposed as critical therapeutic targets for SARS-CoV-2 entry and infection (6, 7).

Considering the time and cost required for developing new drugs, computational drug repurposing is an effective strategy for developing new indications for approved drugs already available for clinical profiles (8, 9). Griseofulvin is an FDA-approved drug that has been primarily used to treat dermatophyte infections (10, 11). Interestingly, it has received renewed interest in recent years, mainly due to its potential to treat cancer (12), and suppress the replication of hepatitis C virus (13). Griseofulvin inhibits cell division by acting on mitotic spindle microtubule and induces cell death in cancer cell lines (12). Additionally, griseofulvin

arrests G2/M phase in human cells by interacting with microtubule polymerization to suppress hepatitis C virus replication (13). Recently, griseofulvin genes in *gsf* gene cluster have been investigated among fungal genomes to identify essential genes involved in griseofulvin production (14).

Molecular docking provides preliminary information for small molecule interactions with receptors (15). Molecular dynamics (MD) simulations seem to be pivotal in drug development to study the behaviour of proteins and other biomolecules in atomic resolution (16). In the current *in silico* study, we performed molecular docking and Molecular Dynamics Simulation analyses to investigate the inhibitory effects of griseofulvin and its derivatives in blocking essential SARS-CoV-2 M proteinase, RdRp, and RDB proteins (involved in its replication and propagation) and ACE2 from human (involved in host cell entry). Our computational approaches evaluated the drug-likeness of griseofulvin and its derivatives against SARS-CoV-2. Our findings revealed that griseofulvin and its derivatives have good binding potential with SARS-CoV-2 main protease and human ACE2 receptor, suggesting that these compounds may have inhibitory effect on SARS-CoV-2 entry and replication viral.

3.4. Materials and methods

3.4.1. Ligand preparation

The ligand 3-D structures were obtained from PubChem in the form of PubChem CIDs. The PubChem CID of the ligand was 441140 for griseofulvin, and CIDs of 464 derivatives of griseofulvin were listed in Supplementary file 1. Open Babel version 2.4.1 was used to generate a co-crystallized ligand (Ligand.pdbqt) file and their optimization.

3.4.2. Receptor preparation

The 3-D protein structures of the receptors were downloaded from the RCSB Protein Data Bank (PDB) as.pdb files. The PDB IDs of Main Proteinase, RNA-dependent RNA polymerase (RdRp), Spike RBD, and ACE2 receptor were 6LU7, 6M71, 6M0J (chain E), 6M0J (chain A) respectively. Chimera version 1.15 was used for protein structure optimization. Due to the missing residues of the viral structures of RdRp protein (PDB 6M71) in comparison with the complete amino acid sequences, protein 7APP was retrieved from PDB and was used as a template to predict homology model of RdRp protein by SWISS-MODELweb server (17). The stereochemical quality of protein structure was validated using PROCHECK by Ramachandran plot (18, 19). Homology modeling result showed 100% homology to 7APP protein, which is nsp7-nsp8-nsp12 SARS-CoV2 RNA-dependent RNA polymerase. The Ramachandran plot of modelled protein depicted 92% of residues lie in favoured regions, followed by 8% in additional allowed regions (Supplementary File 2), indicating a good quality model.

3.4.2. Binding Site Prediction

Computed Atlas of Surface Topography of proteins (CASTp) server was used to determine the binding sites of targeted proteins. The grid box was created around the identified binding pocket to perform virtual screening studies.

3.4.3. Virtual screening and *in Silico* Molecular Docking

PyRx 0.8 (20) from MGLTools (https://ccsb.scripps.edu/mgltools/) was used for the virtual screening using default settings. Ligands with the lowest binding affinity were considered the most stable conformation of the ligands regarding the receptor. Finally, eight hits with the best

docking score were selected for further analysis. Water molecules were manually removed from the PDB file prior to docking, and polar hydrogens were added. Molecular docking was performed for griseofulvin and thirty-two compounds using the Lamarckian genetic algorithm conducted in AutoDock 4 (21). Out of these modes, the two binding modes with the best docking score and interaction with selected protein were saved as a.pdb file and were used for further analysis. The interactions between the receptors and the ligands were visualized using Discovery Studio Visualizer v.20 (which can be downloaded freely from the given link. https://discover.3ds.com/discovery-studio-visualizer-download)

3.4.4. Molecular dynamic simulations

To validate the docking results, atom molecular dynamics simulation (MD) of the complex was performed. The single protein and two best protein-ligand and protein-griseofulvin complexes were analyzed using GROMACS-2021 software package to carry out 100 ns simulations (22) with AMBER99SB force field. The force field parameters for ligands were generated by AnteChamber PYthon Parser interface (ACPYPE) (23). The TIP3P water model was selected for solvating complexes, followed by the addition of sodium and chloride ions to neutralize. Periodic boundary (PBC) conditions were used. Energy minimization was done at 1000 kJ/mol/nm. The system was equilibrated in the NVT and NPT ensembles for 1 ns. To achieve overall charge neutrality of the systems and an ionic strength of 0.15 M, sufficient amounts of Na+ and Cl- counterions were added instead of solvent molecules. To reduce significant forces and relax the simulated systems, an energy reduction procedure was used in the initial step, followed by a relaxation process. The Nose–Hoover thermostat and the Berendsen barostat were employed to keep the temperature and pressure at 310 K and 1.0 bar, respectively (24). The trajectories were generated every 2 fs and saved every 2ps. Post-MD analyses were

performed; this includes root mean square deviation (RMSD), root mean square fluctuations (RMSF), the radius of gyration (Rg), solvent accessible surface area (SASA), secondary structure, and hydrogen bond occupancy.

3.4.5. Drug-like properties of the ligands

The drug likeliness of a molecule is indicated the Lipinski's rule of five parameters (molecular weight less than 500 Da, no more than 5 hydrogen bond donors, number of hydrogen bond acceptors should be less than 1, and LogP should not be greater than 5) (25). SwissADME server (www.swissadme.ch/index.php) was used to obtain Lipinski's rule of five parameters. Hepatotoxicity was also evaluated using the pkCSM server (http://biosig.unimelb.edu.au/pkcsm/prediction).

3.5. Results and Discussion

3.5.1. Virtual screening and molecular docking studies

The proteins and ligands structures were optimized to be in their minimum energy state. Figure 1 depicts ligand binding site prediction of targeted proteins in the hydrophobicity surface model. In this study, Pyrx was used to score the docking quality of ligands and targeted SARS-CoV-2 proteins (Supplementary file 3). The structures were ordered by the lowest free energy values (kcal/mol) corresponding to the high affinity binding site. The top eight ligands were chosen for further analysis using AutoDock 4.2 (Supplementary File 4). The ligand with high affinity can change the conformation of the substrate and subsequently change its function. The structures with the best binding affinities were mainly the best compounds with the most significant interactions in hydrogen bonds. Most of all interactions are shown between amino

acids and ligands (Table 1), including Hydrogen bonds (Green), alkyl and Pi-alkyl (Pink), Pi-Cation (Orange), Pi-sulfur (Yellow), Van der Waals interactions (Light Green), Halogen (Blue), and Carbon hydrogen bond (Gray).

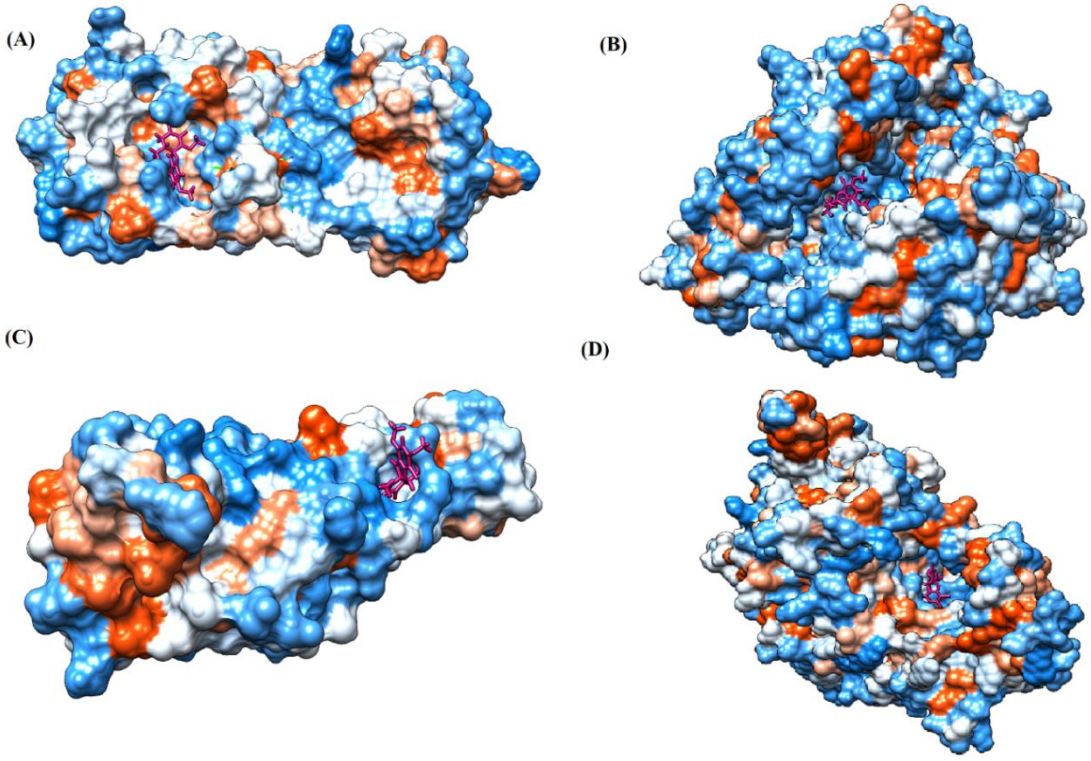

Figure 3.1. Ligand binding site prediction at (A) Mprotease, (B) ACE2, (C) RBD, and (D) RdRp hydrophobicity surface model with ligand binding pocket in the protein structure. Dodger blue for the most hydrophilic, to white, to orange red for the most hydrophobic regions. The ligand molecule (griseofulvin) is shown in bold, colored in pink. Images were obtained by Chimera.

Table 3.1. Molecular docking details of top compounds which are selected for MD analysis. PubChem ID compound (first column) highlighted in red, blue, orange, and green indicate their interactions with Mprotease, ACE2, RdRp, and RBD respectively. The dotted lines in ligand interaction diagram (last column) show the key interacting residues of targeted protein and ligand structure. Moreover, the green, light green, orange, pink, blue, and red dotted lines show conventional Hydrogen Bond, van der Waals, Pi Cation-Anion, Pi-Alkyl, Halogen, and unfavorable Acceptor-Acceptor interactions.

PubChem ID	Binding Energy (kcal/mol)	H-bonds	Hydrophobic interactions	Lipinski Analysis		Ligand interaction diagram
441140 (M1)	-6.80	HIS 41 GLY 143 CYS 145 GLU 166	MET 49 MET 165 ARG 188	Molecular weight Lipophilicity H bond donor H bond acceptor Violations Lipinski Hepatotoxicity	352.7 2.95 0 6 0 Yes No	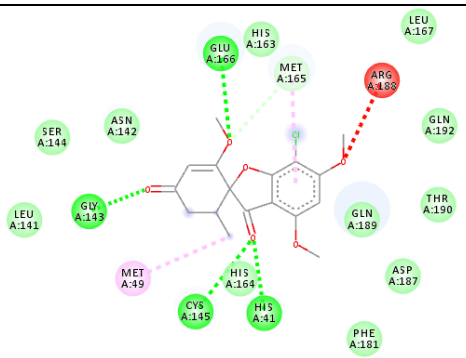
142550537 (M7)	-7.58	HIS 41 GLY 143 GLU 166 THR 190 GLN 192	MET 165 PRO 168 ARG 188 GLN 189 THR 190 GLN 192	Molecular weight Lipophilicity H bond donor H bond acceptor Violations Lipinski Hepatotoxicity	506.7 2.59 0 13 2 Yes No	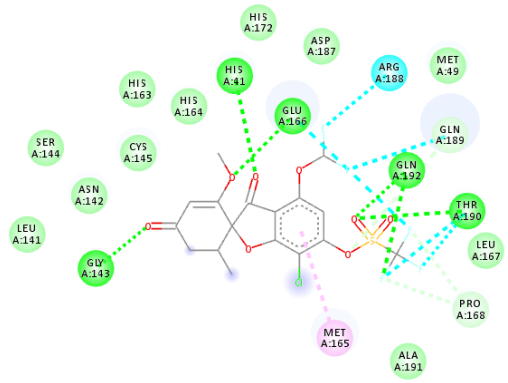
144564153 (M9)	-9.49	MET 165 GLU 166	CYS 44 MET 49 LEU 141 CYS 145 MET 165	Molecular weight Lipophilicity H bond donor H bond acceptor Violations Lipinski Hepatotoxicity	484.9 3.61 1 7 0 Yes No	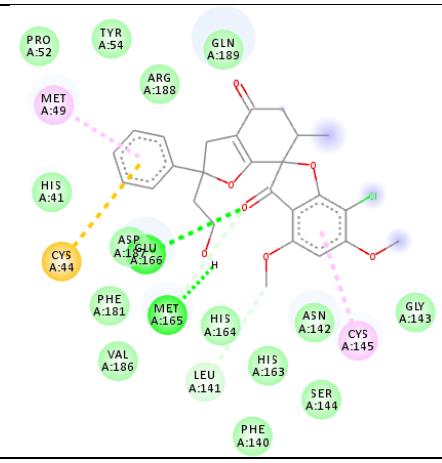

441140 (A7)	-5.2	HIS 401 ARG 514	HIS 378 GLU 398 HIS 401	Molecular weight Lipophilicity H bond donor H bond acceptor Violations Lipinski Hepatotoxicity	352.7 2.95 0 6 0 Yes No	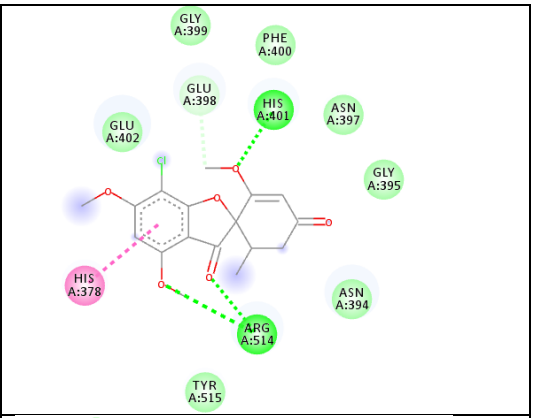
46844082 (A3)	-8.44	ALA 348 ASN 394 ARG 514	GLU 375 HIS 378 HIS 401 GLU 402	Molecular weight Lipophilicity H bond donor H bond acceptor Violations Lipinski Hepatotoxicity	641.1 5.51 0 8 2 Yes No	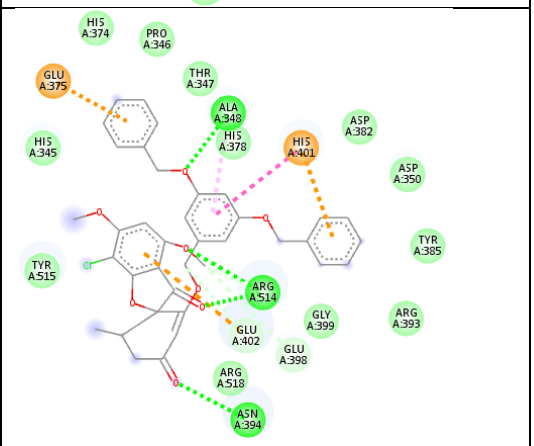
132286359 (A9)	-6.51	ASP 382 GLY 395 PHE 400 HIS 401 GLU 402 ARG 514	GLU 375 HIS 378 HIS 401 GLU 402	Molecular weight Lipophilicity H bond donor H bond acceptor Violations Lipinski Hepatotoxicity	551.3 3.85 2 9 1 Yes No	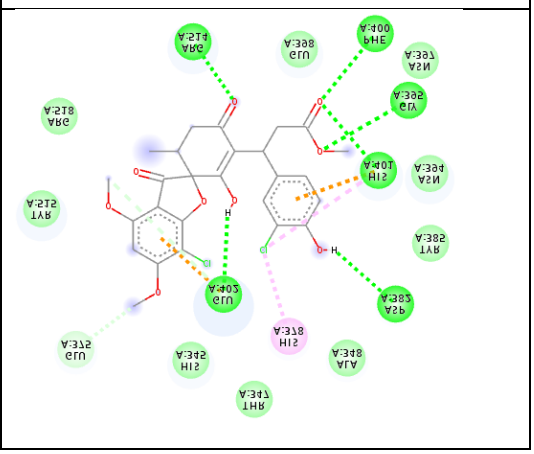

441140 **(Rd7)**	-5.62	LYS 621 CYS 622 LYS 798	ASP 623	Molecular weight Lipophilicity H bond donor H bond acceptor Violations Lipinski Hepatotoxicity	352.7 2.95 0 6 0 Yes No	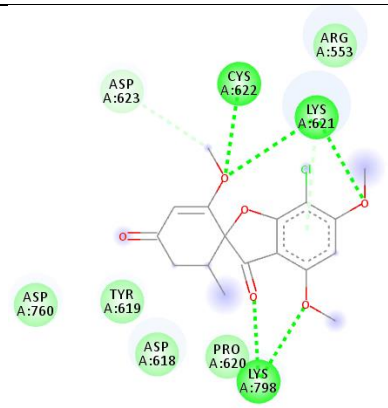
73331209 **(Rd2)**	-7.21	LYS 621 CYS 622 LYS 798	ASP 618 LYS 621 CYS 622 ASP 623	Molecular weight Lipophilicity H bond donor H bond acceptor Violations Lipinski Hepatotoxicity	458.8 3.75 0 7 0 Yes No	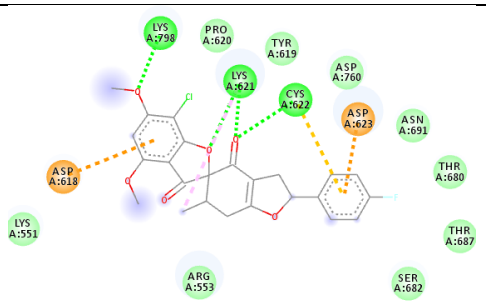
118254151 **(Rd6)**	-6.61	LYS 621 CYS 622 LYS 798	ASP 618 LYS 621 CYS 622 ASP 623 ASN 691	Molecular weight Lipophilicity H bond donor H bond acceptor Violations Lipinski Hepatotoxicity	458.8 3.73 0 7 0 Yes No	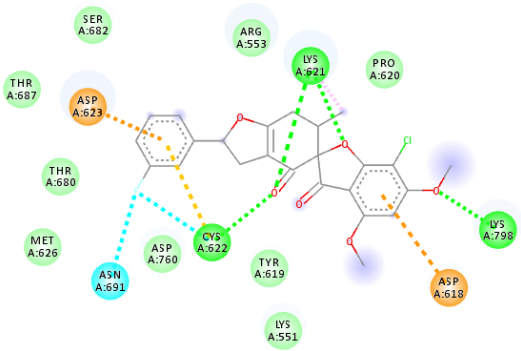
441140 **(Rb1)**	-5.3	GLU 471	LYS 458 GLU 471	Molecular weight Lipophilicity H bond donor H bond acceptor Violations Lipinski Hepatotoxicity	352.7 2.95 0 6 0 Yes No	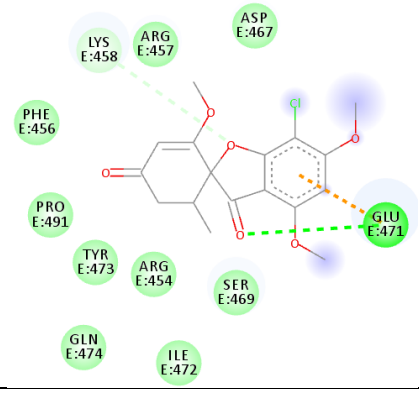

56950846 (Rb3)	-7.21	ARG 457 LYS 458 SER 469	ARG 457 LYS 458 GLU 471 PRO 491	Molecular weight Lipophilicity H bond donor H bond acceptor Violations Lipinski Hepatotoxicity	428.8 3.6 0 6 0 Yes No	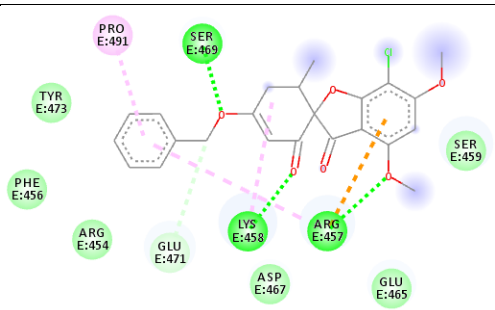
125429633 (Rb9)	-6.5	ARG 457 LYS 458 SER 459 GLU 471 ILE 472	ARG 457 LYS 458 GLU 471 PRO 491	Molecular weight Lipophilicity H bond donor H bond acceptor Violations Lipinski Hepatotoxicity	516.9 3.45 2 9 1 Yes No	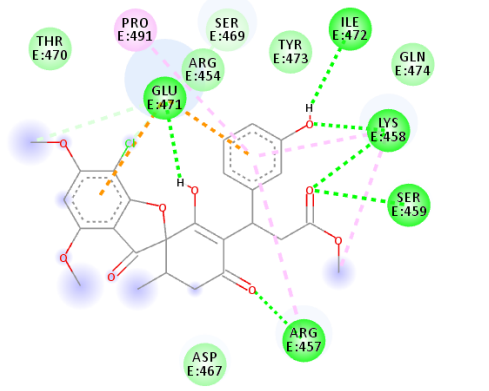

3.5.2. Main Protease (6LU7)

The coronavirus main protease (Mpro) is essential for the proteolytic maturation of the virus. It has been examined as a potential target to stop the spread of infection by inhibiting viral polyprotein cleavage (26, 27). The residues of His41, Gly143, Cys145, Glu166, Gln192, Asn142, Thr190, and Met165 6LU7 form H-bond with carbonyl group while Met49, Met165, Cys145, His41, and Pro168 show π-alkyl interaction with pyridine. Phe140, Leu141, Asn142, Met165, Glu166, Gln189 have van der waals interactions, whereas Met165, and Cys44 show π-sulfur interaction with SO2 group. Amino acids Gln189 and His41 form π-sigma and π-π-T shaped interactions, respectively. Moreover, there are halogen bonds between Arg188, Thr190, His164, His41, Glu166, and Gln181 with chlorine of ligands. The amino acid interactions in the present

study are similar to that in other studies that reported GLU166, CYS 44, CYS145, SER 144 and MET49 play roles in drug interactions (28).

Based on the lower dock score in the catalytic pocket of Main protease, the derivative M9 with -9.49 kcal/mol binding energy was the most effective as it strongly binds to SARS-CoV-2 main protease as confirmed by the AutoDock analysis. Notably, it has been reported that this derivative can be used to treat precancerous hyperproliferative conditions (29). Our *in silico* study revealed that all structures showed good binding energy toward the target protein ranging from −9.49 to −6.8 kcal mol−1.

3.5.3. ACE2

The docking of receptor ACE2 with candidate ligands showed well established bonds with one or more residues in the receptor active site. The residues of Arg514, Glu402, Asn394, Ala348, Asp382, His401, Asp350, Gly394, and Phe400 form strong H-bond interaction with methylene and OH, while His378, Asp382, Asp350, Thr385, Ala348, Glu402, Glu398, and Asn394 involve in weak van der waals interaction. Close examination of the docking pose suggested a fluorine atom of A5 (PubChem ID 118254232) lined with the residues Asp382 and Ala348. The molecular docking results also revealed hydrophobic interactions of residues His401, Glu375, His378, Glu402, Glu398, His378, Ala 348, Arg514, and His345 are dominant interactions in A1, A4, and A5 compounds with PubChem IDs 10574693, 118254131, 118254232 respectively.

The compound A3 (PubChem ID 46844082) exhibited the lowest binding energy with value of -8.44 kcal mol−1, indicating the highest affinity to the ACE2 receptor (Table 1). This compound

is an analogue of griseofulvin in which a npropoxy group has replaced the methoxy group in 2' position exhibits a more substantial inhibiting effect on cancer cells than griseofulvin itself (30). Two-dimensional receptor-ligand interaction diagrams illustrated that A9 (PubChem ID 132286359) compound having best interaction as hydrogenic (Asp382, Gly395, Phe400, His401, Glu402, Arg514) and hydrophobic (Glu375, His378, His401, Glu402) to ACE2 receptor. Since compounds A3 and A9 showed the best binding affinity and interaction with ACE2, these complexes were considered for further MD simulation.

3.5.3. Spike RBD

The amino acids Arg454, Arg457, Lys458, Ser459, Ile468, Se469, Glu471, and Ile472 in the binding cavity can form hydrogen bonds. Molecular docking results suggest that hydrophobic actions of residues Arg454, Phe456, Arg457, Lys458, Arg466, Asp467, Ser469, Glu471, Ile472, Tyr473, and Pro491 with griseofulvin analogues played a predominant role in all compounds except Rb9, with the best result for hydrogen bonds interaction. The Rb3 compound showed the highest binding affinity towards the RBD protein, with the lowest CDocker energy -7.21 kcal mol−1.

3.5.4. RNA dependent RNA polymerase (RdRp)

The Rd2 compound showed a high binding affinity with -7.21 kcal mol−1 to the RdRp receptor (Table 1). The docking pose of Rd2 shows three hydrogen bonds interactions with Lys621, Cys622, and Lys798 amino acids present at the active site of the RdRp protein. It is noteworthy that the H-bonds in griseofulvin and the best interacting compound (PubChem ID 118254151) are identical to those found in Rd2 with the lowest binding energy. The selected

ligand-protein complexes illustrated intermediate binding energy ranging from 5.62-7.21 kcal mol−1 toward the target protein.

3.6. Molecular dynamics simulations

The results in Table 1 suggest that the best inhibitors have strong hydrogen bonds with a large amount of noncovalent interaction. Figure 2 shows two-dimensional (2D) structures of selected best-docked ligand molecules based on the lowest binding energy and highest number of hydrogen bonds. MD simulations were performed for 100 ns to analyze protein structure stability and conformational changes of proteins, griseofulvin-proteins, and the top docked ligand-complexes. The trajectory files from MD simulations were analyzed for root-mean-square deviation (RMSD), root mean square fluctuation (RMSF), radius of gyration (Rg), Solvent Accessible Surface Area (SASA), secondary structure, and H-bond occupancy contributing to investigating the stability and structural dynamics during MD simulations (Table 2-5).

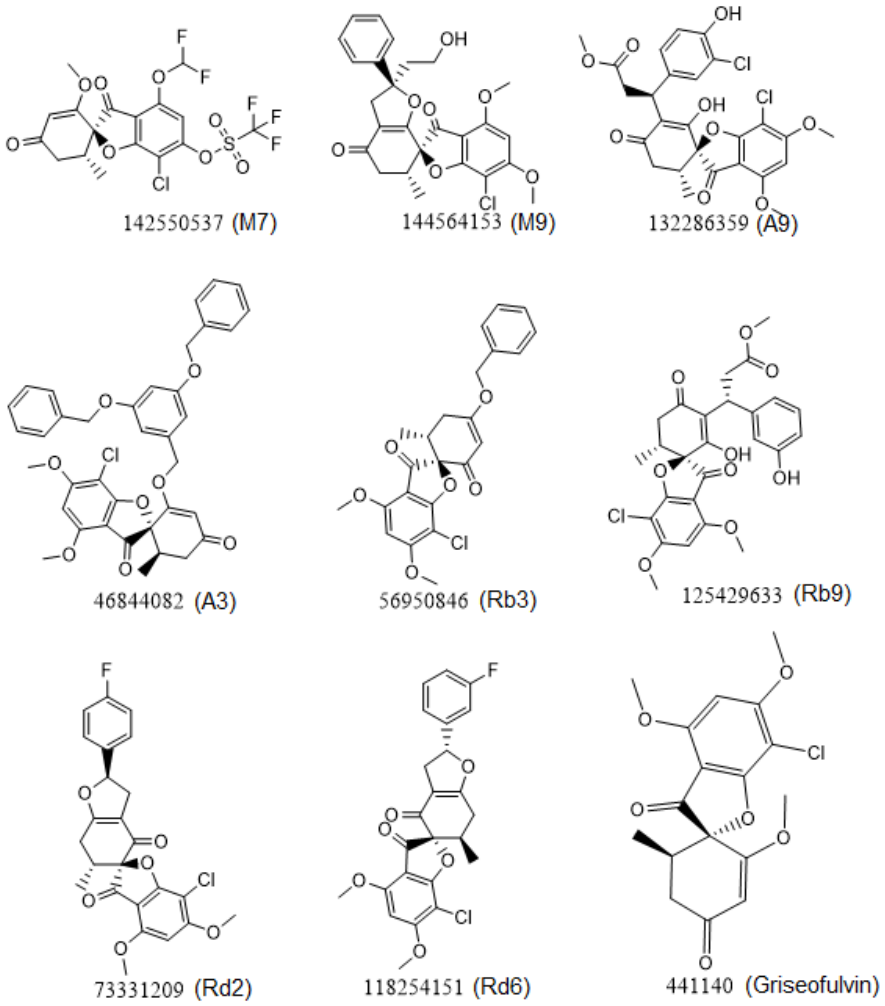

Figure 3.2. Chemical two-dimensional (2D) structures of top selected ligands for MD analysis. The PubChem IDs are listed under the 2D structures.

3.6.1. Structural Dynamics of Mprotease

The M protease is an essential component in the virus life cycle, as it coordinates viral replication and transcription. It cleaves polyproteins in their primary parts and releases replicative proteins. Consequently, this protein is considered a potential target for designing therapeutic drugs to counter SARS-CoV-2.

RMSD is used to measure the deviation between the initial and final position of a protein. The smaller the RMSD, the more stable structures. The average RMSD values of Mprotease and Mprotease –griseofulvin were 4.12 and 3.51 Å followed by M7 (2.35 Å) and M9 (2.79 Å) compounds (Table 2). These values were found to be lower and remained stable during the simulations. This suggests that griseofulvin binds to Mprotease firmly and may block it. RMSF was used to depict the fluctuations at the residue level. RMSF plot showed residues HIS41, Met165, and Glu166 interacting with the active site of Mprotease have less RMSF values compared to Mprotease alone (Fig 3B), indicating the stability of these residues upon binding to Mprotease during the simulation. The radius of gyration (Rg) indicates compactness of protein. Mprotease and Mprotease-griseofulvin average Rg values were revealed to be 22.9 and 21.8 Å respectively (Table 2). This finding suggests that Mprotease-griseofulvin binds significantly more strongly than Mprotease alone. Protein-alone is a control used for comparison in this study. SASA is defined as the surface area of a protein which interacts with its solvent molecules. The average SASA values for Mprotease, Mprotease-griseofulvin, M7 and M9 were estimated to be 13382, 14834, 14885, and 15177 $Å^2$ respectively. This plot suggested an increase in the total SASA of Mprotease, which means the internal residues in Mprotease are accessible to solvent when griseofulvin binds to it (Fig 3D).

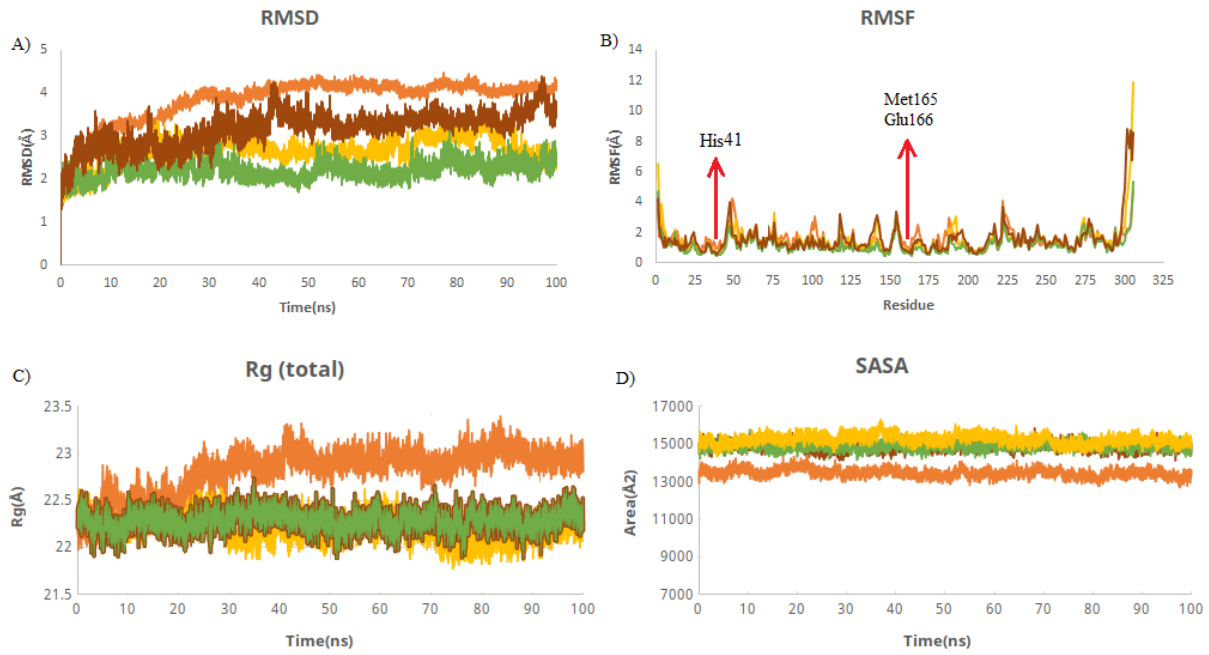

Figure 3.3. Structural dynamics of Mprotein. (A) Root mean square deviation (RMSD), (B) Root mean square fluctuations (RMSF), (C) Radius of the gyration (Rg) plot, (D) Solvent-Accessible Surface Area (SASA). Orange color indicates Mprotease-free form; yellow, green, and brown indicate Mprotease in the complex with M9, M7, and griseofulvin respectively.

Table 3.2. The average of RMSD, RMSF, Rg, and SASA for Mprotease (6LU7) during the last 20 ns of MD simulations. PubChem IDs of derivatives M9 and M7 are 144564153 and 142550537 respectively.

Complex	Mean RMSD (Å)	Mean RMSF (Å)	Mean Rg (Å)	Mean SASA (Å)
Mprotease	4.12±0.08	0.91±0.40	22.99±0.95	13382±199
Mprotease-M9	2.79±0.30	1.2±1.03	22.14±0.11	15177±199
Mprotease-M7	2.35±0.16	1.05±0.49	22.30±0.10	14885±180
Mprotease-griseofulvin	3.51±0.23	1.17±0.65	21.81±0.11	14834±200

3.6.2. Structural Dynamics of Angiotensin-converting enzyme 2 (ACE2)

ACE2, a type I membrane protein, has a role in the renin angiotensin system (RAS), a key component in controlling hydroelectrolyte balance (31). SARS-CoV-2 enters the host body via the respiratory tract and airway, where it binds to ACE2 receptors on human cells (32). ACE2 is expressed in many human organs, including lungs, heart, kidneys, bladder, and small intestine, and it demonstrates viral tissue tropism, which may lead to multiple organ failures (33-35).

The RMSD trajectory measures protein deviation from the reference structure (36). The binding of ligand into the receptor binding pocket provides the conformational stability of the macromolecular system. In all simulations, the complex reaches an equilibrium during the last 20 ns of simulation, as it shows in Table 3. It was revealed that the average RMSD values was decreased by 3.4 Å (from 5.7 to 2.28 Å) upon binding to griseofulvin (Fig 4A). This finding shows the stability of griseofulvin in the active pocket of ACE2. There was minor increase in residual fluctuations. The average Rg values for ACE2 and ACE2-griseofulvin, A3 and A9 compounds were found to be 25.7, 24.9, 24.7, and 25.5 Å. It was found that ACE2-A3 has more tight packing than ACE2 alone. The highest SASA value was observed in A9 (27798 Å)

followed by A3 (26697 Å) and griseofulvin (26532 Å) revealing protein volume expansion and a low variation is expected throughout the simulation time (Table 3).

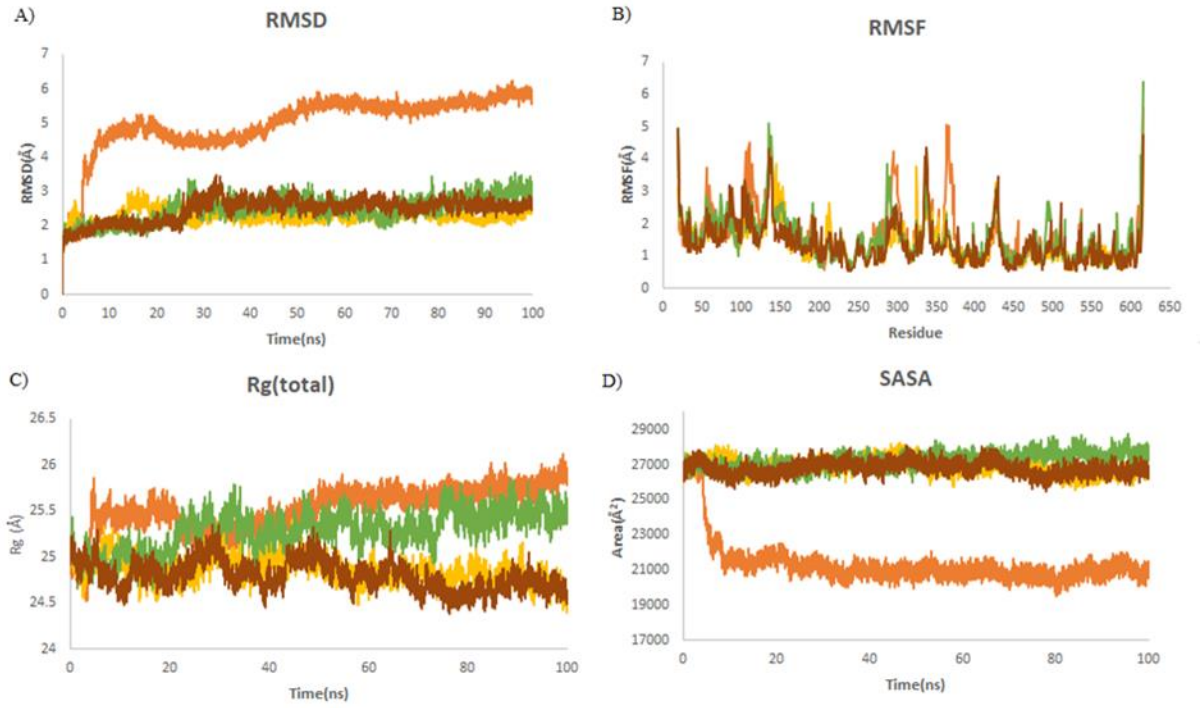

Figure 3.4. Structural dynamics of ACE2. (A) Root mean square deviation (RMSD), (B) Root mean square fluctuations (RMSF), (C) Radius of the gyration (Rg) plot, (D) Sand Solvent-Accessible Surface Area (SASA). Orange color indicates ACE2-free form; yellow, green, and brown indicate ACE2 in the complex with griseofulvin, A9, and A3 respectively.

Table 3.3. The average of RMSD, RMSF, Rg, and SASA for ACE2 during the last 20 ns of MD simulations. PubChem IDs of derivatives A9 and A3 are 132286359 and 46844082 respectively.

Complex	Mean RMSD (Å)	Mean RMSF (Å)	Mean Rg (Å)	Mean SASA (Å)
ACE2	5.70±0.15	0.99±.58	25.7±0.09	20933±385
ACE2-A9	2.85±0.21	1.18±.58	25.5±0.11	27798±334
ACE2-A3	2.63±0.13	1±0.48	24.7±0.9	26697±270
ACE2-griseofulvin	2.28±0.12	1.12±0.48	24.9±0.11	26532±285

3.6.3. Structural Dynamics of RNA-Dependent RNA Polymerase (RdRp)

RdRp plays an essential role in the replication and transcription cycle of RNA viruses, making this protein an appealing antiviral drug candidate for a broad range of viruses (37). RdRp targeted inhibition is unlikely to cause adverse effects due to its absence in mammalian cells (38-40). Thus, repurposing of the RdRp-targeted drugs may represent a promising strategy for COVID-19 treatment (41, 42).

Steady RMSDs with small changes for almost all complexes demonstrated the stability of the complexes throughout the simulation (Fig 5A). No significant fluctuations in the average of RMSFs were observed, which depicted the consistent complex exposure for a favourable conformational cavity of the RdRp molecule (Table 4). The average Rg values were found to be 32, 32.2, 31.9, and 31.9 Å for RdRp, RdRp-griseofulvin, Rd2, and Rd6 respectively (Figure 5C), which means having similar structural packing to RdRp alone. The average SASA values of Rd6 (39078 $Å^2$) and Rd2 (39257 $Å^2$) compounds were found to be the lowest compared to RdRp alone (39625 $Å^2$) (Table 4). It can suggest that the binding of these compounds could reduce protein expansion, probably due to strong binding of Rd6 and Rd2 with RdRp protein. However, a higher SASA value was observed in griseofulvin-RdRp complex, indicating its expansion of protein volume and less fluctuation over time.

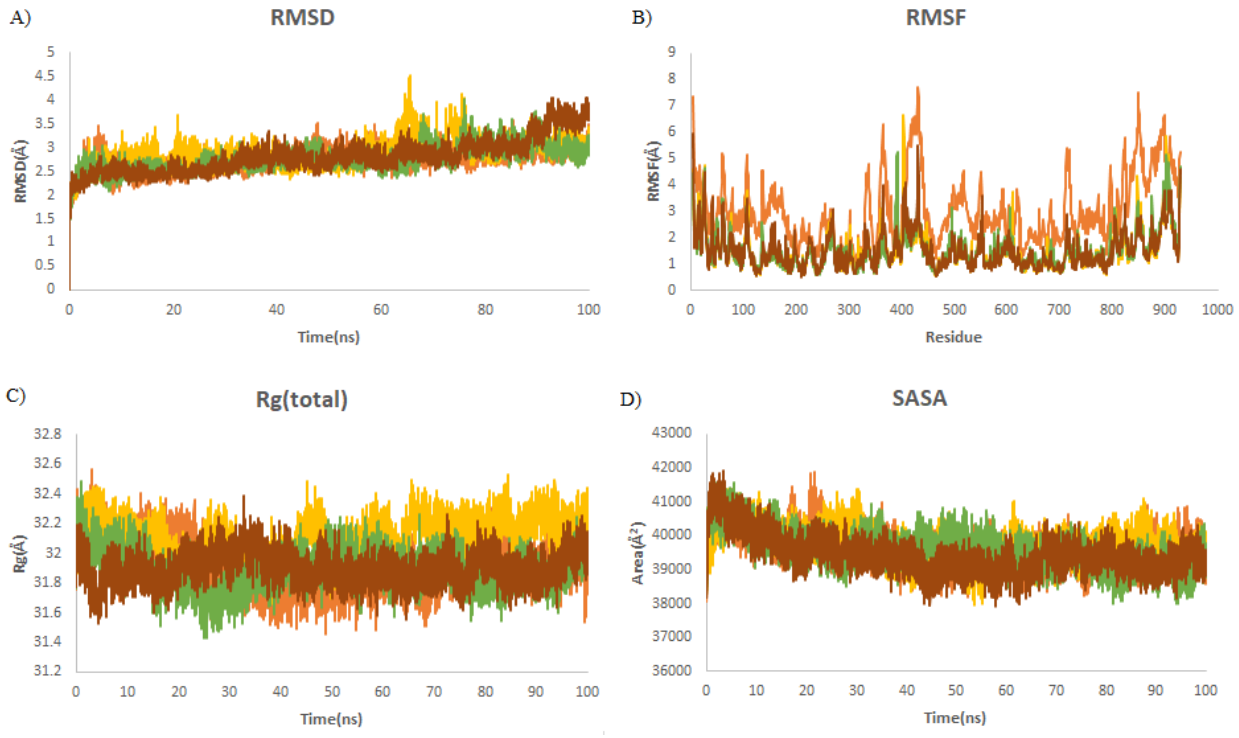

Table 3.4. Structural dynamics of RdRp. (A) Root mean square deviation (RMSD), (B) Root mean square fluctuations (RMSF), (C) Radius of the gyration (Rg) plot, (D) Sand Solvent-Accessible Surface Area (SASA). Orange color indicates RBD-free form; yellow, green, and brown indicate RdRp in the complex with griseofulvin, Rd6, Rd2 respectively.

Table 3.5. The average of RMSD, RMSF, Rg, and SASA for RdRp during the last 20 ns of MD simulations. PubChem IDs of derivatives Rd6 and Rd2 are 118254151 and 73331209 respectively.

Complex	Mean RMSD (Å)	Mean RMSF (Å)	Mean Rg (Å)	Mean SASA (Å)
RdRp	2.9±0.15	0.14±0.06	32±0.11	39625±380

RdRp-Rd6	3.1±0.19	0.14±0.06	31.8±0.1	39078±389
RdRp-Rd2	3.34±0.31	0.13±0.05	31.9±0.1	39257±318
RdRp-griseofulvin	3.1±0.16	0.16±.07	32.2±0.10	39735±381

3.6.4. Structural Dynamics of receptor-binding domain (RBD)

The receptor-binding domain in SARS-CoV-2 S protein binds to human ACE-2 receptor enabling viral entry into host cell (43, 44). The RBD is an attractive antigen for vaccine development since it is the primary target for the majority of neutralizing antibodies produced during a SARS-CoV-2 infection (45).

It is observed from Table 5 that RBD-griseofulvin complex exhibits the lowest RMSD (2.17 Å) than RBD alone (3.47 Å), implying the structural stability of griseofulvin in the active pocket of RBD. The average RMSD values of complexes during the last 20 ns trajectories of MD simulations indicate the fluctuations in the constituent residues were less than 0.2 Å, which is satisfactory (Table 5). Furthermore, the residues Glu471, Lys458, and Arg457 that were found to interact with the binding site of RBD (Fig 6B), showed decreased RMSF values, indicating the most stable residues of this protein during the simulation. The average Rg values for RBD, RBD-griseofulvin, Rb9, and Rb3 were found to be 17.5 Å, 18.1 Å, 18.1 Å, and 18.2 Å, respectively (Figure 6C). The Rg plot depicted there is no significant difference in the packing of RBD upon ligand binding. From the SASA plot in Figure 6D, we can see that the SASA values of RBD-griseofulvin, Rb9 and Rb3 are overall greater than the RBD protein alone, making an increase in the solvent accessible surface area that results in increased stability of the protein.

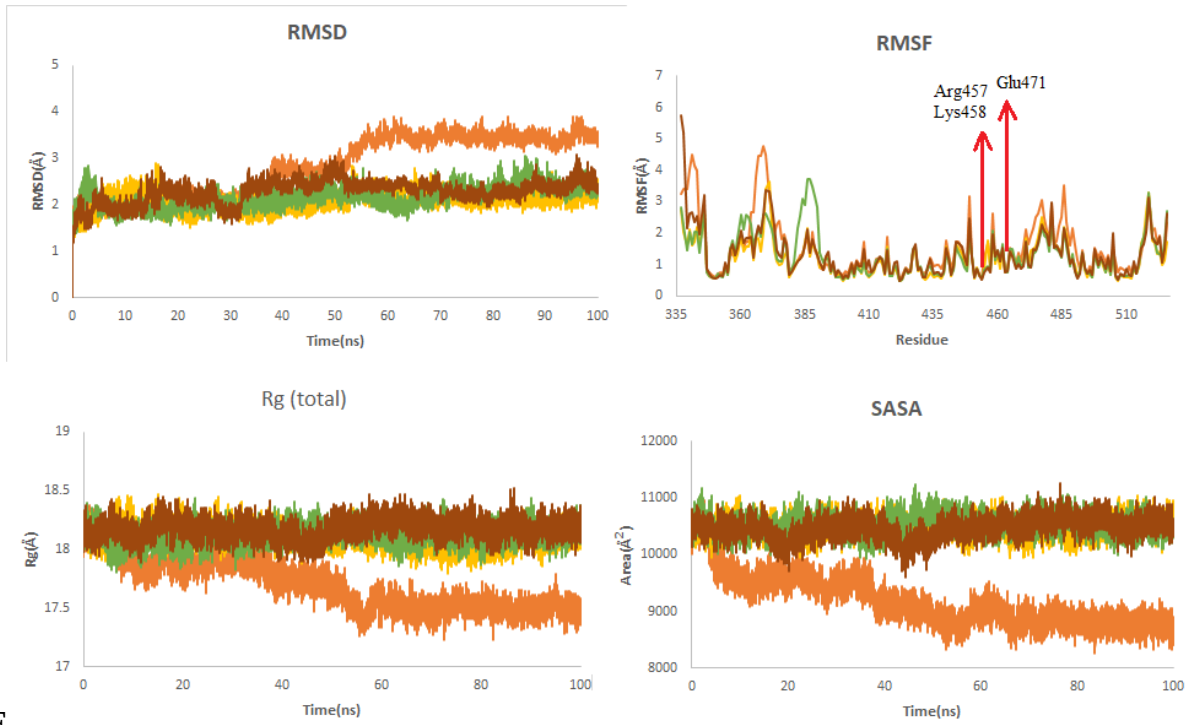

F

mean square fluctuations (RMSF), (C) Radius of the gyration (Rg) plot, (D) Sand Solvent-Accessible Surface Area (SASA). Orange color indicates RBD-free form; yellow, green, and brown indicate RBD in the complex with griseofulvin, Rb9, Rb3 respectively.

Table 3.6. The average of RMSD, RMSF, Rg, and SASA for RBD during the last 20 ns of MD simulations. PubChem IDs of derivatives Rb9 and Rb3 are 125429633 and 56950846 respectively.

Complex	Mean RMSD (Å)	Mean RMSF (Å)	Mean Rg (Å)	Mean SASA (Å)
RBD	3.47±0.12	0.95±0.48	17.5±0.06	8785±128
RBD-Rb9	2.45±0.18	1.2±0.63	18.1±0.07	10514±148
RBD-Rb3	2.41±0.14	1.2±0.63	18.2±0.08	10582±152
RdRp-griseofulvin	2.17±0.19	1.04±0.50	18.1±0.08	10554±155

3.6.5. Secondary structure changes upon ligand binding

The purpose of secondary structure is to identify protein structural characteristics. The average number of secondary structures in complexes remained at approximately equal frequency compared to protein alone over the last 20 ns of MD simulations (Supplementary File 5). This finding suggests the stability of secondary structure of protein upon binding to ligand.

3.6.6. Hydrogen bonding

Hydrogen bond plays an important role in stability of the inhibitor-protein complex. To validate structural stability, the hydrogen bonds paired within 0.35 nm indicating the cutoff distance as per the hydrogen bond were calculated in a solvent environment during the 100 ns MD simulations (Table 6). The residue occupancies corresponding the participation of active site residues remarkably demonstrated that the residues Gln192 and Glu166 were predominant contributors with 77.2% and 76.8% occupancies to the formation of H-bond with Mprotease during simulation. This finding highlights the significance of these residues in the structural state of 6LU7 protein. The highest number of hydrogen bonds of six was found between compound A9 and ACE2 as a receptor, followed by compounds M7 and M1 with five and four hydrogen bonds with Mprotease (6LU7) respectively during the last 20 ns of MD simulations (Supplementary File 6). The results of H-bond analysis are consistent with docking findings, however the number of hydrogen bonds in the two approaches appear to be slightly different, which could be due to ligand-protein dynamics and conformation changes during MD simulation.

Table 3.7. The residue interaction and hydrogen bond (H-bond) percentage occupancy from the simulation trajectories.

Compound	Residue interaction (H-bond occupancy (%))
6LU7-griseofulvin (M1)	Gln192 (17.2) Cys145 (43.4), Glu166 (6.1)
6LU7-142550537 (M7)	Gln192 (77.2), Thr190 (70.2), Gln189 (10.1)
6LU7-144564153 (M9)	Glu166 (76.8), His41 (3.8), His164 (15.1)
ACE2-griseofulvin (A7)	Trp69 (1.7), Ser106 (9.1), Asn117 (2.6), Lys114 (1.9)
ACE2-46844082 (A3)	Trp69 (2.2), Asn117 (24.2), Asn63 (1.15), Arg514 (10.2)
ACE2-132286359 (A9)	Trp69 (7.9), Asn51 (2.6), Asn53 (7.6), Gly104 (3.9)
RdRp-griseofulvin (Rd7)	Cys622 (37.2), Arg555 (17.2), Asp623(1.7)
RdRp-73331209 (Rd2)	Arg553 (2.3), Lys621 (2.1), Asp623 (9.1)
RdRp-118254151 (Rd6)	Arg553 (8.8), Lys621 (1.8), Asp623 (1.52)
RBD-griseofulvin (Rb1)	Asn360 (1.6), Cys391 (2.3), Phe486 (2.8), Ala522 (3.8)
RBD-56950846 (Rb3)	Thr430 (1.4), Lys458 (5.1), Ser459 (39.1), Ala522 (7.8)
RBD-125429633 (Rb9)	Asn460 (6.4), Arg466 (6.8), Asn354 (3.8), Ser349 (3.5)

3.7. Drug-likeness evaluation

The ligands with the greatest potential for inhibiting targeted receptors were analyzed for their drug likeliness through SwissADME (46). A compound seems to be more permeable and quickly absorbed by the body if it meets the Lipinski criteria (25). Remarkably, all studied compounds except derivative A3 were shown to have a molecular weight ranging from 352.7 to 551.3 Daltons with predicted LogP within the range value of 2.59-3.85. They all had less than ten hydrogen bond acceptors and five hydrogen bond donors. These characteristics are in the acceptable range of Lipinski's rule of five (See Methods). Our results showed that none of the

compounds exhibited hepatotoxicity using PkCSM server, which evaluates the hepatotoxic feature. The calculated LogP values, hepatotoxicity, and other features of the bound ligands are illustrated in Table 1.

3.8. Acknowledgments

The computational resources were provided by Compute Canada. This work is supported by the Natural Sciences and Engineering Research Council of Canada (NSERC) Discovery Grant to X.X. (RGPIN/2018-03878), and NSERC Doctoral Scholarship to Y.W. (CGSD/2019-535291).

3.9. References

1. Cascella M, Rajnik M, Aleem A, Dulebohn SC, Di Napoli R. Features, evaluation, and treatment of coronavirus (COVID-19). Statpearls (internet). 2022.

2. Chen J, Lu H. New challenges to fighting COVID-19: Virus variants, potential vaccines, and development of antivirals. Bioscience trends. 2021.

3. Niknam Z, Jafari A, Golchin A, Danesh Pouya F, Nemati M, Rezaei-Tavirani M, et al. Potential therapeutic options for COVID-19: an update on current evidence. European journal of medical research. 2022;27(1):1-15.

4. Cannalire R, Cerchia C, Beccari AR, Di Leva FS, Summa V. Targeting SARS-CoV-2 proteases and polymerase for COVID-19 treatment: state of the art and future opportunities. Journal of medicinal chemistry. 2020.

5. Wu C, Liu Y, Yang Y, Zhang P, Zhong W, Wang Y, et al. Analysis of therapeutic targets for SARS-CoV-2 and discovery of potential drugs by computational methods. Acta Pharmaceutica Sinica B. 2020;10(5):766-88.

6. Zhang H, Penninger JM, Li Y, Zhong N, Slutsky AS. Angiotensin-converting enzyme 2 (ACE2) as a SARS-CoV-2 receptor: molecular mechanisms and potential therapeutic target. Intensive care medicine. 2020;46(4):586-90.

7. Huang Y, Yang C, Xu X-f, Xu W, Liu S-w. Structural and functional properties of SARS-CoV-2 spike protein: potential antivirus drug development for COVID-19. Acta Pharmacologica Sinica. 2020;41(9):1141-9.

8. Ashburn TT, Thor KB. Drug repositioning: identifying and developing new uses for existing drugs. Nature reviews Drug discovery. 2004;3(8):673-83.

9. Rudrapal M, Khairnar SJ, Jadhav AG. Drug repurposing (DR): an emerging approach in drug discovery. Drug Repurposing Hypothesis Mol Asp Ther Appl. 2020.

10. Oxford AE, Raistrick H, Simonart P. Studies in the biochemistry of micro-organisms: griseofulvin, C17H17O6Cl, a metabolic product of Penicillium griseo-fulvum Dierckx. Biochemical Journal. 1939;33(2):240.

11. Lambert DR, Siegle RJ, Camisa C. Griseofulvin and ketoconazole in the treatment of dermatophyte infections. International journal of dermatology. 1989;28(5):300-4.

12. Rebacz B, Larsen TO, Clausen MH, Rønnest MH, Löffler H, Ho AD, et al. Identification of griseofulvin as an inhibitor of centrosomal clustering in a phenotype-based screen. Cancer research. 2007;67(13):6342-50.

13. Jin H, Yamashita A, Maekawa S, Yang P, He L, Takayanagi S, et al. Griseofulvin, an oral antifungal agent, suppresses hepatitis C virus replication in vitro. Hepatology Research. 2008;38(9):909-18.

14. Aris P, Yan L, Wei Y, Chang Y, Shi B, Xia X. Conservation of griseofulvin genes in the gsf gene cluster among fungal genomes. G3. 2022;12(2):jkab399.

15. Agarwal S, Mehrotra R. An overview of molecular docking. JSM chem. 2016;4(2):1024-8.

16. Borhani DW, Shaw DE. The future of molecular dynamics simulations in drug discovery. Journal of computer-aided molecular design. 2012;26(1):15-26.

17. Schwede T, Kopp J, Guex N, Peitsch MC. SWISS-MODEL: an automated protein homology-modeling server. Nucleic acids research. 2003;31(13):3381-5.

18. Laskowski RA, MacArthur MW, Moss DS, Thornton JM. PROCHECK: a program to check the stereochemical quality of protein structures. Journal of applied crystallography. 1993;26(2):283-91.

19. Lovell SC, Davis IW, Arendall III WB, De Bakker PI, Word JM, Prisant MG, et al. Structure validation by Cα geometry: ϕ, ψ and Cβ deviation. Proteins: Structure, Function, and Bioinformatics. 2003;50(3):437-50.

20. Dallakyan S, Olson AJ. Small-molecule library screening by docking with PyRx. Chemical biology: Springer; 2015. p. 243-50.

21. Morris GM, Huey R, Lindstrom W, Sanner MF, Belew RK, Goodsell DS, et al. AutoDock4 and AutoDockTools4: Automated docking with selective receptor flexibility. Journal of computational chemistry. 2009;30(16):2785-91.

22. Lindahl A. Hess, & van der Spoel.(2020). GROMACS 20202 Source code. 2021.

23. Sousa da Silva AW, Vranken WF. ACPYPE-Antechamber python parser interface. BMC research notes. 2012;5(1):1-8.

24. Berendsen HJ, Postma Jv, Van Gunsteren WF, DiNola A, Haak JR. Molecular dynamics with coupling to an external bath. The Journal of chemical physics. 1984;81(8):3684-90.

25. Lipinski CA, Lombardo F, Dominy BW, Feeney PJ. Experimental and computational approaches to estimate solubility and permeability in drug discovery and development settings. Advanced drug delivery reviews. 1997;23(1-3):3-25.

26. Liu X, Zhang B, Jin Z, Yang H, Rao Z. The crytal structure of 2019-nCoV main protease in complex with an inhibitor N3. RCSB Protein Data Bank. 2020;10.

27. Zhou J, Fang L, Yang Z, Xu S, Lv M, Sun Z, et al. Identification of novel proteolytically inactive mutations in coronavirus 3C-like protease using a combined approach. The FASEB Journal. 2019;33(12):14575-87.

28. Liu X, Wang X-J. Potential inhibitors against 2019-nCoV coronavirus M protease from clinically approved medicines. Journal of Genetics and Genomics. 2020;47(2):119.

29. MARION F, LIEBY-MULLER F, GRISONI S, RAHIER N, PEREZ M, SARTORI I, inventorsGRISEOFULVIN DERIVATIVES patent WO/2014/020101. 2014.

30. Krämer A, Rebacz B, Clausen M, Larsen T, Roennest M, Worm K, inventors; Deutsches Krebsforschungszentrum DKFZ, assignee. 2009.

31. Santos RAS, Sampaio WO, Alzamora AC, Motta-Santos D, Alenina N, Bader M, et al. The ACE2/angiotensin-(1–7)/MAS axis of the renin-angiotensin system: focus on angiotensin-(1–7). Physiological reviews. 2017.

32. Lan J, Ge J, Yu J, Shan S, Zhou H, Fan S, et al. Structure of the SARS-CoV-2 spike receptor-binding domain bound to the ACE2 receptor. Nature. 2020;581(7807):215-20.

33. Donoghue M, Hsieh F, Baronas E, Godbout K, Gosselin M, Stagliano N, et al. A novel angiotensin-converting enzyme–related carboxypeptidase (ACE2) converts angiotensin I to angiotensin 1-9. Circulation research. 2000;87(5):e1-e9.

34. Hamming I, Timens W, Bulthuis M, Lely A, Navis Gv, van Goor H. Tissue distribution of ACE2 protein, the functional receptor for SARS coronavirus. A first step in understanding SARS pathogenesis. The Journal of Pathology: A Journal of the Pathological Society of Great Britain and Ireland. 2004;203(2):631-7.

35. Zhang H, Li H-B, Lyu J-R, Lei X-M, Li W, Wu G, et al. Specific ACE2 expression in small intestinal enterocytes may cause gastrointestinal symptoms and injury after 2019-nCoV infection. International Journal of Infectious Diseases. 2020;96:19-24.

36. Sargsyan K, Grauffel C, Lim C. How molecular size impacts RMSD applications in molecular dynamics simulations. Journal of chemical theory and computation. 2017;13(4):1518-24.

37. Campagnola G, Gong P, Peersen OB. High-throughput screening identification of poliovirus RNA-dependent RNA polymerase inhibitors. Antiviral research. 2011;91(3):241-51.

38. Tian L, Qiang T, Liang C, Ren X, Jia M, Zhang J, et al. RNA-dependent RNA polymerase (RdRp) inhibitors: The current landscape and repurposing for the COVID-19 pandemic. European journal of medicinal chemistry. 2021;213:113201.

39. Das K, Aramini JM, Ma L-C, Krug RM, Arnold E. Structures of influenza A proteins and insights into antiviral drug targets. Nature structural & molecular biology. 2010;17(5):530-8.

40. Sampath A, Padmanabhan R. Molecular targets for flavivirus drug discovery. Antiviral research. 2009;81(1):6-15.

41. Wang Y, Anirudhan V, Du R, Cui Q, Rong L. RNA-dependent RNA polymerase of SARS-CoV-2 as a therapeutic target. Journal of medical virology. 2021;93(1):300-10.

42. Zhu W, Chen CZ, Gorshkov K, Xu M, Lo DC, Zheng W. RNA-dependent RNA polymerase as a target for COVID-19 drug discovery. SLAS DISCOVERY: Advancing the Science of Drug Discovery. 2020;25(10):1141-51.

43. Seyran M, Takayama K, Uversky VN, Lundstrom K, Palù G, Sherchan SP, et al. The structural basis of accelerated host cell entry by SARS-CoV-2. The FEBS journal. 2021;288(17):5010-20.

44. Durmaz B, Abdulmajed O, Durmaz R. Mutations observed in the SARS-CoV-2 spike glycoprotein and their effects in the interaction of virus with ACE-2 receptor. Medeniyet medical journal. 2020;35(3):253.

45. Wang C, Li W, Drabek D, Okba N, van Haperen R, Osterhaus AD, et al. A human monoclonal antibody blocking SARS-CoV-2 infection. Nature communications. 2020;11(1):1-6.

46. Daina A, Michielin O, Zoete V. SwissADME: a free web tool to evaluate pharmacokinetics, drug-likeness and medicinal chemistry friendliness of small molecules. Scientific reports. 2017;7(1):1-13.

CHAPTER FOUR

Computational Design of Novel Griseofulvin Derivatives Demonstrating Potential Antibacterial Activity: Insights from Molecular Docking and Molecular Dynamics Simulation

This chapter is published.

Aris P, Mohamadzadeh M, Zarei M, Xia X. Computational Design of Novel Griseofulvin Derivatives Demonstrating Potential Antibacterial Activity: Insights from Molecular Docking and Molecular Dynamics Simulation. International Journal of Molecular Sciences. 2024;25(2):1039.

4.1. Author Contributions

Parisa Aris [1]*, Masoud Mohamadzadeh [2], Maaroof Zarei [2,3] and Xuhua Xia [1,4]*

1. Department of Biology, University of Ottawa, 30 Marie Curie, P.O. Box 450, Ottawa, ON K1N 6N5, Canada

2. Department of Chemistry, Faculty of Sciences, University of Hormozgan, Bandar Abbas 71961, Iran;
masoud.mohamadzadehh@gmail.com (M.M.); mzarei57@gmail.com (M.Z.)

3. Nanoscience, Nanotechnology and Advanced Materials Research Center, University of Hormozgan,
Bandar Abbas 71961, Iran

4. Ottawa Institute of Systems Biology, Ottawa, ON K1H 8M5, Canada

P.A., M.M., and M.Z. designed the study. P.A. and M.M. collected and analyzed the data. P.A. wrote the original draft of the manuscript. M.M. and X.X. reviewed and edited the manuscript.

X.X. designed, supervised, and coordinated the study. All authors have read and agreed to the published version of the manuscript.

4.2. Abstract

In response to the urgent demand for innovative antibiotics, theoretical investigations have been employed to design novel analogs. Because griseofulvin is a potential antibacterial agent, we have designed novel derivatives of griseofulvin to enhance its antibacterial efficacy and to evaluate their interactions with bacterial targets using *in silico* analysis. The results of this study reveal that the newly designed derivatives displayed the most robust binding affinities towards PBP2, tyrosine phosphatase, and FtsZ proteins. Additionally, molecular dynamics (MD) simulations underscored the notable stability of these derivatives when engaged with the FtsZ protein, as evidenced by root mean square deviation (RMSD), root mean square fluctuation (RMSF), radius of gyration (Rg), and solvent-accessible surface area (SASA). Importantly, this observation aligns with expectations, considering that griseofulvin primarily targets microtubules in eukaryotic cells, and FtsZ functions as the prokaryotic counterpart to microtubules. These findings collectively suggest the promising potential of griseofulvin and its designed derivatives as effective antibacterial agents, particularly concerning their interaction with the FtsZ protein. This research contributes to the ongoing exploration of novel antibiotics and may serve as a foundation for future drug development efforts.

4.3. Introduction

A dramatic upsurge in bacterial infections coupled with a growing resistance to existing antibiotics poses a serious threat to the global healthcare system (1, 2). The majority of antibiotics were discovered during the golden age of antibiotic therapy, which started in 1928 with penicillin discovery and peaked in the middle of 1950 (3). However, there has been a gradual decline in antibiotic discovery and development since then, leading to the emergence of drug resistance in many human infections and the current antimicrobial resistance crisis (2, 4). More than half of the known natural product antibiotic classes are produced by filamentous actinomycetes, with the remainder originating from other bacteria and fungi (5).

Griseofulvin is a fungal natural product and secondary polyketide metabolite that was initially isolated from *P. griseofulvum* in 1939 and has since been found in various other fungal species (6-8). A comparative genome analysis of over 250 fungal species revealed that only seven out of the thirteen putative genes in the *gsf* cluster are conserved among most genomes and may play a crucial role in griseofulvin production (9). Griseofulvin has been primarily employed to treat dermatophyte infections, but it has also garnered attention due to its potential in treating colon and breast cancer (10), inhibiting the replication of the hepatitis C virus (HCV) (11), and most recently, its potential therapeutic applications for COVID-19 (12).

Research has shown that griseofulvin can inhibit tubulin polymerization and microtubule dynamics, leading to the suppression of cell division and, ultimately, cell death (13, 14). To understand the molecular interactions of griseofulvin with various β-tubulin isotypes, molecular docking and molecular dynamics simulations were conducted recently (15). Additionally, griseofulvin has been found to bind to keratin cytoskeleton intermediate filament proteins K8

and K18, altering keratin solubility and causing the formation of Mallory bodies (MBs) in hepatocytes (16). While humans and rodents may experience hepatitis and MB formation following griseofulvin treatment, severe hepatitis is more common in rodents due to the stronger binding affinity of griseofulvin to K18 in rodents compared to humans (16).

Due to its low toxicity and wide-ranging applications, griseofulvin has garnered renewed interest in recent years. Previous studies have indicated its promising antibacterial activity against various bacteria, although its effects differ across bacterial species, and the underlying molecular mechanisms remain poorly understood (17). Given the scarcity of newly discovered antibiotics in the past two decades, despite extensive screening of bacterial and fungal secondary metabolites, there is an urgent need to develop more effective antibiotics to address this global crisis.

Schiff bases, or imines, play a vital role in the synthesis of bioactive compounds, including β-lactams (18-20). Key components like 6-aminopenicillanic acid (6-APA) and 7-aminocephalosporanic acid (7-ACA) are essential in the production of penicillins and cephalosporins (21). Through chemical modifications of semisynthetic 6-APA and 7-ACA, more than fifty commercial antibiotics have been developed and manufactured (22). Previously reported, benzenesulfonyl hydrazones are known for their potential antibacterial activity, belonging to a class of compounds with diverse biological activities in medicine, primarily in the areas of antibacterial, antifungal, anticancer, and antidepressant effects (23). Aromatic amine 3,4-dichloroaniline is exclusively used as an intermediate in the chemical industry for synthesizing the antibacterial agent triclocarban, particularly effective against Gram-positive bacteria, such as Staphylococcus aureus (24). Reports suggest that the presence of a methylenedioxy ring in derivatives of methylenedioxy aniline may enhance their antibacterial

activity (25). Notably, morpholine, a strong alkali, is a crucial precursor in antibiotic production (26).

Theoretical studies play a crucial role in accelerating drug development and conserving resources. Several successful examples of computational studies in medicine showcase the transformative impact of theoretical studies on drug development and discovery. From identifying potential targets for the hepatitis C virus (27) to repurposing safe medicines for the treatment of multidrug-resistant tuberculosis bacteria (28), these advancements highlight the versatility of computational approaches. These successes underscore the potential of integrating computational tools into medical research, offering innovative solutions to some of the most challenging healthcare problems. Taking into account the antibacterial potential of the mentioned compounds, we aimed to design novel griseofulvin analogs as antibacterial agents and conducted *in silico* studies to investigate their binding affinities and stability towards potential bacterial targets. We hypothesized that griseofulvin and its newly designed derivatives might have the potential to interact favorably with the ftsZ protein in bacterial cells, considering its structural similarity to microtubules (29), which are the primary targets of griseofulvin.

4.4. Materials and Methods

4.4.1. Design novel derivatives

In this study, we employed molecular hybridization technique for drug design and development (30). This method entails the fusion of pharmacophoric elements from different bioactive compounds to generate novel hybrid compounds with superior affinity and effectiveness compared to their parent drugs. Clarivate Analytics Integrity drug discovery and

development portal, available at https://integrity.clarivate.com/, was used to assess the novelty of designed compounds.

4.4.2. Ligand and Receptor Preparation

We initiated the process by designing the two-dimensional structures of ligands using ChemDraw Software. Subsequently, we created and optimized the three-dimensional molecular structures of these compounds with Chem3D. Ligand preparation was conducted using the Ligprep panel in Maestro. For the receptors, we obtained the three-dimensional protein structures in .pdb format from the RCSB Protein Data Bank (PDB). The PDB IDs corresponding to the Tyrosine phosphatase, Filamenting temperature-sensitive mutant Z (ftsZ), UDP-N-acetylglucosamine enolpyruvyl transferase (murA), Penicillin binding protein 2 (PBP2), DNA gyrase subunit B (GyrB), DNA topoIV, and primase proteins were 2M3V, 3VOB, 1UAE, 1VQQ, 4PRV, 1S16, and 1DDE respectively. These proteins are widely recognized as prominent drug targets. All protein structures were subjected to preparation using the Protein Preparation wizard in Maestro.

4.4.3. Drug-Like Properties of the Ligands

To determine the drug-likeness of the molecules, we employed Lipinski's rule of five parameters, which include criteria such as a molecular weight less than 500 Da, no more than 5 hydrogen bond donors, fewer than 10 hydrogen bond acceptors, and a LogP value not exceeding 5 (31). Lipinski's rule of five parameters was obtained using the SwissADME web-based program (www.swissadme.ch/index.php) (32).

4.4.4. Biological Activity Predictions

The biological activity of the designed derivatives was predicted using the PASS Online web service in the Way2Drug web portal (33). The predictions are grounded in structure-activity relationships (SAR) derived from a diverse training set encompassing various chemical classes. The PASS training set includes approximately 7000 antibacterial drugs, and the prediction accuracy for this activity is approximately 0.92. We provided the structural formulas of the compounds in MOL structure-data files as input to PASS, which yielded predictions, including probabilities for the presence of activity (Pa).

4.4.5. *In Silico* Molecular Docking

The molecular docking analyses were carried out using the Schrödinger Suite 2020-3. To determine the binding sites on the targeted proteins, we utilized the computed Atlas of Surface Topography of Proteins (CASTp) server and constructed a grid box around the identified binding pocket, maintaining the default size of 20 Å. Molecular mechanics generalized born surface area (MM-GBSA) method was used to calculate binding free energy in this study (34). The interactions between the ligands and receptors were visualized using Discovery Studio Visualizer v.20.

4.4.6. Molecular Dynamic Simulations

To validate the docking results, molecular dynamics simulations (MD) were performed. The GROMACS-2021 software package was used to analyze the single protein and the two best protein-ligand complexes through 100 ns simulations (35) with an AMBER99SB force field (36). The force field parameters for the ligands were generated by the Ante Chamber PYthon Parser interface (ACPYPE) (37). The solvation of complexes employed the TIP3P water model, with the addition of sodium and chloride ions to maintain charge neutrality. Periodic boundary

conditions (PBC) were applied, and an energy minimization was performed at 1000 kJ/mol/nm. The systems were equilibrated in the NVT and NPT ensembles for 1 ns, with Na+ and Cl− counterions added to achieve charge neutrality and a 0.15 M ionic strength. The temperature and pressure were controlled at 310 K and 1.0 bar, respectively, using the Nose–Hoover thermostat (38), and the Berendsen barostat (39). Trajectories were saved at 2 ps intervals and analyzed post-simulation, which included parameters such as root mean square deviation (RMSD), root mean square fluctuations (RMSF), radius of gyration (Rg), and solvent-accessible surface area (SASA).

4.5. Results and Discussion

In this research, we employed a pioneering molecular hybridization approach in the realm of drug design and development. This method involves the fusion of pharmacophoric elements extracted from various bioactive compounds, resulting in producing novel hybrid compounds that exhibit elevated affinity and efficacy compared to the parent drugs (30). In this study, the imino group, which consists of a nitrogen atom doubly bonded to a carbon atom, served as a versatile linker in molecular structures, providing versatility in synthetic strategies. Imino linkers are stable under a wide range of conditions, making them suitable for use in diverse chemical reactions without undergoing undesired side reactions. There have been previously reported instances of Schiff bases successfully synthesized through this reaction (40, 41).

4.5.1. Structure analysis of novel derivatives

The MOL files of these compounds were used as input data for similarity searches, employing default parameter settings. Notably, none of the six designed compounds exhibited any similarity with existing pharmaceutical agents within the Clarivate Analytics Integrity

database. Table 1 displays the two-dimensional (2D) structures of these newly designed compounds, along with calculated LogP values and ligand bond characteristics. It's worth mentioning that all the examined compounds had molecular weights falling within the range of 471.89 to 670.03 Daltons, with predicted LogP values ranging from 2.87 to 4.39. Each of the derivatives shared attributes such as possessing no more than 10 hydrogen bond acceptors (except for G2) and no more than five hydrogen bond donors. Even though derivative G2 does not fully comply with Lipinski's rules, there are instances of commercially successful used drugs that exhibit non-compliance with these rules (42), suggesting a reconsideration of Lipinski’s rule of five.

Table 4.1. Chemical 2D structures of the novel derivatives along with the Lipinski analysis.

	RNH_2	Lipinski Analysis		2D Structure
Griseofulvin **+RNH_2**	6-APA	Molecular weight Lipophilicity H bond donors H bond acceptors Violations	551.01 3.19 1 10 1	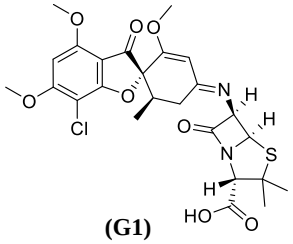 **(G1)**
	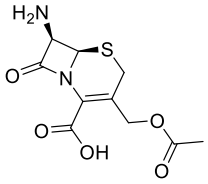 7-ACA	Molecular weight Lipophilicity H bond donors H bond acceptors Violations	607.03 2.87 1 12 2	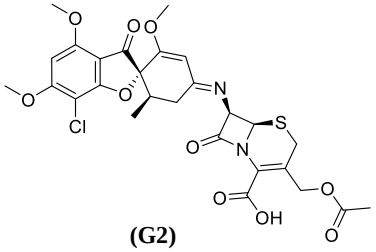 **(G2)**
	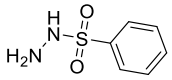 Benzenesulfonyl hydrazine	Molecular weight Lipophilicity H bond donors H bond acceptors Violations	506.96 3.25 1 8 1	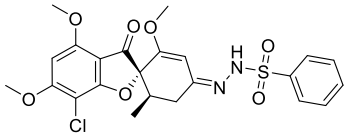 **(G3)**
	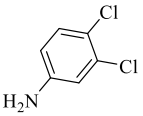 3,4-Dichloroaniline	Molecular weight Lipophilicity H bond donors H bond acceptors Violations	496.77 4.19 0 8 0	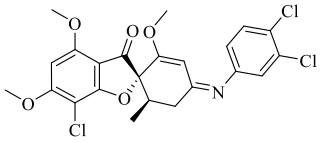 **(G4)**
	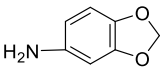 3,4-Methylenedioxy aniline	Molecular weight Lipophilicity H bond donors H bond acceptors Violations	471.89 4.19 0 8 0	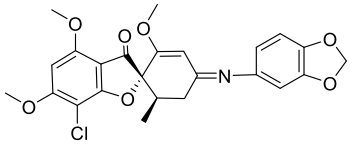 **(G5)**

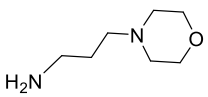

3-Aminopropyl morpholine

Molecular weight	478.97
Lipophilicity	4.39
H bond donors	0
H bond acceptors	8
Violations	0

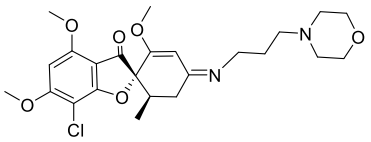

(G6)

To investigate the antibacterial activity of these designed derivatives and comprehend their potential mechanisms of action, we employed an *in silico* approach, involving molecular

docking, molecular dynamics, and Way2Drugs Prediction of Activity Spectra for Substances (PASS). The prediction relies on analyzing the relationships between structure and activity for over 250,000 biologically active compounds. The overall accuracy of predictions is approximately 95% for the entire PASS training set (43). In Table 2, the expected biological activities, particularly focusing on the antibacterial and phosphatase inhibitory effects of the griseofulvin derivatives, are presented. In this study, ciprofloxacin served as the reference drug for activity comparisons. Notably, the results reveal that derivative G2 exhibited antibacterial activity surpassing that of ciprofloxacin. Significantly, all the derivatives exhibited noteworthy potential as inhibitors of phosphatase enzymes, a subject that we will investigate more in-depth in this study.

Table 4.2. Prediction of antibacterial and phosphatase inhibitor activities (Pa) for griseofulvin and derivatives G1-G6.

Compounds	Antibacterial activity (Pa)	phosphatase inhibitor activity (Pa)
G1	0.435	0.803
G2	0.718	0.712
G3	<0.1	0.754
G4	0.304	0.755
G5	0.259	0.727

G6	0.254	0.735
Griseofulvin	0.342	0.803
Ciprofloxacin	0.588	0.301

4.5.2. Molecular Docking Studies

Regarding this prediction, we investigate the potential of the derivatives concerning an important protein phosphatase found in bacteria that plays a pivotal role in regulating various cellular functions (44, 45). This tyrosine phosphatase (PTPs) is an essential virulence factor in pathogenic bacteria such as *Staphylococcus aureus, Mycobacterium tuberculosis, Salmonella typhimurium,* and *Yersinia* sp (45). Notably, Tyrosine phosphatase A (TbpA) from *Pseudomonas aeruginosa* serves as a positive regulator in the formation of biofilms by controlling the concentration of the second messenger cyclic diguanylic acid (c-di-GMP) (46). In this study, derivatives G1-G6 have a strong affinity for Tyrosine phosphatase, with binding energies ranging from -33.65 to -49.01 kcal mol^{-1}. This observation aligns with the predictions made by Way2Drug.

FtsZ is identified as a bacterial homolog to eukaryotic tubulin, forming a dynamic structural framework for the Z-ring, strategically positioned at the midpoint of bacterial cells to govern the process of cytokinesis (29). FtsZ has emerged as a primary target for antibacterial agents due to its indispensable role in cell division across a wide spectrum of bacteria while remaining non-essential in eukaryotes (47, 48). Despite its homology with eukaryotic tubulin, FtsZ shares only a modest 10–18% sequence similarity with tubulin, making it less toxic to eukaryotic cells (49). Our docking analysis at the inter-domain cleft (IDC) has revealed

remarkably strong binding energies between griseofulvin and its derivatives with FtsZ, ranging from -29.48 to -38.59 kcal mol^{-1}.

MurA represents a pivotal target for bacterial replication inhibition since it catalyzes the initial step in peptidoglycan synthesis. In this study, it was observed that the 3-aminopropyl morpholine derivative displayed the most robust binding affinity with MurA, whereas ciprofloxacin did not exhibit any interaction or affinity towards this particular target. Ciprofloxacin, which belongs to the second generation of fluoroquinolones, is known for inhibiting bacterial DNA gyrase and topoisomerase IV (50).

Ciprofloxacin displayed a commendable binding affinity of -38.22 kcal mol^{-1} with GyrB, while G6 exhibited the most favourable binding energy of -41.55 kcal mol^{-1} for this target. Of particular interest, two novel derivatives G3 and G6 demonstrated elevated affinities for DNA topoIV, with binding energies of -40.75 and -40.85 kcal mol^{-1}, surpassing the binding affinity of ciprofloxacin, which was lower when compared to the designed derivatives.

To initiate DNA replication, cellular organisms rely on specialized RNA polymerases called primases to synthesize RNA primers (51). In this study, it was found that G5 and G2 derivatives displayed the most favourable affinity with binding energies of -34.95 and -28.16 kcal mol^{-1} in their interaction with primase, whereas both griseofulvin and ciprofloxacin showed the weakest binding energies, measuring at -17.54 and -18.42 kcal mol^{-1}, in contrast to the new derivatives.

Penicillin-binding proteins (PBPs) are essential proteins in the cell wall peptidoglycan synthesis. Consequently, targeting these proteins could represent one of the most effective strategies for disrupting cell wall biosynthesis. Notably, all of the newly designed derivatives

exhibited the highest affinity for PBP2. In the molecular docking analysis, it was evident that G2 and G3 displayed particularly strong binding affinities, with binding energies of -55.29 and -57.04 kcal mol^{-1}, surpassing the binding energies of other derivatives, which ranged from -40.82 to -52.17 kcal mol^{-1} for PBP2. A comprehensive summary of the binding affinities of these novel analogs, in comparison to the control compounds, for the selected targets is provided in Table 3. Ciprofloxacin served as a control in this study.

Table 4.3. The binding energies (kcal mol^{-1}) of griseofulvin analogs towards bacterial targets from *Pseudomonas aeruginosa*, *Staphylococcus aureus,* and *Escherichia coli*.

	Tyrosine phosphatase (2M3V)	**ftsZ (3VOB)**	**murA (1UAE)**	**PBP2 (1VQQ)**	**GyrB (4PRV)**	**DNA topoIV (1S16)**	**Primase (1DDE)**
G1	-33.65	-29.48	-24.05	-42.09	-30-73	-14.22	-20-02
G2	-33.81	-34.90	-36.90	-55.29	-35.83	-37.57	-28.16
G3	-49.01	-35.62	-34.79	-57.04	-27.77	-40.75	-18.42
G4	-42.85	-35.62	-41.32	-52.17	-38.09	-27.22	-26.86
G5	-36.25	-37.85	-35.57	-49.87	-27.32	-20.58	-34.96
G6	-45.65	-38.59	-46.48	-46.17	-41.55	-40.85	-24.02
Griseofulvin	-22.37	-38.09	-37.94	-40.82	-30.88	-18.85	-17.54
Ciprofloxacin	-25.98	-31.46	0	-43.65	-38.22	-26.65	-18.42

The analysis of hydrogen bonds and hydrophobic interactions involving griseofulvin derivatives, that were subjected to docking with the antibacterial targets listed in Table 4, revealed interesting insights. The outcomes of molecular docking indicated that hydrophobic interactions, including Alkyl, Pi-Anion, and van der Waals forces, played dominant roles in most targets, such as murA, DNA topoIV, and GyrB. In contrast, hydrogen bonds emerged as significant contributors in interactions with Tyrosine phosphatase, ftsZ, and PBP2. Within PBP2,

for instance, the residues Thr216, Arg241, and Ser249 established hydrogen bonds with the carbonyl group of the ligands. In the case of Tyrosine phosphatase, the amino acid Arg106 appeared to be notably vital in facilitating hydrogen bond interactions with the ligands. Furthermore, the amino acid Pro248 in the ftsz protein was observed to form carbon-hydrogen bonds with derivatives G1-G3 and griseofulvin.

Table 4. 4. Molecular docking details of the novel derivatives with antibacterial targets.

Targets	Ligands	Binding Energy (kcal/mol)	H-bonds	Hydrophobic Interaction
Tyrosine phosphatase (2M3V)	G1	-33.65	Arg106	His103, Arg106, Arg117, Leu204
	G2	-33.81	Arg106, Arg117, Ser200	Ser99, Pro101, His103
	G3	-49.01	Arg106, Glu111	Phe81, Ile82, Pro101, His103, Arg106
	G4	-42.85	Arg106	Val79, Ser80, Phe81, Ile82, Ser99, Pro101, His103
	G5	-36.25	Arg106, Ser200	Pro101, Glu111, Ala191, Ala203, Leu204
	G6	-45.65	Arg106	Ser80, Phe81, Ile82, Lys83, Ser99, Glu111, Gly195, Phe202
	Griseofulvin	-22.37	Arg106	Arg106, Glu111, Ala191, Ser198
	Ciprofloxacin	-25.98	Leu100, Arg106	Leu100, Pro101, Glu111, Gly195
ftsZ (3VOB)	G1	-29.48	Val230, Lys243, Leu249	Ile228, Pro248
	G2	-34.90	Gln192	Glu185,Gly227, Ile228, Ala244, Ser246, Pro248, Leu250,
	G3	-35.62	-	Val189, Ile228, Val230, Pro248
	G4	-35.62	Gln192	Lys184, Glu185, Ser246, Leu225, Ala244, Leu250
	G5	-37.85	Ser246	Glu185, Asn188, Gly227, Lys243
	G6	-38.59	-	Met226, Gly227, Val230, Lys243, Ser246
	Griseofulvin	-38.09	Asn188, Gln192, Leu249	Val230, Lys243, Pro248
	Ciprofloxacin	-31.46	-	Gly227, Ile228, Lys243, Ser246, Pro248, Leu249
murA (1UAE)	G1	-24.05	Asn23, Cys115	Lys22, Arg120, Gly114, Pro121, Val327, Phe328, Arg397
	G2	-36.90	Arg120, Gly164	Leu26, Arg91, Ala92, Ile94, Trp95, His125, Val163, Arg120, Lys160, Phe328
	G3	-34.79	Arg120, Lys160	Asn23, Arg91, Alys160, Val161, Val163, Asp305, Phe328, Glu329,
	G4	-41.32	Ser162, Val163, Gly164	Arg91, Trp95, Arg120, Lys160, Val 161, Val 327, Phe328
	G5	-35.57	Thr326	Arg91, Tpr95, Arg120, His125, Val161, Ser162, Val163, Ala297, Pro298, Phe328
	G6	-46.48	Cys115, Val163, Arg120	Asp305, Val327, Phe328
	Griseofulvin	-37.94	Lys22, Arg120	Val163, Pro298, Val327, Phe328
	Ciprofloxacin	0	-	-
	G1	-42.09	Thr216, Ser240, Arg241	Tyr196, Ile192, Lys215
	G2	-55.29	Thr216, Arg241	Ile192, Tyr196, Lys215, Val277

PBP2 (1VQQ)	G3	-57.04	Thr216, Ser240, Arg241	Lys148, Ser149, Arg241, His293
	G4	-52.17	Thr165, Thr216	Arg151, Lys215, Ser240, Pro258, Tyr373
	G5	-49.87	Thr216, Ser240, Arg241	Lys148, Ser149, Thr165, Thr216, Arg241, Val277
	G6	-46.17	Ser240, Arg241	Lys148, Ser149, Thr165, Thr216, Arg241, His293, Met372
	Griseofulvin	-40.82	Ser240, Arg241	Arg241, Val277, His293
	Ciprofloxacin	-43.65	Arg151, Glu170, Thr216, Thr238, Ser240	Val277
GyrB (4PRV)	G1	-30-73	His 38	Thr34, His38, Ile27, Tyr267, Pro274, Arg276, Asp338,
	G2	-35.83	Cys268, Arg276	Phe41, Tyr267, Cys268, Phe269, Pro274, Arg276
	G3	-27.77	His38, Arg276, Asp338	Lys189, Arg190, Glu193, Pro274, Tyr267, Asp338
	G4	-38.09	-	His38, Phe41, Tyr267, Pro274, Arg276
	G5	-27.32	-	Lys189, Glu193, Tyr267, Pro274, Arg276
	G6	-41.55	-	His38, Phe41, Lys189, Tyr228, Pro274, Arg276, Asp338
	Griseofulvin	-30.88	Cys268	Ile266, Tyr267, Cys268, Phe269, Pro274, Arg276
	Ciprofloxacin	-38.22	His38, Glu193	Lys189, Pro274, Arg276
DNA topoIV (1S16)	G1	-14.22	Arg1031, Arg1183	Arg1031, Arg1183, Thr1264, Ser1266, Met1274, Tyr1318
	G2	-37.57	Thr1264, Gln1037	Arg1031, Arg1183, His1186, Leu1262, Thr1264, Ser1266, Thr1273
	G3	-40.75	Ser1182, Thr1264	Met1274
	G4	-27.22	-	Ser1182, Arg1183, His1186, Val1187, Met1274
	G5	-20.58	Arg1183	His1034, Arg1183, His1186, Val1187, Met1274
	G6	-40.85	Lys1189	His1034, Arg1183, His1186, Val1187, Tyr1222, Met1274
	Griseofulvin	-18.85	Arg1183	His1034, Arg1183, His1186, Val1187, Met1274, Pro1272
	Ciprofloxacin	-26.65	Asp1028	Arg1183, His1186, Val1187, Pro1272, Met1274
Primase (1DDE)	G1	-20-02	Lys229, Asp345	Arg146,Arg221, Lys229, Arg221,Tyr230, Asn232, Gly266, Tyr267, Met268, Leu285, Thr287, Asp309, Asp345
	G2	-28.16	Arg146, Lys229	Arg146, Arg221, Lys229, Tyr230, Asn232, Gly266, Tyr267, Met268, Asp269, Gly286, Thr287, Asp309
	G3	-18.42	Asp345	Tyr230, Gly266, Tyr267, Met268, Asp269, Ser284, Asp309, Asp345
	G4	-26.86	Lys229	Tyr230, Glu265, Tyr267
	G5	-34.96	Lys229	Lys229, Tyr230, Asn232, Glu265, Gly266, Tyr267, Met268, Leu285
	G6	-24.02	Arg221, Lys229, Tyr230	Tyr142, Arg146, Gly266, Met268
	Griseofulvin	-17.54	-	Lys229, Tyr230, Gly266, Met268, Asp345, Asp347
	Ciprofloxacin	-18.42	Tyr230, Tyr267, Asp345	Tyr230, Asn232, Asp269, Gly286, Asp345

4.5.3. MD Simulations

The top three docked complexes were subjected to 100 ns of MD simulations to investigate the protein structural stability and conformational changes. Noteworthy, all derivatives exhibited the strongest binding affinity with PBP2. The molecular docking analysis of tyrosine phosphatase is in good agreement with the biological activity prediction by PASS.

Furthermore, the derivatives displayed favourable binding to ftz, a microtubule homolog that griseofulvin might target. The simulations trajectory files were examined for root-mean-square deviation (RMSD), root mean square fluctuation (RMSF), radius of gyration (Rg), and solvent-accessible surface area (SASA).

4.5.3.1. Structural Dynamics of PBP2 (1VQQ)

Molecular dynamics simulations were used to study the complex of PBP2 enzyme and the novel derivatives. The root mean square deviation (RMSD) was calculated to evaluate the stability of these complexes. The RMSD of the enzyme in the absence of ligand exhibited fluctuations around an average value of 0.35 nm. Upon binding of analogs, the RMSD values increased from 0.36 to 0.91 nm, indicating conformational changes in the enzyme upon complex formation. Smaller RMSD values correspond to more steadfast protein structures. RMSF (Root Mean Square Fluctuation) plots were analyzed for both the ligand-free and ligand-bound states. In the absence of the ligand, the enzyme exhibited an average RMSF of 0.19 nm. However, upon ligand binding, the average RMSD values of G2, G4, and G6 were decreased to 0.18, 0.14, and 0.13 nm respectively, indicating the stability of complexes during the simulation. Radius of gyration (Rg) provides insight into the protein's structural compactness. When Rg is smaller, it suggests a more tightly packed protein structure. In the case of the complexes, the average Rg values remained mostly unchanged or slightly decreased, indicating the ligand binding did not significantly alter the structural compactness of PBP2. Solvent Accessible Surface Area analysis (SASA) was used to measure the surface area of a compound that is accessible to solvent molecules. The mean SASA measurements for derivatives remained almost unchanged when they bound to PBP2. This observation implies that the protein undergone conformational changes at a comparatively slow rate and no equilibrium has been reached, as evidenced by its

solvent accessibility. Overall, the analysis suggests that no equilibrium has been reached for this target during the last 20 ns of MD simulations.

Table 4.5. The average of RMSD, RMSF, Rg, and SASA for PBP2 during the last 20 ns of MD simulations.

Complex	Mean RMSD (nm)	Mean RMSF (nm)	Mean Rg (nm)	Mean SASA (nm²)
PBP2	0.35±0.05	0.19±0.1	3.7±0.0	319±3.3
G1	0.36±0.05	0.21±0.1	3.7±0.0	320±3.2
G2	0.71±0.08	0.18±0.08	3.5±0.0	313±3
G3	0.49±0.12	0.25±0.1	3.6±0.0	319±3.1
G4	0.91±0.03	.014±0.05	3.4±0.0	310±3
G5	0.38±0.06	0.21±0.1	3.7±0.0	320±3.3
G6	0.84±0.03	0.13±0.05	3.4±0.0	312±3
Griseofulvin	0.84±0.06	0.17±0.07	3.5±0.0	318±4
Ciprofloxacin	0.39±0.04	0.19±0.08	3.7±0.0	317±3

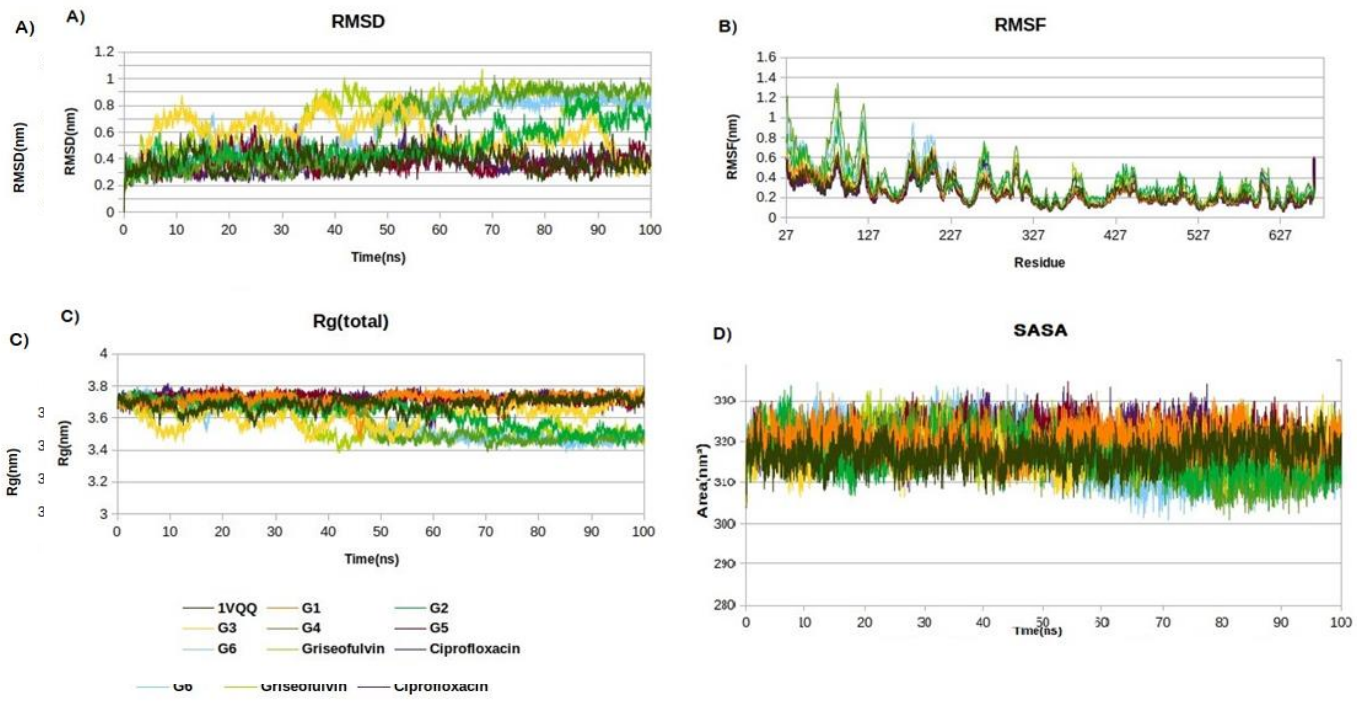

Figure 4.1. Structural dynamics of PBP2 protein. (A) Root mean square deviation (RMSD), (B) root mean square fluctuations (RMSF), (C) radius of gyration (Rg) plot, and (D) solvent-accessible surface area (SASA).

4.5.3.2. Structural Dynamics of Tyrosine Phosphatase (2M3V)

The MD analysis showed the average RMSD values for all derivatives but G3 decreased up to 0.15 nm when binding to tyrosine phosphatase (Table 6). This finding illustrates the stability of these complexes within the active pocket of tyrosine phosphatase, with only a slight increase in residual fluctuations (Fig 2B). Ciprofloxacin demonstrated a significantly elevated Root Mean Square Deviation (RMSD) from 0.73 to 0.85 nm, which is in line with expectations, as tyrosine phosphatase is not a conventional molecular target for ciprofloxacin. The average RMSF and Rg values of the complexes exhibited negligible alterations, indicating their structural packing closely resembles that of tyrosine phosphatase alone. The average SASA values for the derivatives exhibited a notable increase, going from 88 to 118 nm^2. This observation indicates

that the internal residues within tyrosine phosphatase become more accessible to solvents and that there is an expansion in protein volume upon the binding of the derivatives.

Table 4.6. The average of RMSD, RMSF, Rg, and SASA for tyrosine phosphatase protein during the last 20 ns of MD simulations.

Complex	Mean RMSD (nm)	Mean RMSF (nm)	Mean Rg (nm)	Mean SASA (nm²)
Tyrosine Phosphatase	0.73±0.01	0.12±0.7	1.6±0.1	88±2
G1	0.66±0.01	0.15±0.09	1.7±0.1	114±2
G2	0.62±0.01	0.13±0.06	1.7±0.1	113±3
G3	0.77±0.01	0.18±0.1	1.6±0.1	118±2
G4	0.62±0.01	0.11±0.05	1.7±0.1	110±2
G5	0.58±0.01	0.13±0.07	1.7±0.1	109±2
G6	0.61±0.03	0.16±0.13	1.7±0.1	113±2
Griseofulvin	0.72±0.02	0.15±0.12	1.7±0.1	114±2
Ciprofloxacin	0.85±0.04	0.20±0.17	1.7±0.1	117±2

Figure 4.2. Structural dynamics of tyrosine phosphatase protein. (A) Root mean square deviation (RMSD), (B) root mean square fluctuations (RMSF), (C) radius of gyration (Rg) plot, and (D)

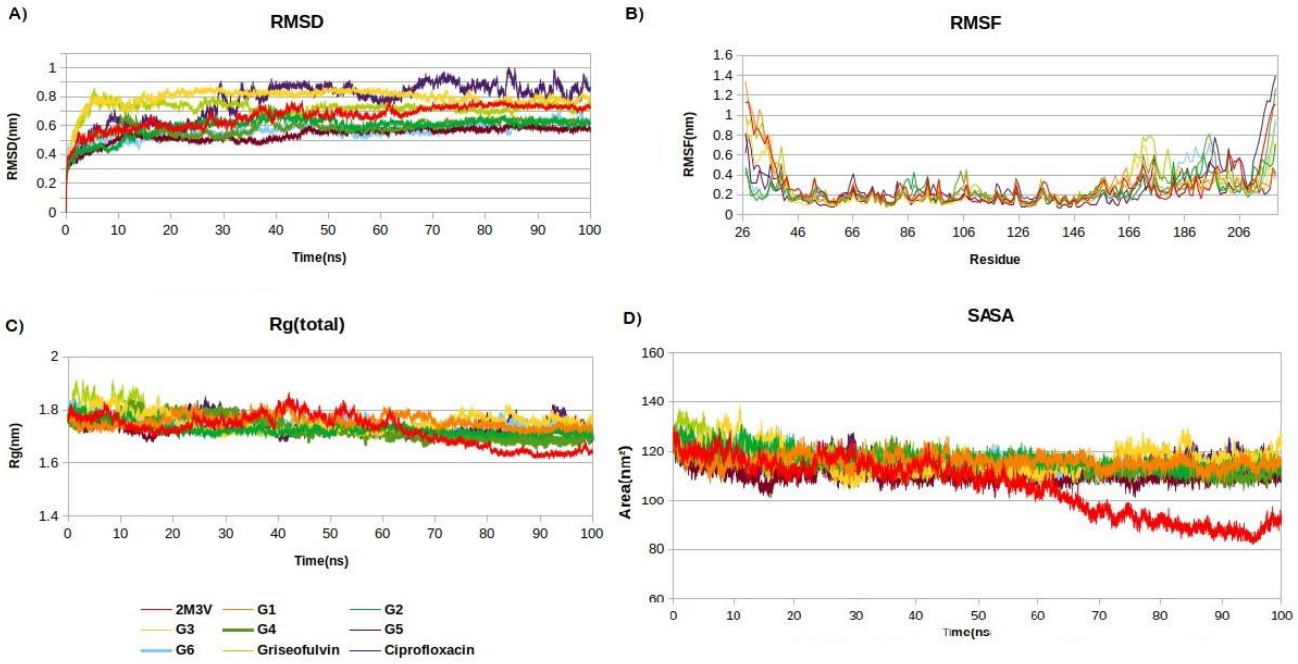

4.5.3.3. Structural Dynamics of ftsZ (3VOB)

The RMSD trajectory assesses the deviation of complexes from the reference structure. When ligands bind to the receptor-binding pocket, they contribute to the conformational stability of the macromolecular system. As shown in Table 7, all complexes displayed a lower RMSD compared to ftsZ alone, signifying the structural stability of the designed derivatives within the active pocket of ftsZ protein. The average RMSF values for the complexes in the final 20 ns of the MD simulations indicated that the fluctuations in their constituent residues remained below 0.2 nm, which is considered satisfactory. The Rg plot indicates that there are no notable variations in the arrangement of ftsZ when ligands are bound. From the SASA plot in Figure 3D, it is evident that the complexes exhibit higher SASA values compared to the standalone ftsZ protein. This indicates an expansion in the solvent-accessible surface area, contributing to enhanced protein stability.

Table 4.7. The average of RMSD, RMSF, Rg, and SASA for ftsZ protein during the last 20 ns of MD simulations.

Complex	Mean RMSD (nm)	Mean RMSF (nm)	Mean Rg (nm)	Mean SASA (nm²)
ftsZ	0.31±0.01	0.11±0.04	1.9±0.0	136±2
G1	0.28±0.01	0.12±0.05	1.9±0.01	137±2
G2	0.27±0.01	0.09±0.04	1.9±0.0	137±3
G3	0.29±0.01	0.11±0.05	1.9±0.0	138±2
G4	0.27±0.01	0.10±0.05	1.9±0.0	138±2
G5	0.33±0.01	0.10±0.04	1.9±0.0	136±2
G6	0.28±0.01	0.12±0.06	1.9±0.0	143±2
Griseofulvin	0.33±0.01	0.10±0.04	1.9±0.0	130±3
Ciprofloxacin	0.29±0.01	0.11±0.04	1.9±0.01	138±2

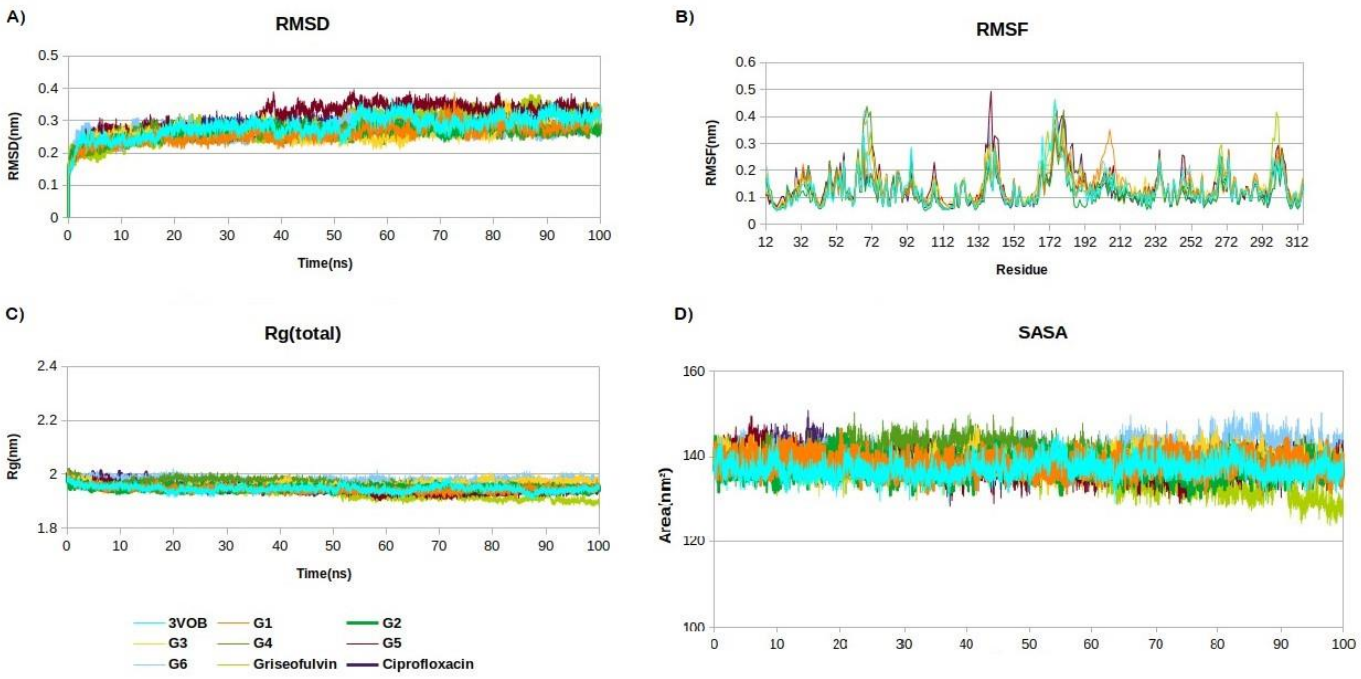

Figure 4.3. Structural dynamics of ftsZ protein. (A) Root mean square deviation (RMSD), (B) root mean square fluctuations (RMSF), (C) radius of gyration (Rg) plot, and (D) solvent-accessible surface area (SASA).

4.6. Funding

This work is supported by the Natural Sciences and Engineering Research Council of Canada (NSERC) Discovery Grant to X.X. (RGPIN/2018-03878). P.A. was supported by an Ontario Graduate Scholarship (2023-2024).

4.7. Acknowledgments

The authors would like to thank the joint editor and referees for their helpful comments that greatly improved the presentation of the study. The computational resources were provided by Compute Canada.

4.8. References

1. Aslam B, Wang W, Arshad MI, Khurshid M, Muzammil S, Rasool MH, et al. Antibiotic resistance: a rundown of a global crisis. Infection and drug resistance. 2018;11:1645.
2. Talebi Bezmin Abadi A, Rizvanov AA, Haertlé T, Blatt NL. World Health Organization report: current crisis of antibiotic resistance. BioNanoScience. 2019;9:778-88.
3. Hutchings MI, Truman AW, Wilkinson B. Antibiotics: past, present and future. Current opinion in microbiology. 2019;51:72-80.
4. Roope LS, Smith RD, Pouwels KB, Buchanan J, Abel L, Eibich P, et al. The challenge of antimicrobial resistance: what economics can contribute. Science. 2019;364(6435):eaau4679.
5. De Simeis D, Serra S. Actinomycetes: A never-ending source of bioactive compounds—An overview on antibiotics production. Antibiotics. 2021;10(5):483.
6. Grove JF, MacMillan J, Mulholland T, Rogers MT. 759. Griseofulvin. Part I. Journal of the Chemical Society (Resumed). 1952:3949-58.
7. Mead ME, Raja HA, Steenwyk JL, Knowles SL, Oberlies NH, Rokas A. Draft genome sequence of the griseofulvin-producing fungus Xylaria flabelliformis strain G536. Microbiology Resource Announcements. 2019;8(38):e00890-19.
8. PARK J-H, CHOI G-J, LEE S-W, LEE H-B, KIM K-M, JUNG H-S, et al. Griseofulvin from Xylaria sp. strain F0010, an endophytic fungus of Abies holophylla and its antifungal activity against plant pathogenic fungi. Journal of Microbiology and Biotechnology. 2005;15(1):112-7.
9. Aris P, Yan L, Wei Y, Chang Y, Shi B, Xia X. Conservation of griseofulvin genes in the gsf gene cluster among fungal genomes. G3 Genes| Genomes| Genetics. 2021.
10. Rebacz B, Larsen TO, Clausen MH, Rønnest MH, Löffler H, Ho AD, et al. Identification of griseofulvin as an inhibitor of centrosomal clustering in a phenotype-based screen. Cancer research. 2007;67(13):6342-50.
11. Rathinasamy K, Jindal B, Asthana J, Singh P, Balaji PV, Panda D. Griseofulvin stabilizes microtubule dynamics, activates p53 and inhibits the proliferation of MCF-7 cells synergistically with vinblastine. Bmc Cancer. 2010;10:1-13.
12. Aris P, Mohamadzadeh M, Wei Y, Xia X. In Silico Molecular Dynamics of Griseofulvin and Its Derivatives Revealed Potential Therapeutic Applications for COVID-19. International journal of molecular sciences. 2022;23(13):6889.

13. Rebacz B, Larsen TO, Clausen MH, Rønnest MH, Löffler H, Ho AD, et al. Identification of griseofulvin as an inhibitor of centrosomal clustering in a phenotype-based screen. Cancer research. 2007;67(13):6342-50.
14. Gull K, Trinci A. Griseofulvin inhibits fungal mitosis. Nature. 1973;244(5414):292-4.
15. Aris P, Mohamadzadeh M, Kruglikov A, Askari Rad M, Xia X. In Silico Exploration of Microtubule Agent Griseofulvin and Its Derivatives Interactions with Different Human β-Tubulin Isotypes. Molecules. 2023;28(5):2384.
16. Aris P, Wei Y, Mohamadzadeh M, Xia X. Griseofulvin: An Updated Overview of Old and Current Knowledge. Molecules. 2022;27(20):7034.
17. Geronikaki A, Kartsev V, Petrou A, Akrivou M, Vizirianakis I, Chatzopoulou FM, et al. Antibacterial activity of griseofulvin analogues as an example of drug repurposing. International journal of antimicrobial agents. 2020;55(3):105884.
18. Venturini A, González J. A CASPT2 and CASSCF approach to the cycloaddition of ketene and imine: A new mechanistic scheme of the staudinger reaction. The Journal of Organic Chemistry. 2002;67(25):9089-92.
19. Taggi AE, Hafez AM, Wack H, Young B, Ferraris D, Lectka T. The development of the first catalyzed reaction of ketenes and imines: catalytic, asymmetric synthesis of β-lactams. Journal of the American Chemical Society. 2002;124(23):6626-35.
20. Mohamadzadeh M, Zarei M, Vessal M. Synthesis, in vitro biological evaluation and in silico molecular docking studies of novel β-lactam-anthraquinone hybrids. Bioorganic Chemistry. 2020;95:103515.
21. Hamilton-Miller J. Development of the semi-synthetic penicillins and cephalosporins. International journal of antimicrobial agents. 2008;31(3):189-92.
22. Rolinson G, Geddes A. The 50th anniversary of the discovery of 6-aminopenicillanic acid (6-APA). International journal of Antimicrobial agents. 2007;29(1):3-8.
23. Popiołek Ł. The bioactivity of benzenesulfonyl hydrazones: A short review. Biomedicine & Pharmacotherapy. 2021;141:111851.
24. Iacopetta D, Catalano A, Ceramella J, Saturnino C, Salvagno L, Ielo I, et al. The different facets of triclocarban: A review. Molecules. 2021;26(9):2811.

25. Laurentiz RS, Gomes WP, Pissurno AP, Santos FA, Santos VCO, Martins CH. Synthesis and antibacterial activity of new lactone 1, 4-dihydroquinoline derivatives. Medicinal Chemistry Research. 2018;27:1074-84.
26. Goudarziafshar H, Rezaeivala M, Khosravi F, Abbasityula Y, Yousefi S, Özbek N, et al. Synthesis, characterization and crystal structures of new Zinc (II) and Nickel (II) complexes containing morpholine moiety and their antibacterial studies. Journal of the Iranian Chemical Society. 2015;12:113-9.
27. Dey D, Biswas P, Paul P, Mahmud S, Ema TI, Khan AA, et al. Natural flavonoids effectively block the CD81 receptor of hepatocytes and inhibit HCV infection: a computational drug development approach. Molecular Diversity. 2023;27(3):1309-22.
28. Kinnings SL, Liu N, Buchmeier N, Tonge PJ, Xie L, Bourne PE. Drug discovery using chemical systems biology: repositioning the safe medicine Comtan to treat multi-drug and extensively drug resistant tuberculosis. PLoS computational biology. 2009;5(7):e1000423.
29. Wang M, Fang C, Ma B, Luo X, Hou Z. Regulation of cytokinesis: FtsZ and its accessory proteins. Current genetics. 2020;66:43-9.
30. Viegas-Junior C, Danuello A, da Silva Bolzani V, Barreiro EJ, Fraga CAM. Molecular hybridization: a useful tool in the design of new drug prototypes. Current medicinal chemistry. 2007;14(17):1829-52.
31. Lipinski CA, Lombardo F, Dominy BW, Feeney PJ. CAS: 528: DC% 2BD3MXitVOhs7o% 3D: Experimental and computational approaches to estimate solubility and permeability in drug discovery and development settings. vol. 46, issue 1-3. Adv Drug Deliv Rev. 2001:3-26.
32. Daina A, Michielin O, Zoete V. SwissADME: a free web tool to evaluate pharmacokinetics, drug-likeness and medicinal chemistry friendliness of small molecules. Scientific reports. 2017;7(1):42717.
33. Druzhilovskiy D, Rudik A, Filimonov D, Gloriozova T, Lagunin A, Dmitriev A, et al. Computational platform Way2Drug: from the prediction of biological activity to drug repurposing. Russian Chemical Bulletin. 2017;66:1832-41.
34. Genheden S, Ryde U. The MM/PBSA and MM/GBSA methods to estimate ligand-binding affinities. Expert opinion on drug discovery. 2015;10(5):449-61.
35. Abraham L, Hess B, Spoel V. GROMACS 2020.3 source code. Zenodo, in. 2020;317.

36. Hornak V, Abel R, Okur A, Strockbine B, Roitberg A, Simmerling C. Comparison of multiple Amber force fields and development of improved protein backbone parameters. Proteins: Structure, Function, and Bioinformatics. 2006;65(3):712-25.
37. Sousa da Silva AW, Vranken WF. ACPYPE-Antechamber python parser interface. BMC research notes. 2012;5:1-8.
38. Hoover WG. Canonical dynamics: Equilibrium phase-space distributions. Physical review A. 1985;31(3):1695.
39. Berendsen HJ, Postma Jv, Van Gunsteren WF, DiNola A, Haak JR. Molecular dynamics with coupling to an external bath. The Journal of chemical physics. 1984;81(8):3684-90.
40. Jarrahpour A, Khalili D, De Clercq E, Salmi C, Brunel JM. Synthesis, antibacterial, antifungal and antiviral activity evaluation of some new bis-Schiff bases of isatin and their derivatives. Molecules. 2007;12(8):1720-30.
41. Jarrahpour A, Motamedifar M, Pakshir K, Hadi N, Zarei M. Synthesis of novel azo Schiff bases and their antibacterial and antifungal activities. Molecules. 2004;9(10):815-24.
42. Chagas CM, Moss S, Alisaraie L. Drug metabolites and their effects on the development of adverse reactions: Revisiting Lipinski's Rule of Five. International journal of pharmaceutics. 2018;549(1-2):133-49.
43. Filimonov D, Poroikov V. Probabilistic approaches in activity prediction: Royal Society of Chemistry, Cambridge, UK; 2008.
44. Whitmore SE, Lamont RJ. Tyrosine phosphorylation and bacterial virulence. International journal of oral science. 2012;4(1):1-6.
45. Kuban-Jankowska A, Kostrzewa T, Gorska-Ponikowska M. Bacterial Protein Tyrosine Phosphatases as Possible Targets for Antimicrobial Therapies in Response to Antibiotic Resistance. Antioxidants. 2022;11(12):2397.
46. Ueda A, Wood TK. Tyrosine phosphatase TpbA of Pseudomonas aeruginosa controls extracellular DNA via cyclic diguanylic acid concentrations. Environmental microbiology reports. 2010;2(3):449-55.
47. Beall B, Lutkenhaus J. FtsZ in Bacillus subtilis is required for vegetative septation and for asymmetric septation during sporulation. Genes & development. 1991;5(3):447-55.
48. Dai K, Lutkenhaus J. ftsZ is an essential cell division gene in Escherichia coli. Journal of bacteriology. 1991;173(11):3500-6.

49. De Pereda JM, Leynadier D, Evangelio JA, Chacón P, Andreu JM. Tubulin secondary structure analysis, limited proteolysis sites, and homology to FtsZ. Biochemistry. 1996;35(45):14203-15.
50. Pan X-S, Ambler J, Mehtar S, Fisher LM. Involvement of topoisomerase IV and DNA gyrase as ciprofloxacin targets in Streptococcus pneumoniae. Antimicrobial agents and chemotherapy. 1996;40(10):2321-6.
51. Lee J-B, Hite RK, Hamdan SM, Sunney Xie X, Richardson CC, Van Oijen AM. DNA primase acts as a molecular brake in DNA replication. Nature. 2006;439(7076):621-4.

CHAPTER FIVE

Conclusions

In the realm of fungal biology and drug discovery, griseofulvin stands as a compelling subject of study due to its broad spectrum of biological activities. Primarily known for its potent antifungal properties, griseofulvin has also shown promising potential as an antiviral agent, particularly against Hepatitis C virus. Recent advancements in genomic research have shed light on the intricate mechanisms of griseofulvin biosynthesis across diverse fungal species, highlighting its evolutionary adaptations and ecological roles within microbial communities.

Despite these strides, significant gaps persist in our understanding of griseofulvin's biosynthetic pathways, necessitating further exploration into the conservation, evolution, and ecological implications of its biosynthetic genes among fungal genomes. This exploration promises insights into how these genes have evolved to confer competitive advantages in fungal ecological niches and may reveal novel strategies for harnessing griseofulvin's therapeutic potential.

Moreover, the development of novel griseofulvin derivatives tailored for antibacterial activity represents a critical frontier in combating the growing challenge of antibiotic resistance. By leveraging computational approaches such as genomics, bioinformatics, molecular modeling, and molecular dynamics simulations, researchers can accelerate the design and optimization of these derivatives. This multidisciplinary approach not only enhances our understanding of structure-activity relationships but also expedites the translation of theoretical insights into practical applications, thereby bolstering the arsenal against resistant bacterial infections.

This study lays a robust foundation for future investigations aimed at unlocking the full therapeutic repertoire of griseofulvin and its derivatives. By integrating cutting-edge technologies and interdisciplinary expertise, researchers can propel the field towards novel therapeutic strategies that address the complexities of fungal infections, viral diseases, and antibiotic resistance on a global scale.

5.1. Conservation of griseofulvin genes in the *gsf* gene cluster among fungal genomes

This study utilizes genomic analysis to elucidate and characterize the gsf genes responsible for griseofulvin biosynthesis across various fungal species. Initially, we sequenced the genome of *P. griseofulvum* strain D-756 and curated additional fungal genomes from the NCBI database for comparative analysis. A total of 11 gsf biosynthetic gene clusters (BGCs) were examined in comparison to the reference BGC from *P. aethiopicum*, which has a well-established biosynthetic pathway.

Our findings indicate that genes such as *gsfH*, *gsfK*, and *gsfR2* may not be crucial for griseofulvin biosynthesis, consistent with previous research (1, 2). Our results suggest that *gsfH*, *gsfK* and *gsfR2* genes may not be essential for griseofulvin biosynthesis, consistent with findings from a previous study (3). Based on gene conservation between fungal species, a total of seven conserved *gsf* genes were determined, out of the thirteen putative *gsf* cluster genes from *P. aethiopicum* (Chooi et al., 2010). Our results are consistent with those verified by Cacho et al., (2013). Furthermore, our finding also revealed that these seven *gsf* genes were not only maintained, but also have shared sequence orders, between fungal species. However, several differences in these *gsf* genes may lead to either loss of function (LOF) or gain of function (GOF).

An interesting question involving these findings is that species that experience benefits for producing griseofulvin (e.g., eliminating other fungal species to reduce competition) would maintain the griseofulvin gene cluster. If a species is freed from competition (e.g., having evolved to exploit a new carbon source or having colonized an area without competing species, or in areas where resources are abundant), then the advantage of producing griseofulvin disappears and the gene cluster would likely degrade or evolve new functions. Additionally, given that griseofulvin can interfere with mitosis and inhibit cell growth, another interesting question involving those griseofulvin-producing fungal species is their underlying detoxification pathway to protect themselves against griseofulvin. Future analyses to compare the genomes of griseofulvin-producing species and griseofulvin susceptible species could help identify the genes involved in the detoxification pathway.

5.2. *In Silico* Molecular Dynamics of Griseofulvin and its Derivatives Revealed Potential Therapeutic Applications for COVID-19

Several antiviral agents and other conventional treatments are being investigated as a treatment for COVID-19, but therapeutic options remain poor (4, 5). The FDA-approved drug, griseofulvin, has gained many intentions due to its low toxicity (6), and wide applications in treating and suppressing dermatophyte infections, cancer, and hepatitis C virus (7-10). Drug-likeness analysis also shows no violation of Lipinski rule and hepatotoxicity for our studied compounds. Consequently, repurposing and developing derivatives of this compound might be a useful strategy for future therapeutic intervention.

Our *in silico* study results of tested compounds showed good-to-significant activity toward target proteins of SARS-CoV-2. Griseofulvin exhibited the best binding affinity with the

most interactions in form of hydrogen bonds to COVID-19 main protease (6LU7), which is essential for replication and transcription of the novel coronavirus (SARS-CoV-2). However, favourable interactions with ACE2, RBD, and RdRb were also identified for griseofulvin.

Among the derivatives, the molecular docking analysis revealed that M9, A3, Rb3, and Rd2 with a binding affinity greater than -7 kcal/mol could act as the best inhibitors of SARS-CoV-2 main protease, ACE2, RBD, and RdRp respectively. The structure of top ligands suggests that functional groups containing oxygen, such as ether group in compounds M9, A3, and Rb3 may provide more possibilities for better interaction and higher affinity toward receptors. Moreover, structures with sulfonyl group in derivative M7 and fluorobenzene group in Rd2, could enhance the interaction between protein and ligand. The docked results were also supported by MD simulation analysis to affirm the stability of the studied complexes on basis of RMSD, RMSF, Rg, hydrogen bonds (H-bond), and SASA values. These results outline the potential activity of griseofulvin and its derivative as inhibitors of COVID-19. Nevertheless, further in vitro and in vivo investigations are required to validate the effectiveness of proposed targets against SARS-CoV-2.

5.3. Computational Design of Novel Griseofulvin Derivatives Demonstrating Potential Antibacterial Activity: Insights from Molecular Docking and Molecular Dynamics Simulation

In this study, a series of novel griseofulvin derivatives were designed and evaluated for antibacterial activity using computer-aided approaches. Data analysis of compounds through a similarity search in the Clarivate Analytics Integrity portal validated their novelty regarding antibacterial activity. Structure analysis of derivatives revealed the presence of substituents like β-lactam moiety (G1 and G2), hydrazine (G3), sulfonyl group (G4), chlorine (G5), and

methylenedioxy ring (G6) groups are beneficial for antibacterial activity. Molecular docking studies and predictions using the PASS server indicated that the derivatives exhibited strong binding modes to the PBP2, tyrosine phosphatase, and ftsZ proteins. However, the MD analysis demonstrated that these complexes lack stability upon binding and do not induce any significant changes in the protein's conformation of PBP2 throughout the simulation. Noteworthy, derivatives G3 and G5 displayed the greatest stability within the active site of tyrosine phosphatase, as evidenced by a decrease in RMSD and an increase in SASA, suggesting enzyme conformational changes upon complex formation. MD simulations unveiled remarkable stability of studied derivative when interacting with ftsZ, as indicated by RMSD, RMSF, Rg, and SASA values. This observation aligns with expectations since griseofulvin targets microtubules in eukaryotes, and ftsZ serves as a microtubule homolog in prokaryotes. These findings underscore the potential efficacy of griseofulvin and its derivatives against bacterial targets, especially the ftsZ protein. This study is constrained by the small number of designed compounds. Notwithstanding this limitation, this research has the potential to offer insights for the advancement of novel derivatives and the enhancement of the antibacterial activity of griseofulvin through a hybridization approach in derivative development. Furthermore, this investigation has the potential to set a benchmark for future endeavors in the design of griseofulvin inhibitor compounds targeting bacterial proteins, laying the foundation or the development of promising antibacterial agents.

5.4. Future work on Advancing Insights into Griseofulvin Biosynthesis, Ecological Dynamics, and Therapeutic Potential

In forthcoming investigations, expanding upon the genomic evidence presented in this study, further exploration into the conservation and evolution of griseofulvin biosynthetic genes

among fungal species could shed light on the ecological and evolutionary dynamics of griseofulvin-producing fungi. Specifically, investigating the circumstances under which these gene clusters are maintained or lost could provide insights into the ecological roles of griseofulvin and the selective pressures acting upon its production. Additionally, elucidating the detoxification pathways employed by griseofulvin-producing fungi to mitigate the cytotoxic effects of griseofulvin presents an intriguing avenue for research. Through comprehensive comparative genomic analyses, key detoxification genes and associated metabolic pathways can be identified, offering profound insights into fungal physiology and adaptive responses.

Furthermore, building upon the promising *in silico* findings regarding the therapeutic potential of griseofulvin and its derivatives against COVID-19, future studies should prioritize in vitro and in vivo validations to ascertain their efficacy and safety profiles. Moreover, the computational design and evaluation of novel griseofulvin derivatives for antibacterial activity offer exciting prospects for the development of potent antibacterial agents. Expanding the scope of derivative design and systematically exploring their interactions with bacterial targets could facilitate the development of enhanced antibacterial therapies, addressing the pressing need for novel antimicrobial agents in the face of rising antibiotic resistance. This comprehensive approach to understanding and harnessing the therapeutic potential of griseofulvin and its derivatives holds promise for advancing both antifungal and antibacterial drug discovery efforts.

5.5. References

1. Chooi Y-H, Cacho R, Tang Y. Identification of the viridicatumtoxin and griseofulvin gene clusters from Penicillium aethiopicum. Chemistry & biology. 2010;17(5):483-94.

2. Cacho RA, Chooi Y-H, Zhou H, Tang Y. Complexity generation in fungal polyketide biosynthesis: a spirocycle-forming P450 in the concise pathway to the antifungal drug griseofulvin. ACS chemical biology. 2013;8(10):2322-30.

3. Banani H, Marcet-Houben M, Ballester A-R, Abbruscato P, González-Candelas L, Gabaldón T, et al. Genome sequencing and secondary metabolism of the postharvest pathogen Penicillium griseofulvum. BMC genomics. 2016;17(1):19.

4. Fatima U, Rizvi SSA, Raina N, Fatima S, Rahman S, Kamal MA, et al. Therapeutic management of COVID-19 patients: Clinical manifestation and limitations. Current pharmaceutical design. 2021;27(41):4223-31.

5. Salasc F, Lahlali T, Laurent E, Rosa-Calatrava M, Pizzorno A. Treatments for COVID-19: Lessons from 2020 and new therapeutic options. Current Opinion in Pharmacology. 2022;62:43-59.

6. Hamdy AK, Sheha MM, Abdel-Hafez AA, Shouman SA. Design, synthesis, and cytotoxicity evaluation of novel griseofulvin analogues with improved water solubility. International journal of medicinal chemistry. 2017;2017.

7. Lambert DR, Siegle RJ, Camisa C. Griseofulvin and ketoconazole in the treatment of dermatophyte infections. International journal of dermatology. 1989;28(5):300-4.

8. Oxford AE, Raistrick H, Simonart P. Studies in the biochemistry of micro-organisms: griseofulvin, C17H17O6Cl, a metabolic product of Penicillium griseo-fulvum Dierckx. Biochemical Journal. 1939;33(2):240.

9. Rebacz B, Larsen TO, Clausen MH, Rønnest MH, Löffler H, Ho AD, et al. Identification of griseofulvin as an inhibitor of centrosomal clustering in a phenotype-based screen. Cancer research. 2007;67(13):6342-50.

10. Jin H, Yamashita A, Maekawa S, Yang P, He L, Takayanagi S, et al. Griseofulvin, an oral antifungal agent, suppresses hepatitis C virus replication in vitro. Hepatology Research. 2008;38(9):909-18.

Appendix A: Supplemental for Chapter 2

File 1

Supplemental Table S1.1. BLASTP showed 22 species that contains at least three homologs with more than 50% similarities to reference Gsf proteins in *Penicillium aethiopicum*.

Species	**Predicted proteins involved**
Penicillium coprophilum	**GsfH,GsfG,GsfE,GsfD,GsfC,GsfB,GsfA,GsfI,GsfJ,GsfR1**
Aspergillus alliaceus	**GsfH,GsfG,GsfF,GsfD,GsfC,GsfB,GsfA,GsfI**
Aspergillus burnettii	**GsfH,GsfG,GsfF,GsfD,GsfC,GsfB,GsfA,GsfI**
Aspergillus pseudoviridinutans	**GsfR2,GsfA,GsfH**
Penicillium polonicum	**GsfR2,GsfK,GsfR1,GsfJ,GsfB,GsfH**
Penicillium freii	**GsfR2,GsfK,GsfR1,GsfJ**
Aspergillus oryzae	**GsfH,GsfE,GsfI**
Penicillium antarcticum	**GsfH,GsfG,GsfD**
Aspergillus ellipticus	**GsfH,GsfE,GsfD**
Aspergillus sclerotioniger	**GsfK,GsfD,GsfE**
Xylaria multiplex	**GsfG,GsfF,GsfD**
Aspergillus hancockii	**GsfA,GsfD,GsfH,GsfK,GsfR2**
Aspergillus glaucus	**GsfG,GsfD,GsfR2**
Penicillium solitum	**GsfG,GsfD,GsfB,GsfR1,GsfK,GsfR2**
Penicillium arizonense	**GsfH, GsfI, GsfJ, GsfK, GsfR1, GsfR2**
Penicillium expansum	**GsfH, GsfJ, GsfR1**
Aspergillus nidulans	**GsfE, GsfH, GsfJ, GsfR1**
Aspergillus japonicus	**GsfH, GsfI, GsfJ, GsfR1**
Aspergillus mulundensis	**GsfH, GsfI, GsfJ, GsfR2**

Aspergillus aculeatus	**GsfH, GsfI, GsfJ, GsfR2**
Aspergillus uvarum	**GsfH, GsfJ, GsfR3**
Aspergillus saccharolyticus	**GsfH, GsfJ, GsfR3**

Supplemental Table S1.2. Overview of the retrieved fungal genomes analyzed in this study. Highlighted in bold are the identified species in this study that harbor *gsf* BGCs in their genomes.

Species	GeneBank Accession number	Strain	Class	Order
Arthonia radiata	**PSQN00000000.1**	**EZ20314**	**Arthoniomycetes**	**Arthoniales**
Ascochyta rabiei	**RYYQ00000000.1**	**Me14**	**Dothideomycetes**	**Pleosporales**
Aureobasidium melanogenum	**AYEN00000000.1**	**CBS 110374**	**Dothideomycetes**	**Dothideales**
Aureobasidium namibiae	**AYEM00000000.1**	**CBS 147.97**	**Dothideomycetes**	**Dothideales**
Aureobasidium pullulans	**AYEO00000000.1**	**EXF-150**	**Dothideomycetes**	**Dothideales**
Aureobasidium subglaciale	**AYYB00000000.1**	**EXF-2481**	**Dothideomycetes**	**Dothideales**
Baudoinia panamericana	**AEIF00000000.1**	**UAMH 10762**	**Dothideomycetes**	**Mycosphaerellales**
Cenococcum geophilum	**LKKR00000000.1**	**1.58**	**Dothideomycetes**	**Mytilinidiales**
Cercospora berteroae	**PNEN00000000.1**	**CBS538.71**	**Dothideomycetes**	**Mycosphaerellales**
Cladosporium cladosporioides	**NOXB00000000.1**	**TYU**	**Dothideomycetes**	**Cladosporiales**
Cladosporium sphaerospermum	**JAHARS000000000.1**	**F4_7S_F1_F**	**Dothideomycetes**	**Cladosporiales**
Clohesyomyces aquaticus	**MCFA00000000.1**	**CBS 115471**	**Dothideomycetes**	**Pleosporales**
Coniosporium apollinis	**AJKL00000000.1**	**CBS 100218**	**Dothideomycetes**	**-**
Corynespora cassiicola	**JAEMHE000000000.1**	**CC01**	**Dothideomycetes**	**Pleosporales**

Cryomyces antarcticus	**AYQD00000000.1**	**CCFEE 534**	**Dothideomycetes**	**incertae sedis**
Curvularia geniculata	**JACADS000000000.1**	**P1**	**Dothideomycetes**	**Pleosporales**
Diplodia corticola	**MNUE00000000.1**	**CBS 112549**	**Dothideomycetes**	**Botryosphaeriales**
Dothistroma pini	**MWSO00000000.1**	**CBS 116487**	**Dothideomycetes**	**Mycosphaerellales**
Epicoccum nigrum	**NCTX00000000.1**	**ICMP 19927**	**Dothideomycetes**	**Pleosporales**
Exserohilum turcicum	**AIHT00000000.1**	**Et28A**	**Dothideomycetes**	**Pleosporales**
Exutisphaerella laricina	**AWYE00000000.2**	**CBS 326.52**	**Dothideomycetes**	**Mycosphaerellales**
Glonium stellatum	**LKAO00000000.1**	**CBS 207.34**	**Dothideomycetes**	**Mytilinidiales**
Helminthosporium solani	**AWWW00000000.1**	**B-AC-16A**	**Dothideomycetes**	**Pleosporales**
Lasiodiplodia theobromae	**QCYV00000000.1**	**AM2As**	**Dothideomycetes**	**Botryosphaeriales**
Leptoxyphium fumago	**LSHF00000000.1**	**SC3815**	**Dothideomycetes**	**Capnodiales**
Macrophomina phaseolina	**PPFZ00000000.1**	**M11-12**	**Dothideomycetes**	**Botryosphaeriales**
Microcyclospora pomicola	**NHNY00000000.1**	**SP1-49Fa**	**Dothideomycetes**	**Capnodiales**
Microcyclospora tardicrescens	**PXOE00000000.1**	**HJS1936**	**Dothideomycetes**	**Capnodiales**
Microcyclosporella mali	**NHNU00000000.1**	**UMD1a**	**Dothideomycetes**	**Mycosphaerellales**
Mycosphaerella arachidis	**LIHB00000000.1**	**CALF-13A**	**Dothideomycetes**	**Mycosphaerellales**
Mycosphaerelloides madeirae	**NHNV00000000.1**	**CBS 112895**	**Dothideomycetes**	**Mycosphaerellales**
Neofusicoccum parvum	**AORE00000000.1**	**UCRNP2**	**Dothideomycetes**	**Botryosphaeriales**
Neoscytalidium dimidiatum	**FLVB00000000.1**	**-**	**Dothideomycetes**	**Botryosphaeriales**
Nigrograna mackinnonii	**JGVQ00000000.1**	**E5202H**	**Dothideomycetes**	**Pleosporales**
Nothophaeocryptopus gaeumannii	**MWSP00000000.1**	**CBS 267.37**	**Dothideomycetes**	**Mycosphaerellales**
Ochroconis constricta	**AZYM00000000.1**	**UM 578**	**Dothideomycetes**	**Venturiales**

Paraphaeosphaeria sporulosa	**LXPO00000000.1**	**AP3s5-JAC2a**	**Dothideomycetes**	**Pleosporales**
Passalora fulva	**AMRR00000000.1**	**CBS 131901**	**Dothideomycetes**	**Mycosphaerellales**
Periconia macrospinosa	**PCYO00000000.1**	**DSE2036**	**Dothideomycetes**	**Pleosporales**
Phoma herbarum	**BCGR00000000.1**	**JCM 15942**	**Dothideomycetes**	**Pleosporales**
Phyllosticta capitalensis	**LOEO00000000.1**	**Gm33**	**Dothideomycetes**	**Botryosphaeriales**
Pseudocercospora eumusae	**LFZN00000000.1**	**CBS 114824**	**Dothideomycetes**	**Mycosphaerellales**
Pseudopyrenochaeta lycopersici	**NHZP00000000.1**	**CRA-PAV_ER 1518**	**Dothideomycetes**	**Pleosporales**
Pyrenophora seminiperda	**ATLS00000000.1**	**CCB06**	**Dothideomycetes**	**Pleosporales**
Rachicladosporium antarcticum	**NAJO00000000.1**	**CCFEE 5527**	**Dothideomycetes**	**Cladosporiales**
Ramichloridium luteum	**MTSC00000000.1**	**CPC 18961**	**Dothideomycetes**	**Mycosphaerellales**
Ramularia collo-cygni	**FJUY00000000.1**	**URUG2**	**Dothideomycetes**	**Mycosphaerellales**
Sphaerulina musiva	**AEFD00000000.1**	**SO2202**	**Dothideomycetes**	**Mycosphaerellales**
Sporothrix brasiliensis	**AWTV00000000.1**	**5110**	**Dothideomycetes**	**Mycosphaerellales**
Stagonosporopsis tanaceti	**JUDZ00000000.1**	**CBS 131484**	**Dothideomycetes**	**Pleosporales**
Stemphylium lycopersici	**QGDG00000000.1**	**CIDEFI 212**	**Dothideomycetes**	**Pleosporales**
Venturia carpophila	**JACTAK000000000.1**	**ZJHZ1-1-1**	**Dothideomycetes**	**Venturiales**
Verruconis gallopava	**JYBX00000000.1**	**CBS 43764**	**Dothideomycetes**	**Venturiales**
Zasmidium angulare	**NHNX00000000.1**	**GA2-2.7B1a**	**Dothideomycetes**	**Mycosphaerellales**
Zymoseptoria ardabiliae	**AFIV00000000.1**	**STIR04_1.1.2**	**Dothideomycetes**	**Mycosphaerellales**

Zymoseptoria brevis	**JYJE00000000.1**	**ZB163**	**Dothideomycetes**	**Mycosphaerellales**
Beverwykella pulmonaria	**BCHH00000000.1**	**JCM 9230**	**Dothideomycetes;**	**Pleosporales**
Bipolaris cookei	**NRSV00000000.1**	**LSLP18.3**	**Dothideomycetes;**	**Pleosporales**
Botryosphaeria dothidea	**WWBZ00000000.2**	**sdau11-99**	**Dothideomycetes;**	**Botryosphaeriales**
Amauroascus mutatus	**LJPJ00000000.1**	**UAMH 3576**	**Eurotiomycetes**	**Onygenales**
Ascosphaera apis	**AZGZ00000000.1**	**ARSEF 7405**	**Eurotiomycetes**	**Onygenales**
Aspergillus aculeatus	**ATCC 16872**	**MRCK00000000.1**	**Eurotiomycetes**	**Eurotiales**
Aspergillus aculeatus	**ATCC 16872**	**MRCK00000000.1**	**Eurotiomycetes**	**Eurotiales**
Aspergillus alliaceus	**IBT 14317**	**STFQ00000000.1**	**Eurotiomycetes**	**Eurotiales**
Aspergillus alliaceus	**CBS 536.65**	**SWAS00000000.1**	**Eurotiomycetes**	**Eurotiales**
Aspergillus burnettii	**FRR 5400**	**SPNV00000000.1**	**Eurotiomycetes**	**Eurotiales**
Aspergillus ellipticus	**CBS 707.79**	**PSSY00000000.1**	**Eurotiomycetes**	**Eurotiales**
Aspergillus glaucus	**CBS 516.65**	**LSTL00000000.1**	**Eurotiomycetes**	**Eurotiales**
Aspergillus hancockii	**FRR 3425**	**MBFL00000000**	**Eurotiomycetes**	**Eurotiales**
Aspergillus japonicus	**CBS 114.51**	**PSTF00000000.1**	**Eurotiomycetes**	**Eurotiales**
Aspergillus mulundensis	**DSM 5745**	**PVWQ00000000.1**	**Eurotiomycetes**	**Eurotiales**
Aspergillus mulundensis	**DSM 5745**	**NW_020797888.1**	**Eurotiomycetes**	**Eurotiales**
Aspergillus nidulans	**FGSC A4**	**AACD00000000.1**	**Eurotiomycetes**	**Eurotiales**
Aspergillus oryzae	**RIB40**	**BA000049.1**	**Eurotiomycetes**	**Eurotiales**
Aspergillus pseudoviridinutans	**IFM 55266**	**BHVY00000000.1**	**Eurotiomycetes**	**Eurotiales**
Aspergillus saccharolyticus	**JOP 1030-1**	**MSFQ00000000.1**	**Eurotiomycetes**	**Eurotiales**
Aspergillus sclerotioniger	**CBS 115572**	**MSFK00000000.1**	**Eurotiomycetes**	**Eurotiales**
Aspergillus uvarum	**CBS 121591**	**MSFT00000000.1**	**Eurotiomycetes**	**Eurotiales**
Blastomyces dermatitidis	**ACBT00000000.1**	**ER-3**	**Eurotiomycetes**	**Onygenales**
Byssoonygena ceratinophila	**LJPH00000000.1**	**UAMH 5669**	**Eurotiomycetes**	**Onygenales**

Capronia coronata	**AMWN00000000.1**	**CBS 617.96**	**Eurotiomycetes**	**Chaetothyriales**
Chrysosporium queenslandicum	**LJPI00000000.1**	**CBS 280.77**	**Eurotiomycetes**	**Onygenales**
Cladophialophora bantiana	**JYBT00000000.1**	**CBS 173.52**	**Eurotiomycetes**	**Chaetothyriales**
Coccidioides immitis	**AAEC00000000.3**	**RS**	**Eurotiomycetes**	**Onygenales**
Cyphellophora europaea	**AOBU00000000.1**	**CBS 101466**	**Eurotiomycetes**	**Chaetothyriales**
Elaphomyces granulatus	**NPHW00000000.1**	**OSC145934**	**Eurotiomycetes**	**Eurotiales**
Emergomyces africanus	**LGUA00000000.1**	**CBS 136260**	**Eurotiomycetes**	**Onygenales**
Emmonsia crescens	**PDND00000000.1**	**UAMH4076**	**Eurotiomycetes**	**Onygenales**
Endocarpon pusillum	**APWS00000000.1**	**Z07020**	**Eurotiomycetes**	**Verrucariales**
Exophiala alcalophila	**BCHY00000000.1**	**JCM 1751**	**Eurotiomycetes**	**Chaetothyriales**
Fonsecaea erecta	**LVYI00000000.1**	**CBS 125763**	**Eurotiomycetes**	**Chaetothyriales**
Helicocarpus griseus	**PDNB00000000.1**	**UAMH5409**	**Eurotiomycetes**	**Onygenales**
Histoplasma capsulatum	**AAJI00000000.1**	**NAm1**	**Eurotiomycetes**	**Onygenales**
Knufia petricola	**NMUC00000000.1**	**MA 5789**	**Eurotiomycetes**	**Chaetothyriales;**
Malbranchea cinnamomea	**FQSS00000000.2**	**-**	**Eurotiomycetes**	**Onygenales**
Microsporum canis	**ABVF00000000.1**	**CBS 113480**	**Eurotiomycetes**	**Onygenales**
Monascus purpureus	**WXEU00000000.1**	**YJX-8**	**Eurotiomycetes**	**Eurotiales**
Nannizzia gypsea	**ABQE00000000.1**	**CBS 118893**	**Eurotiomycetes**	**Onygenales**
Onygena corvina	**JWPT00000000.1**	**CBS 281.48**	**Eurotiomycetes**	**Onygenales**
Ophidiomyces ophidiicola	**MWKM00000000.1**	**MYCO-ARIZ AN0400001**	**Eurotiomycetes**	**Onygenales**
Paecilomyces niveus	**QEIL00000000.1**	**Cornell orchards no. 7**	**Eurotiomycetes**	**Eurotiales**
Paracoccidioides brasiliensis	**ABKI00000000.2**	**Pb18**	**Eurotiomycetes**	**Onygenales**
Penicillium aethiopicum	**IBT 5753**	**GU574478.1**	**Eurotiomycetes**	**Eurotiales**
Penicillium antarcticum	**IBT 31811**	**MDYN00000000.1**	**Eurotiomycetes**	**Eurotiales**
Penicillium arizonense	**CBS 141311**	**LXJU00000000.1**	**Eurotiomycetes**	**Eurotiales**
Penicillium biforme	**FM169**	**CBXO000000000.1**	**Eurotiomycetes**	**Eurotiales**
Penicillium brasilianum	**HKI JENA**	**CDHK00000000.1**	**Eurotiomycetes**	**Eurotiales**

Penicillium camemberti	**FM 013**	**CBVV000000000.1**	**Eurotiomycetes**	**Eurotiales**
Penicillium capsulatum	**WQ-2011**	**JPLR00000000.1**	**Eurotiomycetes**	**Eurotiales**
Penicillium carneum	**LCP05634**	**CBXS000000000.1**	**Eurotiomycetes**	**Eurotiales**
Penicillium chrysogenum	**P2niaD18**	**JMSF00000000.1**	**Eurotiomycetes**	**Eurotiales**
Penicillium citrinum	**JCM 22607**	**BCKA00000000.1**	**Eurotiomycetes**	**Eurotiales**
Penicillium coprophilum	**IBT 31321**	**MDDG00000000.1**	**Eurotiomycetes**	**Eurotiales**
Penicillium decumbens	**IBT 11843**	**MDYL00000000.1**	**Eurotiomycetes**	**Eurotiales**
Penicillium digitatum	**PDC 102**	**LHSL00000000.1**	**Eurotiomycetes**	**Eurotiales**
Penicillium digitatum	**Pd1**	**AKCU00000000.1**	**Eurotiomycetes**	**Eurotiales**
Penicillium expansum	**MD-8**	**JQFZ00000000.1**	**Eurotiomycetes**	**Eurotiales**
Penicillium flavigenum	**IBT 14082**	**MLQL00000000.1**	**Eurotiomycetes**	**Eurotiales**
Penicillium freii	**DAOM 242723**	**LLXE00000000.1**	**Eurotiomycetes**	**Eurotiales**
Penicillium fuscoglaucum	**FM041**	**CBXP000000000.1**	**Eurotiomycetes**	**Eurotiales**
Penicillium griseofulvum	**D-756**	**This study**	**Eurotiomycetes**	**Eurotiales**
Penicillium griseofulvum	**MRI314**	**LWCZ00000000.1**	**Eurotiomycetes**	**Eurotiales**
Penicillium griseofulvum	**PG3**	**LHQR00000000.1**	**Eurotiomycetes**	**Eurotiales**
Penicillium italicum	**GL-Gan1**	**LWEC00000000.1**	**Eurotiomycetes**	**Eurotiales**
Penicillium janthinellum	**NCIM1366**	**NPFE00000000.1**	**Eurotiomycetes**	**Eurotiales**
Penicillium marneffei	**ATCC 18224**	**ABAR00000000.1**	**Eurotiomycetes**	**Eurotiales**
Penicillium nalgiovense	**IBT 13039**	**MOOB00000000.1**	**Eurotiomycetes**	**Eurotiales**
Penicillium nordicum	**UASWS BFE487**	**JNNR00000000.1**	**Eurotiomycetes**	**Eurotiales**
Penicillium oxalicum	**114-2**	**AGIH00000000.1**	**Eurotiomycetes**	**Eurotiales**
Penicillium paneum	**FM227**	**CBXN000000000.1**	**Eurotiomycetes**	**Eurotiales**
Penicillium paxilli	**ATCC 26601**	**AOTG00000000.1**	**Eurotiomycetes**	**Eurotiales**
Penicillium polonicum	**F7**	**WBOJ00000000.1**	**Eurotiomycetes**	**Eurotiales**
Penicillium rolfsii	**F1880**	**QMFL00000000.1**	**Eurotiomycetes**	**Eurotiales**
Penicillium roqueforti	**FM164**	**CBMR000000000.1**	**Eurotiomycetes**	**Eurotiales**
Penicillium rubens Wisconsin	**54-1255**	**GCA_000226395.1**	**Eurotiomycetes**	**Eurotiales**
Penicillium sclerotiorum	**113**	**MJCA00000000.1**	**Eurotiomycetes**	**Eurotiales**

Penicillium solitum	**IBT 29525**	**MDYO00000000.1**	**Eurotiomycetes**	**Eurotiales**
Penicillium solitum	**RS1**	**JYNM00000000.2**	**Eurotiomycetes**	**Eurotiales**
Penicillium steckii	**IBT 24891**	**MLKD00000000.1**	**Eurotiomycetes**	**Eurotiales**
Penicillium subrubescens	**CBS 132785**	**MNBE00000000.1**	**Eurotiomycetes**	**Eurotiales**
Penicillium verrucosum	**BFE808**	**LAKW00000000.2**	**Eurotiomycetes**	**Eurotiales**
Penicillium vulpinum	**IBT 29486**	**MDYP01000001.1**	**Eurotiomycetes**	**Eurotiales**
Phaeomoniella chlamydospora	**LCWF00000000.1**	**UCRPC4**	**Eurotiomycetes**	**Phaeomoniellales**
Phialophora americana	**JYCC00000000.1**	**CBS 27337**	**Eurotiomycetes**	**Chaetothyriales**
Polytolypa hystricis	**PDNA00000000.1**	**UAMH7299**	**Eurotiomycetes**	**Onygenales**
Rasamsonia emersonii	**LASV00000000.1**	**CBS 393.64**	**Eurotiomycetes**	**Eurotiales**
Rhinocladiella mackenziei	**JYBU00000000.1**	**CBS 650.93**	**Eurotiomycetes**	**Chaetothyriales**
Talaromyces borbonicus	**NBSA00000000.1**	**SV-2017a**	**Eurotiomycetes**	**Eurotiales**
Thermoascus crustaceus	**BCIC00000000.1**	**JCM 12817**	**Eurotiomycetes**	**Eurotiales**
Trichophyton benhamiae	**ABSU00000000.1**	**CBS 112371**	**Eurotiomycetes**	**Onygenales**
Uncinocarpus reesii	**AAIW00000000.1**	**1704**	**Eurotiomycetes**	**Onygenales**
Xeromyces bisporus	**CCCX00000000.1**	**FRR 0525**	**Eurotiomycetes**	**Eurotiales**
Cetradonia linearis	**QKZZ00000000.1**	**BA2**	**Lecanoromycetes**	**Lecanorales**
Evernia prunastri	**NKYR00000000.1**	**FR SP7-11**	**Lecanoromycetes**	**Lecanorales**
Gyalolechia flavorubescens	**AUPK00000000.1**	**KoLRI002931**	**Lecanoromycetes**	**Teloschistales**
Lasallia hispanica	**PKMA00000000.1**	**C0002**	**Lecanoromycetes**	**Umbilicariales**
Pseudevernia furfuracea	**NKYQ00000000.1**	**AKPM 0122M**	**Lecanoromycetes**	**Lecanorales**
Ramalina intermedia	**PEKF00000000.1**	**YAF0013**	**Lecanoromycetes**	**Lecanorales**

Umbilicaria muehlenbergii	**JFDN00000000.1**	**KoLRI No. LF000956**	**Lecanoromycetes**	**Umbilicariales**
Articulospora tetracladia	**PYIV00000000.1**	**NNIBRFG329**	**Leotiomycetes**	**Helotiales**
Ascocoryne sarcoides	**AIAA00000000.1**	**NRRL 50072**	**Leotiomycetes**	**Helotiales**
Blumeria graminis	**CAJHIT000000000.1**	**THUN-12**	**Leotiomycetes**	**Erysiphales**
Botrytis paeoniae	**PQXI00000000.1**	**Bp0003**	**Leotiomycetes**	**Helotiales**
Cadophora malorum	**JAFJYH000000000.1**	**M34**	**Leotiomycetes**	**Helotiales**
Cairneyella variabilis	**AYLM00000000.1**	**VPRI 42388**	**Leotiomycetes**	**Helotiales**
Chlorociboria aeruginascens	**NCSK00000000.2**	**IHIA39**	**Leotiomycetes**	**Helotiales**
Ciborinia camelliae	**LGKQ00000000.1**	**ICMP 19812**	**Leotiomycetes**	**Helotiales**
Cladonia macilenta	**AUPP00000000.1**	**KoLRI003786**	**Leotiomycetes**	**Lecanorales**
Clarireedia homoeocarpa	**LNKV00000000.1**	**HRI11**	**Leotiomycetes**	**Helotiales**
Coleophoma crateriformis	**PDLN00000000.1**	**BP5796**	**Leotiomycetes**	**Helotiales**
Diplocarpon rosae	**JAANDC000000000.1**	**DiKAZ_180**	**Leotiomycetes**	**Helotiales**
Erysiphe necator	**JAFBAW000000000.1**	**NAFU1**	**Leotiomycetes**	**Erysiphales**
Glarea lozoyensis	**ALVE00000000.1**	**ATCC 20868**	**Leotiomycetes**	**Helotiales**
Hyaloscypha bicolor	**LXPI00000000.1**	**E**	**Leotiomycetes**	**Helotiales**
Hymenoscyphus fraxineus	**FXXO00000000.1**	**-**	**Leotiomycetes**	**Helotiales**
Marssonina brunnea	**AFXC00000000.1**	**MB_m1**	**Leotiomycetes**	**Helotiales**
Monilinia aucupariae	**NGKF00000000.1**	**LMK 733**	**Leotiomycetes**	**Helotiales**
Myriosclerotinia curreyana	**NGKJ00000000.1**	**LMK 759**	**Leotiomycetes**	**Helotiales**
Oidiodendron maius	**JMDP00000000.1**	**Zn**	**Leotiomycetes**	**-**
Pezicula radicicola	**PDUO00000000.1**	**NRRL 12192**	**Leotiomycetes**	**Helotiales**
Pseudogymnoascus destructans	**LAJJ00000000.1**	**20631-21**	**Leotiomycetes**	**Incertae sedis**
Rhynchosporium agropyri	**FJUX00000000.1**	**04CH-RAC-A.6.1**	**Leotiomycetes**	**Helotiales**
Rutstroemia sydowiana	**JWJB00000000.1**	**CBS 115975**	**Leotiomycetes**	**Helotiales**
Venustampulla echinocandica	**NPIC00000000.1**	**BP 5553**	**Leotiomycetes**	**Helotiales**

Arthrobotrys flagrans	**SAEB00000000.1**	**CBS H-5679**	**Orbiliomycetes**	**Orbiliales**
Dactylellina haptotyla	**AQGS00000000.1**	**CBS 200.50**	**Orbiliomycetes**	**Orbiliales**
Drechslerella stenobrocha	**ASQI00000000.1**	**248**	**Orbiliomycetes**	**Orbiliales**
Orbilia oligospora	**ADOT00000000.1**	**ATCC 24927**	**Orbiliomycetes**	**Orbiliales**
Morchella eximia	**QMFK00000000.1**	**MG90**	**Pezizomycetes**	**Pezizales**
Tuber borchii	**NESQ00000000.1**	**Tbo3840**	**Pezizomycetes**	**Pezizales**
Amorphotheca resinae	**MADK00000000.1**	**ATCC 22711**	**sordariomyceta**	**Leotiomycetes**
Annulohypoxylon stygium	**QLPL00000000.1**	**MG137**	**Sordariomycetes**	**Xylariales**
Aciculosporium take	**AFQZ00000000.1**	**MAFF-241224**	**Sordariomycetes**	**Hypocreales**
Akanthomyces lecanii	**AZHF00000000.1**	**RCEF 1005**	**Sordariomycetes**	**Hypocreales**
Albophoma yamanashiensis	**BCKH00000000.1**	**JCM 11844**	**Sordariomycetes**	**Hypocreales**
Ambrosiella xylebori	**PCDO00000000.1**	**CBS 110.61**	**Sordariomycetes**	**Microascales**
Aquanectria penicillioides	**PYIU00000000.1**	**NNIBRFG19**	**Sordariomycetes**	**Hypocreales**
Basipetospora chlamydospora	**BCHP00000000.1**	**JCM 23157**	**Sordariomycetes**	**Microascales**
Beauveria bassiana	**ADAH00000000.1**	**ARSEF 2860**	**Sordariomycetes**	**Hypocreales**
Ceratocystiopsis brevicomis	**PCDN00000000.1**	**CBS 137839**	**Sordariomycetes**	**Ophiostomatales**
Ceratocystis adiposa	**LXGU00000000.1**	**CBS136.34**	**Sordariomycetes**	**Microascales**
Chaetomium cochliodes	**LSBY00000000.1**	**CCM F-232**	**Sordariomycetes**	**Sordariales**
Claviceps fusiformis	**AFRA00000000.1**	**PRL 1980**	**Sordariomycetes**	**Hypocreales**
Clonostachys rosea	**JADCTT000000000.1**	**CanS41**	**Sordariomycetes**	**Hypocreales**
Colletotrichum chlorophyti	**MPGH00000000.1**	**NTL11**	**Sordariomycetes**	**Glomerellales**
Coniella lustricola	**NSBW00000000.1**	**B22-T-1**	**Sordariomycetes**	**Diaporthales**
Coniochaeta hoffmannii	**NXFW00000000.1**	**CBS 245.38**	**Sordariomycetes**	**Coniochaetales**
Cordyceps cicadae	**MWMN00000000.1**	**CC02**	**Sordariomycetes**	**Hypocreales**
Corinectria fuckeliana	**WPDH00000000.1**	**CBS 125109**	**Sordariomycetes**	**Hypocreales**
Davidsoniella virescens	**LJZU00000000.1**	**CMW17339**	**Sordariomycetes**	**Microascales**
Diaporthe ampelina	**LWAD00000000.1**	**S3MP**	**Sordariomycetes**	**Diaporthales**
Didymobotryum rigidum	**BCKI00000000.1**	**JCM 8837**	**Sordariomycetes**	**-**
Endocalyx cinctus	**BCKC00000000.1**	**JCM 7946**	**Sordariomycetes**	**Xylariales**

Epichloe amarillans	**AFRF00000000.1**	**E57**	**Sordariomycetes**	**Hypocreales**
Esteya vermicola	**PCDM00000000.1**	**CBS 115803**	**Sordariomycetes**	**Ophiostomatales**
Falciphora oryzae	**JNVV00000000.1**	**R5-6-1**	**Sordariomycetes**	**Magnaporthales**
Furcasterigmium furcatum	**BCIA00000000.1**	**JCM 9210**	**Sordariomycetes**	**Glomerellales**
Fusarium azukicola	**MAEG00000000.1**	**NRRL 54364**	**Sordariomycetes**	**Hypocreales**
Geosmithia morbida	**JAANYQ000000000.1**	**1262**	**Sordariomycetes**	**Hypocreales**
Graphilbum fragrans	**LLKO00000000.1**	**CBS 138720**	**Sordariomycetes**	**Ophiostomatales**
Grosmannia clavigera	**ACXQ00000000.2**	**kw1407**	**Sordariomycetes**	**Ophiostomatales**
Huntiella bhutanensis	**MJMS00000000.1**	**CMW 8217**	**Sordariomycetes**	**Microascales**
Hypoxylon pulicicidum	**CADCWX000000000.1**	**ATCC 74245**	**Sordariomycetes**	**Xylariales**
Ilyonectria destructans	**MPHF00000000.1**	**C1**	**Sordariomycetes**	**Hypocreales**
Juglanconis juglandina	**MUZJ00000000.1**	**CBS 121083**	**Sordariomycetes**	**Diaporthales**
Knoxdaviesia capensis	**LNGK00000000.1**	**CMW40890**	**Sordariomycetes**	**Microascales**
Kretzschmaria deusta	**MLHU00000000.3**	**DSM 104547**	**Sordariomycetes**	**Xylariales**
Lanzia echinophila	**JWJA00000000.1**	**CBS 111548**	**Sordariomycetes**	**Helotiales**
Lecanicillium fungicola	**FWCC00000000.1**	**-**	**Sordariomycetes**	**Hypocreales**
Lecanosticta acicola	**NXEF00000000.1**	**B3_MdHEF**	**Sordariomycetes**	**Hypocreales**
Leptographium lundbergii	**LDEF00000000.1**	**CBS 138716**	**Sordariomycetes**	**Ophiostomatales**
Madurella mycetomatis	**LCTW00000000.2**	**mm55**	**Sordariomycetes**	**Sordariales**
Magnaporthiopsis incrustans	**PYSR00000000.1**	**M35**	**Sordariomycetes**	**Magnaporthales**
Memnoniella echinata	**JCM 22618**	**BCHF00000000.1**	**Sordariomycetes**	**Hypocreales**
Metarhizium acridum	**ADNI00000000.1**	**CQMa 102**	**Sordariomycetes**	**Hypocreales**
Mollisia scopiformis	**LKNI00000000.1**	**CBS 120377**	**Sordariomycetes**	**Helotiales**
Neonectria ditissima	**LDPL00000000.1**	**RS 324p**	**Sordariomycetes**	**Hypocreales**
Neurospora africana	**CAPO000000000.2**	**FGSC 1740**	**Sordariomycetes**	**Sordariales**
Ophioceras dolichostomum	**PYST00000000.1**	**CBS 114926**	**Sordariomycetes**	**Magnaporthales**
Ophiocordyceps australis	**NJET00000000.1**	**Map64**	**Sordariomycetes**	**Hypocreales**

Ophiostoma ips	**NTMB00000000.1**	**CBS 138721**	**Sordariomycetes**	**Ophiostomatales**
Periglandula ipomoeae	**AFRD00000000.1**	**IasaF13**	**Sordariomycetes**	**Hypocreales**
Phialocephala subalpina	**FJOG00000000.1**	**UAMH 11012**	**Sordariomycetes**	**Helotiales**
Pseudomassariella vexata	**MCFJ00000000.1**	**CBS 129021**	**Sordariomycetes**	**Xylariales**
Pyricularia grisea	**RRCK00000000.1**	**NI907**	**Sordariomycetes**	**Magnaporthales**
Raffaelea albimanens	**PCDJ00000000.1**	**CBS 271.70**	**Sordariomycetes**	**Ophiostomatales**
Reticulascus tulasneorum	**LSAX00000000.1**	**NRRL18230**	**Sordariomycetes**	**Glomerellales**
Rosellinia necatrix	**BBSO00000000.2**	**W97**	**Sordariomycetes**	**Xylariales**
Samsoniella hepiali	**LNDK00000000.2**	**FENG**	**Sordariomycetes**	**Hypocreales**
Sarocladium oryzae	**BCHE00000000.1**	**JCM 12450**	**Sordariomycetes**	**Hypocreales**
Scedosporium apiospermum	**JOWA00000000.1**	**IHEM 14462**	**Sordariomycetes**	**Microascales**
Sclerotinia borealis	**AYSA00000000.1**	**F-4128**	**Sordariomycetes**	**Helotiales**
Sordaria macrospora	**CABT00000000.2**	**Strain: k-hell**	**Sordariomycetes**	**Sordariales**
Stachybotrys chartarum	**LDEE00000000.1**	**1511**	**Sordariomycetes**	**Hypocreales**
Thielaviopsis ethacetica	**BCFY00000000.1**	**JCM 6961**	**Sordariomycetes**	**Microascales**
Tolypocladium capitatum	**NRSZ00000000.1**	**CBS 113982**	**Sordariomycetes**	**Hypocreales**
Trichoderma arundinaceum	**PXOA00000000.1**	**IBT 40837**	**Sordariomycetes**	**Hypocreales**
Trichothecium ovalisporum	**PXOC00000000.1**	**DAOM 186447**	**Sordariomycetes**	**Hypocreales**
Verticillium albo-atrum	**NMXJ00000000.1**	**PD747**	**Sordariomycetes**	**Glomerellales**
Xylaria flabelliformis	**G536**	**VFLP00000000.1**	**Sordariomycetes**	**Xylariales**
Xylaria longipes	**NQIL00000000.1**	**IHI A66**	**Sordariomycetes**	**Xylariales**
Xylaria multiplex	**DSM 110363**	**WUBL00000000.1**	**Sordariomycetes**	**Xylariales**
Xylaria polymorpha	**NQIM00000000.1**	**DSM 105756**	**Sordariomycetes**	**Xylariales**
Xylaria striata	**LOBO00000000.1**	**RK1-1**	**Sordariomycetes**	**Xylariales**
Xylona heveae	**JXCS00000000.1**	**TC161**	**Sordariomycetes**	**Xylariales**
Symbiotaphrina buchneri	**BCIG00000000.1**	**JCM 9740**	**Xylonomycetes**	**Symbiotaphrinales**

File 2

Dataset S1. Fungal genomes that have potential to produce griseofulvin acccording the previous studies or search via GenBank. NA=Not Available, SP=Some Partial sequence available.

	Accession Number (mentioned in the article)	Accession Number (via search in GenBank)	Reference
Penicillium aethiopicum	**GU574478**	**-**	**1**
Penicillium griseofulvum **strain PG3**	**LHQR00000000.1**	**-**	**2**
Xylaria cubensis (flabelliformis)	**VFLP00000000**	**-**	**3**
Penicillium brasilianum	**NA**	**CDHK00000000.1**	**4**
Penicillium canescens	**NA**	**SP**	**5**
Penicillium marinum	**NA**	**SP**	**6**
Penicillium waksmanii	**NA**	**SP**	**7**
Penicillium janthinellum	**NA**	**NPFE00000000.1**	**8**
Penicillium sclerotigenum	**NA**	**SP**	**9**
Abieticola koreana	**NA**	**NA**	**10**
Stachybotrys levispora	**NA**	**SP**	**11**
Penicillium persicinum	**NA**	**SP**	**12**
Penicillium coprophilum	**NA**	**MDDG00000000.1**	**13**
Penicillium dipodomyicola	**NA**	**SP**	**14**
Penicillium coprobium	**NA**	**SP**	**14**
Penicillium concentricum	**NA**	**SP**	**14**
Penicillium vulpinum	**NA**	**MDYP00000000.1**	**14**
Penicillium formosanum	**NA**	**SP**	**14**
Penicillium clavigerum	**NA**	**SP**	**14**
Penicillium lanosum	**NA**	**SP**	**15**
Penicillium raistrickii	**NA**	**SP**	**15**
Penicillium soppii	**NA**	**SP**	**15**
Penicillium murcianum	**NA**	**SP**	**15**
Penicillium nigricans	**NA**	**NA**	**15**
Penicillium nodusitatum	**NA**	**NA**	**15**
Penicillium yarmokense	**NA**	**SP**	**15**

Penicillium lanosum Westling	**NA**	**SP**	**16**
Penicillium jensenii	**NA**	**SP**	**16**
Penicillium janczewskii	**NA**	**SP**	**16**
Memnoniella echinata	**NA**	**NA**	**17**

References

1. Chooi Y-H, Cacho R, Tang Y. Identification of the viridicatumtoxin and griseofulvin gene clusters from Penicillium aethiopicum. Chemistry & biology. 2010;17(5):483-94.
2. Banani H, Marcet-Houben M, Ballester A-R, Abbruscato P, González-Candelas L, Gabaldón T, et al. Genome sequencing and secondary metabolism of the postharvest pathogen Penicillium griseofulvum. BMC genomics. 2016;17(1):19.
3. Mead ME, Raja HA, Steenwyk JL, Knowles SL, Oberlies NH, Rokas A. Draft Genome Sequence of the Griseofulvin-Producing Fungus Xylaria flabelliformis Strain G536. Microbiology resource announcements. 2019;8(38):e00890-19.
4. Tang H-Y, Zhang Q, Li H, Gao J-M. Antimicrobial and allelopathic metabolites produced by Penicillium brasilianum. Natural product research. 2015;29(4):345-8.
5. Roullier C, Bertrand S, Blanchet E, Peigné M, Robiou du Pont T, Guitton Y, et al. Time dependency of chemodiversity and biosynthetic pathways: an LC-MS metabolomic study of marine-sourced penicillium. Marine drugs. 2016;14(5):103.
6. Jadulco R, Edrada RA, Ebel R, Berg A, Schaumann K, Wray V, et al. New Communesin Derivatives from the Fungus Penicillium sp. Derived from the Mediterranean Sponge Axinella v errucosa. Journal of natural products. 2004;67(1):78-81.
7. Petit K, Mondeguer F, Roquebert M, Biard J, Pouchus Y. Detection of griseofulvin in a marine strain of Penicillium waksmanii by ion trap mass spectrometry. Journal of microbiological methods. 2004;58(1):59-65.
8. Xue C, Li T, Deng Z, Fu H, Lin W. Janthinolide AB, two new 2, 5-piperazinedione derivatives from the endophytic Penicillium janthinellum isolated from the soft coral Dendronephthya sp. Die Pharmazie. 2006;61(12):1041-4.
9. Clarke S, McKenzie M. Penicillium sclerotigenum: a new source of Griseofulvin. Nature. 1967;213(5075):504-5.
10. Lee HB, Mun HY, Nguyen TTT, Kim J-C, Stone JK. Abieticola koreana gen. et sp. nov., a griseofulvin-producing endophytic xylariaceous ascomycete from Korea. Mycotaxon. 2016;131(4):749-64.
11. Ribeiro AI, Costa ES, Thomasi SS, Brandão DFR, Vieira PC, Fernandes JoB, et al. Biological and chemical control of Sclerotinia sclerotiorum using Stachybotrys levispora and its secondary metabolite griseofulvin. Journal of agricultural and food chemistry. 2018;66(29):7627-32.
12. Wang L, Zhou H-B, Frisvad JC, Samson RA. Penicillium persicinum, a new griseofulvin, chrysogine and roquefortine C producing species from Qinghai province, China. Antonie van leeuwenhoek. 2004;86(2):173-9.
13. Nielsen JC, Grijseels S, Prigent S, Ji B, Dainat J, Nielsen KF, et al. Global analysis of biosynthetic gene clusters reveals vast potential of secondary metabolite production in Penicillium species. Nature microbiology. 2017;2(6):1-9.
14. Frisvad JC, Samson RA. Polyphasic taxonomy of Penicillium subgenus Penicillium. A guide to identification of food and air-borne terverticillate Penicillia and their mycotoxins. Studies in mycology. 2004;49(1):1-174.

15. Larsen TO, Smedsgaard J, Nielsen KF, Hansen ME, Frisvad JC. Phenotypic taxonomy and metabolite profiling in microbial drug discovery. Natural product reports. 2005;22(6):672-95.
16. Samson RA, Pitt JI. Modern concepts in Penicillium and Aspergillus classification: Springer Science & Business Media; 2013.
17. Jarvis BB, Zhou Y, Jiang J, Wang S, Sorenson W, Hintikka E-L, et al. Toxigenic molds in water-damaged buildings: dechlorogriseofulvins from Memnoniella echinata. Journal of natural products. 1996;59(6):553-4.

Dataset S2. List of gene cluster families (GCFs) at griseofulvin biosynthetic gene clusters (BGCs) according antiSMASH and BiG-SCAPE analysis.

GCF Identifier	BGC Identifier	antiSMASH Classification	Most similar known cluster - MIBiG	First blast result (antiSMASH data)	Number of proteins with BLAST hits to this cluster	Cumulative BLAST score	Significant hits (MIBiG BGC-ID)
FAM 00011	*Penicillium griseofulvum* D-756	Type I PKS (Polyketide synthase)	griseofulvin biosynthetic gene cluster	Penicillium aethiopicum GU574478.4	9	9323	BGC0000077, griseofulvin gene cluster
	Penicillium griseofulvum MRI314	Type I PKS (Polyketide synthase)	griseofulvin biosynthetic gene cluster	Penicillium aethiopicum GU574478.5	6	5525	BGC0000077, griseofulvin gene cluster
	Penicillium griseofulvum PG3	Type I PKS (Polyketide synthase)	griseofulvin biosynthetic gene cluster	Penicillium aethiopicum GU574478.6	10	9271	BGC0000077, griseofulvin gene cluster
	Xylaria flabelliformis G536	Type I PKS (Polyketide synthase)	griseofulvin biosynthetic gene cluster	Penicillium aethiopicum GU574478.7	7	7391	BGC0000077, griseofulvin gene cluster
	Aspergillus alliaceus CBS 536.65	Type I PKS (Polyketide synthase)	griseofulvin biosynthetic gene cluster	Penicillium aethiopicum GU574478.1	9	7494	BGC0000077, griseofulvin gene cluster
	Aspergillus alliaceus IBT 14317	Type I PKS (Polyketide synthase)	griseofulvin biosynthetic gene cluster	Penicillium aethiopicum GU574478.2	9	7509	BGC0000077, griseofulvin gene cluster
	Aspergillus burnettii FRR 5400	Type I PKS (Polyketide synthase)	griseofulvin biosynthetic gene cluster	Penicillium aethiopicum GU574478.2	9		BGC0000077, griseofulvin gene cluster
	Penicillium aethiopicum IBT 5753	Type I PKS (Polyketide synthase)	griseofulvin biosynthetic gene cluster	Penicillium aethiopicum GU574478.9	13	17411	BGC0000077, griseofulvin gene cluster
	Penicillium coprophilum IBT 31321	Type I PKS (Polyketide synthase)	griseofulvin biosynthetic gene cluster	Penicillium aethiopicum GU574478.11	9	8452	BGC0000077, griseofulvin gene cluster

FAM 00010	*Penicillium vulpinum* IBT 29486	Type I PKS (Polyketide synthase)	griseofulvin biosynthetic gene cluster	Penicillium aethiopicum GU574478.3	7	7159	BGC000007, griseofulvin gene cluster
FAM 00006	*Memnoniella echinata* JCM 22618	Type I PKS (Polyketide synthase)	griseofulvin biosynthetic gene cluster	Penicillium aethiopicum GU574478.8	7	6483	BGC000007, griseofulvin gene cluster
FAM 00008	*Penicillium capsulatum* LiaoWQ-2011	Type I PKS (Polyketide synthase)	griseofulvin biosynthetic gene cluster	Penicillium aethiopicum GU574478.10	9	8232	BGC000007, griseofulvin gene cluster

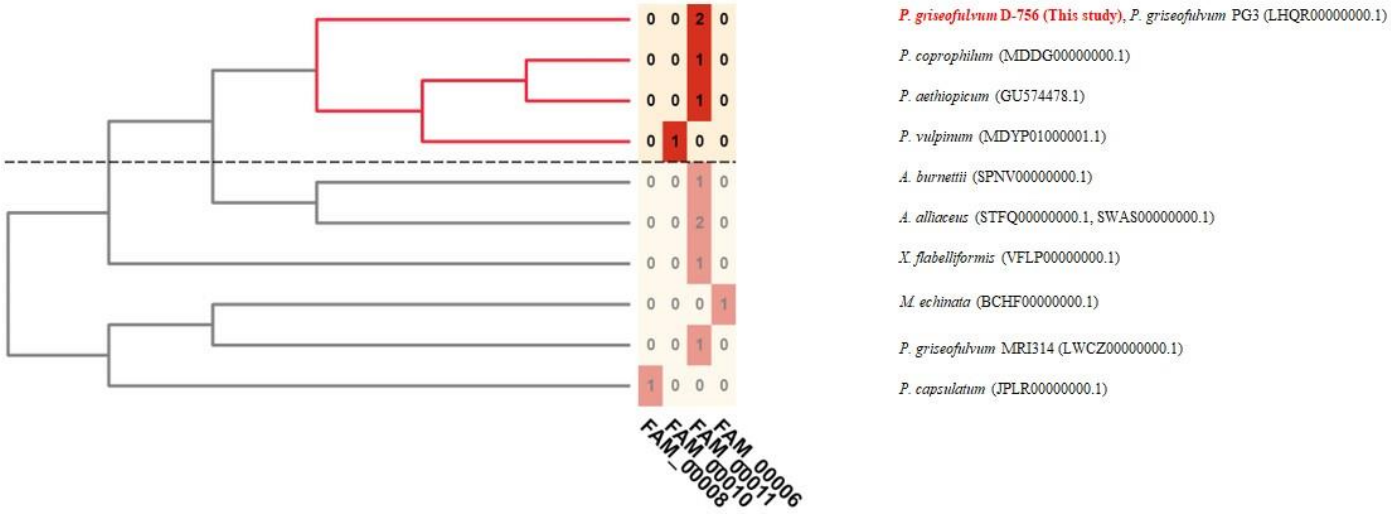

Fig S1. Phylogenetic tree of gsf gene cluster based on BiG-SCAPE analysis. Absent-present table of gene cluster families (GSFs) are also provided. The red highlighted species (*P.griseofulvum* D-756) is the stain that we sequenced in this study.

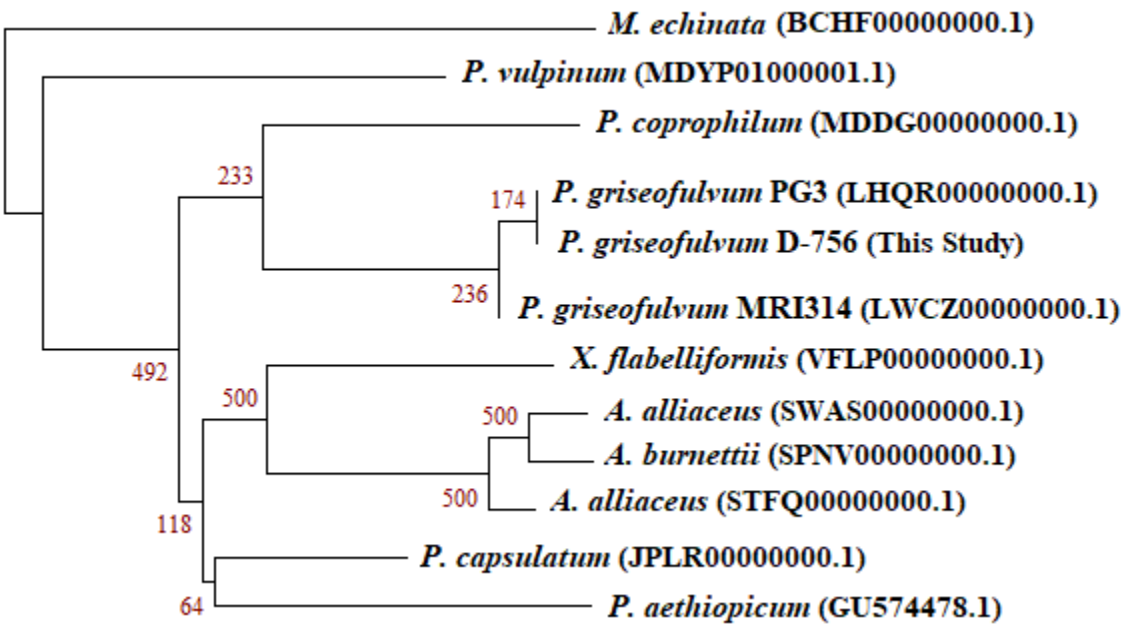

Fig S2. The unrooted phylogenetic tree was constructed by FastME approach. Supporting bootstrap values are based on 500 replicates. The *M. echinata* was used as an outgroup.

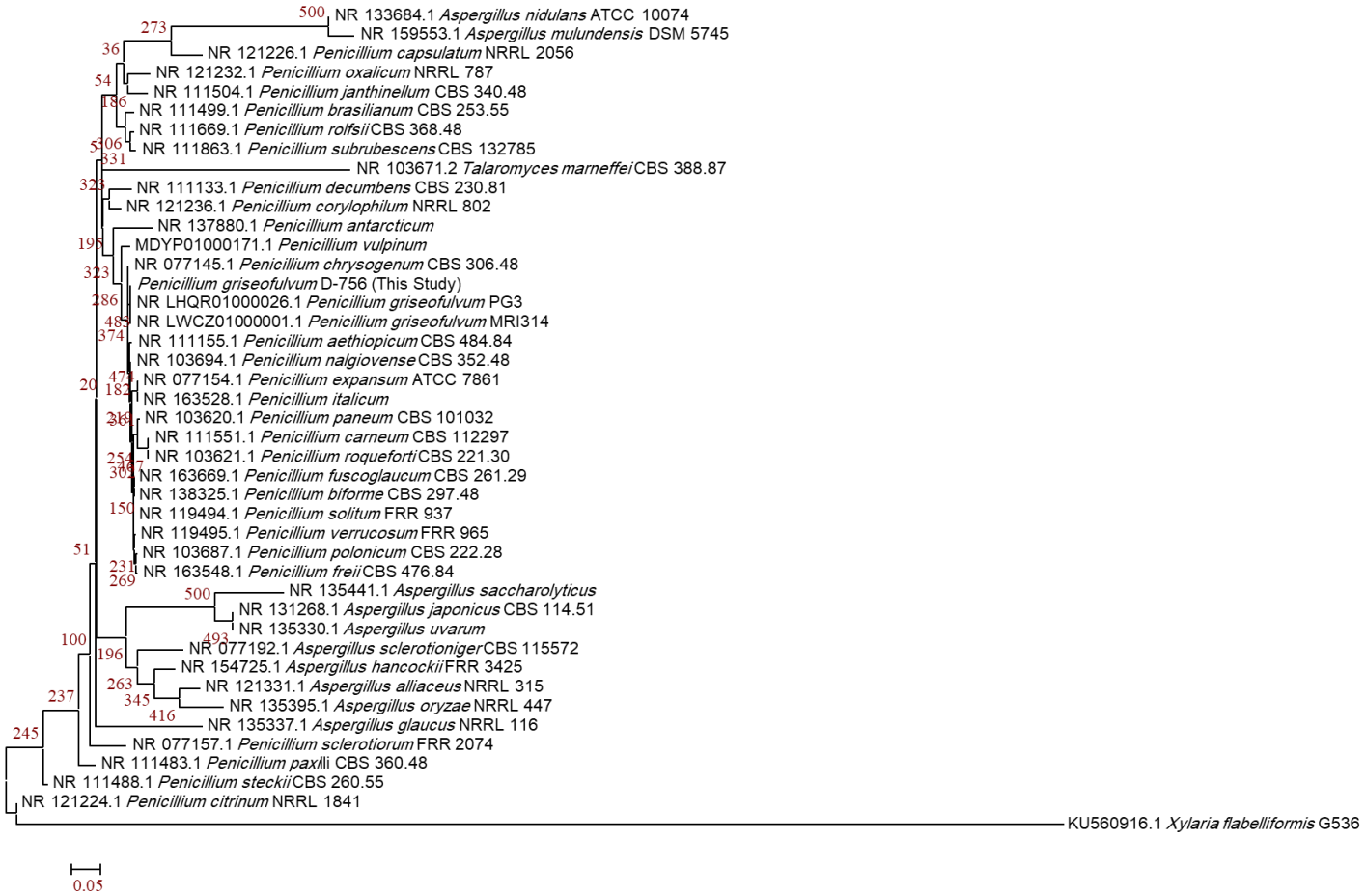

Fig S3. The unrooted phylogenetic tree was constructed by the maximum likelihood-based PhyML approach, using aligned nucleotide sequences of ITS region of fungal species. Supporting bootstrap values are based on 500 replicates. The *X. flabelliformis* was used as an outgroup.

Dataset S3. The BLASTN comparison of *gsf* genes between *P. griseofulvum* strain D-756 and *P. griseofulvum* strain PG3.

	Max Score	Total Score	Query Coverage (%)	E Value	Identity (%)
gsfR1	**2637**	**2668**	**67**	**0**	**99.86**
gsfJ	**3048**	**3048**	**100**	**0**	**99.94**
gsfI	**2891**	**2891**	**100**	**0**	**99.94**
gsfA	**8882**	**8882**	**100**	**0**	**99.92**

gsfB	**2223**	**2223**	**100**	**0**	**99.13**
gsfC	**2149**	**2149**	**100**	**0**	**100**
gsfD	**2143**	**2143**	**100**	**0**	**100**
gsfE	**2040**	**2040**	**100**	**0**	**100**
gsfF	**2652**	**2652**	**100**	**0**	**100**

Dataset S4. Functional domains of griseofulvin gene cluster among the surveyed species according to Pfam database. The green and pink color codes show the present and absent the gsf genes respectively. The check mark shows the presence of the functional domain, which are listed under the gene name and are in red. The functional domain has been lost from some genes, which are shown in red boxes. It seems that there is no functional domain in *gsfR1* and *gsfE*.

Dataset S5. The discription of Pfam domains located in *gsf* genes.

Pfam Accession Number	Name	Description
PF00172	Zn_clus	Fungal Zn(2)-Cys(6) binuclear cluster domain
PF00106	adh_short	short chain dehydrogenase
PF07690	MFS_1	Major Facilitator Superfamily
PF04820	Trp_halogenase	Tryptophan halogenase
PF16073	SAT	Starter unit:ACP transacylase in aflatoxin biosynthesis
PF02801	Ketoacyl-synt_C	Beta-ketoacyl synthase, C-terminal domain

PF00550	PP-binding	Phosphopantetheine attachment site
PF00109	ketoacyl-synt	Beta-ketoacyl synthase, N-terminal domain
PF00698	Acyl_transf_1	Acyl transferase domain
PF14765	PS-DH	Polyketide synthase dehydratase
PF00891	Methyltransf_2	O-methyltransferase domain
PF08100	Dimerisation	Dimerisation domain
PF00067	p450	Cytochrome P450
PF12796	PF12796	Ankyrin repeats
PF00857	Isochorismatase	Isochorismatase family

File 3

Table S9. Annotations of query cluster of putative gsf genes cluster in *Xylaria flabelliformis.*

Table of genes, locations, and strands of subject cluster.

Table of genes	**locations**		**Strands**
FHL15_010255	1400	3324	+
FHL15_010256	3825	4740	+
FHL15_010257	5785	11451	+
FHL15_010258	11684	13122	-
FHL15_010259	14159	15350	-
FHL15_010260	15782	17102	+
FHL15_010261	17371	18868	-
FHL15_010262	19168	21204	+
FHL15_010263	22439	23981	+
FHL15_010264	24341	25397	-
FHL15_010265	25721	27398	+
FHL15_010266	28519	29636	-

Table of Blast hits.

Gene	**Size (bp/aa)**	**BLASTP Homolog**	**Identity/Coverage (%)**	**BLAST Score**	**E value**
FHL15_010255 (gsfI)	1596/522	Halogenase gsfI; AltName: Full=Griseofulvin	84/95	945	3.80E-275

		synthesis protein I [Penicillium aethiopicum]			
FHL15_010257 (gsfA)	5265/1754	Non-reducing polyketide synthase gsfA; AltName: Full=Griseofulvin synthesis protein A; AltName: Full=Norlichexanthone synthase [Penicillium aethiopicum]	81/92	2852	0
FHL15_010258 (gsfB)	1260/419	O-methyltransferase gsfB; AltName: Full=Griseofulvin synthesis protein B [Penicillium aethiopicum]	81/99	720	2.10E-207
FHL15_010259 (gsfC)	1191/396	O-methyltransferase gsfC; AltName: Full=Griseofulvin synthesis protein C [Penicillium aethiopicum]	83/98	654	1.30E-187
FHL15_010260 (gsfD)	1188/395	O-methyltransferase gsfD; AltName: Full=Griseofulvin synthesis protein D [Penicillium aethiopicum]	85/48	651	6.60E-187
FHL15_010261 (gsfE)	1299/432	Short chain dehydrogenase gsfE; AltName: Full=Griseofulvin synthesis protein E [Penicillium aethiopicum]	82/99	690	1.40E-198
FHL15_010262 (gsfF)	1611/536	Cytochrome P450 monooxygenase gsfF; AltName: Full=Griseofulvin synthesis protein F; Flags: Precursor [Penicillium aethiopicum]	83/97	879	2.00E-255

Table S10. Annotations of query cluster of putative gsf genes cluster in *P. griseofulvum* stain D-756.

Table of genes, locations, and strands of subject cluster.

Table of genes	**locations**		**Strands**
FUN_007659	1357708	1359221	-
FUN_007660	1359553	1360696	+

FUN_007661	1364595	1366305	-
FUN_007662	1366829	1367960	+
FUN_007663	1368567	1369881	-
FUN_007664	1370302	1371493	+
FUN_007665	1372214	1373662	+
FUN_007666	1374873	1380039	-
FUN_007667	1381317	1383267	-
FUN_007668	1384079	1386122	-
FUN_007669	1386761	1389034	+
FUN_007670	1389212	1391112	-

Table of Blast hits.

Gene	**Size (bp/aa)**	**BLASTP Homolog**	**Identity/Coverage (%)**	**BLAST Score**	**E value**
FUN_007661 (gsfF)	1470/490	Cytochrome P450 monooxygenase gsfF; AltName: Full=Griseofulvin synthesis protein F; Flags: Precursor [Penicillium aethiopicum]	87/85	862	2.30E-250
FUN_007662 (gsfE)	1131/377	Short chain dehydrogenase gsfE; AltName: Full=Griseofulvin synthesis protein E [Penicillium aethiopicum]	83/88	704	1.10E-202
FUN_007663 (gsfD)	1188/396	O-methyltransferase gsfD; AltName: Full=Griseofulvin synthesis protein D [Penicillium aethiopicum]	79/84	671	1.10E-192
FUN_007664 (gsfC)	1191/397	O-methyltransferase gsfC; AltName: Full=Griseofulvin synthesis protein C [Penicillium aethiopicum]	84/85	663	2.90E-190
FUN_007665 (gsfB)	1260/420	O-methyltransferase gsfB; AltName: Full=Griseofulvin synthesis protein B [Penicillium aethiopicum]	81/81	723	1.90E-208
FUN_007666 (gsfA)	4935/1645	Non-reducing polyketide synthase gsfA; AltName: Full=Griseofulvin synthesis protein A; AltName: Full=Norlichexanthone synthase [Penicillium aethiopicum]	80/81	2720	0

FUN_007667 (gsfI)	1605/535	Halogenase gsfI; AltName: Full=Griseofulvin synthesis protein I [Penicillium aethiopicum]	87/93	1002	2.10E-292
FUN_007668 (gsfJ)	1692/564	Probable efflux pump gsfJ; AltName: Full=Griseofulvin synthesis protein J [Penicillium aethiopicum]	80/81	878	8.10E-255
FUN_007669 (gsfR1)	2163/721	Probable transcription factor gsfR1; AltName: Full=Griseofulvin synthesis protein R1 [Penicillium aethiopicum]	80/80	1100	0.00E+00

Table S11. Annotations of query cluster of putative gsf genes cluster in *A. burnettii*.

Table of genes	**locations**		**Strands**
ETB97_011395	73116	74031	+
ETB97_011396	75941	77080	+
ETB97_011397	79181	80268	+
ETB97_011398	82544	83709	-
ETB97_011399	85095	87026	+
ETB97_011400	89496	95177	+
ETB97_011401	95409	96848	-
ETB97_011402	97240	97556	-
ETB97_011403	97636	98827	-
ETB97_011404	99356	100553	+
ETB97_011405	101639	102130	-
ETB97_011406	104456	104893	-
ETB97_011407	105518	107224	+
ETB97_011408	107796	108781	-
ETB97_011409	109450	109876	-

Table of Blast hits.

Gene	**Size (bp/aa)**	**BLASTP Homolog**	**Identity/Coverage (%)**	**BLAST Score**	**E value**

ETB97_011398 (gsfR1)	774/258	Probable transcription factor gsfR1; AltName: Full=Griseofulvin synthesis protein R1 [Penicillium aethiopicum]	84/85	319	6.60E-87
ETB97_011399 (gsfI)	1590/530	Halogenase gsfI; AltName: Full=Griseofulvin synthesis protein I [Penicillium aethiopicum]	87/85	967	9.50E-282
ETB97_011400 (gsfA)	5370/1790	Non-reducing polyketide synthase gsfA; AltName: Full=Griseofulvin synthesis protein A; AltName: Full=Norlichexanthone synthase [Penicillium aethiopicum]	85/99	3035	0
ETB97_011401 (gsfB)	1260/420	O-methyltransferase gsfB; AltName: Full=Griseofulvin synthesis protein B [Penicillium aethiopicum]	83/99	717	1.00E-206
ETB97_011403 (gsfC)	1191/397	O-methyltransferase gsfC; AltName: Full=Griseofulvin synthesis protein C [Penicillium aethiopicum]	86/97	674	9.60E-194
ETB97_011405 (gsfD)	681/227	O-methyltransferase gsfD; AltName: Full=Griseofulvin synthesis protein D [Penicillium aethiopicum]	86/85	239	3.70E-63
ETB97_011406 (gsfE)	771/257	Short chain dehydrogenase gsfE; AltName: Full=Griseofulvin synthesis protein E [Penicillium aethiopicum]	86/85	162	3.50E-40
ETB97_011407 (gsfF)	1518/506	Cytochrome P450 monooxygenase gsfF; AltName: Full=Griseofulvin synthesis protein F; Flags: Precursor [Penicillium aethiopicum]	85/98	895	3.40E-260
ETB97_011408 (gsfG)	918/396	GsfG [Penicillium aethiopicum]	82/90	171	1.60E-42

File 4

Table S1. BLASTN Hits for *Penicillium griseofulvum* strain D-756 against *P. aethiopicum* (GU574478) as query.

Query accession	**Subject accession**	**Subject Range**	**CDS feature**	**Identity (%)**	**Alignment length**	**Mismatches**	**Gap opens**	**Query start**	**Query end**	**E-value**	**Bit score**
GU574478.1	Query_159513	Scaffold4_1380732-1374850	gsfA	80.63	5932	1075	34	21314	27220	0	5432
GU574478.1	Query_159513	Scaffold4_1366534-1362353	gsfF/G	74.098	4297	873	77	34790	38961	0	2601
GU574478.1	Query_159513	Scaffold4_1389042-1386617	gsfR1	81.032	2462	425	14	13029	15484	0	2310

GU574478.1	Query_159513	Scaffold4_1383523-1381238	gsfI	78.846	2340	408	25	18691	20997	0	1955
GU574478.1	Query_159513	Scaffold4_1386335-1384074	gsfJ	78.496	2274	446	17	15910	18152	0	1859
GU574478.1	Query_159513	Scaffold4_1370065-1368568	gsfD	80.744	1506	256	14	31417	32896	0	1377
GU574478.1	Query_159513	Scaffold4_1373719-1372005	gsfB	77.765	1718	354	14	27598	29290	0	1339
GU574478.1	Query_159513	Scaffold4_1371540-1370341	gsfC	82.848	1201	205	1	29935	31135	0	1234
GU574478.1	Query_159513	Scaffold4_1367962-1366830	gsfE	83.201	1137	187	2	33256	34392	0	1185
GU574478.1	Query_60369	Scaffold2_7546078-7544786	gsfR2	78.588	1303	268	5	9787	11088	0	1080
GU574478.1	Query_60369	Scaffold2_7544382-753273	gsfK	75.336	1115	230	7	11520	12594	0	781
GU574478.1	Query_43451	Scaffold5_3249325-3247855	gsfH	75.397	1512	256	30	40442	41878	0	1020

Table S2. BLASTN Hits for *Penicillium vulpinum* strain IBT 29486 against *P. aethiopicum* (GU574478) as query.

Query accession	**Subject accession**	**Subject Range**	**CDS feature**	**Identity (%)**	**Alignment length**	**Mismatches**	**Gap opens**	**Query start**	**Query end**	**E-value**	**Bit score**
GU574478.1	MDYP01000001.1_Penicillium	25888-19984	gsfA	81.393	5928	1052	26	21315	27214	0	5647
GU574478.1	MDYP01000001.1_Penicillium	15657-11228	gsfC/D/E	76.318	4476	938	43	29996	34395	0	3210
GU574478.1	MDYP01000001.1_Penicillium	33967-31576	gsfR1	80.116	2414	451	11	13041	15447	0	2167
GU574478.1	MDYP01000001.1_Penicillium	31141-28898	gsfJ	78.675	2265	447	21	15913	18162	0	1846
GU574478.1	MDYP01000001.1_Penicillium	9808-7862	gsfF/G	74.848	1976	438	28	36023	37968	0	1251

GU574478.1	MDYP01000001.1_Penicillium	18310-16769	gsfB	76.943	1544	342	7	27567	29098	0	1161
GU574478.1	MDYP01000001.1_Penicillium	28205-26636	gsfI	74.194	1612	357	21	18867	20461	0	991
GU574478.1	MDYP01000001.1_Penicillium	10825-99801	gsfF	73.07	1062	219	17	34776	35807	3.30E-17	610

Table S3. BLASTN Hits for *Penicillium capsulatum* strain LiaoWQ-2011 (JPLR01000013.1) against *P. aethiopicum* (GU574478) as query.

Query accession	**Subject accession**	**Subject Range**	**CDS feature**	**Identity (%)**	**Alignment length**	**Mismatches**	**Gap opens**	**Query start**	**Query end**	**E-value**	**Bit score**
GU574478.1	JPLR01000013.1	21320-27244	gsfA	84.362	5947	889	17	19294	25221	0	6493
GU574478.1	JPLR01000013.1	27508-34722	gsfB/C/D/E	78.814	7354	1315	80	25674	32923	0	6097
GU574478.1	JPLR01000013.1	34897-38405	gsfF/G	79.844	3582	613	30	33198	36743	0	3168
GU574478.1	JPLR01000013.1	13052-15463	gsfR1	85.081	2413	342	5	10667	13062	0	2723
GU574478.1	JPLR01000013.1	18685-21281	gsfI	81.298	2620	439	21	16383	18974	0	2468
GU574478.1	JPLR01000013.1	15726-18385	gsfJ	79.585	2699	469	27	13122	15777	0	2336

Table S4. BLASTN Hits for *Penicillium coprophilum* strain IBT 31321 (MDDG01000006.1) against *P. aethiopicum* (GU574478) as query.

Query accession	**Subject accession**	**Subject Range**	**CDS feature**	**Identity (%)**	**Alignment length**	**Mismatches**	**Gap opens**	**Query start**	**Query end**	**E-value**	**Bit score**
GU574478.1	MDDG01000006.1	25850-20003	gsfA	79.68	5876	1150	23	21335	27194	0	5150
GU574478.1	MDDG01000006.1	12063-8177	gsfF/G	74.121	3984	824	70	34787	38660	0	2408
GU574478.1	MDDG01000006.1	17084-14083	gsfC/D	77.844	3033	589	34	29996	32976	0	2362
GU574478.1	MDDG01000006.1	34094-31778	gsfR1	79.837	2336	421	5	13041	15345	0	2113

GU574478.1	MDDG01000006.1	28440-26332	gsfI	79.185	2147	397	23	18868	21002	0	1799
GU574478.1	MDDG01000006.1	31368-29126	gsfJ	77.025	2259	484	15	15910	18149	0	1699
GU574478.1	MDDG01000006.1	13535-12407	gsfE	83.88	1129	182	0	33265	34393	0	1216
GU574478.1	MDDG01000006.1	19441-17916	gsfB	76.225	1531	346	8	27656	29173	0	1101

Table S5. BLASTN Hits for *Penicillium griseofulvum* strain MRI314 (LWCZ00000000.1) against *P. aethiopicum* (GU574478) as query.

Query accession	**Subject accession**	**Subject Range**	**CDS feature**	**Identity (%)**	**Alignment length**	**Mismatches**	**Gap opens**	**Query start**	**Query end**	**E-value**	**Bit score**
GU574478.1	LWCZ01000522.1	12550-6668	gsfA	80.614	5932	1076	34	21314	27220	0	5427
GU574478.1	LWCZ01000522.1	20861-18436	gsfR1	81.072	2462	424	14	13029	15484	0	2315
GU574478.1	LWCZ01000522.1	15342-13056	gsfI	78.907	2342	404	25	18691	20997	0	1966
GU574478.1	LWCZ01000522.1	18154-15893	gsfJ	78.54	2274	445	17	15910	18152	0	1864
GU574478.1	LWCZ01000522.1	1869-372	gsfD	80.677	1506	257	14	31417	32896	0	1372
GU574478.1	LWCZ01000522.1	5538-3954	gsfB	78.878	1586	324	7	27598	29173	0	1329
GU574478.1	LWCZ01000522.1	3344-2145	gsfC	82.848	1201	205	1	29935	31135	0	1234

File 5

Table S1. Gsf Domain analysis of *P. capsulatum* using NCBI CDD.

Query	**Hit type**	**PSSM-ID**	**From**	**To**	**E-Value**	**Bitscore**	**Accession**	**Short name**
gsfR1	specific	213391	2	275	1.37E-14	75.1736	cd12148	fungal_TF_MHR
gsfJ	specific	341045	29	413	9.45E-86	267.507	cd17502	MFS_Azr1_MDR_like
gsfI	superfamily	380163	32	285	6.49E-19	89.0048	cl38964	halo_ClmS superfamily

gsfA	specific	225858	250	1034	8.17E-171	541.66	COG3321	PksD
	specific	275325	1061	1377	2.05E-93	304.929	TIGR04532	PT_fungal_PKS
	superfamily	415491	5	118	1.10E-15	78.0221	cl08282	Acyl_transf_1 superfamily
	specific	395435	1456	1514	6.49E-08	50.6377	pfam00550	PP-binding
gsfB	superfamily	418430	251	391	7.49E-22	92.8537	cl17173	AdoMet_MTases superfamily
gsfC	superfamily	418430	228	372	5.03E-15	73.2085	cl17173	AdoMet_MTases superfamily
gsfD	superfamily	418430	192	333	2.93E-15	73.5937	cl17173	AdoMet_MTases superfamily
	superfamily	414963	68	105	0.00381713	35.9864	cl06920	dimerization2 superfamily
gsfE	specific	187652	14	323	1.48E-107	318.421	cd08948	5beta-POR_like_SDR_a
gsfF	specific	410683	1	364	8.61E-146	419.294	cd11060	CYP57A1-like

Table S2. Gsf Domain analysis of *P. griseofulvum* MRI314 using NCBI CDD.

Query	**Hit type**	**PSSM-ID**	**From**	**To**	**E-Value**	**Bitscore**	**Accession**	**Short name**
gsfD	superfamily	418430	184	371	3.19E-12	65.1193	cl17173	AdoMet_MTases superfamily
	superfamily	414963	68	110	8.04E-05	40.994	cl06920	dimerization2 superfamily
gsfC	superfamily	418430	228	374	9.56E-17	78.2161	cl17173	AdoMet_MTases superfamily
	superfamily	131763	62	339	7.59E-06	47.3532	cl25581	C20_methyl_CrtF superfamily
gsfB	superfamily	418430	237	383	1.42E-21	91.6981	cl17173	AdoMet_MTases superfamily
gsfA	specific	225858	64	825	6.03E-156	493.895	COG3321	PksD
	specific	275325	852	1170	2.34E-96	310.322	TIGR04532	PT_fungal_PKS
	superfamily	415491	5	65	2.47E-07	52.9841	cl08282	Acyl_transf_1 superfamily
gsfI	superfamily	380163	8	328	1.35E-26	112.887	cl38964	halo_ClmS superfamily
gsfJ	specific	341045	56	473	4.39E-78	247.477	cd17502	MFS_Azr1_MDR_like
	superfamily	182502	149	324	8.76E-07	51.2707	cl32521	PRK10504 superfamily

Table S3. Gsf Domain analysis of *P. griseofulvum* PG3 using NCBI CDD.

Query	Hit type	PSSM-ID	From	To	E-Value	Bitscore	Accession	Short name
gsfJ	specific	341045	65	482	3.99E-78	247.862	cd17502	MFS_Azr1_MDR_like
	superfamily	182502	158	333	8.86E-07	51.2707	cl32521	PRK10504 superfamily
gsfI	superfamily	380163	8	328	1.35E-26	112.887	cl38964	halo_ClmS superfamily
gsfA	specific	225858	250	1098	0	588.269	COG3321	PksD
	specific	275325	1125	1443	1.46E-95	310.707	TIGR04532	PT_fungal_PKS
	superfamily	415491	5	118	3.03E-17	82.6445	cl08282	Acyl_transf_1 superfamily
gsfB	superfamily	418430	237	383	1.42E-21	91.6981	cl17173	AdoMet_MTases superfamily
gsfC	superfamily	418430	228	374	9.56E-17	78.2161	cl17173	AdoMet_MTases superfamily
	superfamily	131763	62	339	7.59E-06	47.3532	cl25581	C20_methyl_CrtF superfamily
gsfD	superfamily	418430	184	371	3.44E-12	65.1193	cl17173	AdoMet_MTases superfamily
	superfamily	414963	68	110	1.24E-05	43.3052	cl06920	dimerization2 superfamily
gsfE	specific	187652	17	304	5.51E-98	292.998	cd08948	5beta-POR_like_SDR_a
gsfF	specific	410683	19	404	2.39E-160	458.199	cd11060	CYP57A1-like

Table S4. Gsf Domain analysis of *P. griseofulvum* D-756 using NCBI CDD.

Query	Hit type	PSSM-ID	From	To	E-Value	Bitscore	Accession	Short name
gsfF	superfamily	425388	19	170	2.96E-58	187.789	cl41757	cytochrome_P450 superfamily
gsfE	specific	187652	17	324	9.30E-111	325.354	cd08948	5beta-POR_like_SDR_a
gsfD	superfamily	418430	184	371	3.44E-12	65.1193	cl17173	AdoMet_MTases superfamily
	superfamily	414963	68	110	1.24E-05	43.3052	cl06920	dimerization2 superfamily
gsfC	superfamily	418430	228	374	9.56E-17	78.2161	cl17173	AdoMet_MTases superfamily

	superfamily	131763	62	339	7.59E-06	47.3532	cl25581	C20_methyl_CrtF superfamily
gsfB	superfamily	418430	237	383	1.42E-21	91.6981	cl17173	AdoMet_MTases superfamily
gsfA	specific	225858	46	825	2.08E-155	496.592	COG3321	PksD
	specific	275325	852	1170	5.08E-96	311.092	TIGR04532	PT_fungal_PKS
	specific	395435	1279	1337	7.10E-08	50.2525	pfam00550	PP-binding
	superfamily	415491	5	65	2.79E-07	52.9841	cl08282	Acyl_transf_1 superfamily
gsfI	superfamily	380163	8	328	1.35E-26	112.887	cl38964	halo_ClmS superfamily
gsfJ	specific	341045	56	473	4.39E-78	247.477	cd17502	MFS_Azr1_MDR_like
	superfamily	182502	149	324	8.76E-07	51.2707	cl32521	PRK10504 superfamily

Table S5. Gsf Domain analysis of *P. coprophilum* using NCBI CDD.

Query	**Hit type**	**PSSM-ID**	**From**	**To**	**E-Value**	**Bitscore**	**Accession**	**Short name**
gsfG	specific	403870	181	265	4.82E-18	77.4662	pfam12796	Ank_2
	specific	269836	25	46	7.20E-07	45.7886	cd14688	bZIP_YAP
	superfamily	215625	129	306	2.69E-06	48.711	cl33658	PLN03192 superfamily
gsfE	specific	187652	4	314	2.46E-107	317.265	cd08948	5beta-POR_like_SDR_a
gsfD	superfamily	418430	184	333	1.08E-08	54.7189	cl17173	AdoMet_MTases superfamily
	superfamily	414963	63	110	2.92E-05	42.1496	cl06920	dimerization2 superfamily
gsfC	superfamily	418430	231	372	6.04E-15	73.2085	cl17173	AdoMet_MTases superfamily
	superfamily	131763	62	339	4.98E-05	44.6568	cl25581	C20_methyl_CrtF superfamily
gsfB	superfamily	418430	251	392	7.99E-18	81.2977	cl17173	AdoMet_MTases superfamily
gsfA	specific	225858	395	1271	0	624.863	COG3321	PksD
	specific	275325	1298	1616	2.92E-95	311.092	TIGR04532	PT_fungal_PKS
	specific	406473	20	263	4.03E-44	160.84	pfam16073	SAT

	specific	395435	1726	1784	2.93E-07	49.0969	pfam00550	PP-binding
gsfI	superfamily	380163	8	372	1.21E-43	162.963	cl38964	halo_ClmS superfamily
gsfJ	specific	341045	81	486	2.60E-99	304.872	cd17502	MFS_Azr1_MDR_like
gsfR1	specific	213391	2	322	7.33E-22	97.5152	cd12148	fungal_TF_MHR

Table S6. Gsf Domain analysis of *P. vulpinum* using NCBI CDD.

Query	**Hit type**	**PSSM-ID**	**From**	**To**	**E-Value**	**Bitscore**	**Accession**	**Short name**
gsfD	superfamily	418430	180	321	2.54E-14	70.8973	cl17173	AdoMet_MTases superfamily
	superfamily	414963	68	110	9.50E-06	43.3052	cl06920	dimerization2 superfamily
gsfB	superfamily	418430	235	296	1.23E-07	51.2521	cl17173	AdoMet_MTases superfamily
gsfA	specific	225858	223	990	3.48E-152	491.584	COG3321	PksD
	specific	275325	1019	1332	4.23E-91	298.381	TIGR04532	PT_fungal_PKS
	superfamily	415491	1	107	1.61E-14	74.5553	cl08282	Acyl_transf_1 superfamily
	specific	223314	1435	1506	1.29E-08	53.0672	COG0236	AcpP
gsfJ	superfamily	421695	61	359	1.43E-49	169.666	cl28910	MFS superfamily

Table S7. Gsf Domain analysis of *P. aethiopicum* using NCBI CDD.

Query	**Hit type**	**PSSM-ID**	**From**	**To**	**E-Value**	**Bitscore**	**Accession**	**Short name**
gsfR2	specific	214501	6	45	3.99E-11	57.3698	smart00066	GAL4
gsfK	specific	187586	5	251	1.77E-66	205.607	cd05325	carb_red_sniffer_like_SDR_c
gsfR1	specific	213391	157	519	7.17E-26	110.612	cd12148	fungal_TF_MHR
gsfJ	specific	341045	61	461	1.91E-102	312.19	cd17502	MFS_Azr1_MDR_like
gsfI	superfamily	380163	8	372	7.68E-44	163.348	cl38964	halo_ClmS superfamily

gsfA	specific	225858	395	1271	0	633.723	COG3321	PksD
	specific	275325	1298	1616	4.68E-95	310.322	TIGR04532	PT_fungal_PKS
	specific	406473	20	272	1.57E-43	158.914	pfam16073	SAT
	specific	395435	1726	1784	1.68E-07	49.4821	pfam00550	PP-binding
gsfB	superfamily	418430	251	391	3.79E-24	99.0169	cl17173	AdoMet_MTases superfamily
gsfC	superfamily	418430	228	372	4.59E-16	76.2901	cl17173	AdoMet_MTases superfamily
gsfD	superfamily	418430	214	355	1.99E-12	65.5045	cl17173	AdoMet_MTases superfamily
	superfamily	414963	63	110	1.06E-05	43.3052	cl06920	dimerization2 superfamily
gsfE	specific	187652	4	314	6.76E-111	326.51	cd08948	5beta-POR_like_SDR_a
gsfG	specific	403870	168	250	1.87E-18	78.2366	pfam12796	Ank_2
	specific	394980	266	295	2.26E-05	40.7006	pfam00023	Ank

Table S8. Gsf Domain analysis of *A. alliaceus* (SWAS00000000.1) using NCBI CDD.

Query	**Hit type**	**PSSM-ID**	**From**	**To**	**E-Value**	**Bitscore**	**Accession**	**Short name**
gsfI	superfamily	380163	41	239	1.50E-16	80.9156	cl38964	halo_ClmS superfamily
gsfA	specific	225858	84	867	9.77E-172	539.349	COG3321	PksD
	specific	275325	894	1212	2.35E-99	319.952	TIGR04532	PT_fungal_PKS
	specific	395435	1280	1316	0.000142873	41.0078	pfam00550	PP-binding
gsfB	superfamily	418430	169	309	1.19E-21	90.9277	cl17173	AdoMet_MTases superfamily
gsfC	superfamily	418430	228	374	1.43E-15	74.7493	cl17173	AdoMet_MTases superfamily
gsfE	superfamily	419666	4	129	6.19E-30	109.257	cl21454	NADB_Rossmann superfamily
gsfF	specific	410683	69	498	0	520.602	cd11060	CYP57A1-like

Table S9. Gsf Domain analysis of *A. alliaceus* (STFQ00000000.1) using NCBI CDD.

Query	**Hit type**	**PSSM-ID**	**From**	**To**	**E-Value**	**Bitscore**	**Accession**	**Short name**

gsfI	superfamily	380163	41	239	3.26E-17	83.2268	cl38964	halo_ClmS superfamily
gsfA	specific	225858	84	867	1.60E-170	535.882	COG3321	PksD
	specific	275325	894	1212	5.78E-99	319.182	TIGR04532	PT_fungal_PKS
	specific	395435	1280	1316	0.000142873	41.0078	pfam00550	PP-binding
gsfB	superfamily	418430	277	417	9.65E-22	92.8537	cl17173	AdoMet_MTases superfamily
gsfC	superfamily	418430	228	374	4.08E-16	76.2901	cl17173	AdoMet_MTases superfamily
	superfamily	131763	74	339	0.000145251	43.116	cl25581	C20_methyl_CrtF superfamily
gsfE	superfamily	419666	4	129	6.19E-30	109.257	cl21454	NADB_Rossmann superfamily
gsfF	superfamily	425388	60	169	7.45E-42	144.647	cl41757	cytochrome_P450 superfamily

Table S10. Gsf Domain analysis of *A. burnettii* (SPNV00000000.1) using NCBI CDD.

Query	**Hit type**	**PSSM-ID**	**From**	**To**	**E-Value**	**Bitscore**	**Accession**	**Short name**
gsfA	specific	225858	395	1271	0	644.894	COG3321	PksD
	specific	275325	1298	1616	3.87E-98	319.182	TIGR04532	PT_fungal_PKS
	specific	406473	20	251	6.71E-42	154.292	pfam16073	SAT
	specific	395435	1727	1783	3.85E-07	48.7117	pfam00550	PP-binding
gsfB	superfamily	418430	251	391	3.01E-21	90.9277	cl17173	AdoMet_MTases superfamily
gsfC	superfamily	418430	228	374	2.15E-15	74.3641	cl17173	AdoMet_MTases superfamily
gsfE	superfamily	419666	148	255	1.22E-20	88.8419	cl21454	NADB_Rossmann superfamily
	superfamily	419666	2	85	7.52E-08	52.2479	cl21454	NADB_Rossmann superfamily
gsfF	specific	410683	69	498	0	520.987	cd11060	CYP57A1-like
gsfG	specific	403870	177	261	1.40E-19	81.3182	pfam12796	Ank_2
	superfamily	215625	124	302	7.75E-07	50.2518	cl33658	PLN03192 superfamily
	specific	269836	26	52	1.17E-05	42.3218	cd14688	bZIP_YAP

gsfI	superfamily	380163	8	376	3.65E-44	164.504	cl38964	halo_ClmS superfamily

Table S11. Gsf Domain analysis of *X.flabelliformis* using NCBI CDD.

Query	**Hit type**	**PSSM-ID**	**From**	**To**	**E-Value**	**Bitscore**	**Accession**	**Short name**
gsfI	superfamily	380163	8	334	1.53E-45	167.971	cl38964	halo_ClmS superfamily
gsfA	specific	225858	375	1237	0	610.996	COG3321	PksD
	specific	275325	1264	1582	5.16E-100	324.574	TIGR04532	PT_fungal_PKS
	superfamily	415491	20	243	8.60E-24	101.904	cl08282	Acyl_transf_1 superfamily
	specific	395435	1692	1748	4.17E-07	48.3265	pfam00550	PP-binding
gsfB	superfamily	418430	251	391	4.42E-22	93.2389	cl17173	AdoMet_MTases superfamily
gsfC	superfamily	418430	220	374	1.13E-16	77.8309	cl17173	AdoMet_MTases superfamily
gsfD	superfamily	418430	182	372	4.10E-13	67.8157	cl17173	AdoMet_MTases superfamily
	superfamily	414963	68	110	4.29E-06	44.4608	cl06920	dimerization2 superfamily
gsfE	specific	187652	59	369	2.22E-107	319.576	cd08948	5beta-POR_like_SDR_a
gsfF	specific	410683	69	498	2.92E-178	508.275	cd11060	CYP57A1-like

Table S12. Gsf Domain analysis of *M. echinata* using NCBI CDD.

Query	**Hit type**	**PSSM-ID**	**From**	**To**	**E-Value**	**Bitscore**	**Accession**	**Short name**
gsfA	specific	225858	413	1288	0	651.827	COG3321	PksD
	specific	275325	1315	1633	3.51E-99	322.263	TIGR04532	PT_fungal_PKS
	specific	406473	20	280	1.32E-36	139.269	pfam16073	SAT
	specific	395435	1737	1793	7.69E-07	47.9413	pfam00550	PP-binding
gsfB	superfamily	418430	251	393	3.00E-25	102.098	cl17173	AdoMet_MTases superfamily

gsfC	superfamily	418430	228	372	5.76E-18	81.6829	cl17173	AdoMet_MTases superfamily
	superfamily	131763	87	339	1.42E-06	49.6644	cl25581	C20_methyl_CrtF superfamily
gsfD	superfamily	418430	182	372	6.37E-14	70.1269	cl17173	AdoMet_MTases superfamily
	superfamily	414963	63	110	2.23E-06	45.2312	cl06920	dimerization2 superfamily
gsfE	specific	187652	4	313	4.02E-108	319.191	cd08948	5beta-POR_like_SDR_a
gsfF	specific	410683	40	425	6.49E-151	442.406	cd11060	CYP57A1-like
gsfI	superfamily	380163	6	145	1.85E-12	67.0484	cl38964	halo_ClmS superfamily

Appendix A: Supplemental for Chapter 3

File 1

Table S1. The PubChem CID of 464 griseofulvin derivatives.

CID ID	Compound Name	Molecular Weight	Molecular Formula
3512	Gris-PEG	352.8	C17H17ClO6
10097	7-Chloro-3',4,6-trimethoxy-5'-methylspiro[1-benzofuran-2,6'-cyclohex-2-ene]-1',3-dione	352.8	C17H17ClO6
31336	(2S)-7-chloro-3',4,6-trimethoxy-5'-methylspiro[1-benzofuran-2,4'-cyclohex-2-ene]-1',3-dione	352.8	C17H17ClO6

161302	6-Demethylgriseofulvin	338.74	C16H15ClO6
176431	Dtxsid80949069	338.74	C16H15ClO6
195521	2'-Demethoxy-2'-methyldehydrogriseofulvin	334.7	C17H15ClO5
195522	7-Chloro-4,6-dimethoxy-3',5'-dimethylspiro[1-benzofuran-2,4'-cyclohex-2-ene]-1',3-dione	336.8	C17H17ClO5
253250	Spiro[benzofuran-2(3H),1'-[2]cyclohexene]-3,4'-dione, 7-chloro-4,6-dimethoxy-6'-methyl-2'-(methylthio)-	368.8	C17H17ClO5S
289550	7-Chloro-4,6-dimethoxy-1-benzofuran-3(2h)-one	228.63	C10H9ClO4
298140	Spiro[benzofuran-2(3H),1'-[3]cyclohexene]-2',3-dione, 7-chloro-4,6-dimethoxy-6'-methyl-	322.74	C16H15ClO5
441140	Griseofulvin	352.8	C17H17ClO6
566721	Spiro[benzofuran-2(3H),1'-[3]cyclohexene]-2',3-dione,7-chloro-6-hydroxy-4,4'-dimethoxy-6'-methyl-	338.74	C16H15ClO6
574586	Spiro[benzofuran-2(3H),1'-[3]cyclohexene]-2',3-dione,7-chloro-4,4',6-trimethoxy-3',6'-dimethyl-	366.8	C18H19ClO6
586839	Spiro[benzofuran-2(3H),1'-[2]cyclohexene]-3,4'-dione,7-chloro-4-hydroxy-2',6-dimethoxy-6'-methyl-, methanesulfonate	416.8	C17H17ClO8S
586858	Spiro[benzofuran-2(3H),1'-[2]cyclohexene]-3,4'-dione,5,7-dichloro-2',4,6-trimethoxy-6'-methyl-, (2S-trans)-	387.2	C17H16Cl2O6
592609	Spiro[benzofuran-2(3H),1'-[2]cyclohexene]-3,4'-dione,7-chloro-2',4,6-trimethoxy-3',6'-dimethyl-	366.8	C18H19ClO6
611914	7-Chloro-4,6-dimethoxy-5'-methylspiro[1-benzofuran-2,4'-cyclohex-2-ene]-1',3-dione	322.74	C16H15ClO5
611918	Spiro[benzofuran-2(3H),1'-[2]cyclohexene]-3,4'-dione,2',7-dichloro-4,6-dimethoxy-6'-methyl-	357.2	C16H14Cl2O5
612127	Spiro[benzofuran-2(3H),1'-[2]cyclohexene]-3,4'-dione,7-chloro-5'-hydroxy-2',4,6-trimethoxy-6'-methyl-, [1'S-(1'alpha,5'beta,6'beta)]-	368.8	C17H17ClO7
617268	Spiro[benzofuran-2(3H),1'-cyclohexane]-2',3,4'-trione,7-chloro-6-methoxy-4,6'-dimethyl-	322.74	C16H15ClO5
617713	Spiro[benzofuran-2(3H),1'-cyclohexane]-2',3,4'-trione,7-chloro-4-hydroxy-6-methoxy-6'-methyl-	324.71	C15H13ClO6
617901	Spiro[benzofuran-2(3H),1'-cyclohexane]-2',3,4'-trione,7-chloro-6-hydroxy-4-methoxy-6'-methyl-	324.71	C15H13ClO6
620242	Spiro[benzofuran-2(3H),1'-[3]cyclohexene]-2',3-dione, 7-chloro-4,6-dimethoxy-6'-methyl-4'-(methylthio)-	368.8	C17H17ClO5S
620360	Spiro[benzofuran-2(3H),1'-cyclohexane]-2',3-dione, 7-chloro-4,4',6-trimethoxy-6'-methyl-	354.8	C17H19ClO6
620368	Spiro[benzofuran-2(3H),1'-cyclohexane]-3,4'-dione, 7-chloro-2',4,6-trimethoxy-6'-methyl-	354.8	C17H19ClO6

620370	Spiro[benzofuran-2(3H),1'-[3]cyclohexene]-2',3-dione,4',7-dichloro-4,6-dimethoxy-6'-methyl-	357.2	C16H14Cl2O5
620371	Spiro[benzofuran-2(3H),1'-cyclohexan]-3-one,7-chloro-4'-hydroxy-2',4,6-trimethoxy-6'-methyl-	356.8	C17H21ClO6
620374	Spiro[benzofuran-2(3H),1'-cyclohexane]-2',3,4'-trione,3',7-dichloro-4,6-dimethoxy-6'-methyl-	373.2	C16H14Cl2O6
622712	Spiro[benzofuran-2(3H),1'-cyclohexane]-2',3-dione, 7-chloro-4,6-dimethoxy-6'-methyl-	324.75	C16H17ClO5
626596	Spiro[benzofuran-2(3H),1'-cyclohexane]-2',3,4'-trione, 7-chloro-4,6-dimethoxy-3',3',6'-trimethyl-	366.8	C18H19ClO6
629676	Spiro[benzofuran-2(3H),1'-cyclohexane]-3,4'-dione, 7-chloro-4,6-dimethoxy-2'-methyl-	324.75	C16H17ClO5
630845	Spiro[benzofuran-2(3H),1'-cyclohexane]-2',3,4'-trione, 7-chloro-4,6-dimethoxy-6'-methyl-	338.74	C16H15ClO6
631655	Griseophenone	350.7	C17H15ClO6
941385	(2S,6'R)-7-chloro-2',4,6-trimethoxy-6'-methyl-3H-spiro[1-benzofuran-2,1'-cyclohexan]-2'-ene-3,4'-dione	352.8	C17H17ClO6
978391	(2S,5'S)-7-chloro-3',4,6-trimethoxy-5'-methylspiro[1-benzofuran-2,4'-cyclohex-2-ene]-1',3-dione	352.8	C17H17ClO6
978395	(2R,5'R)-7-chloro-3',4,6-trimethoxy-5'-methylspiro[1-benzofuran-2,4'-cyclohex-2-ene]-1',3-dione	352.8	C17H17ClO6
3082005	Dehydrogriseofulvin	350.7	C17H15ClO6
4125561	7-Chloro-4'-hydroxy-2',4,6-trimethoxy-6'-methyl-3H-spiro[benzofuran-2,1'-cyclohex[2]EN]-3-one	354.8	C17H19ClO6
5126442	7-Chloro-3'-hydroxy-4,6-dimethoxy-5'-methylspiro[1-benzofuran-2,4'-cyclohex-2-ene]-1',3-dione	338.74	C16H15ClO6
5702061	(5'R)-7-chloro-3',4,6-trimethoxy-5'-methylspiro[1-benzofuran-2,4'-cyclohex-2-ene]-1',3-dione	352.8	C17H17ClO6
6452395	Desmethylgriseofulvin	338.74	C16H15ClO6
6604225	(2S,3'S,5'R)-7-chloro-3',4,6-trimethoxy-5'-methylspiro[1-benzofuran-2,4'-cyclohexane]-1',3-dione	354.8	C17H19ClO6
6713927	(2S,5'R)-7-chloro-3',4,6-trimethoxy-5'-methylspiro[benzofuran-2,4'-cyclohexane]-1',3-dione	354.8	C17H19ClO6
9974417	6-O-Demethyl Griseofulvin	338.74	C16H15ClO6
10019062	(2S,6'R)-2',4-Dimethoxy-6'beta-methyl-7-chlorospiro[benzofuran-2(3H),1'-[2]cyclohexene]-3,4'-dione	322.74	C16H15ClO5
10045461	(2S,6'R)-2',4,5,6-Tetramethoxy-6'beta-methyl-7-chlorospiro[benzofuran-2(3H),1'-[2]cyclohexene]-3,4'-dione	382.8	C18H19ClO7
10406626	(2S,6'R)-2',4,6-Trimethoxy-5,6'beta-dimethyl-7-chlorospiro[benzofuran-2(3H),1'-[2]cyclohexene]-3,4'-dione	366.8	C18H19ClO6

10407853	5-Chlorogriseofulvin	387.2	C17H16Cl2O6
10497262	(2R,6'R)-2'-(Methylthio)-4-methoxy-6'beta-methyl-7-chlorospiro[benzofuran-2(3H),1'-[2]cyclohexene]-3,4'-dione	338.8	C16H15ClO4S
10574693	(2S,5'S)-7-chloro-4,6-dimethoxy-3'-methylsulfanyl-5'-phenylspiro[1-benzofuran-2,4'-cyclohex-2-ene]-1',3-dione	430.9	C22H19ClO5S
10596108	(2S,5'R)-7-chloro-3'-ethylsulfanyl-4,6-dimethoxy-5'-methylspiro[1-benzofuran-2,4'-cyclohex-2-ene]-1',3-dione	382.9	C18H19ClO5S
10619960	(2R,6'R)-2'-(Methylthio)-4,6-dimethoxy-5,6'beta-dimethyl-7-chlorospiro[benzofuran-2(3H),1'-[2]cyclohexene]-3,4'-dione	382.9	C18H19ClO5S
10621755	(2S,5'S)-7-chloro-3',4,6-trimethoxy-5'-phenylspiro[1-benzofuran-2,6'-cyclohex-2-ene]-1',3-dione	414.8	C22H19ClO6
10623284	(2R,5'S)-7-chloro-4,6-dimethoxy-3'-methylsulfinyl-5'-phenylspiro[1-benzofuran-2,4'-cyclohex-2-ene]-1',3-dione	446.9	C22H19ClO6S
10642700	(2S,6'R)-7-Chloro-2',4,6-trimethoxy-6'-ethylspiro[benzofuran-2(3H),1'-[2]cyclohexene]-3,4'-dione	366.8	C18H19ClO6
10643661	(2R,5'R)-7-chloro-5'-ethyl-4,6-dimethoxy-3'-methylsulfanylspiro[1-benzofuran-2,4'-cyclohex-2-ene]-1',3-dione	382.9	C18H19ClO5S
10668598	(2S,5'R)-7-chloro-3'-ethylsulfinyl-4,6-dimethoxy-5'-methylspiro[1-benzofuran-2,4'-cyclohex-2-ene]-1',3-dione	398.9	C18H19ClO6S
10687333	(2S,6'R)-2',6-Dimethoxy-6'beta-methyl-7-chlorospiro[benzofuran-2(3H),1'-[2]cyclohexene]-3,4'-dione	322.74	C16H15ClO5
10690292	7-Chloro-3'-ethoxy-4,6-dimethoxy-5'-methylspiro[1-benzofuran-2,4'-cyclohex-2-ene]-1',3-dione	366.8	C18H19ClO6
10691346	(2R)-4,6-Dimethoxy-4'-(ethylthio)-6'beta-methyl-7-chlorospiro[benzofuran-2(3H),1'-[3]cyclohexene]-2',3-dione	382.9	C18H19ClO5S
10691458	(2S,5'R)-7-chloro-4,6-dimethoxy-5'-methyl-3'-methylsulfinylspiro[1-benzofuran-2,4'-cyclohex-2-ene]-1',3-dione	384.8	C17H17ClO6S
10693960	(2R,5'S)-7-chloro-4,6-dimethoxy-3'-methylsulfanyl-5'-phenylspiro[1-benzofuran-2,4'-cyclohex-2-ene]-1',3-dione	430.9	C22H19ClO5S
10712095	(2R,6'R)-2'-(Methylthio)-6-methoxy-6'beta-methyl-7-chlorospiro[benzofuran-2(3H),1'-[2]cyclohexene]-3,4'-dione	338.8	C16H15ClO4S
10715802	(2S,5'R)-7-chloro-5'-ethyl-3'-ethylsulfanyl-4,6-dimethoxyspiro[1-benzofuran-2,6'-cyclohex-2-ene]-1',3-dione	396.9	C19H21ClO5S
10761572	7-Chloro-4,6-dimethoxy-6'-methyl-2'-(methylthio)-spiro(benzofuran-2(3H),1'-(2)cyclohexene)-3,4'-dione, cis-(+/-)-	368.8	C17H17ClO5S
10763672	(2R,6'R)-2'-(Methylthio)-4,6-dimethoxy-5,7-dichloro-6'beta-methylspiro[benzofuran-2(3H),1'-[2]cyclohexene]-3,4'-dione	403.3	C17H16Cl2O5S
10785158	(2S,5'R)-7-chloro-5'-ethyl-3',4,6-trimethoxyspiro[1-benzofuran-2,6'-cyclohex-2-ene]-1',3-dione	366.8	C18H19ClO6
10787864	(2R,5'R)-7-chloro-5'-ethyl-3'-ethylsulfinyl-4,6-dimethoxyspiro[1-benzofuran-2,4'-cyclohex-2-ene]-1',3-dione	412.9	C19H21ClO6S

10787978	(2S)-2',4,6-Trimethoxy-6'beta-phenyl-7-chlorospiro[benzofuran-2(3H),1'-[2]cyclohexene]-3,4'-dione	414.8	C22H19ClO6
10810786	(2R)-2'-(Ethylthio)-4,6-dimethoxy-6'beta-ethyl-7-chlorospiro[benzofuran-2(3H),1'-[2]cyclohexene]-3,4'-dione	396.9	C19H21ClO5S
10810923	(2R,5'R)-7-chloro-5'-ethyl-4,6-dimethoxy-3'-methylsulfinylspiro[1-benzofuran-2,4'-cyclohex-2-ene]-1',3-dione	398.9	C18H19ClO6S
10837041	(2R)-2'-(Ethylthio)-4,6-dimethoxy-6'beta-phenyl-7-chlorospiro[benzofuran-2(3H),1'-[2]cyclohexene]-3,4'-dione	444.9	C23H21ClO5S
11603327	(2S)-7-chloro-4,6-dimethoxy-5'-methyl-3'-propoxyspiro[1-benzofuran-2,4'-cyclohex-2-ene]-1',3-dione	380.8	C19H21ClO6
11794329	(2S,5'R)-7-chloro-5'-ethyl-4,6-dimethoxy-3'-methylsulfanylspiro[1-benzofuran-2,4'-cyclohex-2-ene]-1',3-dione	382.9	C18H19ClO5S
13735050	7-Chloro-2-[(2-hydroxy-3-oxo-5-propan-2-ylcyclohepta-1,4,6-trien-1-yl)-(4-methoxyphenyl)methyl]-4,6-dimethoxy-1-benzofuran-3-one	511	C28H27ClO7
14067764	ethyl 2-[4-[(Z)-(7-chloro-4,6-dimethoxy-3-oxo-1-benzofuran-2-ylidene)methyl]phenoxy]-2-methylpropanoate	446.9	C23H23ClO7
14565581	(2S,6'R)-7-Chloro-4,6-dimethoxy-6'-methylspiro[benzofuran-2(3H),1'-[2]cyclohexene]-3,4'-dione	322.74	C16H15ClO5
14565583	(3'R,5'R)-7-chloro-4,6-dimethoxy-3',5'-dimethylspiro[1-benzofuran-2,4'-cyclohexane]-1',3-dione	338.8	C17H19ClO5
14565584	(3'R,5'S)-7-chloro-4,6-dimethoxy-3',5'-dimethylspiro[1-benzofuran-2,4'-cyclohexane]-1',3-dione	338.8	C17H19ClO5
14565585	(2S,6'R)-7-Chloro-4,6-dimethoxy-2',6'-dimethylspiro[benzofuran-2(3H),1'-[2]cyclohexene]-3,4'-dione	336.8	C17H17ClO5
14565587	(2S,5'R)-3'-(bromomethyl)-7-chloro-4,6-dimethoxy-5'-methylspiro[1-benzofuran-2,4'-cyclohex-2-ene]-1',3-dione	415.7	C17H16BrClO5
14565589	(2S,5'S,6'R)-6'-bromo-3'-(bromomethyl)-7-chloro-4,6-dimethoxy-5'-methylspiro[1-benzofuran-2,4'-cyclohex-2-ene]-1',3-dione	494.6	C17H15Br2ClO5
14589751	(2Z)-7-Chloro-2-ethylidene-4,6-dimethoxybenzofuran-3(2H)-one	254.66	C12H11ClO4
14589753	(2Z)-7-Chloro-4,6-dimethoxy-2-propylidenebenzofuran-3(2H)-one	268.69	C13H13ClO4
14589759	7-chloro-4,6-dimethoxy-2-methylene-3(2H)-benzofuranone	240.64	C11H9ClO4
14589761	7-Chloro-6',6'-dimethyl-2',4,6-trimethoxyspiro[benzofuran-2(3H),1'-[2]cyclohexene]-3,4'-dione	366.8	C18H19ClO6
14706665	7-Chloro-4,6-dimethoxy-6'-methyl-2'-(methylthio)-spiro(benzofuran-2(3H),1'-(2)cyclohexene)-3,4'-dione, trans-(+/-)-	368.8	C17H17ClO5S
14737140	2-Phenyl-methylene-7-chloro-4,6-dimethoxy-3(2H)-benzofuranone	316.7	C17H13ClO4
14760418	2,2-Bis(hydroxymethyl)-4,6-dimethoxy-7-chlorobenzofuran-3(2H)-one	288.68	C12H13ClO6
15086460	4'-O-Demethyl Griseofulvin	338.74	C16H15ClO6

20841686	(2S)-7-chloro-4-hydroxy-3',6-dimethoxy-5'-methylspiro[1-benzofuran-2,4'-cyclohex-2-ene]-1',3-dione	338.74	C16H15ClO6
21123948	(2S)-7-chloro-6-hydroxy-3',4-dimethoxy-5'-methylspiro[1-benzofuran-2,4'-cyclohex-2-ene]-1',3-dione	338.74	C16H15ClO6
21629991	(2R,5'R)-7-chloro-2'-hydroxy-4,6-dimethoxy-3',5'-dimethylspiro[1-benzofuran-2,4'-cyclohex-2-ene]-1',3-dione	352.8	C17H17ClO6
21677661	Isogriseofulvin	352.8	C17H17ClO6
21677662	(2S,5'R)-7-chloro-4,6-dimethoxy-5'-methylspiro[1-benzofuran-2,6'-cyclohex-2-ene]-1',3-dione	322.74	C16H15ClO5
21820746	7-Chloro-2'-hydroxy-4,5',6-trimethoxy-3'-methylspiro[1-benzofuran-2,4'-cyclohexa-2,5-diene]-1',3-dione	366.7	C17H15ClO7
22216755	(2S)-5,7-dichloro-3',4,6-trimethoxy-5'-methylspiro[1-benzofuran-2,4'-cyclohex-2-ene]-1',3-dione	387.2	C17H16Cl2O6
23424082	7-Chloro-3'-ethoxy-4,6-dimethoxy-5'-methylspiro[1-benzofuran-2,6'-cyclohex-2-ene]-1',3-dione	366.8	C18H19ClO6
23424318	7-Chloro-4,6-dimethoxy-5'-methyl-3'-propoxyspiro[1-benzofuran-2,4'-cyclohex-2-ene]-1',3-dione	380.8	C19H21ClO6
23424319	7-Chloro-4,6-dimethoxy-5'-methyl-3'-propoxyspiro[1-benzofuran-2,6'-cyclohex-2-ene]-1',3-dione	380.8	C19H21ClO6
23424320	3'-Butoxy-7-chloro-4,6-dimethoxy-5'-methylspiro[1-benzofuran-2,4'-cyclohex-2-ene]-1',3-dione	394.8	C20H23ClO6
23424321	3'-Butoxy-7-chloro-4,6-dimethoxy-5'-methylspiro[1-benzofuran-2,6'-cyclohex-2-ene]-1',3-dione	394.8	C20H23ClO6
23424413	7-Chloro-3',6-diethoxy-4-methoxy-5'-methylspiro[1-benzofuran-2,4'-cyclohex-2-ene]-1',3-dione	380.8	C19H21ClO6
23424433	7-Chloro-3'-hexoxy-4,6-dimethoxy-5'-methylspiro[1-benzofuran-2,6'-cyclohex-2-ene]-1',3-dione	422.9	C22H27ClO6
23424466	[3,4,5-Triacetyloxy-6-(7-chloro-4,6-dimethoxy-5'-methyl-3,3'-dioxospiro[1-benzofuran-2,6'-cyclohexene]-1'-yl)oxyoxan-2-yl]methyl acetate	669	C30H33ClO15
23955821	7-Chloro-3'-hydroxy-4,6-dimethoxy-5'-methylspiro[1-benzofuran-2,6'-cyclohexa-2,4-diene]-1',3-dione	336.72	C16H13ClO6
25171426	(2S,5'R)-3'-butoxy-7-chloro-4,6-dimethoxy-5'-methylspiro[1-benzofuran-2,4'-cyclohex-2-ene]-1',3-dione	394.8	C20H23ClO6
25171427	(2S,5'R)-7-chloro-4,6-dimethoxy-5'-methyl-3'-pentoxyspiro[1-benzofuran-2,4'-cyclohex-2-ene]-1',3-dione	408.9	C21H25ClO6
25171428	(2S,5'R)-7-chloro-3'-hexoxy-4,6-dimethoxy-5'-methylspiro[1-benzofuran-2,4'-cyclohex-2-ene]-1',3-dione	422.9	C22H27ClO6
25171429	(2S,5'R)-7-chloro-4,6-dimethoxy-5'-methyl-3'-pent-4-enoxyspiro[1-benzofuran-2,4'-cyclohex-2-ene]-1',3-dione	406.9	C21H23ClO6
25171430	(2S,5'R)-7-chloro-3'-(cyclopropylmethoxy)-4,6-dimethoxy-5'-methylspiro[1-benzofuran-2,4'-cyclohex-2-ene]-1',3-dione	392.8	C20H21ClO6

25171632	(2S,5'R)-7-chloro-3'-cyclopentyloxy-4,6-dimethoxy-5'-methylspiro[1-benzofuran-2,4'-cyclohex-2-ene]-1',3-dione	406.9	C21H23ClO6
25171633	(2S,5'R)-7-chloro-4,6-dimethoxy-5'-methyl-3'-phenylmethoxyspiro[1-benzofuran-2,4'-cyclohex-2-ene]-1',3-dione	428.9	C23H21ClO6
25171634	(2S,5'R)-7-chloro-4-ethoxy-3',6-dimethoxy-5'-methylspiro[1-benzofuran-2,4'-cyclohex-2-ene]-1',3-dione	366.8	C18H19ClO6
25171635	(2S,5'R)-7-chloro-3',6-dimethoxy-5'-methyl-4-phenylmethoxyspiro[1-benzofuran-2,4'-cyclohex-2-ene]-1',3-dione	428.9	C23H21ClO6
25171636	(2S,5'R)-7-chloro-3',4,6-trimethoxy-2',5'-dimethylspiro[1-benzofuran-2,4'-cyclohex-2-ene]-1',3-dione	366.8	C18H19ClO6
25171637	(2S,3'R,5'S)-7-chloro-4,6-dimethoxy-3'-methyl-5'-phenylmethoxyspiro[1-benzofuran-2,4'-cyclohexane]-1',3-dione	430.9	C23H23ClO6
25171846	(2S,3'E,5'R)-7-chloro-3'-hydroxyimino-1',4,6-trimethoxy-5'-methylspiro[1-benzofuran-2,6'-cyclohexene]-3-one	367.8	C17H18ClNO6
25171847	(2S,5'R)-7-chloro-4,6-dimethoxy-5'-methyl-3'-propan-2-yloxyspiro[1-benzofuran-2,4'-cyclohex-2-ene]-1',3-dione	380.8	C19H21ClO6
25171849	(2S,5'R)-7-chloro-4,6-dimethoxy-5'-methyl-3'-(naphthalen-1-ylmethoxy)spiro[1-benzofuran-2,4'-cyclohex-2-ene]-1',3-dione	478.9	C27H23ClO6
25172057	(2R,5'R)-3'-benzylsulfanyl-7-chloro-4,6-dimethoxy-5'-methylspiro[1-benzofuran-2,4'-cyclohex-2-ene]-1',3-dione	444.9	C23H21ClO5S
40455568	(2R)-7-chloro-3',4,6-trimethoxy-5'-methylspiro[1-benzofuran-2,4'-cyclohexa-2,5-diene]-1',3-dione	350.7	C17H15ClO6
44139468	(2S,5'R)-7-chloro-4,6-dimethoxy-5'-methyl-3'-[(4-methylphenyl)methoxy]spiro[1-benzofuran-2,4'-cyclohex-2-ene]-1',3-dione	442.9	C24H23ClO6
44139586	(2S,5'R)-3'-(1-adamantylmethoxy)-7-chloro-4,6-dimethoxy-5'-methylspiro[1-benzofuran-2,4'-cyclohex-2-ene]-1',3-dione	487	C27H31ClO6
44139587	(2S,5'R)-7-chloro-3'-(cyclopropylmethoxy)-4,6-dimethoxy-5'-methylspiro[1-benzofuran-2,6'-cyclohex-2-ene]-1',3-dione	392.8	C20H21ClO6
44139588	(2S,5'R)-7-chloro-4,6-dimethoxy-5'-methyl-3'-(2-phenylethoxy)spiro[1-benzofuran-2,4'-cyclohex-2-ene]-1',3-dione	442.9	C24H23ClO6
44139589	(2S,5'R)-7-chloro-4,6-dimethoxy-5'-methyl-3'-[(4-phenylphenyl)methoxy]spiro[1-benzofuran-2,4'-cyclohex-2-ene]-1',3-dione	505	C29H25ClO6
44139590	(2S,5'R)-7-chloro-3'-cyclopentyloxy-4,6-dimethoxy-5'-methylspiro[1-benzofuran-2,6'-cyclohex-2-ene]-1',3-dione	406.9	C21H23ClO6
44148513	Griseofulvin 4'-oxime	367.8	C17H18ClNO6
44565921	4-O-Demethyl Griseofulvin	338.74	C16H15ClO6
44565973	(2S,5'R)-7-chloro-3'-ethoxy-4,6-dimethoxy-5'-methylspiro[1-benzofuran-2,4'-cyclohex-2-ene]-1',3-dione	366.8	C18H19ClO6
44565974	(2S,6'R)-7-Chloro-2'-propoxy-4,6-dimethoxy-6'-methylspiro[benzofuran-2(3H),1'-[2]cyclohexene]-3,4'-dione	380.8	C19H21ClO6

44566031	(2S,5'R)-7-chloro-4,6-dimethoxy-5'-methyl-3'-phenoxyspiro[1-benzofuran-2,4'-cyclohex-2-ene]-1',3-dione	414.8	C22H19ClO6
44566051	(2S,3'S,5'R)-7-chloro-3',6-dihydroxy-1',4-dimethoxy-5'-methylspiro[1-benzofuran-2,6'-cyclohexene]-3-one	340.75	C16H17ClO6
44566064	(2S,2'S,4'S,6'R)-7-chloro-4'-hydroxy-2',4,6-trimethoxy-6'-methylspiro[1-benzofuran-2,1'-cyclohexane]-3-one	356.8	C17H21ClO6
44566065	(2S,3'Z,5'R)-7-chloro-3'-hydroxyimino-1',4,6-trimethoxy-5'-methylspiro[1-benzofuran-2,6'-cyclohexene]-3-one	367.8	C17H18ClNO6
44566068	(2R,5'R)-7-chloro-4,6-dimethoxy-2',2',5'-trimethylspiro[1-benzofuran-2,4'-cyclohexane]-1',3,3'-trione	366.8	C18H19ClO6
44566075	(2S,5'R)-2'-benzyl-7-chloro-3'-hydroxy-4,6-dimethoxy-5'-methylspiro[1-benzofuran-2,4'-cyclohex-2-ene]-1',3-dione	428.9	C23H21ClO6
44566076	(2S,5'R)-7-chloro-2'-iodo-3',4,6-trimethoxy-5'-methylspiro[1-benzofuran-2,4'-cyclohex-2-ene]-1',3-dione	478.7	C17H16ClIO6
44566077	(2S,5'R)-7-chloro-2'-iodo-4,6-dimethoxy-5'-methyl-3'-propoxyspiro[1-benzofuran-2,4'-cyclohex-2-ene]-1',3-dione	506.7	C19H20ClIO6
44566078	(2S,5'R)-7-chloro-2'-iodo-4,6-dimethoxy-5'-methyl-3'-phenylmethoxyspiro[1-benzofuran-2,4'-cyclohex-2-ene]-1',3-dione	554.8	C23H20ClIO6
46843899	(2S,5'R)-7-chloro-3'-[(4-chlorophenyl)methoxy]-4,6-dimethoxy-5'-methylspiro[1-benzofuran-2,4'-cyclohex-2-ene]-1',3-dione	463.3	C23H20Cl2O6
46843961	(2S,5'R)-7-chloro-3'-[(4-iodophenyl)methoxy]-4,6-dimethoxy-5'-methylspiro[1-benzofuran-2,4'-cyclohex-2-ene]-1',3-dione	554.8	C23H20ClIO6
46843962	(2S,5'R)-7-chloro-3'-[(3-iodophenyl)methoxy]-4,6-dimethoxy-5'-methylspiro[1-benzofuran-2,4'-cyclohex-2-ene]-1',3-dione	554.8	C23H20ClIO6
46843963	(2S,5'R)-7-chloro-3'-[(2-iodophenyl)methoxy]-4,6-dimethoxy-5'-methylspiro[1-benzofuran-2,4'-cyclohex-2-ene]-1',3-dione	554.8	C23H20ClIO6
46843964	(2S,5'R)-7-chloro-3'-[[4-(hydroxymethyl)phenyl]methoxy]-4,6-dimethoxy-5'-methylspiro[1-benzofuran-2,4'-cyclohex-2-ene]-1',3-dione	458.9	C24H23ClO7
46843965	(2S,5'R)-3'-[[4-(bromomethyl)phenyl]methoxy]-7-chloro-4,6-dimethoxy-5'-methylspiro[1-benzofuran-2,4'-cyclohex-2-ene]-1',3-dione	521.799	C24H22BrClO6
46844022	(2S,5'R)-7-chloro-3'-[(2-chlorophenyl)methoxy]-4,6-dimethoxy-5'-methylspiro[1-benzofuran-2,4'-cyclohex-2-ene]-1',3-dione	463.3	C23H20Cl2O6
46844023	(2S,5'R)-3'-[(3-bromophenyl)methoxy]-7-chloro-4,6-dimethoxy-5'-methylspiro[1-benzofuran-2,4'-cyclohex-2-ene]-1',3-dione	507.8	C23H20BrClO6
46844024	(2S,5'R)-7-chloro-3'-[(4-fluorophenyl)methoxy]-4,6-dimethoxy-5'-methylspiro[1-benzofuran-2,4'-cyclohex-2-ene]-1',3-dione	446.8	C23H20ClFO6
46844079	4-[[(2S,5'R)-7-chloro-4,6-dimethoxy-5'-methyl-3,3'-dioxospiro[1-benzofuran-2,6'-cyclohexene]-1'-yl]oxymethyl]benzonitrile	453.9	C24H20ClNO6
46844082	(2S,5'R)-3'-[[3,5-bis(phenylmethoxy)phenyl]methoxy]-7-chloro-4,6-dimethoxy-5'-methylspiro[1-benzofuran-2,4'-cyclohex-2-ene]-1',3-dione	641.1	C37H33ClO8

46844083	(2S,5'R)-3'-[(4-butoxyphenyl)methoxy]-7-chloro-4,6-dimethoxy-5'-methylspiro[1-benzofuran-2,4'-cyclohex-2-ene]-1',3-dione	501	C27H29ClO7
46844137	(2S,5'R)-7-chloro-4,6-dimethoxy-5'-methyl-3'-[[4-(trifluoromethyl)phenyl]methoxy]spiro[1-benzofuran-2,4'-cyclohex-2-ene]-1',3-dione	496.9	C24H20ClF3O6
46844138	(2S,5'R)-7-chloro-3'-decoxy-2'-iodo-4,6-dimethoxy-5'-methylspiro[1-benzofuran-2,4'-cyclohex-2-ene]-1',3-dione	604.9	C26H34ClIO6
51401507	(2S,3'R,5'R)-7-chloro-3',4,6-trimethoxy-5'-methylspiro[1-benzofuran-2,4'-cyclohexane]-1',3-dione	354.8	C17H19ClO6
56691266	7-Chloro-2',4,6-trimethoxy-6'-methylspiro[1-benzofuran-2,4'-cyclohex-2-ene]-1',3-dione	352.8	C17H17ClO6
56924745	(2S,5'R)-3',7-dichloro-4,6-dimethoxy-5'-methylspiro[1-benzofuran-2,6'-cyclohex-2-ene]-1',3-dione	357.2	C16H14Cl2O5
56924746	(2R,5'R)-3',7-dichloro-4,6-dimethoxy-5'-methylspiro[1-benzofuran-2,4'-cyclohex-2-ene]-1',3-dione	357.2	C16H14Cl2O5
56924747	(2S,5'R)-7-chloro-3',6-dimethoxy-5'-methyl-4-(naphthalen-1-ylmethoxy)spiro[1-benzofuran-2,4'-cyclohex-2-ene]-1',3-dione	478.9	C27H23ClO6
56950704	(2S,5'R)-7-chloro-3',6-dimethoxy-5'-methyl-4-pentoxyspiro[1-benzofuran-2,4'-cyclohex-2-ene]-1',3-dione	408.9	C21H25ClO6
56950842	(2S,5'R)-7-chloro-4,6-dimethoxy-3'-[(2-methoxyphenyl)methoxy]-5'-methylspiro[1-benzofuran-2,4'-cyclohex-2-ene]-1',3-dione	458.9	C24H23ClO7
56950843	(2S,5'R)-7-chloro-4,6-dimethoxy-3'-[(3-methoxyphenyl)methoxy]-5'-methylspiro[1-benzofuran-2,4'-cyclohex-2-ene]-1',3-dione	458.9	C24H23ClO7
56950844	(2S,5'R)-7-chloro-4,6-dimethoxy-3'-[(4-methoxyphenyl)methoxy]-5'-methylspiro[1-benzofuran-2,4'-cyclohex-2-ene]-1',3-dione	458.9	C24H23ClO7
56950845	(2S,5'R)-7-chloro-4,6-dimethoxy-3'-[(3-methoxyphenyl)methoxy]-5'-methylspiro[1-benzofuran-2,6'-cyclohex-2-ene]-1',3-dione	458.9	C24H23ClO7
56950846	(2S,5'R)-7-chloro-4,6-dimethoxy-5'-methyl-3'-phenylmethoxyspiro[1-benzofuran-2,6'-cyclohex-2-ene]-1',3-dione	428.9	C23H21ClO6
57390407	(2S,5'R)-7-chloro-3'-ethoxy-4,6-dimethoxy-5'-methylspiro[1-benzofuran-2,6'-cyclohex-2-ene]-1',3-dione	366.8	C18H19ClO6
57392201	(2S,5'R)-7-chloro-6-ethoxy-3',4-dimethoxy-5'-methylspiro[1-benzofuran-2,4'-cyclohex-2-ene]-1',3-dione	366.8	C18H19ClO6
57393956	(2S,5'R)-7-chloro-4,6-dimethoxy-5'-methyl-3'-propan-2-yloxyspiro[1-benzofuran-2,6'-cyclohex-2-ene]-1',3-dione	380.8	C19H21ClO6
57395698	(2S,5'R)-7-chloro-4,6-dimethoxy-5'-methyl-3'-propoxyspiro[1-benzofuran-2,6'-cyclohex-2-ene]-1',3-dione	380.8	C19H21ClO6
57397525	Rel-Griseofulvic Acid	338.74	C16H15ClO6
57397526	(2S,5'R)-7-chloro-3',6-dihydroxy-4-methoxy-5'-methylspiro[1-benzofuran-2,4'-cyclohex-2-ene]-1',3-dione	324.71	C15H13ClO6

67096429	(2S,6'R)-7-Chloro-2',4,6-trimethoxy-6'-methyl-3H,4'H-spiro[1-benzofuran-2,1'-cyclohex-2-ene]-3,4'-dione	705.5	C34H34Cl2O12
67363532	2-aminoacetic acid;(2S,5'R)-7-chloro-3',4,6-trimethoxy-5'-methylspiro[1-benzofuran-2,4'-cyclohex-2-ene]-1',3-dione	427.8	C19H22ClNO8
67892219	(2S,5'R)-7-chloro-3',4,6-trimethoxy-5'-methylspiro[1-benzofuran-2,4'-cyclohex-2-ene]-1',3-dione;prop-2-en-1-amine	409.9	C20H24ClNO6
68024713	(2S)-7-chloro-3'-hexoxy-4-hydroxy-6-methoxyspiro[1-benzofuran-2,4'-cyclohex-2-ene]-1',3-dione	394.8	C20H23ClO6
68727568	(5'R)-7-chloro-3',4,6-trimethoxy-2',5'-dimethylspiro[1-benzofuran-2,4'-cyclohex-2-ene]-1',3-dione	366.8	C18H19ClO6
68727702	(2S,5'R)-7-chloro-4,6-dimethoxy-5'-methyl-3'-prop-2-enoxyspiro[1-benzofuran-2,4'-cyclohex-2-ene]-1',3-dione	378.8	C19H19ClO6
70039744	(2S,5'R)-7-chloro-3',4,6-trimethoxy-5'-methylspiro[1-benzofuran-2,4'-cyclohex-2-ene]-1',3-dione;1,4-dioxane	440.9	C21H25ClO8
70355234	(2S,5'R)-7-chloro-3',4,6-trimethoxy-5'-methylspiro[1-benzofuran-2,4'-cyclohex-2-ene]-1',3-dione;sulfane	386.8	C17H19ClO6S
70658189	7-Chloro-6-(hydroxymethyl)-3',4-dimethoxy-5'-methylspiro[1-benzofuran-2,4'-cyclohex-2-ene]-1',3-dione	352.8	C17H17ClO6
70870984	(2S,5'R)-7-chloro-3'-[2-(2-iodophenyl)ethyl]-4,6-dimethoxy-5'-methylspiro[1-benzofuran-2,4'-cyclohex-2-ene]-1',3-dione	552.8	C24H22ClIO5
70876805	(2S,5'R)-7-chloro-4,6-dimethoxy-5'-methyl-3'-(2-phenylethyl)spiro[1-benzofuran-2,4'-cyclohex-2-ene]-1',3-dione	426.9	C24H23ClO5
71043635	(2S)-7-chloro-3'-(cyclopropylmethoxy)-4,6-dimethoxyspiro[1-benzofuran-2,4'-cyclohex-2-ene]-1',3-dione	378.8	C19H19ClO6
71312580	Griseofulvin 13C17	369.64	C17H17ClO6
71317160	Griseofulvic acid	338.74	C16H15ClO6
71317161	(2S,5'R)-7-chloro-3',6-dimethoxy-5'-methyl-4-(trideuterio(113C)methoxy)spiro[1-benzofuran-2,4'-cyclohex-2-ene]-1',3-dione	356.77	C17H17ClO6
71318420	3(2H)-Benzofuranone, 7-chloro-4,6-dimethoxy-2-(phenylmethylene)-	316.7	C17H13ClO4
71318422	3(2H)-Benzofuranone, 5-chloro-4,6-dimethoxy-2-(phenylmethylene)-	316.7	C17H13ClO4
71737790	7-Chloro-4,6-dimethoxy-6'-methyl-2'-(methylthio)-spiro(benzofuran-2(3H),1'-(2)cyclohexene)-3,4'-dione	368.8	C17H17ClO5S
71763716	(2S)-2'-[[4-(Trimethylsilyl)benzyl]oxy]-4,6-dimethoxy-6'beta-methyl-7-chlorospiro[benzofuran-2(3H),1'-[2]cyclohexene]-3,4'-dione	501	C26H29ClO6Si
71763717	(2S,5'R)-7-chloro-3'-[(4-(125I)iodanylphenyl)methoxy]-4,6-dimethoxy-5'-methylspiro[1-benzofuran-2,4'-cyclohex-2-ene]-1',3-dione	552.8	C23H20ClIO6
71764910	(2S,5'R)-7-chloro-3'-[(2-(125I)iodanylphenyl)methoxy]-4,6-dimethoxy-5'-methylspiro[1-benzofuran-2,4'-cyclohex-2-ene]-1',3-dione	552.8	C23H20ClIO6

71764911	(2S,5'R)-7-chloro-3'-[(3-(125I)iodanylphenyl)methoxy]-4,6-dimethoxy-5'-methylspiro[1-benzofuran-2,4'-cyclohex-2-ene]-1',3-dione	552.8	C23H20ClIO6
71777464	(2R,5'R)-7-chloro-4,6-dimethoxy-5'-methylspiro[1-benzofuran-2,4'-cyclohexane]-1',3,3'-trione	338.74	C16H15ClO6
72726987	Ethyl2-[4-[(7-chloro-4,6-dimethoxy-3-oxo-1-benzofuran-2-ylidene)methyl]phenoxy]-2-methylpropanoate	446.9	C23H23ClO7
73053256	(2S,5'R)-7-chloro-4,6-dimethoxy-5'-methyl-3'-methylsulfonylspiro[1-benzofuran-2,4'-cyclohex-2-ene]-1',3-dione	400.8	C17H17ClO7S
73330625	(2S,2'S,6'R)-7-chloro-4,6-dimethoxy-6'-methyl-2'-phenylspiro[1-benzofuran-2,5'-2,3,6,7-tetrahydro-1-benzofuran]-3,4'-dione	440.9	C24H21ClO6
73330762	(2S,2'R,6'R)-7-chloro-4,6-dimethoxy-2',6'-dimethyl-2'-phenylspiro[1-benzofuran-2,7'-5,6-dihydro-3H-1-benzofuran]-3,4'-dione	454.9	C25H23ClO6
73330763	(2S,6'R)-7-chloro-4,6-dimethoxy-6'-methyl-2',2'-diphenylspiro[1-benzofuran-2,5'-6,7-dihydro-3H-1-benzofuran]-3,4'-dione	517	C30H25ClO6
73330764	(2S,6'R)-7-chloro-4,6-dimethoxy-6'-methyl-2',2'-diphenylspiro[1-benzofuran-2,7'-5,6-dihydro-3H-1-benzofuran]-3,4'-dione	517	C30H25ClO6
73330766	methyl 4-[(2S,2'S,6'R)-7-chloro-4,6-dimethoxy-6'-methyl-3,4'-dioxospiro[1-benzofuran-2,7'-2,3,5,6-tetrahydro-1-benzofuran]-2'-yl]benzoate	498.9	C26H23ClO8
73330910	methyl 4-[(2S,2'R,6'R)-7-chloro-4,6-dimethoxy-6'-methyl-3,4'-dioxospiro[1-benzofuran-2,7'-2,3,5,6-tetrahydro-1-benzofuran]-2'-yl]benzoate	498.9	C26H23ClO8
73330911	2-[(2S,2'R,6'R)-7-chloro-4,6-dimethoxy-6'-methyl-3,4'-dioxo-2'-phenylspiro[1-benzofuran-2,7'-5,6-dihydro-3H-1-benzofuran]-2'-yl]ethyl acetate	527	C28H27ClO8
73330912	(2S,2'R,6'R)-7-chloro-2'-(4-hydroxybutyl)-4,6-dimethoxy-6'-methyl-2'-phenylspiro[1-benzofuran-2,7'-5,6-dihydro-3H-1-benzofuran]-3,4'-dione	513	C28H29ClO7
73331060	(2S,2'S,6'R)-7-chloro-2'-(3,4-dichlorophenyl)-4,6-dimethoxy-6'-methylspiro[1-benzofuran-2,7'-2,3,5,6-tetrahydro-1-benzofuran]-3,4'-dione	509.8	C24H19Cl3O6
73331205	(2S,2'R,6'R)-7-chloro-2'-(3,4-dichlorophenyl)-4,6-dimethoxy-6'-methylspiro[1-benzofuran-2,7'-2,3,5,6-tetrahydro-1-benzofuran]-3,4'-dione	509.8	C24H19Cl3O6
73331208	(2S,2'S,6'R)-7-chloro-2'-(4-fluorophenyl)-4,6-dimethoxy-6'-methylspiro[1-benzofuran-2,5'-2,3,6,7-tetrahydro-1-benzofuran]-3,4'-dione	458.9	C24H20ClFO6
73331209	(2S,2'R,6'R)-7-chloro-2'-(4-fluorophenyl)-4,6-dimethoxy-6'-methylspiro[1-benzofuran-2,5'-2,3,6,7-tetrahydro-1-benzofuran]-3,4'-dione	458.9	C24H20ClFO6
73331344	(2S,6'R)-7-chloro-2'-(2-fluorophenyl)-4,6-dimethoxy-6'-methylspiro[1-benzofuran-2,5'-2,3,6,7-tetrahydro-1-benzofuran]-3,4'-dione	458.9	C24H20ClFO6
73331345	(2S,2'S,6'R)-7-chloro-2'-(3-fluorophenyl)-4,6-dimethoxy-6'-methylspiro[1-benzofuran-2,7'-2,3,5,6-tetrahydro-1-benzofuran]-3,4'-dione	458.9	C24H20ClFO6
73331346	(2S,2'R,6'R)-7-chloro-2'-(3-fluorophenyl)-4,6-dimethoxy-6'-methylspiro[1-benzofuran-2,7'-2,3,5,6-tetrahydro-1-benzofuran]-3,4'-dione	458.9	C24H20ClFO6
73331347	(2S,2'R,6'R)-7-chloro-2'-(4-fluorophenyl)-4,6-dimethoxy-6'-methylspiro[1-benzofuran-2,7'-2,3,5,6-tetrahydro-1-benzofuran]-3,4'-dione	458.9	C24H20ClFO6

73331348	(2S,2'S,6'R)-7-chloro-2'-(2-fluorophenyl)-4,6-dimethoxy-6'-methylspiro[1-benzofuran-2,7'-2,3,5,6-tetrahydro-1-benzofuran]-3,4'-dione	458.9	C24H20ClFO6
73331349	(2S,2'R,6'R)-7-chloro-2'-(2-fluorophenyl)-4,6-dimethoxy-6'-methylspiro[1-benzofuran-2,7'-2,3,5,6-tetrahydro-1-benzofuran]-3,4'-dione	458.9	C24H20ClFO6
73331487	(2S,2'S,6'R)-7-chloro-4,6-dimethoxy-6'-methyl-2'-[4-(trifluoromethyl)phenyl]spiro[1-benzofuran-2,7'-2,3,5,6-tetrahydro-1-benzofuran]-3,4'-dione	508.9	C25H20ClF3O6
73331488	(2S,2'R,6'R)-7-chloro-4,6-dimethoxy-6'-methyl-2'-[4-(trifluoromethyl)phenyl]spiro[1-benzofuran-2,7'-2,3,5,6-tetrahydro-1-benzofuran]-3,4'-dione	508.9	C25H20ClF3O6
73331490	(2S,2'R,6'R)-7-chloro-4,6-dimethoxy-6'-methyl-2'-phenylspiro[1-benzofuran-2,7'-2,3,5,6-tetrahydro-1-benzofuran]-3,4'-dione	440.9	C24H21ClO6
73331491	(2S,2'S,6'R)-7-chloro-4,6-dimethoxy-6'-methyl-2'-phenylspiro[1-benzofuran-2,7'-2,3,5,6-tetrahydro-1-benzofuran]-3,4'-dione	440.9	C24H21ClO6
73331628	(2S,2'R,6'R)-2'-(2-bromoethyl)-7-chloro-4,6-dimethoxy-6'-methyl-2'-phenylspiro[1-benzofuran-2,7'-5,6-dihydro-3H-1-benzofuran]-3,4'-dione	547.8	C26H24BrClO6
73331629	(2S,2'S,6'R)-2'-(2-bromoethyl)-7-chloro-4,6-dimethoxy-6'-methyl-2'-phenylspiro[1-benzofuran-2,7'-5,6-dihydro-3H-1-benzofuran]-3,4'-dione	547.8	C26H24BrClO6
73331632	(2R,2'R,6'S)-7-chloro-6'-hydroxy-4,6-dimethoxy-2'-methyl-6'-phenylspiro[1-benzofuran-2,1'-2,3,5,7,8,9-hexahydrobenzo[7]annulene]-3,4'-dione	482.9	C27H27ClO6
73331772	(2R,2'R,6'R)-7-chloro-6'-hydroxy-4,6-dimethoxy-2'-methyl-6'-phenylspiro[1-benzofuran-2,1'-2,3,5,7,8,9-hexahydrobenzo[7]annulene]-3,4'-dione	482.9	C27H27ClO6
74426566	3'-Benzylsulfanyl-7-chloro-4,6-dimethoxy-5'-methylspiro[1-benzofuran-2,4'-cyclohex-2-ene]-1',3-dione	444.9	C23H21ClO5S
75218801	3'-[[4-(Bromomethyl)phenyl]methoxy]-7-chloro-4,6-dimethoxy-5'-methylspiro[1-benzofuran-2,4'-cyclohex-2-ene]-1',3-dione	521.799	C24H22BrClO6
75218823	7-Chloro-3'-[(2-chlorophenyl)methoxy]-4,6-dimethoxy-5'-methylspiro[1-benzofuran-2,4'-cyclohex-2-ene]-1',3-dione	463.3	C23H20Cl2O6
75218824	3'-[(3-Bromophenyl)methoxy]-7-chloro-4,6-dimethoxy-5'-methylspiro[1-benzofuran-2,4'-cyclohex-2-ene]-1',3-dione	507.8	C23H20BrClO6
75218825	7-Chloro-3'-[(4-fluorophenyl)methoxy]-4,6-dimethoxy-5'-methylspiro[1-benzofuran-2,4'-cyclohex-2-ene]-1',3-dione	446.8	C23H20ClFO6
75218847	3'-[(4-Butoxyphenyl)methoxy]-7-chloro-4,6-dimethoxy-5'-methylspiro[1-benzofuran-2,4'-cyclohex-2-ene]-1',3-dione	501	C27H29ClO7
75218864	7-Chloro-4,6-dimethoxy-5'-methyl-3'-[[4-(trifluoromethyl)phenyl]methoxy]spiro[1-benzofuran-2,4'-cyclohex-2-ene]-1',3-dione	496.9	C24H20ClF3O6
75641496	7-Chloro-4,6-dimethoxy-5'-methyl-3,3'-dioxospiro[1-benzofuran-2,6'-cyclohexene]-1'-olate	337.73	C16H14ClO6-
76964619	(2S)-7-Chloro-2'-methylthio-4,6-dimethoxy-6'alpha-methylspiro[benzofuran-2(3H),1'-cyclohexan]-2'-ene-3,4'-dione	368.8	C17H17ClO5S

76968174	(2R,5'S)-7-chloro-4,6-dimethoxy-5'-methyl-3'-methylsulfanylspiro[1-benzofuran-2,4'-cyclohex-2-ene]-1',3-dione	368.8	C17H17ClO5S
76970921	(2R,5'S)-7-chloro-3',4,6-trimethoxy-5'-methylspiro[1-benzofuran-2,6'-cyclohex-2-ene]-1',3-dione	352.8	C17H17ClO6
76973167	(2S,5'R)-7-chloro-4,6-dimethoxy-5'-methyl-3'-(trideuterio(113C)methoxy)spiro[1-benzofuran-2,4'-cyclohex-2-ene]-1',3-dione	356.77	C17H17ClO6
76973812	(+)-Griseofulvin	355.8	C17H17ClO6
84820866	Dimethyl 7-chloro-4,4',6-trimethoxy-6'-methyl-2',3-dioxospiro[1-benzofuran-2,5'-cyclohex-3-ene]-1',5-dicarboxylate	468.8	C21H21ClO10
85199072	7-Chloro-3'-ethylsulfanyl-4,6-dimethoxy-5'-methylspiro[1-benzofuran-2,4'-cyclohex-2-ene]-1',3-dione	382.9	C18H19ClO5S
89050851	CID 89050851	452.7	C24H22BClO6
89054741	(2S,5'R)-7-chloro-4,6-dimethoxy-5'-methyl-3'-[(Z,2E)-2-prop-2-enylidenehex-3-enoxy]spiro[1-benzofuran-2,4'-cyclohex-2-ene]-1',3-dione	458.9	C25H27ClO6
89798228	(2S,5'R)-7-chloro-6-(hydroxymethyl)-3',4-dimethoxy-5'-methylspiro[1-benzofuran-2,4'-cyclohex-2-ene]-1',3-dione	352.8	C17H17ClO6
90958864	7-Chloro-4,6-dimethoxy-5'-methyl-3'-[(2-methylphenyl)methoxy]spiro[1-benzofuran-2,4'-cyclohex-2-ene]-1',3-dione	442.9	C24H23ClO6
91035900	7-chloro-4,6-dimethoxy-7'-methyl-3'-octylspiro[1-benzofuran-2,8'-3,4,6,7-tetrahydro-2H-chromene]-3,5'-dione	491	C27H35ClO6
91109362	7-Chloro-2'-ethyl-4,6-dimethoxy-5'-methyl-3'-propoxyspiro[1-benzofuran-2,4'-cyclohex-2-ene]-1',3-dione	408.9	C21H25ClO6
91564943	7-Chloro-3'-[(3-ethylphenyl)methoxy]-4,6-dimethoxy-5'-methylspiro[1-benzofuran-2,4'-cyclohex-2-ene]-1',3-dione	456.9	C25H25ClO6
91820110	Desmethyl-dehydro-griseofulvin	336.72	C16H13ClO6
92222230	(2R,3'S,5'R)-7-chloro-3'-hydroxy-1',4,6-trimethoxy-5'-methylspiro[1-benzofuran-2,6'-cyclohexene]-3-one	354.8	C17H19ClO6
92222231	(2R,3'S,5'S)-7-chloro-3'-hydroxy-1',4,6-trimethoxy-5'-methylspiro[1-benzofuran-2,6'-cyclohexene]-3-one	354.8	C17H19ClO6
92222232	(2R,3'R,5'R)-7-chloro-3'-hydroxy-1',4,6-trimethoxy-5'-methylspiro[1-benzofuran-2,6'-cyclohexene]-3-one	354.8	C17H19ClO6
92222233	(2R,3'R,5'S)-7-chloro-3'-hydroxy-1',4,6-trimethoxy-5'-methylspiro[1-benzofuran-2,6'-cyclohexene]-3-one	354.8	C17H19ClO6
92860931	(2S,6'R)-4,4'-Dimethoxy-6-hydroxy-6'beta-methyl-7-chlorospiro[benzofuran-2(3H),1'-[3]cyclohexene]-3,2'-dione	338.74	C16H15ClO6
95988133	(2R,6'R)-7-chloro-2',4,6-trimethoxy-6'-methylspiro[1-benzofuran-2,4'-cyclohex-2-ene]-1',3-dione	352.8	C17H17ClO6
95988134	(2R,6'S)-7-chloro-2',4,6-trimethoxy-6'-methylspiro[1-benzofuran-2,4'-cyclohex-2-ene]-1',3-dione	352.8	C17H17ClO6

95988135	(2S,6'R)-7-chloro-2',4,6-trimethoxy-6'-methylspiro[1-benzofuran-2,4'-cyclohex-2-ene]-1',3-dione	352.8	C17H17ClO6
95988136	(2S,6'S)-7-chloro-2',4,6-trimethoxy-6'-methylspiro[1-benzofuran-2,4'-cyclohex-2-ene]-1',3-dione	352.8	C17H17ClO6
98058924	(2R,5'R)-7-chloro-6-hydroxy-4-methoxy-5'-methylspiro[1-benzofuran-2,4'-cyclohexane]-1',3,3'-trione	324.71	C15H13ClO6
98058925	(2R,5'S)-7-chloro-6-hydroxy-4-methoxy-5'-methylspiro[1-benzofuran-2,4'-cyclohexane]-1',3,3'-trione	324.71	C15H13ClO6
98058926	(2S,5'R)-7-chloro-6-hydroxy-4-methoxy-5'-methylspiro[1-benzofuran-2,4'-cyclohexane]-1',3,3'-trione	324.71	C15H13ClO6
98058927	(2S,5'S)-7-chloro-6-hydroxy-4-methoxy-5'-methylspiro[1-benzofuran-2,4'-cyclohexane]-1',3,3'-trione	324.71	C15H13ClO6
98125634	dimethyl (1'S,2R,6'R)-7-chloro-4,4',6-trimethoxy-6'-methyl-2',3-dioxospiro[1-benzofuran-2,5'-cyclohex-3-ene]-1',5-dicarboxylate	468.8	C21H21ClO10
98125635	dimethyl (1'S,2R,6'S)-7-chloro-4,4',6-trimethoxy-6'-methyl-2',3-dioxospiro[1-benzofuran-2,5'-cyclohex-3-ene]-1',5-dicarboxylate	468.8	C21H21ClO10
98125636	dimethyl (1'R,2R,6'R)-7-chloro-4,4',6-trimethoxy-6'-methyl-2',3-dioxospiro[1-benzofuran-2,5'-cyclohex-3-ene]-1',5-dicarboxylate	468.8	C21H21ClO10
98125637	dimethyl (1'R,2R,6'S)-7-chloro-4,4',6-trimethoxy-6'-methyl-2',3-dioxospiro[1-benzofuran-2,5'-cyclohex-3-ene]-1',5-dicarboxylate	468.8	C21H21ClO10
98159926	(2S,3'R,5'S)-7-chloro-3'-hydroxy-1',4,6-trimethoxy-5'-methylspiro[1-benzofuran-2,6'-cyclohexene]-3-one	354.8	C17H19ClO6
98159927	(2S,3'R,5'R)-7-chloro-3'-hydroxy-1',4,6-trimethoxy-5'-methylspiro[1-benzofuran-2,6'-cyclohexene]-3-one	354.8	C17H19ClO6
99908084	ethyl 2-[4-[(E)-(7-chloro-4,6-dimethoxy-3-oxo-1-benzofuran-2-ylidene)methyl]phenoxy]-2-methylpropanoate	446.9	C23H23ClO7
101288398	(2S)-7-Chloro-5'beta-hydroxy-2',4,6-trimethoxy-6'beta-methylspiro[benzofuran-2(3H),1'-[2]cyclohexene]-3,4'-dione	368.8	C17H17ClO7
101592379	7-Chloro-4,6-dimethoxyspiro[benzofuran-2(3H),1'-cyclohexane]-3,4'-dione	310.73	C15H15ClO5
101592382	(2S,6'S)-7-Chloro-2',4,6-trimethoxy-6'-ethylspiro[benzofuran-2(3H),1'-[2]cyclohexene]-3,4'-dione	366.8	C18H19ClO6
101749852	2-(1-Methyl-3-oxobutyl)-3-oxo-4,6-dimethoxy-7-chloro-2,3-dihydrobenzofuran-2-carboxylic acid tert-butyl ester	412.9	C20H25ClO7
101749855	3-Oxo-4,6-dimethoxy-7-chloro-2,3-dihydrobenzofuran-2-carboxylic acid tert-butyl ester	328.74	C15H17ClO6
102066898	2-(Demethoxy)ethylthio-griseofulvin	382.9	C18H19ClO5S
102066899	(2R)-4,6-Dimethoxy-4'-(ethylthio)-6'beta-ethyl-7-chlorospiro[benzofuran-2(3H),1'-[3]cyclohexene]-2',3-dione	396.9	C19H21ClO5S
102102400	(2S)-2'-[[3-(Trimethylsilyl)benzyl]oxy]-4,6-dimethoxy-6'beta-methyl-7-chlorospiro[benzofuran-2(3H),1'-[2]cyclohexene]-3,4'-dione	501	C26H29ClO6Si

102102401	(2S)-2'-[[2-(Trimethylsilyl)benzyl]oxy]-4,6-dimethoxy-6'beta-methyl-7-chlorospiro[benzofuran-2(3H),1'-[2]cyclohexene]-3,4'-dione	501	C26H29ClO6Si
102239942	7-Chloro-4,4',6-trimethoxyspiro[benzofuran-2(3H),1'-cyclohexan]-3'-ene-2',3-dione	338.74	C16H15ClO6
118207010	(2S,4'R)-7-chloro-4,6-dimethoxy-4'-methylspiro[1-benzofuran-2,5'-7-oxabicyclo[4.1.0]heptane]-2',3-dione	338.74	C16H15ClO6
118207067	(2R,5'R)-7-chloro-4,6-dimethoxy-5'-methyl-3'-methylsulfonylspiro[1-benzofuran-2,4'-cyclohex-2-ene]-1',3-dione	400.8	C17H17ClO7S
118218025	(5'R)-3'-benzylsulfanyl-7-chloro-4,6-dimethoxy-5'-methylspiro[1-benzofuran-2,4'-cyclohex-2-ene]-1',3-dione	444.9	C23H21ClO5S
118254083	(2S,2'S,6'R)-7-chloro-4,6-dimethoxy-2',6'-dimethyl-2'-phenylspiro[1-benzofuran-2,7'-5,6-dihydro-3H-1-benzofuran]-3,4'-dione	454.9	C25H23ClO6
118254099	(2S,7'R)-7-chloro-2'-ethoxy-4,6-dimethoxy-7'-methylspiro[1-benzofuran-2,6'-3,4,7,8-tetrahydro-2H-chromene]-3,5'-dione	422.9	C21H23ClO7
118254103	(2S,3'R,6'R)-7-chloro-4,6-dimethoxy-6'-methyl-3'-phenylspiro[1-benzofuran-2,5'-2,3,6,7-tetrahydro-1-benzofuran]-3,4'-dione	440.9	C24H21ClO6
118254121	(2S,6'R)-7-chloro-4'-hydroxy-4,6-dimethoxy-6'-methyl-2'-phenylspiro[1-benzofuran-2,7'-3,4,5,6-tetrahydro-2H-1-benzofuran]-3-one	442.9	C24H23ClO6
118254131	(2S,3'S,6'R)-7-chloro-4,6-dimethoxy-6'-methyl-3'-phenylspiro[1-benzofuran-2,5'-2,3,6,7-tetrahydro-1-benzofuran]-3,4'-dione	440.9	C24H21ClO6
118254142	(2S,3'R)-7-chloro-4,6-dimethoxy-3'-methylspiro[1-benzofuran-2,4'-3,6-dihydro-2H-benzo[c]chromene]-1',3-dione	426.8	C23H19ClO6
118254145	(3'R)-7-chloro-4,6-dimethoxy-3'-methylspiro[1-benzofuran-2,4'-3,6-dihydro-2H-benzo[c]chromene]-1',3-dione	426.8	C23H19ClO6
118254151	(2S,2'R,6'R)-7-chloro-2'-(3-fluorophenyl)-4,6-dimethoxy-6'-methylspiro[1-benzofuran-2,5'-2,3,6,7-tetrahydro-1-benzofuran]-3,4'-dione	458.9	C24H20ClFO6
118254179	(2S,5'R)-3'-(1-benzofuran-2-yl)-7-chloro-4,6-dimethoxy-5'-methylspiro[1-benzofuran-2,4'-cyclohex-2-ene]-1',3-dione	438.9	C24H19ClO6
118254182	(2S,2'R,6'R)-7-chloro-2'-(2-hydroxyethyl)-4,6-dimethoxy-6'-methyl-2'-phenylspiro[1-benzofuran-2,7'-5,6-dihydro-3H-1-benzofuran]-3,4'-dione	484.9	C26H25ClO7
118254190	(2S,7'R)-7-chloro-2'-ethoxy-4,6-dimethoxy-7'-methylspiro[1-benzofuran-2,8'-3,4,6,7-tetrahydro-2H-chromene]-3,5'-dione	422.9	C21H23ClO7
118254213	(2S,2'S,6'R)-7-chloro-2'-(4-hydroxybutyl)-4,6-dimethoxy-6'-methyl-2'-phenylspiro[1-benzofuran-2,7'-5,6-dihydro-3H-1-benzofuran]-3,4'-dione	513	C28H29ClO7
118254214	(2S,2'S,6'R)-7-chloro-2'-(3-fluorophenyl)-4,6-dimethoxy-6'-methylspiro[1-benzofuran-2,5'-2,3,6,7-tetrahydro-1-benzofuran]-3,4'-dione	458.9	C24H20ClFO6
118254216	(2S,2'R,6'R)-7-chloro-4,6-dimethoxy-6'-methyl-2'-phenylspiro[1-benzofuran-2,5'-2,3,6,7-tetrahydro-1-benzofuran]-3,4'-dione	440.9	C24H21ClO6
118254219	(2S,5'R)-7-chloro-4,6-dimethoxy-5'-methyl-3'-phenylspiro[1-benzofuran-2,4'-cyclohex-2-ene]-1',3-dione	398.8	C22H19ClO5

118254227	(2S,2'S,6'R)-7-chloro-2'-(2-hydroxyethyl)-4,6-dimethoxy-6'-methyl-2'-phenylspiro[1-benzofuran-2,7'-5,6-dihydro-3H-1-benzofuran]-3,4'-dione	484.9	C26H25ClO7
118254232	(2S,2'S,6'R)-7-chloro-2'-(4-fluorophenyl)-4,6-dimethoxy-6'-methylspiro[1-benzofuran-2,7'-2,3,5,6-tetrahydro-1-benzofuran]-3,4'-dione	458.9	C24H20ClFO6
118254246	2-[(2S,2'S,6'R)-7-chloro-4,6-dimethoxy-6'-methyl-3,4'-dioxo-2'-phenylspiro[1-benzofuran-2,7'-5,6-dihydro-3H-1-benzofuran]-2'-yl]ethyl acetate	527	C28H27ClO8
118263228	7-chloro-4,6-dimethoxy-7'-methylspiro[1-benzofuran-2,8'-3,4,6,7-tetrahydro-2H-chromene]-3,5'-dione	378.8	C19H19ClO6
118263231	(5R,6R)-7'-chloro-4',6'-dimethoxy-5-methylspiro[1,2,3,3a,4,5,7,7a-octahydroindene-6,2'-1-benzofuran]-3'-one	350.8	C19H23ClO4
118263233	7-Chloro-4,6-dimethoxy-2',6'-dimethyl-4'-methylidenespiro[1-benzofuran-2,7'-2,3,5,6-tetrahydro-1-benzofuran]-3-one	376.8	C20H21ClO5
118263237	(2R,6'R)-7-chloro-4,6-dimethoxy-2',3',3',6'-tetramethylspiro[1-benzofuran-2,5'-2,4,6,7-tetrahydro-1-benzofuran]-3-one	392.9	C21H25ClO5
118263241	(2R,7'R)-7-chloro-4,6-dimethoxy-2',3',3',4',4',7'-hexamethylspiro[1-benzofuran-2,6'-2,5,7,8-tetrahydrochromene]-3-one	435	C24H31ClO5
118263242	(2S,3'R)-7-chloro-4,6-dimethoxy-3'-methylspiro[1-benzofuran-2,2'-7-oxabicyclo[4.1.0]heptane]-3-one	324.75	C16H17ClO5
118263243	(2S,5'R)-7-chloro-3'-hydroxy-4-methoxy-5',6-dimethylspiro[1-benzofuran-2,4'-cyclohex-2-ene]-1',3-dione	322.74	C16H15ClO5
118263244	(2S,6'R)-7-chloro-2'-(2-hydroxyethyl)-4,6-dimethoxy-6'-methyl-2'-phenylspiro[1-benzofuran-2,7'-5,6-dihydro-3H-1-benzofuran]-3,4'-dione	484.9	C26H25ClO7
118263245	(2R,6'R)-7-chloro-4,6-dimethoxy-2',3',6'-trimethylspiro[1-benzofuran-2,5'-6,7-dihydro-4H-1-benzofuran]-3-one	376.8	C20H21ClO5
118263246	2-[(2S,6'R)-7-chloro-4,6-dimethoxy-6'-methyl-3,4'-dioxo-2'-phenylspiro[1-benzofuran-2,7'-5,6-dihydro-3H-1-benzofuran]-2'-yl]ethyl acetate	527	C28H27ClO8
118263247	(2S,6'R)-2'-(2-bromoethyl)-7-chloro-4,6-dimethoxy-6'-methyl-2'-phenylspiro[1-benzofuran-2,7'-5,6-dihydro-3H-1-benzofuran]-3,4'-dione	547.8	C26H24BrClO6
118263248	(2R,2'Z,5'R)-7-chloro-2'-(dimethylaminomethylidene)-4,6-dimethoxy-5'-methylspiro[1-benzofuran-2,4'-cyclohexane]-1',3,3'-trione	393.8	C19H20ClNO6
118263250	(2S,2'S,7'R)-7-chloro-2'-ethoxy-4,6-dimethoxy-7'-methylspiro[1-benzofuran-2,6'-3,4,7,8-tetrahydro-2H-chromene]-3,5'-dione	422.9	C21H23ClO7
118263251	(2S,2'R,7'R)-7-chloro-2'-ethoxy-4,6-dimethoxy-7'-methylspiro[1-benzofuran-2,8'-3,4,6,7-tetrahydro-2H-chromene]-3,5'-dione	422.9	C21H23ClO7
118263264	(2S,3'R)-7-chloro-4,6-dimethoxy-3',7',7',8',8'-pentamethylspiro[1-benzofuran-2,2'-bicyclo[4.2.0]oct-1(6)-ene]-3-one	390.9	C22H27ClO4
118263268	(2S,2'R,4'R)-7-chloro-2'-hydroxy-4,6-dimethoxy-4',7',7',8',8'-pentamethylspiro[1-benzofuran-2,3'-bicyclo[4.2.0]oct-1(6)-ene]-3-one	406.9	C22H27ClO5
118263269	(2S,2'S,4'R)-7-chloro-2'-hydroxy-4,6-dimethoxy-4',7',7',8',8'-pentamethylspiro[1-benzofuran-2,3'-bicyclo[4.2.0]oct-1(6)-ene]-3-one	406.9	C22H27ClO5

118263272	(2S,4'R)-7-chloro-4,6-dimethoxy-4',7',7',8',8'-pentamethylspiro[1-benzofuran-2,5'-bicyclo[4.2.0]oct-1(6)-ene]-2',3-dione	404.9	C22H25ClO5
118263273	(2R,4'R)-7-chloro-4,6,6'-trimethoxy-4'-methylspiro[1-benzofuran-2,5'-7-oxabicyclo[4.1.0]heptane]-2',3-dione	368.8	C17H17ClO7
118267042	(2S,4'R)-7-chloro-2'-ethyl-4,6-dimethoxy-1',4'-dimethylspiro[1-benzofuran-2,3'-cyclohexene]-3-one	350.8	C19H23ClO4
118267045	(2S,3'S,5'R)-7-chloro-3'-hydroxy-4,6-dimethoxy-1',2',5'-trimethylspiro[1-benzofuran-2,4'-cyclohexene]-3-one	352.8	C18H21ClO5
118267046	(2S,5'R)-7-chloro-4,6-dimethoxy-2',3',5'-trimethylspiro[1-benzofuran-2,4'-cyclohex-2-ene]-1',3-dione	350.8	C18H19ClO5
118267049	(2S,4'R,6'S)-7-chloro-6'-hydroxy-4,6-dimethoxy-1',2',4'-trimethylspiro[1-benzofuran-2,3'-cyclohexene]-3-one	352.8	C18H21ClO5
118267052	(2S,4'R,6'R)-7-chloro-6'-hydroxy-4,6-dimethoxy-1',2',4'-trimethylspiro[1-benzofuran-2,3'-cyclohexene]-3-one	352.8	C18H21ClO5
118267073	7-Chloro-4,6-dimethoxy-2',6'-dimethylspiro[1-benzofuran-2,7'-2,3,5,6-tetrahydro-1-benzofuran]-3,4'-dione	378.8	C19H19ClO6
118267096	(2S,5'R)-7-chloro-4,6-dimethoxy-3',5'-dimethyl-2'-[(1Z)-3-methylbuta-1,3-dienyl]spiro[1-benzofuran-2,6'-cyclohex-2-ene]-1',3-dione	402.9	C22H23ClO5
118267097	(2S,3'R,5'R)-7-chloro-3'-hydroxy-4,6-dimethoxy-1',2',5'-trimethylspiro[1-benzofuran-2,4'-cyclohexene]-3-one	352.8	C18H21ClO5
118267131	(3'R)-7-chloro-4,6-dimethoxy-3',5'-dimethylspiro[1-benzofuran-2,4'-cyclohexane]-1',3-dione	338.8	C17H19ClO5
119091269	3(2H)-Benzofuranone, 7-chloro-4-ethoxy-6-methoxy-	242.65	C11H11ClO4
122400007	(3R,6S)-3-Hydroxy-6-((2S,6'R)-3,4'-dioxo-6,2'-dimethoxy-7-chloro-6'-methylspiro[benzofuran-2(3H),1'-[2]cyclohexene]-4-yl)oxycyclohexene-1-carboxylic acid methyl ester	492.9	C24H25ClO9
122400012	(5S,6R)-5-Hydroxy-6-((2S,6'R)-3,4'-dioxo-6,2'-dimethoxy-7-chloro-6'-methylspiro[benzofuran-2(3H),1'-[2]cyclohexene]-4-yl)oxycyclohexene-1-carboxylic acid methyl ester	492.9	C24H25ClO9
123214764	3'-Butan-2-yl-7-chloro-2'-(2-ethylphenyl)-4,6-dimethoxy-5'-methylspiro[1-benzofuran-2,4'-cyclohex-2-ene]-1',3-dione	483	C28H31ClO5
123282608	7-chloro-2'-ethoxy-4,6-dimethoxy-7'-methylspiro[1-benzofuran-2,6'-3,4,7,8-tetrahydro-2H-chromene]-3,5'-dione	422.9	C21H23ClO7
123293391	2-(7-chloro-4,6-dimethoxy-6'-methyl-3,4'-dioxo-2'-phenylspiro[1-benzofuran-2,7'-5,6-dihydro-3H-1-benzofuran]-2'-yl)ethyl acetate	527	C28H27ClO8
123350254	7-Chloro-4,6-dimethoxy-4'-methylspiro[1-benzofuran-2,5'-7-oxabicyclo[4.1.0]heptane]-2',3-dione	338.74	C16H15ClO6
123361815	7-Chloro-5'-hydroxy-4,6-dimethoxy-3'-methylspiro[1-benzofuran-2,2'-cyclohexane]-1',3-dione	340.75	C16H17ClO6
123396595	1',7-Dichloro-4,6-dimethoxy-5'-methyl-3'-methylidenespiro[1-benzofuran-2,6'-cyclohexene]-3-one	355.2	C17H16Cl2O4

123704177	2'-(2-bromoethyl)-7-chloro-4,6-dimethoxy-6'-methyl-2'-phenylspiro[1-benzofuran-2,7'-5,6-dihydro-3H-1-benzofuran]-3,4'-dione	547.8	C26H24BrClO6
123825667	(2S,5'R)-7-chloro-3'-imino-4,6-dimethoxy-5'-methylspiro[1-benzofuran-2,4'-cyclohexane]-1',3-dione	337.75	C16H16ClNO5
123836216	7-Chloro-4,6-dimethoxy-6'-methyl-3'-phenylspiro[1-benzofuran-2,5'-2,3,6,7-tetrahydro-1-benzofuran]-3,4'-dione	440.9	C24H21ClO6
123846923	(2R,5'R)-7-chloro-2'-(dimethylaminomethylidene)-4,6-dimethoxy-5'-methylspiro[1-benzofuran-2,4'-cyclohexane]-1',3,3'-trione	393.8	C19H20ClNO6
123872201	7-Chloro-4,6,6'-trimethoxy-4'-methylspiro[1-benzofuran-2,5'-7-oxabicyclo[4.1.0]heptane]-2',3-dione	368.8	C17H17ClO7
124024037	7-Chloro-3'-imino-4,6-dimethoxy-5'-methylspiro[1-benzofuran-2,4'-cyclohexane]-1',3-dione	337.75	C16H16ClNO5
124301775	(2S,5'S)-7-chloro-3',4,6-trimethoxy-5'-methylspiro[1-benzofuran-2,6'-cyclohex-2-ene]-1',3-dione	352.8	C17H17ClO6
124301776	(2R,5'R)-7-chloro-3',4,6-trimethoxy-5'-methylspiro[1-benzofuran-2,6'-cyclohex-2-ene]-1',3-dione	352.8	C17H17ClO6
124307480	(2R,5'S)-7-chloro-6-hydroxy-3',4-dimethoxy-5'-methylspiro[1-benzofuran-2,4'-cyclohex-2-ene]-1',3-dione	338.74	C16H15ClO6
124397086	(2R,5'S)-7-chloro-4-hydroxy-3',6-dimethoxy-5'-methylspiro[1-benzofuran-2,4'-cyclohex-2-ene]-1',3-dione	338.74	C16H15ClO6
125427757	methyl(3R)-3-[(2S,4'R)-7-chloro-2'-hydroxy-4,6-dimethoxy-4'-methyl-3,6'-dioxospiro[1-benzofuran-2,3'-cyclohexene]-1'-yl]-3-(4-methoxyphenyl)propanoate	530.9	C27H27ClO9
125427758	methyl(3S)-3-[(2S,4'R)-7-chloro-2'-hydroxy-4,6-dimethoxy-4'-methyl-3,6'-dioxospiro[1-benzofuran-2,3'-cyclohexene]-1'-yl]-3-(4-methoxyphenyl)propanoate	530.9	C27H27ClO9
125428416	methyl(3R)-3-[(2S,4'R)-7-chloro-2'-hydroxy-4,6-dimethoxy-4'-methyl-3,6'-dioxospiro[1-benzofuran-2,3'-cyclohexene]-1'-yl]-4-methylpentanoate	466.9	C23H27ClO8
125428417	methyl(3S)-3-[(2S,4'R)-7-chloro-2'-hydroxy-4,6-dimethoxy-4'-methyl-3,6'-dioxospiro[1-benzofuran-2,3'-cyclohexene]-1'-yl]-4-methylpentanoate	466.9	C23H27ClO8
125428702	methyl(3R)-3-[(2S,4'R)-7-chloro-2'-hydroxy-4,6-dimethoxy-4'-methyl-3,6'-dioxospiro[1-benzofuran-2,3'-cyclohexene]-1'-yl]-3-[4-(2-methylprop-2-enoxy)phenyl]propanoate	571	C30H31ClO9
125428703	methyl(3S)-3-[(2S,4'R)-7-chloro-2'-hydroxy-4,6-dimethoxy-4'-methyl-3,6'-dioxospiro[1-benzofuran-2,3'-cyclohexene]-1'-yl]-3-[4-(2-methylprop-2-enoxy)phenyl]propanoate	571	C30H31ClO9
125428749	methyl(3R)-3-[(2S,4'R)-7-chloro-2'-hydroxy-4,6-dimethoxy-4'-methyl-3,6'-dioxospiro[1-benzofuran-2,3'-cyclohexene]-1'-yl]-3-phenylpropanoate	500.9	C26H25ClO8
125428750	methyl(3S)-3-[(2S,4'R)-7-chloro-2'-hydroxy-4,6-dimethoxy-4'-methyl-3,6'-dioxospiro[1-benzofuran-2,3'-cyclohexene]-1'-yl]-3-phenylpropanoate	500.9	C26H25ClO8
125429126	methyl(3R)-3-[(2S,4'R)-7-chloro-2'-hydroxy-4,6-dimethoxy-4'-methyl-3,6'-dioxospiro[1-benzofuran-2,3'-cyclohexene]-1'-yl]-3-(3-chloro-4-hydroxyphenyl)propanoate	551.4	C26H24Cl2O9

125429127	methyl(3S)-3-[(2S,4'R)-7-chloro-2'-hydroxy-4,6-dimethoxy-4'-methyl-3,6'-dioxospiro[1-benzofuran-2,3'-cyclohexene]-1'-yl]-3-(3-chloro-4-hydroxyphenyl)propanoate	551.4	C26H24Cl2O9
125429177	methyl(3R)-3-[(2S,4'R)-7-chloro-2'-hydroxy-4,6-dimethoxy-4'-methyl-3,6'-dioxospiro[1-benzofuran-2,3'-cyclohexene]-1'-yl]-3-(4-hydroxyphenyl)propanoate	516.9	C26H25ClO9
125429178	methyl(3S)-3-[(2S,4'R)-7-chloro-2'-hydroxy-4,6-dimethoxy-4'-methyl-3,6'-dioxospiro[1-benzofuran-2,3'-cyclohexene]-1'-yl]-3-(4-hydroxyphenyl)propanoate	516.9	C26H25ClO9
125429419	methyl(3S)-3-[(2S,4'R)-7-chloro-2'-hydroxy-4,6-dimethoxy-4'-methyl-3,6'-dioxospiro[1-benzofuran-2,3'-cyclohexene]-1'-yl]-3-(2,4-dimethoxyphenyl)propanoate	561	C28H29ClO10
125429420	methyl(3R)-3-[(2S,4'R)-7-chloro-2'-hydroxy-4,6-dimethoxy-4'-methyl-3,6'-dioxospiro[1-benzofuran-2,3'-cyclohexene]-1'-yl]-3-(2,4-dimethoxyphenyl)propanoate	561	C28H29ClO10
125429426	2-[4-[(1S)-1-[(2S,4'R)-7-chloro-2'-hydroxy-4,6-dimethoxy-4'-methyl-3,6'-dioxospiro[1-benzofuran-2,3'-cyclohexene]-1'-yl]-3-methoxy-3-oxopropyl]phenoxy]acetic acid	575	C28H27ClO11
125429427	2-[4-[(1R)-1-[(2S,4'R)-7-chloro-2'-hydroxy-4,6-dimethoxy-4'-methyl-3,6'-dioxospiro[1-benzofuran-2,3'-cyclohexene]-1'-yl]-3-methoxy-3-oxopropyl]phenoxy]acetic acid	575	C28H27ClO11
125429497	methyl(3S)-3-[(2S,4'R)-7-chloro-2'-hydroxy-4,6-dimethoxy-4'-methyl-3,6'-dioxospiro[1-benzofuran-2,3'-cyclohexene]-1'-yl]-3-(4-oxochromen-3-yl)propanoate	569	C29H25ClO10
125429498	methyl(3R)-3-[(2S,4'R)-7-chloro-2'-hydroxy-4,6-dimethoxy-4'-methyl-3,6'-dioxospiro[1-benzofuran-2,3'-cyclohexene]-1'-yl]-3-(4-oxochromen-3-yl)propanoate	569	C29H25ClO10
125429633	methyl(3R)-3-[(2S,4'R)-7-chloro-2'-hydroxy-4,6-dimethoxy-4'-methyl-3,6'-dioxospiro[1-benzofuran-2,3'-cyclohexene]-1'-yl]-3-(3-hydroxyphenyl)propanoate	516.9	C26H25ClO9
125429634	methyl(3S)-3-[(2S,4'R)-7-chloro-2'-hydroxy-4,6-dimethoxy-4'-methyl-3,6'-dioxospiro[1-benzofuran-2,3'-cyclohexene]-1'-yl]-3-(3-hydroxyphenyl)propanoate	516.9	C26H25ClO9
125429840	methyl(3R)-3-[(2S,4'R)-7-chloro-2'-hydroxy-4,6-dimethoxy-4'-methyl-3,6'-dioxospiro[1-benzofuran-2,3'-cyclohexene]-1'-yl]-3-(3,4,5-trifluorophenyl)propanoate	554.9	C26H22ClF3O8
125429841	methyl(3S)-3-[(2S,4'R)-7-chloro-2'-hydroxy-4,6-dimethoxy-4'-methyl-3,6'-dioxospiro[1-benzofuran-2,3'-cyclohexene]-1'-yl]-3-(3,4,5-trifluorophenyl)propanoate	554.9	C26H22ClF3O8
125429985	methyl(3R)-3-[(2S,4'R)-7-chloro-2'-hydroxy-4,6-dimethoxy-4'-methyl-3,6'-dioxospiro[1-benzofuran-2,3'-cyclohexene]-1'-yl]-5-methylhexanoate	480.9	C24H29ClO8
125429986	methyl(3S)-3-[(2S,4'R)-7-chloro-2'-hydroxy-4,6-dimethoxy-4'-methyl-3,6'-dioxospiro[1-benzofuran-2,3'-cyclohexene]-1'-yl]-5-methylhexanoate	480.9	C24H29ClO8
127053184	(2S,5'R)-7-chloro-4-(difluoromethoxy)-6-methoxy-5'-methyl-3'-phenylmethoxyspiro[1-benzofuran-2,4'-cyclohex-2-ene]-1',3-dione	464.8	C23H19ClF2O6

127053185	(2S,5'R)-7-chloro-6-(difluoromethoxy)-4-methoxy-5'-methyl-3'-phenylmethoxyspiro[1-benzofuran-2,4'-cyclohex-2-ene]-1',3-dione	464.8	C23H19ClF2O6
127253416	methyl3-[(2S,4'R)-7-chloro-2'-hydroxy-4,6-dimethoxy-4'-methyl-3,6'-dioxospiro[1-benzofuran-2,3'-cyclohexene]-1'-yl]-3-(4-octoxyphenyl)propanoate	629.1	C34H41ClO9
129010273	(2R)-7-chloro-3',4,6-trimethoxy-5'-methylspiro[1-benzofuran-2,4'-cyclohex-2-ene]-1',3-dione	352.8	C17H17ClO6
129603773	methyl(3R)-3-[(2S,4'R)-7-chloro-2'-hydroxy-4,6-dimethoxy-4'-methyl-3,6'-dioxospiro[1-benzofuran-2,3'-cyclohexene]-1'-yl]-3-(4-octoxyphenyl)propanoate	629.1	C34H41ClO9
129603774	methyl(3S)-3-[(2S,4'R)-7-chloro-2'-hydroxy-4,6-dimethoxy-4'-methyl-3,6'-dioxospiro[1-benzofuran-2,3'-cyclohexene]-1'-yl]-3-(4-octoxyphenyl)propanoate	629.1	C34H41ClO9
129894712	methyl3-[(2S,4'R)-7-chloro-2'-hydroxy-4,6-dimethoxy-4'-methyl-3,6'-dioxospiro[1-benzofuran-2,3'-cyclohexene]-1'-yl]-3-(4-methoxyphenyl)propanoate	530.9	C27H27ClO9
129894893	methyl3-[(2S,4'R)-7-chloro-2'-hydroxy-4,6-dimethoxy-4'-methyl-3,6'-dioxospiro[1-benzofuran-2,3'-cyclohexene]-1'-yl]-3-phenylpropanoate	500.9	C26H25ClO8
129895030	methyl3-[(2S,4'R)-7-chloro-2'-hydroxy-4,6-dimethoxy-4'-methyl-3,6'-dioxospiro[1-benzofuran-2,3'-cyclohexene]-1'-yl]-4-methylpentanoate	466.9	C23H27ClO8
129895087	methyl3-[(2S,4'R)-7-chloro-2'-hydroxy-4,6-dimethoxy-4'-methyl-3,6'-dioxospiro[1-benzofuran-2,3'-cyclohexene]-1'-yl]-3-[4-(2-methylprop-2-enoxy)phenyl]propanoate	571	C30H31ClO9
129895176	methyl3-[(2S,4'R)-7-chloro-2'-hydroxy-4,6-dimethoxy-4'-methyl-3,6'-dioxospiro[1-benzofuran-2,3'-cyclohexene]-1'-yl]-3-(4-hydroxyphenyl)propanoate	516.9	C26H25ClO9
129895205	2-[4-[1-[(2S,4'R)-7-chloro-2'-hydroxy-4,6-dimethoxy-4'-methyl-3,6'-dioxospiro[1-benzofuran-2,3'-cyclohexene]-1'-yl]-3-methoxy-3-oxopropyl]phenoxy]acetic acid	575	C28H27ClO11
129895222	methyl3-[(2S,4'R)-7-chloro-2'-hydroxy-4,6-dimethoxy-4'-methyl-3,6'-dioxospiro[1-benzofuran-2,3'-cyclohexene]-1'-yl]-3-(3-chloro-4-hydroxyphenyl)propanoate	551.4	C26H24Cl2O9
129895373	methyl3-[(2S,4'R)-7-chloro-2'-hydroxy-4,6-dimethoxy-4'-methyl-3,6'-dioxospiro[1-benzofuran-2,3'-cyclohexene]-1'-yl]-3-(2,4-dimethoxyphenyl)propanoate	561	C28H29ClO10
129895443	methyl3-[(2S,4'R)-7-chloro-2'-hydroxy-4,6-dimethoxy-4'-methyl-3,6'-dioxospiro[1-benzofuran-2,3'-cyclohexene]-1'-yl]-5-methylhexanoate	480.9	C24H29ClO8
129895451	methyl3-[(2S,4'R)-7-chloro-2'-hydroxy-4,6-dimethoxy-4'-methyl-3,6'-dioxospiro[1-benzofuran-2,3'-cyclohexene]-1'-yl]-3-(3-hydroxyphenyl)propanoate	516.9	C26H25ClO9
129895481	methyl3-[(2S,4'R)-7-chloro-2'-hydroxy-4,6-dimethoxy-4'-methyl-3,6'-dioxospiro[1-benzofuran-2,3'-cyclohexene]-1'-yl]-3-(4-oxochromen-3-yl)propanoate	569	C29H25ClO10

129895618	methyl3-[(2S,4'R)-7-chloro-2'-hydroxy-4,6-dimethoxy-4'-methyl-3,6'-dioxospiro[1-benzofuran-2,3'-cyclohexene]-1'-yl]-3-(3,4,5-trifluorophenyl)propanoate	554.9	C26H22ClF3O8
131770040	6-Methyl-griseofulvin	336.8	C17H17ClO5
131964492	(2S,5'R)-7-chloro-6-hydroxy-3'-methoxy-5'-methyl-4-[2-(oxan-2-yloxy)ethoxy]spiro[1-benzofuran-2,4'-cyclohex-2-ene]-1',3-dione	452.9	C22H25ClO8
131964498	(2S,5'R)-7-chloro-3',4-dimethoxy-6-(2-methoxyethoxy)-5'-methylspiro[1-benzofuran-2,4'-cyclohex-2-ene]-1',3-dione	396.8	C19H21ClO7
131964505	(2S,5'R)-7-chloro-6-(2-hydroxyethoxy)-3',4-dimethoxy-5'-methylspiro[1-benzofuran-2,4'-cyclohex-2-ene]-1',3-dione	382.8	C18H19ClO7
131964506	(2S,5'R)-7-chloro-3',6-dimethoxy-5'-methyl-4-[2-(oxan-2-yloxy)ethoxy]spiro[1-benzofuran-2,4'-cyclohex-2-ene]-1',3-dione	466.9	C23H27ClO8
131975182	(5'R)-7-chloro-3',6-dimethoxy-5'-methyl-4-[2-(oxan-2-yloxy)ethoxy]spiro[1-benzofuran-2,4'-cyclohex-2-ene]-1',3-dione	466.9	C23H27ClO8
131975184	(2S,5'R)-7-chloro-3'-hydroxy-6-methoxy-5'-methyl-4-[2-(oxan-2-yloxy)ethoxy]spiro[1-benzofuran-2,4'-cyclohex-2-ene]-1',3-dione	452.9	C22H25ClO8
132285856	methyl 3-(7-chloro-4'-hydroxy-4,6-dimethoxy-6'-methyl-2',3-dioxo-3H-spiro[1-benzofuran-2,1'-cyclohex[3]en]-3'-yl)-3-[4-(octyloxy)phenyl]propanoate	629.1	C34H41ClO9
132285940	methyl 3-(7-chloro-4'-hydroxy-4,6-dimethoxy-6'-methyl-2',3-dioxo-3H-spiro[1-benzofuran-2,1'-cyclohex[3]en]-3'-yl)-3-(4-methoxyphenyl)propanoate	530.9	C27H27ClO9
132285949	methyl 3-(7-chloro-4'-hydroxy-4,6-dimethoxy-6'-methyl-2',3-dioxo-3H-spiro[1-benzofuran-2,1'-cyclohex[3]en]-3'-yl)-3-(4-hydroxyphenyl)propanoate	516.9	C26H25ClO9
132286067	methyl 3-(7-chloro-4'-hydroxy-4,6-dimethoxy-6'-methyl-2',3-dioxo-3H-spiro[1-benzofuran-2,1'-cyclohex[3]en]-3'-yl)-3-(3-hydroxyphenyl)propanoate	516.9	C26H25ClO9
132286090	methyl 3-(7-chloro-4'-hydroxy-4,6-dimethoxy-6'-methyl-2',3-dioxo-3H-spiro[1-benzofuran-2,1'-cyclohex[3]en]-3'-yl)-4-methylpentanoate	466.9	C23H27ClO8
132286165	{4-[1-(7-chloro-4'-hydroxy-4,6-dimethoxy-6'-methyl-2',3-dioxo-3H-spiro[1-benzofuran-2,1'-cyclohex[3]en]-3'-yl)-3-methoxy-3-oxopropyl]phenoxy}acetic acid	575	C28H27ClO11
132286322	methyl 3-(7-chloro-4'-hydroxy-4,6-dimethoxy-6'-methyl-2',3-dioxo-3H-spiro[1-benzofuran-2,1'-cyclohex[3]en]-3'-yl)-3-phenylpropanoate	500.9	C26H25ClO8
132286340	methyl 3-(7-chloro-4'-hydroxy-4,6-dimethoxy-6'-methyl-2',3-dioxo-3H-spiro[1-benzofuran-2,1'-cyclohex[3]en]-3'-yl)-3-(2,4-dimethoxyphenyl)propanoate	561	C28H29ClO10
132286359	methyl 3-(7-chloro-4'-hydroxy-4,6-dimethoxy-6'-methyl-2',3-dioxo-3H-spiro[1-benzofuran-2,1'-cyclohex[3]en]-3'-yl)-3-(3-chloro-4-hydroxyphenyl)propanoate	551.4	C26H24Cl2O9
132286397	methyl 3-(7-chloro-4'-hydroxy-4,6-dimethoxy-6'-methyl-2',3-dioxo-3H-spiro[1-benzofuran-2,1'-cyclohex[3]en]-3'-yl)-3-(4-oxo-4H-chromen-3-yl)propanoate	569	C29H25ClO10

132286457	methyl 3-(7-chloro-4'-hydroxy-4,6-dimethoxy-6'-methyl-2',3-dioxo-3H-spiro[1-benzofuran-2,1'-cyclohex[3]en]-3'-yl)-3-(3,4,5-trifluorophenyl)propanoate	554.9	C26H22ClF3O8
132286496	methyl 3-(7-chloro-4'-hydroxy-4,6-dimethoxy-6'-methyl-2',3-dioxo-3H-spiro[1-benzofuran-2,1'-cyclohex[3]en]-3'-yl)-3-{4-[(2-methylprop-2-en-1-yl)oxy]phenyl}propanoate	571	C30H31ClO9
132286528	methyl 3-(7-chloro-4'-hydroxy-4,6-dimethoxy-6'-methyl-2',3-dioxo-3H-spiro[1-benzofuran-2,1'-cyclohex[3]en]-3'-yl)-5-methylhexanoate	480.9	C24H29ClO8
133688441	(2R,5'S)-7-chloro-3',6-dimethoxy-5'-methyl-4-(trideuterio(113C)methoxy)spiro[1-benzofuran-2,4'-cyclohex-2-ene]-1',3-dione	356.77	C17H17ClO6
134126306	3'-Butylsulfanyl-7-chloro-4,6-dimethoxy-5'-methylspiro[1-benzofuran-2,4'-cyclohex-2-ene]-1',3-dione	410.9	C20H23ClO5S
134126307	7-Chloro-4,6-dimethoxy-5'-methyl-3'-propylsulfanylspiro[1-benzofuran-2,4'-cyclohex-2-ene]-1',3-dione	396.9	C19H21ClO5S
135027778	methyl(3R,6S)-3-[(2S,5'R)-7-chloro-1',6-dimethoxy-5'-methyl-3,3'-dioxospiro[1-benzofuran-2,6'-cyclohexene]-4-yl]oxy-6-hydroxycyclohexene-1-carboxylate	492.9	C24H25ClO9
137467367	(2S)-7-chloro-3'-hydroxy-6-(2-hydroxyethoxy)-4-methoxyspiro[1-benzofuran-2,4'-cyclohex-2-ene]-1',3-dione	354.74	C16H15ClO7
137467368	[(2S,5'R)-7-chloro-6-(2-hydroxyethoxy)-1'-methoxy-5'-methyl-3,3'-dioxospiro[1-benzofuran-2,6'-cyclohexene]-4-yl] hypoiodite	494.7	C17H16ClIO7
137467381	(2S,5'R)-7-chloro-3',6-dihydroxy-5'-methyl-4-[2-(oxan-2-yloxy)ethoxy]spiro[1-benzofuran-2,4'-cyclohex-2-ene]-1',3-dione	438.9	C21H23ClO8
137467397	(2S)-7-chloro-3',4-dimethoxy-6-(2-methoxyethoxy)spiro[1-benzofuran-2,4'-cyclohex-2-ene]-1',3-dione	382.8	C18H19ClO7
137467447	(2S)-7-chloro-3',6-dihydroxy-4-methoxyspiro[1-benzofuran-2,4'-cyclohex-2-ene]-1',3-dione	310.68	C14H11ClO6
137467524	(2S)-7-chloro-3',4-dihydroxy-6-methoxyspiro[1-benzofuran-2,4'-cyclohex-2-ene]-1',3-dione	310.68	C14H11ClO6
137467528	(2S,5'R)-7-chloro-3',4-dihydroxy-6-methoxy-5'-methylspiro[1-benzofuran-2,4'-cyclohex-2-ene]-1',3-dione	324.71	C15H13ClO6
137641183	(2S,5'R)-7-chloro-4,6-dimethoxy-5'-methyl-3'-[(1S)-1-phenylethoxy]spiro[1-benzofuran-2,4'-cyclohex-2-ene]-1',3-dione	442.9	C24H23ClO6
137647518	(2S,5'R)-7-chloro-5-fluoro-3',4,6-trimethoxy-5'-methylspiro[1-benzofuran-2,4'-cyclohex-2-ene]-1',3-dione	370.8	C17H16ClFO6
137652147	(2S,5'R)-7-chloro-4,6-dimethoxy-5'-methyl-3'-[(1R)-1-phenylethoxy]spiro[1-benzofuran-2,4'-cyclohex-2-ene]-1',3-dione	442.9	C24H23ClO6
137658162	(2S,5'R,6'R)-7-chloro-6'-hydroxy-3',4,6-trimethoxy-5'-methylspiro[1-benzofuran-2,4'-cyclohex-2-ene]-1',3-dione	368.8	C17H17ClO7
138490235	[(2S,5'R)-7-chloro-1',4-dimethoxy-5'-methyl-3,3'-dioxospiro[1-benzofuran-2,6'-cyclohexene]-6-yl] trifluoromethanesulfonate	470.8	C17H14ClF3O8S

138496616	[(2S,5'R)-7-chloro-1',4-dimethoxy-5'-methyl-3,3'-dioxospiro[1-benzofuran-2,6'-cyclohexene]-6-yl] trifluoromethanesulfinate	454.8	C17H14ClF3O7S
138514334	(2S,5'R)-7-chloro-4-(difluoromethoxy)-3'-hydroxy-5'-methyl-6-(trifluoromethylsulfanyloxy)spiro[1-benzofuran-2,4'-cyclohex-2-ene]-1',3-dione	460.8	C16H10ClF5O6S
138514335	(2S,5'R)-7-chloro-4-(difluoromethoxy)-3'-hydroxy-6-methoxy-5'-methylspiro[1-benzofuran-2,4'-cyclohex-2-ene]-1',3-dione	374.72	C16H13ClF2O6
138514336	(2S,5'R)-7-chloro-4-(difluoromethoxy)-3',6-dihydroxy-5'-methylspiro[1-benzofuran-2,4'-cyclohex-2-ene]-1',3-dione	360.69	C15H11ClF2O6
138514463	(2S,5'R)-7-chloro-3'-hydroxy-4-methoxy-5'-methyl-6-(trifluoromethylsulfanyloxy)spiro[1-benzofuran-2,4'-cyclohex-2-ene]-1',3-dione	424.8	C16H12ClF3O6S
138514465	(2S,5'R)-7-chloro-3'-hydroxy-6-(2-hydroxyethoxy)-4-methoxy-5'-methylspiro[1-benzofuran-2,4'-cyclohex-2-ene]-1',3-dione	368.8	C17H17ClO7
139584816	6'-Hydroxygriseofulvin	368.8	C17H17ClO7
139588134	7-chloro-2,5,6-trimethoxy-6-methylspiro(benzofuran-2(3H),1-(2) cyclohexene)-3,4-dione	352.8	C17H17ClO6
142550519	(2S,5'R)-7-chloro-4-(difluoromethoxy)-3',6-dimethoxy-5'-methylspiro[1-benzofuran-2,4'-cyclohex-2-ene]-1',3-dione	388.7	C17H15ClF2O6
142550524	(2S,5'R)-7-chloro-1',4-dimethoxy-5'-methyl-3,3'-dioxospiro[1-benzofuran-2,6'-cyclohexene]-6-carbaldehyde	350.7	C17H15ClO6
142550537	[(2S,5'R)-7-chloro-4-(difluoromethoxy)-1'-methoxy-5'-methyl-3,3'-dioxospiro[1-benzofuran-2,6'-cyclohexene]-6-yl] trifluoromethanesulfonate	506.8	C17H12ClF5O8S
142550538	(2S,5'R)-7-chloro-4-(difluoromethoxy)-6-hydroxy-3'-methoxy-5'-methylspiro[1-benzofuran-2,4'-cyclohex-2-ene]-1',3-dione	374.72	C16H13ClF2O6
144564060	but-2-ene;(2S)-7-chloro-4,6-dimethoxy-2',3',6'-trimethylspiro[1-benzofuran-2,1'-cyclohexane]-3-one	394.9	C22H31ClO4
144564061	(2S)-7-chloro-4,6-dimethoxy-2',3',6'-trimethylspiro[1-benzofuran-2,1'-cyclohexane]-3-one	338.8	C18H23ClO4
144564067	3-[(2S)-7-chloro-4,6-dimethoxy-3-oxo-2-[(Z)-prop-1-enyl]-1-benzofuran-2-yl]butanal	338.8	C17H19ClO5
144564118	(2S)-7-chloro-2'-ethoxy-4,6-dimethoxy-7'-methylspiro[1-benzofuran-2,8'-3,4,6,7-tetrahydro-2H-chromene]-3,5'-dione;ethane	452.9	C23H29ClO7
144564119	(2S)-7-chloro-2'-ethoxy-4,6-dimethoxy-7'-methylspiro[1-benzofuran-2,8'-3,4,6,7-tetrahydro-2H-chromene]-3,5'-dione	422.9	C21H23ClO7
144564145	(2S,3'R,6'R)-7-chloro-4,6-dimethoxy-6'-methyl-3'-phenyl-6'-sulfanylspiro[1-benzofuran-2,5'-3,7-dihydro-2H-1-benzofuran]-3,4'-dione	472.9	C24H21ClO6S
144564153	(2S)-7-chloro-2'-(2-hydroxyethyl)-4,6-dimethoxy-6'-methyl-2'-phenylspiro[1-benzofuran-2,7'-5,6-dihydro-3H-1-benzofuran]-3,4'-dione	484.9	C26H25ClO7
146559679	(2S)-7-chloro-6-(2-hydroxyethoxy)-3',4-dimethoxyspiro[1-benzofuran-2,4'-cyclohex-2-ene]-1',3-dione	368.8	C17H17ClO7

147116578	methyl (7R,8S)-7'-chloro-4',6'-dimethoxy-7-methyl-3',5-dioxo-4-phenylspiro[1,4,6,7-tetrahydronaphthalene-8,2'-1-benzofuran]-2-carboxylate	508.9	C28H25ClO7
147554571	(2S)-7-chloro-4,6-dimethoxy-2-[(2S)-propan-2-yl]-2-prop-1-enyl-1-benzofuran-3-one;yttrium	397.66	C16H17ClO4Y-2
147554572	(2S)-7-chloro-4,6-dimethoxy-2-propan-2-yl-2-prop-1-enyl-1-benzofuran-3-one	310.77	C16H19ClO4
148240297	C=12C(=O)COC2=C(Cl)C(OC)=CC=1OCC1=CC=CC=C1	304.72	C16H13ClO4
153852916	CC(CC(C)=O)C1OC2=C(C(=CC(=C2C1=O)OC)OC)Cl	312.74	C15H17ClO5
153852917	O=C(CCC1OC2=C(C(=CC(=C2C1=O)OC)OC)Cl)C	298.72	C14H15ClO5
153989287	(2S,5'R)-7-chloro-1',4-dimethoxy-5'-methyl-3,3'-dioxospiro[1-benzofuran-2,6'-cyclohexene]-6-carboxylate	365.7	C17H14ClO7-
154178022	COC(=O)C1(OC2=C(Cl)C(OC)=CC(OC)=C2C1=O)C(C)CC(C)=O	370.8	C17H19ClO7
154388188	COC(=O)C1(CCC(C)=O)OC2=C(Cl)C(OC)=CC(OC)=C2C1=O	356.75	C16H17ClO7
154593892	(2S,5'R)-7-chloro-4-(difluoromethoxy)-6-ethyl-3'-methoxy-5'-methylspiro[1-benzofuran-2,4'-cyclohex-2-ene]-1',3-dione	386.8	C18H17ClF2O5
157058015	NULL	472.8	C17H16ClF3O8S
157376471	NULL	755.6	C39H40Cl2O11
161262405	NULL	433.7	C19H17ClO4Y-2
161262406	NULL	346.8	C19H19ClO4
161267575	NULL	526.9	C28H24ClFO7
161564856	NULL	350.8	C18H19ClO5
161564857	NULL	380.9	C20H25ClO5
161564859	NULL	422.9	C23H31ClO5
161564860	NULL	457	C26H29ClO5
162294201	NULL	338.8	C18H23ClO4
162294202	NULL	447.7	C20H19ClO4Y-2
162294203	NULL	360.8	C20H21ClO4

File 2

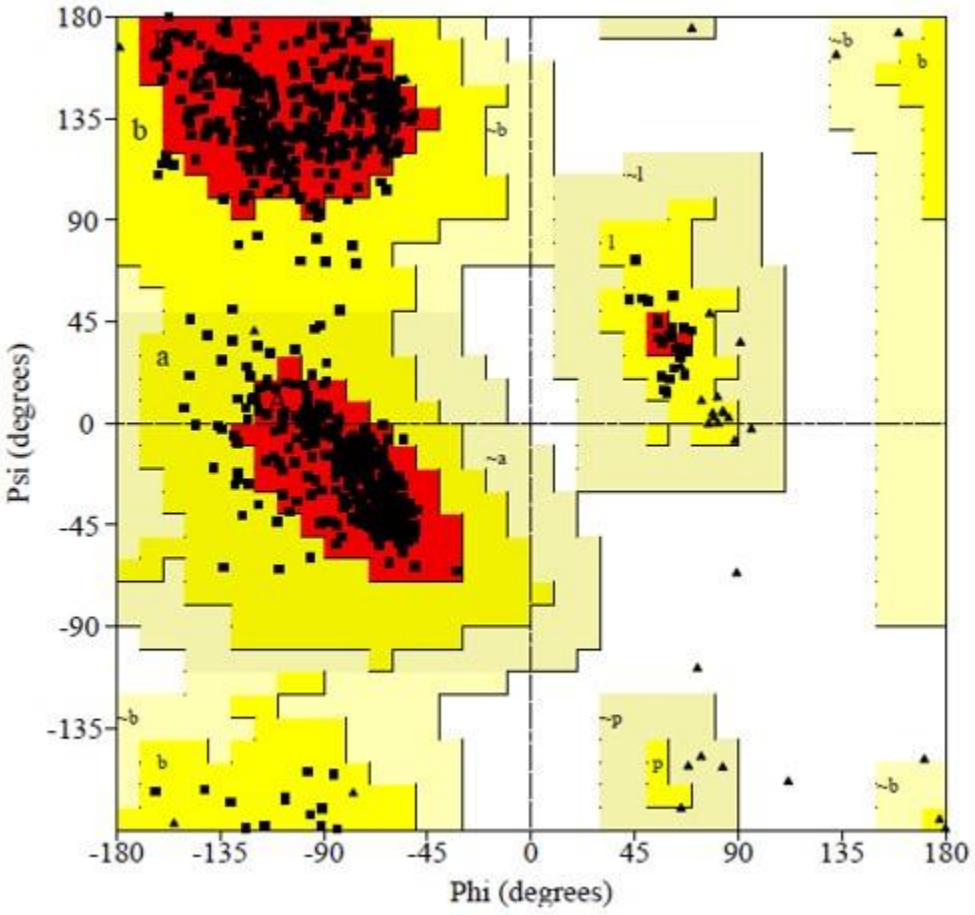

Fig S1. Ramachandran plot analysis of RdRp protein. Here, red region indicates favored region, yellow region for allowed and light yellow shows generously allowed region and white for disallowed region. Phi and Psi angels determine torsion angels.

Table S1. Ramachandran plot statistics of RdRp.

Ramachandran plot statistics	**RdRp**	
	Residue	**%**
Residues in the most favored regions [A,B,L]	960	92.00%
Residues in the additional allowed regions [a,b,l,p]	84	8%
Residues in the generously allowed regions [a,b,l,p]	0	0%
Residues in the disallowed regions [xx]	0	0%
Number of non-glycine and non-proline residues	1044	100%
Number of end residues (excl. Gly and Pro)	11	
Number of glycine residues (shown as triangles)	48	
Number of proline residues	35	
Total number of residues	1138	

File 3

Table S1. Molecular docking details of ligands interaction with Mprotease (6LU7)

PubChem ID	Binding Energy (kcal/mol)	H-bonds	Hydrophobic interactions	Ligand interaction diagram	Lipinski Analysis	
CID_25171849 (M2)	-8.86	GLY 143	HIS 41 MET 49 LEU 141 MET 165 GLU 166 HIS 172 GLN 189	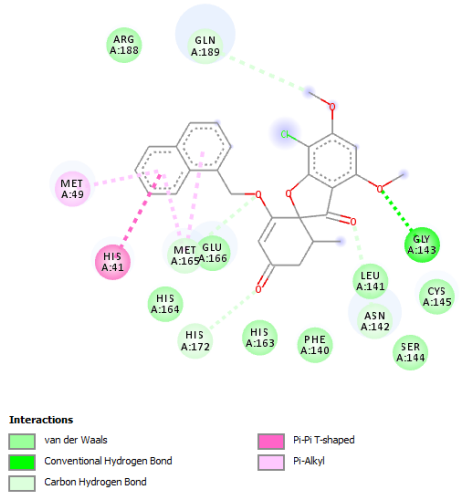	Molecular weight (<500 Da) Lipophilicity (LogP<5) H bond donor (<5) H bond acceptor (<10) Violations Lipinski Hepatotoxicity	478.9 3.29 0 6 0 Yes No

CID_73330910 (M3)	-8.65	GLU 166 GLN 192	HIS 41 ASN 142 CYS 145 MET 165 PRO 168 GLN 189	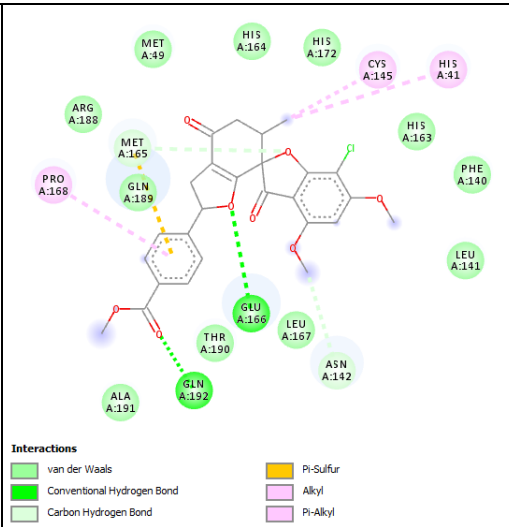	Molecular weight (<500 Da) Lipophilicity (LogP<5) H bond donor (<5) H bond acceptor (<10) Violations Lipinski Hepatotoxicity	498.9 4.08 0 8 0 Yes No
CID_73331488 (M4)	-8.08	GLN 192	HIS 41 PHE 140 CYS 145 MET 165 GLU 166 PRO 168 GLN 189 THR 190 ALA 191	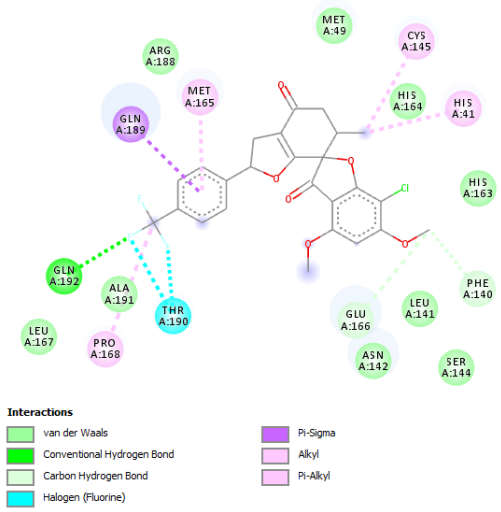	Molecular weight (<500 Da) Lipophilicity (LogP<5) H bond donor (<5) H bond acceptor (<10) Violations Lipinski Hepatotoxicity	508.8 4.00 0 9 1 Yes No

CID_118254214 (M5)	-8.09	ASN 142 GLU 166	HIS 41 MET 49 PHE 140 LEU 141 HIS 164 MET 165 GLU 166	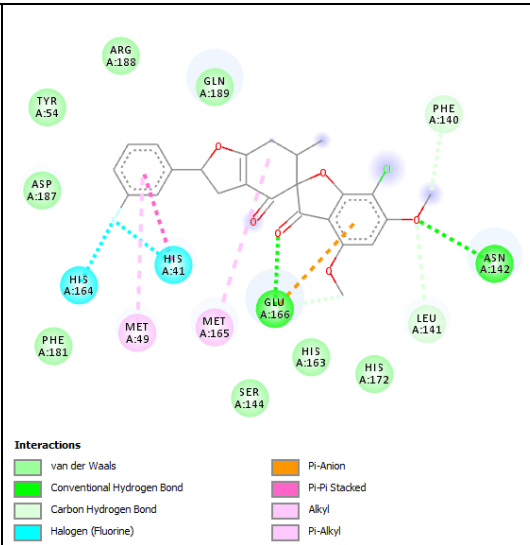	Molecular weight (<500 Da) Lipophilicity (LogP<5) H bond donor (<5) H bond acceptor (<10) Violations Lipinski Hepatotoxicity	458.8 3.83 0 7 0 Yes No
CID_138490235 (M6)	-7.76	HIS 41 GLY 143 GLU 166 THR 190 GLN 192	MET 165 GLU 166 PRO 168 GLN 189 THR 190	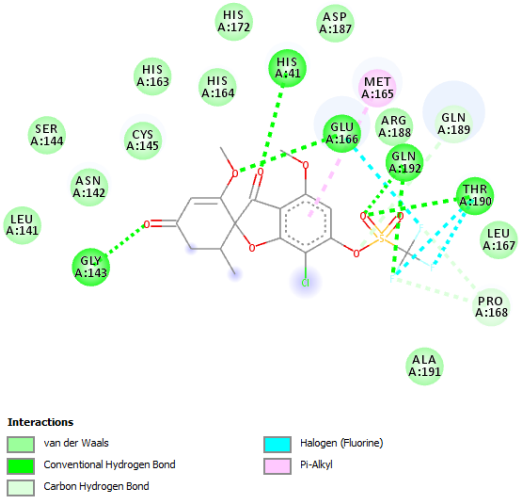	Molecular weight (<500 Da) Lipophilicity (LogP<5) H bond donor (<5) H bond acceptor (<10) Violations Lipinski Hepatotoxicity	470.8 2.84 0 11 1 Yes No

CID_118254145 (M8)	-8.28	GLU 166	HIS 41 CYS 145 MET 165	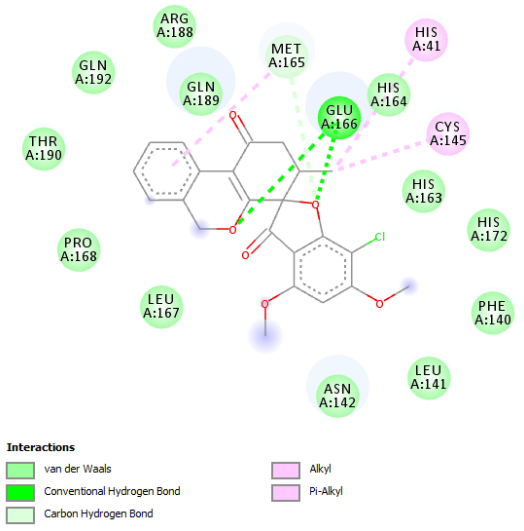	Molecular weight (<500 Da) Lipophilicity (LogP<5) H bond donor (<5) H bond acceptor (<10) Violations Lipinski Hepatotoxicity	426.85 3.45 0 6 0 Yes No

Table S2. Molecular docking details of ligands interaction with human B-Tubulin.

PubChem ID	Binding Energy (kcal/mol)	H- bonds	Hydrophobic interactions	Ligand interaction diagram
7331205	-9.1	-	LYS19 VAL23 ASP26 ALA233 LEU217 PHE272 LEU230 LEU275	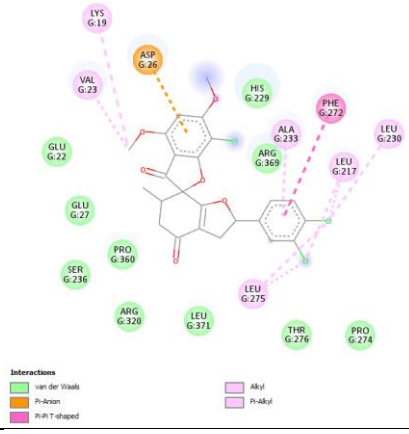
25171849	-9.1	ARG320	LEU230 HIS229 PHE272 ALA233 LYS19 VAL23 ASP26	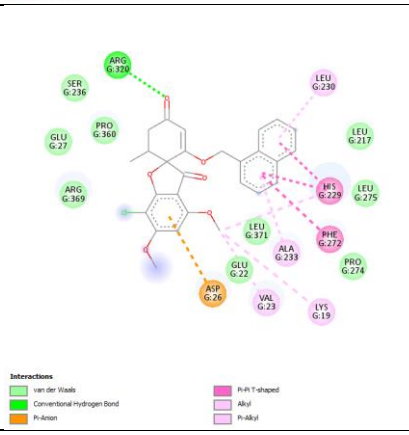

46844082	-9.1	-	LEU217 HIS229 LEU230 PRO360 ALA233 PHE272	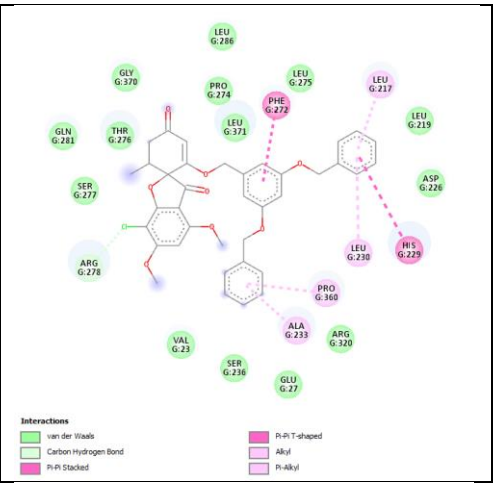
73330764	-8.8	-	LEU371 ARG369 ALA233 HIS229 ASP26 VAL23 LYS19	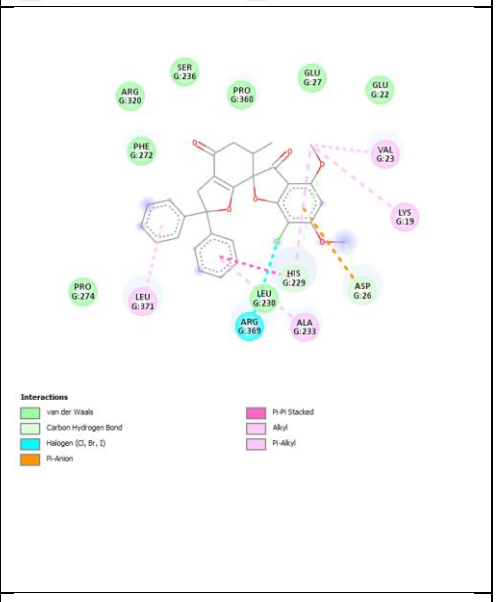
73330911	-8.8	-	LEU371 LEU230 ARG369 ASP26 LYS19 VAL23	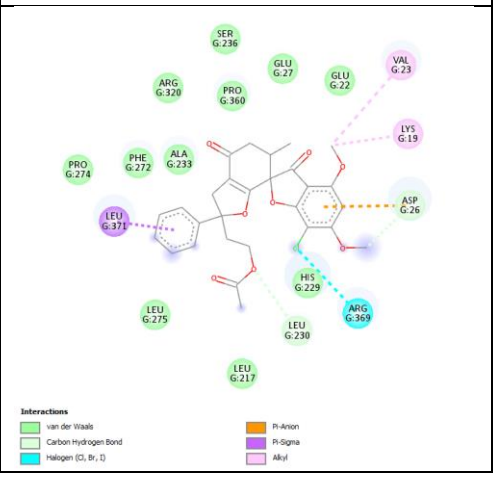

73331060	-8.8	-	LEU371 ARG369 ASP26 LYS19 VAL23	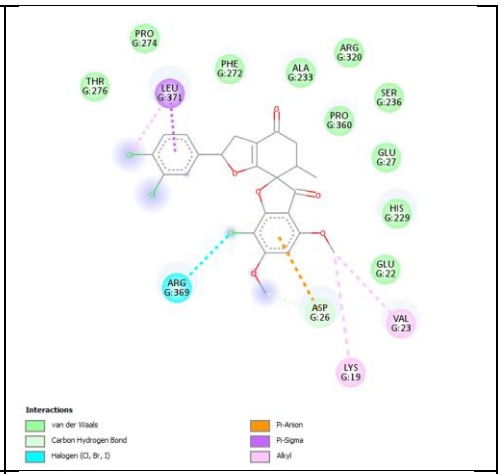
73331209	-8.7	THR276	PRO274 LEU230 ALA233 HIS229 CYS213 ASP226 LEU217 LEU219 LEU275 GLN281 LEU371 LEU286	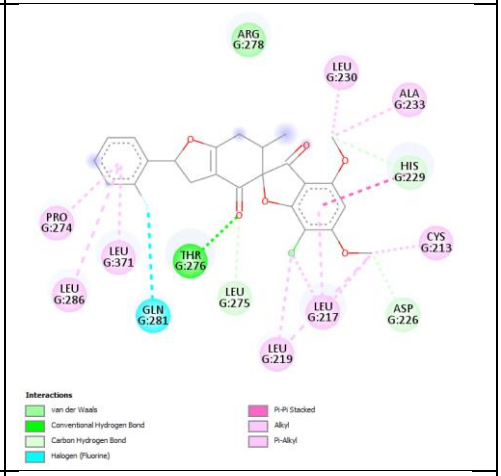
73331488E	-9.3	-	LEU217 LEU230 ALA233 PHE272 ARG369 ASP26 VAL23	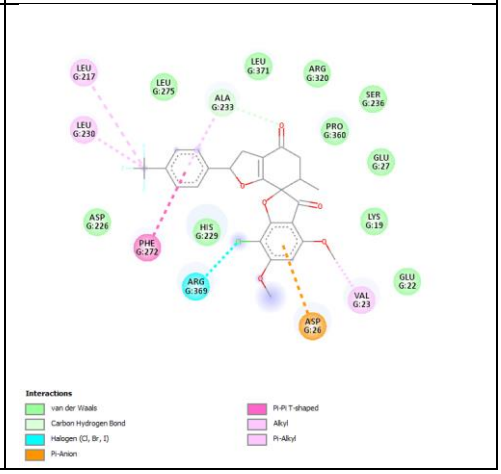

118263246	-8.8	-	LEU371 VAL23 LYS19 ASP26 ARG369 LEU230	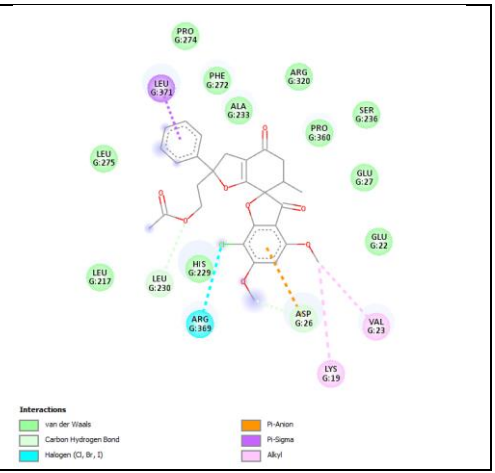

Table S3. Molecular docking details of ligands interaction with Rbd.

PubChem ID	Binding Energy (kcal/mol)	H-bonds	Hydrophobic interactions	Ligand interaction diagram	Lipinski Analysis	
CID_7331772 (Rb2)	-5.92	ARG 457 LYS 458 SER 459	ARG 454 ARG 457 LYS 458 ASP 467 GLU 471 PRO 491	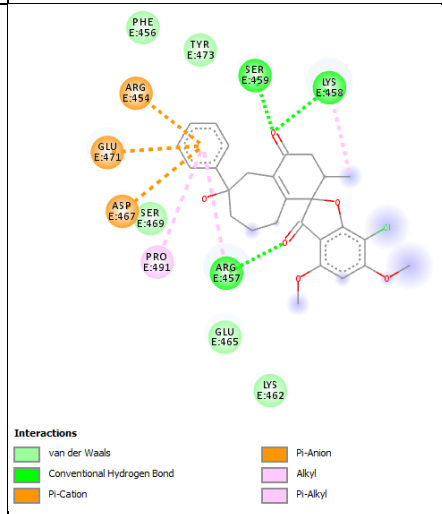	Molecular weight (<500 Da) Lipophilicity (LogP<5) H bond donor (<5) H bond acceptor (<10) Violations Lipinski Hepatotoxicity	417.5 3.47 0 5 0 Yes No

CID_73330911 (Rb4)	-7.07	ARG 457 LYS 458 SER 459	ARG 454 ARG 457 SER 469 GLU 471 PRO 491	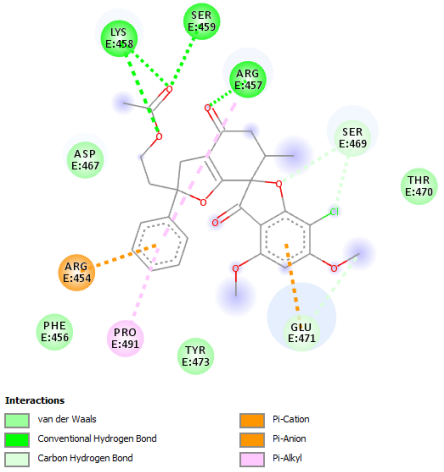	Molecular weight (<500 Da) Lipophilicity (LogP<5) H bond donor (<5) H bond acceptor (<10) Violations Lipinski Hepatotoxicity	526.9 4.27 0 8 1 Yes No
CID_73331346 (Rb5)	-6.08	ARG 454 ARG 457 GLU 471	ARG 454 ARG 457 ASP 467 SER 469 GLU 471 PRO 491	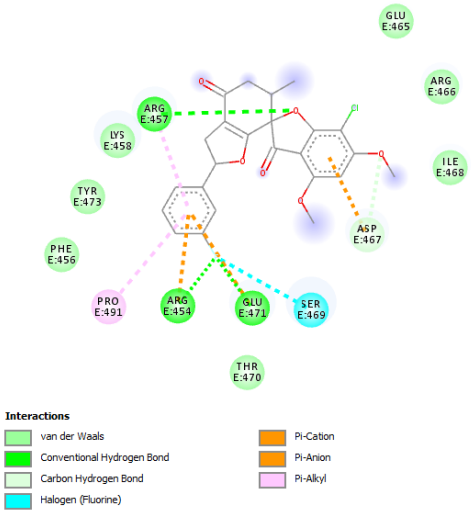	Molecular weight (<500 Da) Lipophilicity (LogP<5) H bond donor (<5) H bond acceptor (<10) Violations Lipinski Hepatotoxicity	458.8 3.73 0 7 0 Yes No

CID_73331488 (Rb6)	-5.49	ILE 468 ARG 454	PHE 456 ARG 457 LYS 458 ASP 467 GLU 471 TYR 473 PRO 491	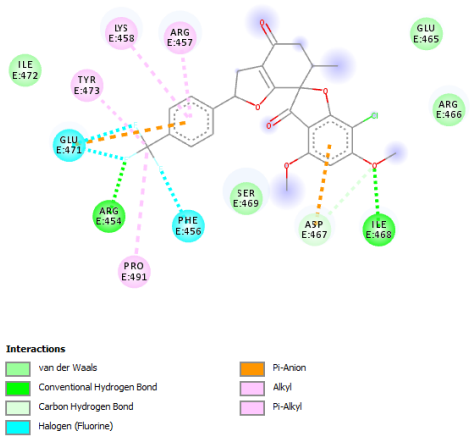	Molecular weight (<500 Da) Lipophilicity (LogP<5) H bond donor (<5) H bond acceptor (<10) Violations Lipinski Hepatotoxicity	508.8 4.00 0 9 1 Yes No
CID_118254214 (Rb7)	-6.68	ARG 457 LYS 458 ILE 468 SER 469	ARG 466 ILE 472 TYR 473 PRO 491	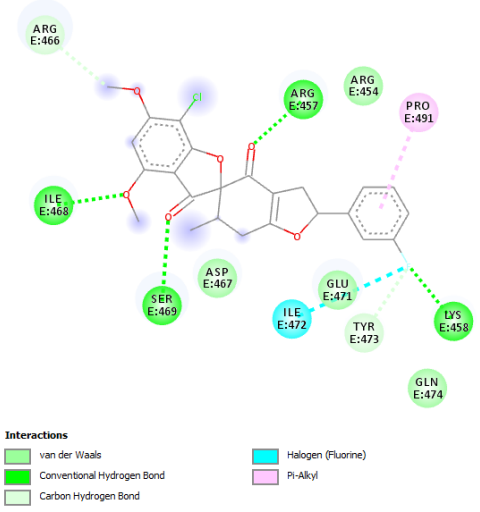	Molecular weight (<500 Da) Lipophilicity (LogP<5) H bond donor (<5) H bond acceptor (<10) Violations Lipinski Hepatotoxicity	458.8 3.83 0 7 0 Yes No

CID_118263246 (Rb8)	-7.02	ARG 457 LYS 458 SER 459	ARG 454 ARG 457 ASP 467 SER 469 GLU 471 PRO 491	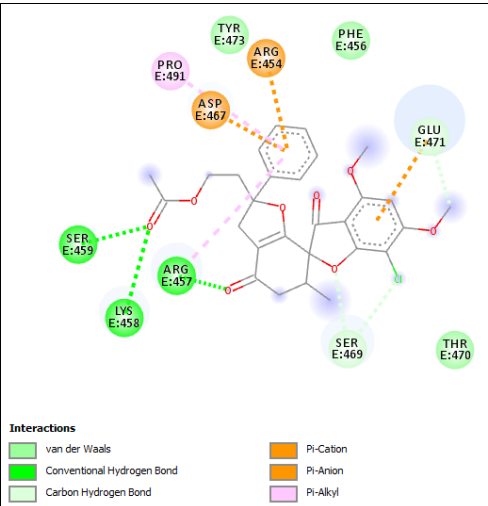	Molecular weight (<500 Da) Lipophilicity (LogP<5) H bond donor (<5) H bond acceptor (<10) Violations Lipinski Hepatotoxicity	526.9 4.27 0 8 1 Yes No

Table S4. Molecular docking details of ligands interaction with RdRp

.

CID_56924747 (Rd1)	-6.48	CYS 622	ASP 761 Glu 811 CYS 813	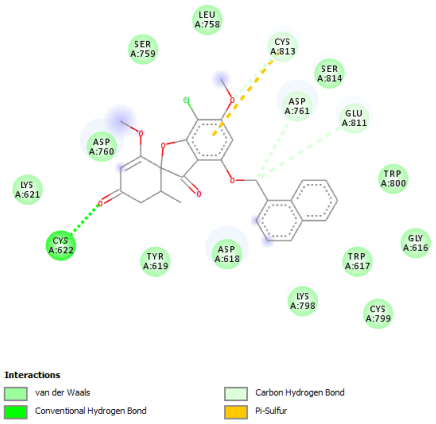	Molecular weight (<500 Da) Lipophilicity (LogP<5) H bond donor (<5) H bond acceptor (<10) Violations Lipinski Hepatotoxicity	478.9 3.68 0 6 0 Yes No
PubChem ID	**Binding Energy (kcal/mol)**	**H- bonds**	**Hydrophobic interactions**	**Ligand interaction diagram**	**Lipinski Analysis**	
CID_46844082 (Rd3)	-6.58	LYS 551 TYR 619 LYS 621	ASP 618 CYS 622 LYS 798	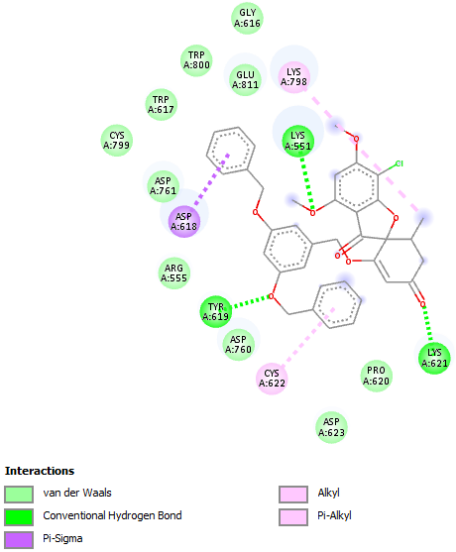	Molecular weight (<500 Da) Lipophilicity (LogP<5) H bond donor (<5) H bond acceptor (<10) Violations Lipinski Hepatotoxicity	641.1 5.51 0 8 2 Yes No

CID_118254216 (Rd4)	-6.62	LYS 621 CYS 622 LYS 798	ASP 618 CYS 622 ASP 623	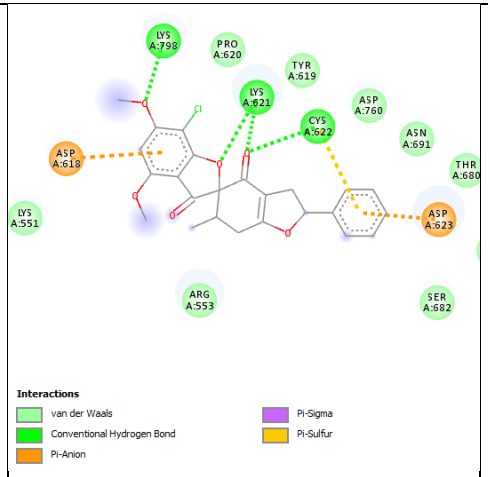	Molecular weight (<500 Da) Lipophilicity (LogP<5) H bond donor (<5) H bond acceptor (<10) Violations Lipinski Hepatotoxicity	440.8 3.65 0 6 0 Yes No
CID_73331060 (Rd5)	-6.87	LYS 621 LYS 798	LYS 621 CYS 622 ASP 623	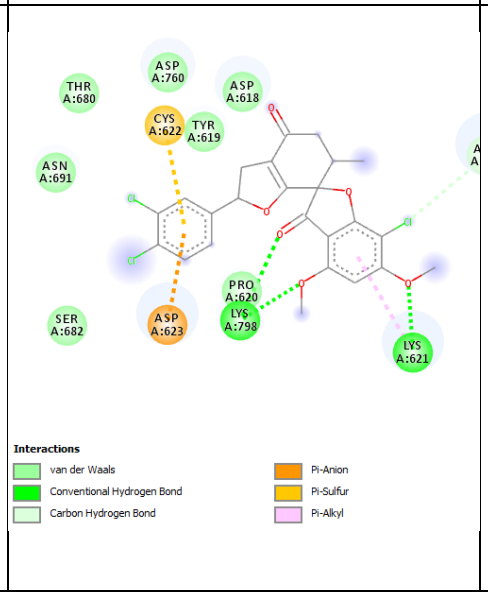	Molecular weight (<500 Da) Lipophilicity (LogP<5) H bond donor (<5) H bond acceptor (<10) Violations Lipinski Hepatotoxicity	509.7 4.09 0 6 1 Yes No

CID_73331487 (Rd8)	-6.01	-	ASP 618 PRO 620 LYS 621 ASP 761	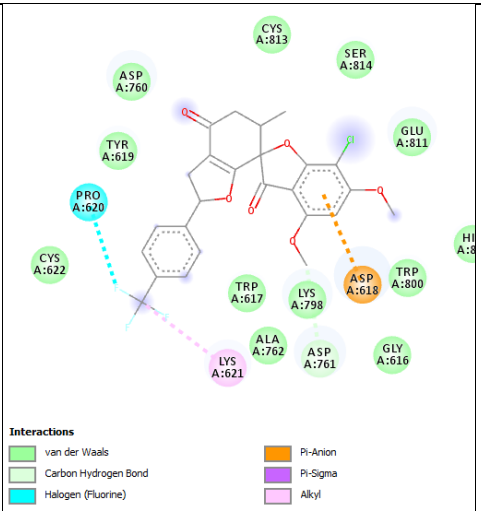	Molecular weight (<500 Da) Lipophilicity (LogP<5) H bond donor (<5) H bond acceptor (<10) Violations Lipinski Hepatotoxicity	508.8 4.01 0 9 1 Yes No
CID_73330763 (Rd9)	-6.84	ARG 555	HIS 439 ILE 548 ALA 550 ASP 618 LYS 798	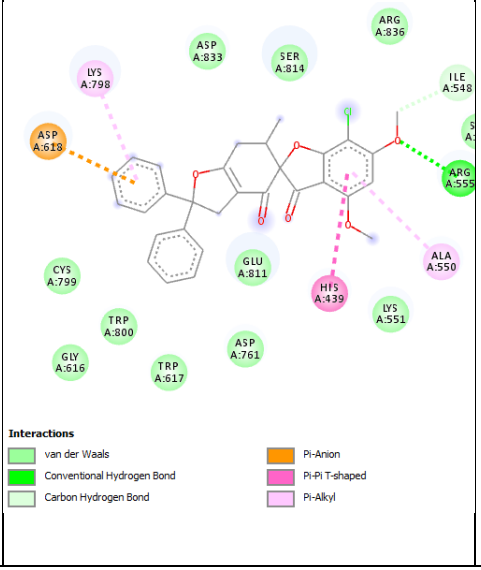	Molecular weight (<500 Da) Lipophilicity (LogP<5) H bond donor (<5) H bond acceptor (<10) Violations Lipinski Hepatotoxicity	516.9 4.22 0 6 1 Yes No

File 4

Table S5. Secondary structure changes upon ligand binding.

Complex	**Coil**	**B-Sheet**	**B-Bridge**	**Bend**	**Turn**	**A-Helix**
6LU7	88.2±3.05	74.3±2.2	3.5±.95	32.8±3.4	47.6±4.4	53.2±3.2
6lu7-144564153	82.1±3.5	78.7±3.6	6.6±1.3	26.2±2.8	47.7±4.7	55.2±4.2
6lu7-142550537	81.2±2.4	80.9±2.1	6.1±0.6	22.06±3.2	52.5±4.9	51.7±5.1
6lu7-griseofulvin	79.1±2.9	79.2±2.4	5.2±0.98	33.6±3.1	45.2±4.9	51.5±4.3
ACE2	96.9±3.4	20.23±3.7	5.07±1.7	57.1±4.9	83.9±7.8	286.5±8.1
ACE2-132286359	97.6±3.2	23.35±2.7	3.89±1.1	56.1±4.6	68.8±7.2	326.7±6.4
ACE2-46844082	87.7±3.2	21.97±2.7	4.2±1.3	56.8±4.5	72.5±7.6	325.1±6.9
ACE2-griseofulvin	90.5±3.4	24.6±3.8	2.5±1.4	60.7±4.5	69.3±8.7	314±7.5
RBD	64.6±2.9	46.4±3.7	5.2±1.9	30.6±2.7	23.1±4.2	6.6±2.8
RBD-griseofulvin	59.6±2.3	52±2.3	3.8±1.4	26.2±2.3	23.9±4.2	8.41±3.25
RBD-125429633	64.8±2.8	47.3±2.6	4.5±1.5	28.4±2.9	22.8±3.75	8.75±3.5
RBD-56950846	61.4±2.4	51.8±2.4	3.1±1.5	28.2±2.5	22.3±4.1	9.2±3.6
RdRp	176.8±5	155.1±4.2	13.5±2.7	87.6±5.5	113.2±8.1	325±6.8
RdRp-griseofulvin	186.1±6	142.8±4.4	15.1±1.9	83.3±6.1	120.5±8.5	327.1±6.8
RdRp-118254151	185.6±6.6	139.5±6.3	14.4±2.5	89.1±5.5	105±7.6	335±6.3
RdRp-73331209	179.1±6.6	151.6±1.1	14.2±1.9	87.8±6.1	122.2±8.1	326.1±6.2

File 5

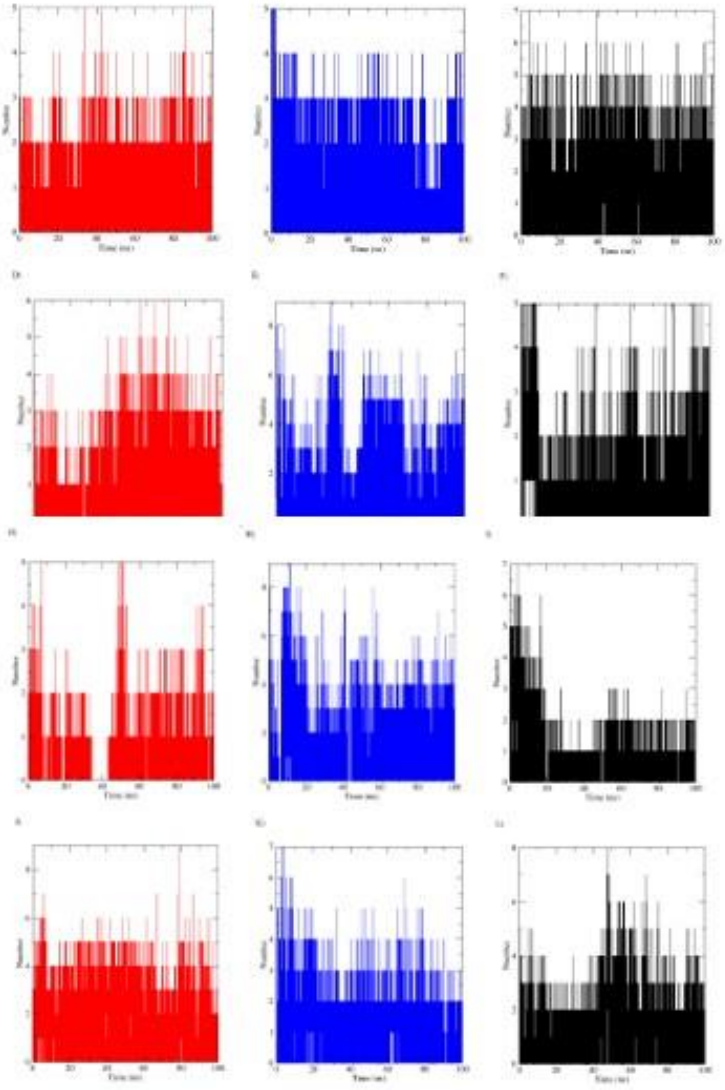

Fig S2. Hydrogen bonds analysis of best docked complexes. A) Mprotease- griseofulvin (M1), B) Mprotease-142550537 (M7), C) Mprotease-144564153 (M9), D) ACE2-griseofulvin (A7), E) ACE2-132286359 (A9), F) ACE2-46844082 (A3), G) RBD-griseofulvin (Rb1), H) RBD-125429633 (Rb9), I) RBD-56950846 (Rb3), J) RdRp-griseofulvin (Rd7), K) RdRp-73331209 (Rd2), L) RdRp-118254151 (Rd6).